Study of a voltage-gated ion channel reconstituted in Giant Unilamellar Vesicles

Sophie Aimon

THESE DE DOCTORAT

de l'UNIVERSITE PARIS VI

Institut Curie

Ecole doctorale ED P2MC 389, Physique

présentée par :

Sophie AIMON

pour obtenir le grade de Docteur de l'Université Paris VI

Study of a Voltage-Gated Potassium Channel in Giant Unilamellar Vesicles

soutenue le 29 septembre 2011, devant le jury composé de :

Mr. Luis BAGATOLLI	Examinateur
Mme Martine BEN AMAR	Examinatrice
Mr. Laurent BOURDIEU	Examinateur
Mr. Rob PHILLIPS	Rapporteur
Mr. Kenton SWARTZ	Rapporteur
Mme Patricia BASSEREAU	Directrice de thèse

Remerciements

Je souhaite tout d'abord remercier ma directrice de thèse, Patricia Bassereau, pour m'avoir fait confiance dès le début. La liberté que tu m'as accordée mais aussi ton dynamisme et ton enthousiasme m'ont encouragés tout au long de la thèse. Je suis aussi très reconnaissante de la gestion subtile que tu as eu des moments critiques. En particulier, sans ton soutien pendant l'écriture du manuscrit (qui a été un peu sportive je l'avoue), la fin de thèse aurait probablement été beaucoup plus compliquée.

Gilman Toombes m'a aussi encadrée pendant les quatre années de thèse. Merci de m'avoir toujours poussée à être honnête avant tout. Merci de m'avoir montré la nécessité de réfléchir profondément aux questions scientifiques qui sous tendent notre recherche, de garder un esprit critique vif, mais aussi de ne pas avoir peur de chercher l'information où elle se trouve pour résoudre les problèmes techniques quotidiens.

Surtout, merci à vous deux pour m'avoir montré que la recherche est un plaisir si on garde l'esprit curieux et que l'on cherche toutes les occasions pour échanger nos idées. J'espère que j'ai intégré au moins une partie de cet enseignement précieux et je m'attacherais à garder cet état d'esprit pendant tout le temps où je ferais de la recherche.

I also want to thank Rob Phillips and Kenton Swartz for their careful review of my thesis despite of the really little time they had. Thank you Rob Phillips, for your very detailed and useful comments on the thesis. Thank you Kenton Swartz, for your contagious enthusiasm for science and for the interesting discussion we had about KvAP. Un merci tout particulier à Laurent Bourdieu qui a aussi été mon tuteur pendant ces quatre ans. Merci beaucoup pour ta disponibilité et ton soutien toujours bienveillant lorsque je venais te demander conseil. Thank you Luis Bagatolli for your interesting comments about GUVs. Merci enfin à la présidente Martine Ben Amar pour m'avoir suivie depuis le master.

Je souhaite aussi remercier les collaborateurs du projet " neurone artificiel "; Luis Dinis, Jean François Joanny, David Lacoste et Jacques Prost. Merci d'avoir permis à ce projet de voir le jour. Thank you Daniel Schmidt for teaching me KvAP purification and the BLM technique and Rod MacKinnon for allowing me to come to your lab. Merci à John Manzi pour l'aide lors des purifications, Fahima Faqir pour les plasmides et Daniel Levy, Manuela Dezi et Aurelie Di Cicco pour toute votre collaboration et votre savoir en ce qui concerne les protéines membranaires. I also want to thank the group of Pr. José Manuel González Ros for their kind welcome in Elche. In particular, thanks to Jose Antonio Larrosa Poveda for showing me the reconstitution technique with the platinum wires and thanks to Asia Fernandez for teaching me how to patch clamp on multilamellar vesicles. Merci aussi à Ernesto Ambroggio pour nous avoir montré ta chambre à fil qui a largement inspiré la notre. Merci à Mathieu Pinot et Jean Baptiste Manneville pour votre collaboration avec la manip de FRAP sur les tubes, et, pour le projet de suivi de molécule unique, merci à Marianne Renner et Antoine Triller pour la comparaison avec les neurones, mais aussi à Matthew Turner pour la partie théorique. Je tiens aussi à remercier Andrew Callan-Jones pour avoir adapté la théorie de couplage entre la densité des protéines et la courbure au cas de protéines transmembranaires avec deux insertions.

Merci aussi à Ivan Lopez-Montero pour les expériences avec le récepteur à acetylcholine et Francisco Barrantes pour nous avoir fourni la protéine. J'aimerais aussi remercier Rania Ghossoub et Alexandre Benmerah pour votre collaboration avec les cellules à cils.

Thanks also to members of the Owe Orwar group, in particular to Tatsiana Lobovkina, Brigitte Bauer, et merci à Karin Aubrey, Maxime Dahan, Marc Gielen, Pierre Paoletti, Nicolas Chiaruttini (" accessoirement "), et tous les autres gentils chercheurs qui nous ont montré leur manips et ont discuté de science avec nous. Thanks to members of the Cold Spring Harbor Laboratory School for Drosophila Neurobiology for exchanges about KvCh enrichment in curved membranes in a biological context. Je souhaite aussi remercier les collègues du bureau 204b et tous les membres de l'UMR 168 et au-delà qui ont fait de ces quatre années un plaisir. Je souhaite en particulier remercier les mécaniciens, Benoit Lemaire et Remi Fert mais aussi les secrétaires, Agnès Vérin, Laurence Turpin et Nicole Blandeau. Merci pour votre aide et votre gentillesse. Un grand merci aussi à ceux avec qui j'ai partagé des cafés et quelques verres lors de soirées en tous genres.

Je tiens bien sûr à remercier chaleureusement les membres de l'équipe Bassereau pour les aspects scientifiques mais aussi pour les petites attentions qui font la différence, surtout dans les moments difficiles. Merci Yegor pour avoir effectué les mesures de tracking de Qdot. Merci Benoît pour avoir monté le set up de pince optique et m'avoir montré comment faire les experiences de tubes. Merci Stéphanie pour le soutien quotidien. Je tiens aussi à remercier Aurélien pour toute l'aide en biochimie et Pierre pour les conseils pertinents à la fin de la thèse. Un grand merci à Marie pour m'avoir si bien encadrée en M2. Merci aux anciens, Ludwig, Darius, Faris, Pia et Gerbrand, pour m'avoir accueillie, et merci à Bidisha, Alessia, Bibhu et Nathalie, pour m'avoir accompagnée. Merci à Clément pour les discussions sur les tubes et la dynamique de la membrane en présence d'inclusions. Merci Gamal, Aurore et Thomas pour la relecture in extremis et nécessaire du manuscrit. Merci Alice pour être une collaboratrice aquaporine si efficace, et Coline pour m'avoir poussée à mes limites à la course à pied. Ayakochan, anata no nintai ni kansha shimasu. Merci à Sandrine et Mahassine pour le stepmania et tout le reste. Enfin un merci particulier à Matthias pour reprendre le flambeau de notre projet difficile. Keep it up!

Merci à mes proches de m'avoir supportée dans cette aventure. Merci à Pierre, Sarah, Romain, Ghislaine et Denis Pezet pour avoir été une deuxième famille pendant une bonne partie de la thèse. Merci à Noémie pour avoir supporté le bazar et le bruit à des horaires impossibles, mais aussi pour avoir été là pour partager les projets, les difficultés et les bons repas. Merci aux amies d'enfance et d'adolescence que j'ai eu le plaisir de retrouver à Paris, aux anciens de Clermont, du master et de Curie que j'ai la chance de recroiser de temps en temps. Une pensée particulière pour les amis précieux qui ont été présents dans les moments particulièrement difficiles de cette fin de thèse.

Merci aux familles Aimon et Deschamps pour être toujours aussi présentes. En particulier, un tendre merci à ma mamie Mimie pour tout le soutien. Merci à Nicolas Aimon pour avoir sauvé ma soutenance grâce à la technique du pomodoro. Merci aussi de m'avoir accueillie à Boston; j'espère qu'on se retrouve bientôt là-bas! Je souhaite aussi remercier mes parents. Merci pour le soutien financier mais aussi merci de m'avoir inculqué le plaisir

de la science sans m'imposer d'orientation lors de mes études. Merci aussi d'avoir si bien organisé mon pot de thèse!

Enfin, malgré le fait d'avoir été si bien entourée, il y a eu des moments pendant lesquels des personnes qui ne me connaissent pas (sauf Brad) m'ont grandement aidée à maintenir ma motivation. Je souhaite en particulier remercier Christophe André, Bill Clinton, Stanislas Dehaene, Tohru Fujisawa, John Kabat-Zinn, Masashi Kishimoto, Brad Mehldau, Hayao Miyazaki, Barack Obama et Joanne Rowling.

Pardon à tous ceux que j'ai oublié ou que je n'ai pas remercié suffisamment faute de temps et de place. Merci encore à tous et bon courage si vous vous apprêtez à lire cette thèse.

Chapter 1

Introduction

Voltage-gated ion channels are trans-membrane proteins implied in cell excitability. They are pores that open as a function of voltage and selectively let specific ions cross the membrane without their counter ions. This flux of ions will either further increase or dampen the initial potential change. This regulation of membrane potential is at the basis of the action potential, which is the electrochemical signal that for example propagates along neuronal axons, thus allowing long distance communication between neurons. The Hodgkin and Huxley theory, that first described the mechanisms underlying this action potential, includes the role of the ion channels only, but totally neglects the potential effects of the surrounding membrane. However, membrane could influence the action potential at two different levels:

- At a molecular and individual level, the membrane properties can affect the functioning of a single voltage-gated channel
- At a larger scale, the membrane can influence the channel distribution by its geometry, but also by more subtle effects due to the interplay between the ion channel activity and membrane physical properties and shape.

My PhD work is part of a large project initiated between our experimental group (P. Bassereau) and membrane theoreticians (J.F. Joanny and J. Prost at the Curie Institute, D. Lacoste at the ESPCI). In the long-term, they aim at developing a biomimetic model of neuron and providing a description of the action potential dynamics based on the physics of non-equilibrium membranes.

From a molecular perspective, the general structure of the voltage gated channels is now known (see for example figure 2.19). They are formed of a central pore that selectively lets a specific ion cross the membrane. Surrounding it are four voltage sensors that change

conformation when a voltage is applied to the membrane which leads to pore opening. As these channels have many contacts with the surrounding membrane due to their cruciform shape (see figure C.1), membrane specific composition but also mechanical properties can have an important role on their function.

Besides, a large amount of theoretical and experimental work has been made in the past 30 years to understand and characterize membrane mechanical properties. A particularly successful model has been the elasticity theory, which is a continuum theory that ignores molecular details of the lipid bilayer, and describes membrane mechanical properties using macroscopic parameters such as membrane tension, curvature and thickness.

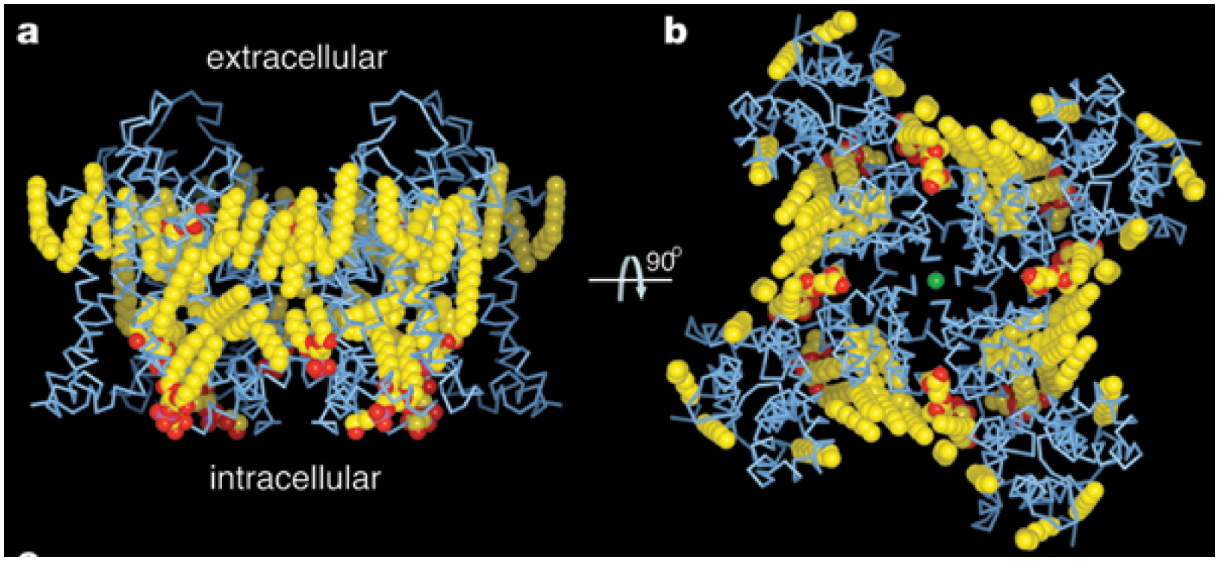

Figure 1.1: Structure of a voltage-gated potassium channel, Kv1.2, embedded in lipids. a) side view, b) top view. From [1].

Recently, some groups have started to study the effects of the membrane properties on channel activity and lateral distribution in membranes, but also reversely to understand the effect of the channel on membrane properties. Deciphering these questions is a hard task with living cell as there is a constant regulation of membrane parameters by the cell itself. Some in vitro systems have been developed, but they usually have some drawbacks that are not compatible with a full control of each of the relevant parameters. Reconstitution of voltage-gated ion channels into giant unilamellar vesicle (GUVs) is a good alternative option as they have been widely used to investigate membrane mechanics and allow to control at once membrane composition, tension and curvature.

The purpose of this thesis is to

- Build a model reconstituted system, while keeping the channels functional, in which all relevant parameters could be controlled to study the coupling between voltage-gated ion channels and the surrounding membrane,
- Use this reconstituted system to perform physics experiments addressing new ques-

tions that could not be solved in the absence of the adequate in vitro system: for instance, to understand the effect of membrane curvature on protein distribution and diffusion.

In the next chapter, I will introduce general points on neurons and action potential and on the global structure of voltage-gated channels. As membrane physical properties are central to my experiments, I will briefly summarize the essential points of the physics of the membrane that are necessary to analyze my work. Eventually, I will review published work on the already studied effects of the membrane on voltage-gated ion channels.

In chapter 3, I present the channel that we used as a model for voltage gated channels, KvAP, a bacterial analog of eukaryotic voltage gated channels. In this chapter, I also describe the protocol for purification and reconstitution in small liposomes that I used for all the other experiments presented in this thesis. I also present the fluorescent labeling method, and show with electrophysiology measurements (BLMs) that labeling did not affect the channel function.

Chapter 4 reports the method for KvAP reconstitution into giant unilamellar vesicles that I have developed (see figure C.4). I will show that it is possible to prepare optically defect-free GUVs from the liposomes described in chapter 3. Channel density and homogeneity in GUVs are quantified via confocal microscopy while patch-clamp is used to measure the activity of the reconstituted channels. We thus have been able to develop a method to reconstitute KvAP in unilamellar giant liposomes, at a controlled density and keeping their functionality.

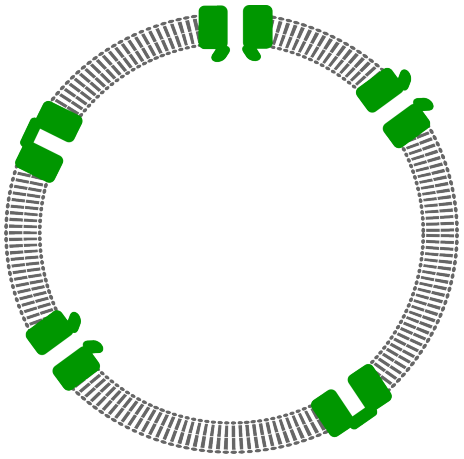

Figure 1.2: Cartoon of a giant unilamellar vesicle containing reconstituted KvAP (in green).

The first question we tackled with our system was the effect of membrane curvature on the channel distribution, as described in chapter 5. To study this effect, I pulled a membrane nano-tube from a GUV and could set the tube radius between 10 nm and 200 nm by varying the tension of the GUV membrane. The concentrations of channels in the tube and GUV were measured via confocal microscopy.

In chapter 6, I present another interesting experiment that was possible with the reconstituted channels in GUVs and the tube pulling technique. The goal here was to measure

the effect of membrane confinement on channel and lipid lateral diffusion. Diffusion was measured by tracking single channels labeled with quantum dots in membrane tubes of different radii.

Finally, in the conclusion, I will summarize the results from my thesis and present some perspectives of the work.

Chapter 2

Introducing voltage-gated ion channels and membranes

In this chapter I will describe how the voltage-dependent gating of ion channels permit neurons to signal rapidly via the propagation of action potentials. I will then summarize the biophysical properties of cell membranes, and describe how cellular excitabililty can be modulated by interactions between ion channels and the surrounding membrane. Finally, I will describe the model system I developed during my thesis to study voltage-gated ion channel biophysics.

2.1 Biophysics of neuronal excitability

Neurons rapidly transport and process information in the brain and nervous system. As shown in figure 2.1, a typical neuron has a cell body, called a soma, a branched tree-like structure called the dendrites and a long cable-like projection called the axon. Signals between neurons are transmitted chemically or electrically at specialized junctions, called synapses (inset of figure 2.1). Signals received in the post-synaptic terminals of the dendritic tree cause current to flow into or out of the cell, thereby raising or lowering the membrane potential (the voltage of the cell interior relative to the surrounding medium). If these input signals drive the membrane potential of the soma above a threshold, the neuron fires and an electro-chemical excitation, called an action potential, is initiated and actively propagates along the axon. This signal is then transmitted to other neurons via synapses along the axon and in the axon terminal. Note that speed, frequency and shape of the action potential are crucial parameters for information processing as they will affect timing and intensity of dendritic inputs which will in turn determine if the neuron fires or

not.

The remainder of this section describes the biophysics of the action potential and the properties of the voltage-gated ion channels that produce it.

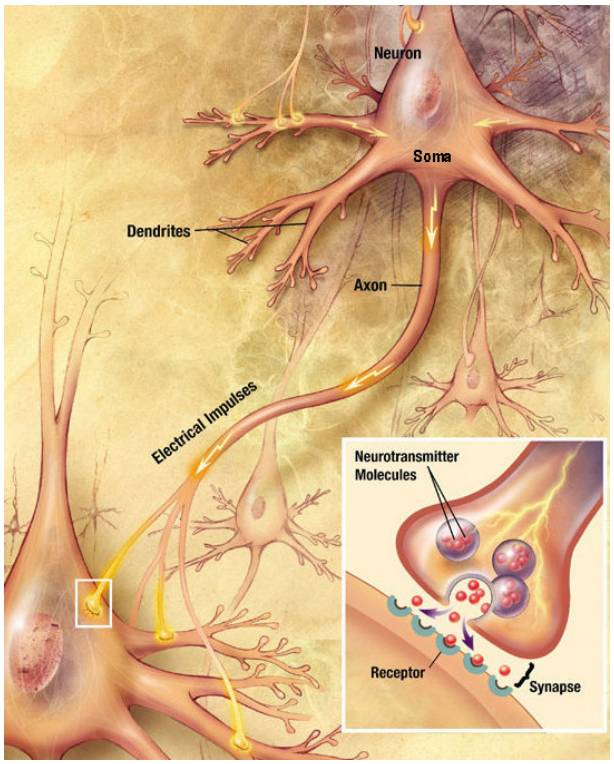

Figure 2.1: Illustration of information flux between neurons. From http://en.wikipedia.org/wiki/Neuron.

2.1.1 Action Potential

Cells actively pump ionic species across the cell membrane to generate concentration gradients and maintain a resting membrane potential (typically -70mV to -80mV for neurons). In excitable cells (e.g. neurons, muscle cells, endocrine cells, some plant cells and even bacteria [2]), stimuli which depolarize the membrane above a threshold (-55mV for example for a typical neuron) can induce an action potential, a short-lasting event in which the cell membrane potential rises rapidly ($\sim$ 1 millisecond) to a very positive value (up to +100mV) before returning back to its initial resting level.

This section describes the biophysical and biochemical processes underlying the action potential in neurons.

2.1.1.1 Membrane Potential

The cell (plasma) membrane consists of proteins embedded in a lipid bilayer. The hydrophobic core of the membrane acts as a barrier around the cell. While some small

molecules such as water, O_2 and CO_2 can cross the lipid bilayer (e.g. water permeability $\sim 10^{-5}$ m/s [3]), charged species such as ions and most hydrophilic molecules (e.g. glucose, amino acids) are essentially impermeable (ionic permeability $\sim 10^{-13}$ m/s [4]). Consequently, the passage of ions across the membrane relies upon proteins which form channels, pumps and transporters. As the intra and extra-cellular solutions are far more conductive than the membrane, any net charge rapidly accumulates at the interior and exterior surfaces of the membrane leading to a transmembrane voltage. Electrically the membrane resembles a capacitor and resistor in parallel.

In the absence of any active processes, the concentration of ions in the cell could equilibrate with the exterior due to ionic diffusion through channels and transporters and there would be no potential difference (0 mV membrane potential). However, pumps in the cell membrane actively transfer ions across the membrane. For example, using the chemical energy obtained by the hydrolysis of ATP, the sodium-potassium exchanger undergoes a cycle which exports three Na^+ ions and imports two K^+ ions into the intracellular space. Each cycle of the pump lowers the intracellular Na^+ concentration, increases the intracellular K^+ concentration, and removes one elementary charge from inside the cell.

Ion	Extracellular concentration (mM)	Intracellular concentration (mM)	$\frac{[\text{Ion}]_o}{[\text{Ion}]_i}$	Equilibrium potential (mV)
Na^+	145	12	12	+67
K^+	4	155	0.026	–98
Ca^{2+}	1.5	100 nM	15,000	+129
Cl^-	123	4.2	29	–90

Figure 2.2: Ion concentrations and Nernst potential (or equilibrium potential) for mammalian skeletal muscle. From [5].

Thus, the activity of pumps creates concentration gradients (see second and third column of the table figure 2.2 for concentrations in a typical mammalian cell) and a membrane potential through the net import/export of an ionic species. These ionic concentration gradients, in turn, drive passive diffusion of ions through channels and transporters, which limits the concentration gradient and establishes the resting membrane potential.

For example, if a pore selective for potassium (i.e. a potassium channel) opens in the membrane with 0mV membrane potential, potassium ions will diffuse from inside the cell (high concentration) to outside the cell (low concentration). However, as those positively charged ions cross the membrane, the membrane potential (inside the cell) will decrease and this electrostatic force will reduce the rate at which potassium ions leave the cell. The inward flux of potassium ions induced by the electric field across the membrane would exactly counteract the outward diffusive flux (net flux of potassium equals zero) when the membrane potential is at the Nernst potential for potassium, E_K, defined as:

$$E_K = \frac{k_b T}{q} ln \frac{[K]_o}{[K]_i}, \tag{2.1}$$

where k_b is the Boltzmann constant, T is the temperature, q is the elementary charge, $[K]_o$ and $[K]_i$ are the potassium concentrations outside and inside the cell respectively. The last column of table 2.2 presents the Nernst potential for different ions.

In a cell, a similar equation can be written to take into account that different ion types (e.g. Na^+, K^+, Cl^-) diffuse across a membrane. The membrane potential is then given by the Goldman equation:

$$E_m = \frac{k_b T}{q} log(\frac{P_{K^+}[K^+]_{out} + P_{Na^+}[Na^+]_{out} + P_{Cl^-}[Cl^-]_{in}}{P_{K^+}[K^+]_{in} + P_{Na^+}[Na^+]_{in} + P_{Cl^-}[Cl^-]_{out}}) \tag{2.2}$$

where Pi is the membrane permeability for the ion i .

In neurons, at rest, sodium channels are closed whereas some potassium channels are opened so the potassium concentration gradient sets the membrane potential at approximately -70 mV [5].

2.1.1.2 Hodgkin-Huxley model

In 1952, before the discovery of ion channels, Hodgkin and Huxley proposed that the action potential in the giant squid axon was due to changes in membrane conductance to specific ions [6], therefore changing membrane potential with the same mechanism as described above. They received the Nobel price in 1963 for this disovery. The corresponding equivalent circuit is shown in figure 2.3. Hodgkin and Huxley also proposed that those conductances themselves depend on membrane voltage following a well defined kinetic model.

The currents underlying an action potential spike are shown in figure 2.4A. If membrane is depolarized above a threshold of -40 mV, sodium enters the cell. This increases the membrane potential which further increases membrane permeability to sodium. This positive feedback leads to a fast increase of the membrane potential. After approximately 1 ms, membrane permeability for potassium increases and potassium starts to go out of the cell. Meanwhile, permeability of the membrane for sodium decreases. K^+ outflow leads to a decrease of membrane potential back to the resting potential.

2.1.1.3 Action potential propagation

As shown in figure 2.4B, membrane depolarisation at a specific point of the membrane produces asymmetric currents, which lead to membrane depolarisation and initiation of the action potential further away along the axon. Note that without this active process, the axon would behave like an electric cable and the signal would decay with a characteristic length of $\lambda = \sqrt{\frac{ar_m}{2r_a}}$, where a is the axon radius, r_m is membrane resistance per unit area, and r_a is the cytoplasm resistivity. λ is of the order of 0.1 to 1 mm.

An action potential only propagates in one direction starting at the neuron soma and downstream along the axon. This directivity results from the inhibition of sodium permeability just after the action potential (we will see in section 2.1.2.5 that this corresponds

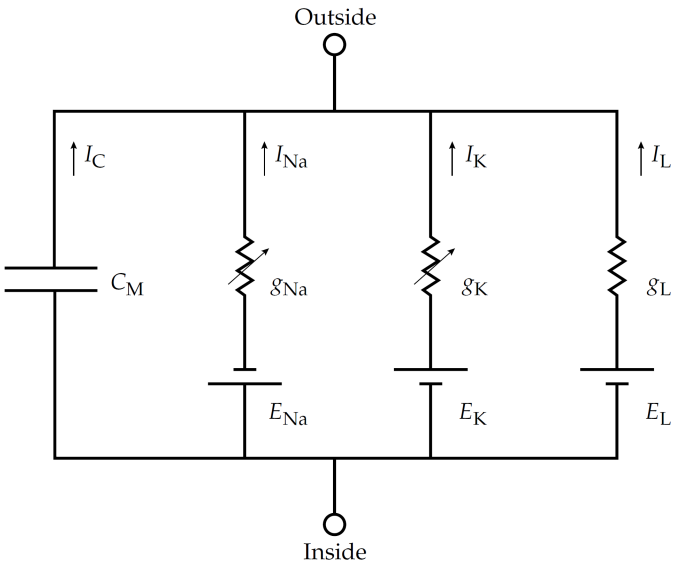

Figure 2.3: Circuit equivalent to the squid giant axon membrane. C_M represents membrane capacitance. Generators, E_i, correspond to the Nernst potential, while g_i represent variable membrane conductance of the difference ions (i=Na^+,K^+) . g_L is a non specific leak conductance. From [5].

to ion channel inactivation). Indeed, at any given point along the axon, sodium permeability upstream is temporarily disabled (for a time longer than the action potential) which prevents the membrane to respond to membrane depolarization and thus ensures the unidirectionality of the action potential propagation.

2.1.2 Voltage-gated ion channels

Hodgkin and Huxley's already suspected that there were discrete sites of the membrane where the conductance was changing with voltage [7].

Those "active patches" in the axon membrane must thus have the following properties:

- Be selective for specific ions
- Have a "gate" that opens as a function of voltage
- Have a mechanism (different from the gate opening) that allows the pore to close again after some time (inactivation)

They should hence have at least three distinct states following a simplistic kinetic model:

The molecules underlying the action potential (the voltage gated channels) have now been identified and studied thoroughly with both functional studies, such as patch-clamp

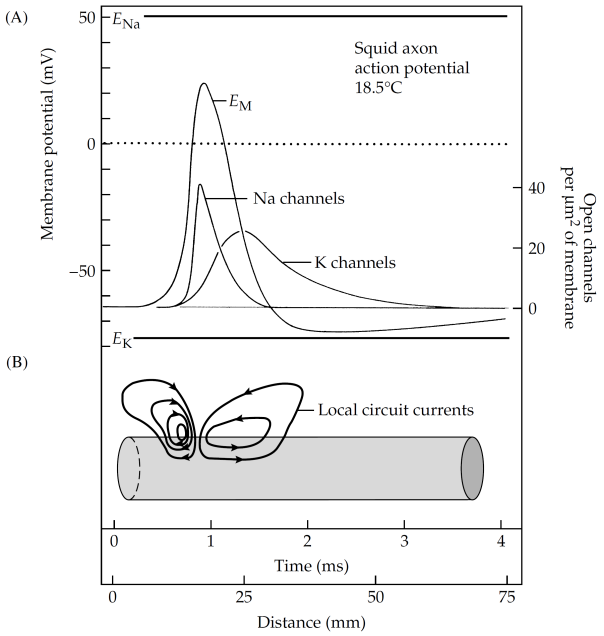

Figure 2.4: A) Membrane conductance to specific ions and membrane potential during action potential in the squid axon. B) Local currents in the axon during action potential propagation. From [5].

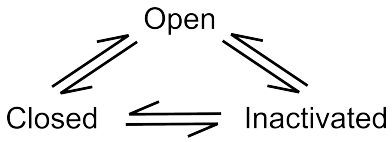

on cells or purified and reconstituted channels in model membranes, and structural methods, including Xray crystallography, Nuclear Magnetic Resonance, Electron Spin Resonance, Electron microscopy et caet.[7].

2.1.2.1 Patch clamp measurements

To test Hodgkin and Huxley's theory, and find evidence of the presence of these ion channels in cells, E. Neher and B. Sakmann in the 70s invented a new technique to isolate a small piece of cell membrane: the patch-clamp technique. They received the Nobel Prize for this in 1991. The technique is described in figure 2.5A. In practice, a small piece of cell membrane is aspired in a clean micropipette containing an electrode (with an open tip with a diameter usually less than one micron). This allows a strong adhesion of the membrane to the glass very tightly and thus, suppresses almost completely leaking currents between the glass and the membrane. Under these conditions, currents can only go through the patch of membrane. Several recording modes are then possible as shown in figure 2.5C:

- On-cell mode: the pipette is kept in contact with the entire cell. This way the small patch of membrane has a much higher resistance than the rest of the cell, and hence

is the conductance limiting element. This geometry thus allows to measure basically only the current going through the small patch of membrane.

- Whole-cell mode: it is used to measure the current going through the whole cell. For this, it is necessary to break the patch in the pipette either by a strong aspiration or by applying a short and strong electric pulse.

- Excised patch mode: it is used to ensure that the current going through the patch will be measured without the contribution of the rest of the cell body, and also to control the media on both sides of the membrane. The patch can be detached from the cell by pulling either from the on-cell mode (inside-out configuration) or from the whole-cell mode (outside-out configuration).

All the configurations are described in details in [8].

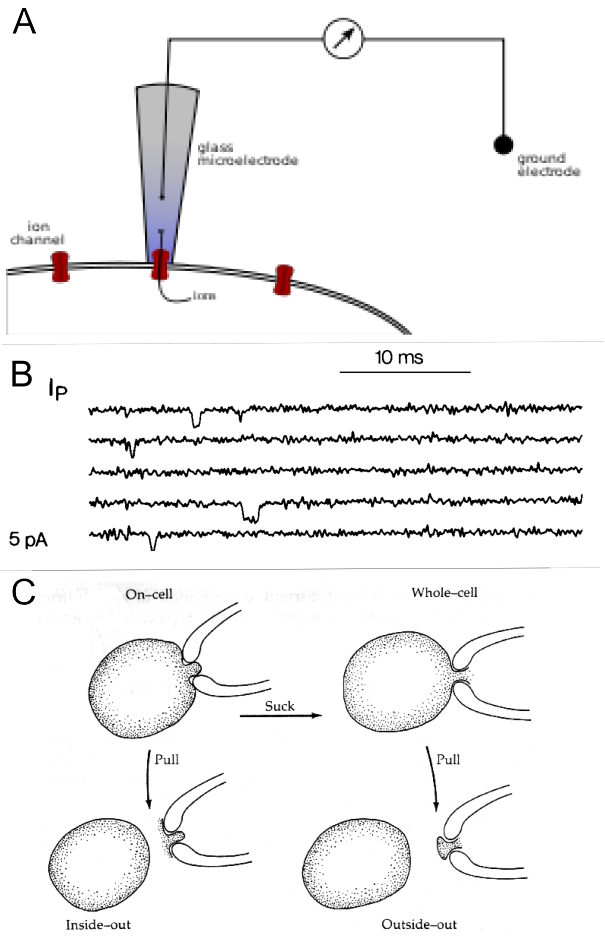

Figure 2.5: A) Patch-clamp method as historically designed by Neher and Sakmann. B) Early patch-clamp recording on rat muscle cells. One can see the step-like currents characteristic of single channel opening and closing. From [9]. C) Different patch clamp recording methods. From [5].

This patch clamp technique allowed Neher and Sakmann to detect step-like currents as shown in figure 2.5B. These are characteristic of single channels opening and closing. Note that the opening is stochastic.

Single channel conductance range from 4 to 240 pS, and most channels have a conductance on the order of 10 pS [5]. Thus, measuring the signal from a single channel requires suppressing as much as possible the leak current between the membrane and the glass pipette. As those conductances are small, the noise from the seal between the membrane and the glass pipette must be really low. This is achieved by the strong adhesion between glass and membrane, leading to a seal resistance on the order of tens of giga ohm (a "gigaseal"). It is also necessary to have very sensitive systems to measure low currents of the order of a few pA and to electrically isolate the set-up.

Other techniques for studying channels purified and reconstituted in membranes have also been developed. They will be discussed in section 4.1.1 of chapter 4.

2.1.2.2 Global structure

The elucidation of the structure of several members of the voltage-gated channels superfamily in the last decade has played an important role for our understanding of voltage-gated ion channels.

Voltage gated channels have a global structure similar to that shown in figure 2.8. They are either tetramers (Kv channels) or monomers made of four repeated motifs (Nav channels and Cav channels). The voltage sensor is constituted of 4 alpha helices (S1 to S4 at the exterior of the channel) while the 2 remaining helices (S5 and S6) form the pore (in the interior).

2.1.2.3 Pore structure

The backbone of the pore is highly conserved in all those ion channels. Its structure was discovered with the structure of KcsA [11], a bacterial channel that does not have the voltage sensor domains (see figure 2.7). It is a tetramer, where each monomer contains two membrane-spanning alpha helices. The ion selectivity filter is formed by the P-loop domain between those two trans-membrane helices. The amino acid sequence in the P loop is also quite conserved in many different ion channels. Selectivity for specific ions is controlled by this pore sequence. For example, the exchange of one amino acid can change a pore selective for potassium like KcsA (containing the characteristic TVGYG sequence for potassium channels that we will also find in KvAP in chapter 3) which is 1000 times more selective for potassium than sodium, into a pore selective for sodium (NaK with TVGDG in the pore sequence) [12]. It can be surprising that some channels let potassium go through but not sodium, even though sodium is much smaller than potassium. This was explained by the fact that the pore residues replace the water molecules in the ion hydration shell[13].

It should also be noted that the pore can be blocked by different molecules (charybdotoxin from scorpion venom, for example) that perfectly fit in the entrance of the pore [7].

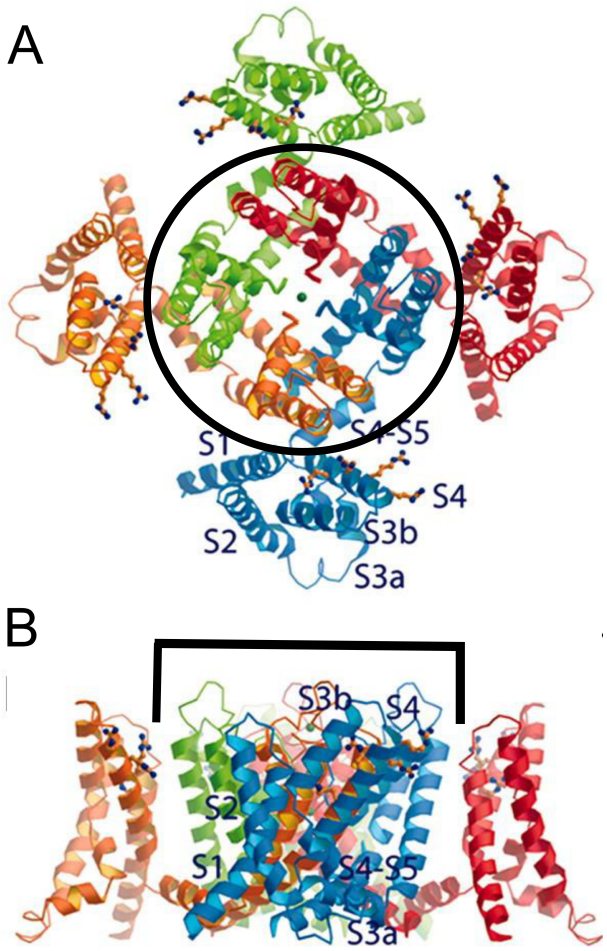

Figure 2.6: Model for the structure of a voltage gated potassium channel (KvAP). A) Top view. B) Side view. The black line delimitates the pore while the voltage sensors are on the outside. From [10].

2.1.2.4 Voltage gating

The underlying mechanism responsible for voltage gating has been a matter of debate since the discovery of the structure of a voltage gated ion channel in the activated state, approximately 10 years ago [14] by the group of Rod Mackinnon.

Electrophysiology measurements had shown that the equivalent of approximately 3 positive charges per monomer cross the membrane when the channel changes conformation just before opening the gate (note that this leads to a typical electric potential energy of ~ 20 kT).

Two basic mechanisms could lead to this change in potential energy during channel conformation change:

- Charged residues could move through the membrane

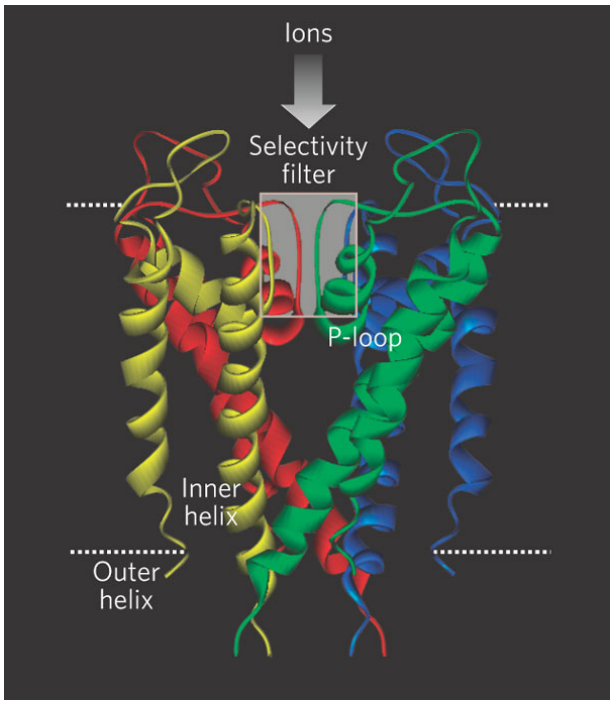

Figure 2.7: Structure of KscA, a model for voltage gated channels pore. From [12, 11].

- The channel could change the electric field around itself (for example by creating water crevices)

Some consensus now starts to arise concerning the conformational changes between the resting and the activated states. The current hypothesis is illustrated in figure 2.8A and B. When an electric field induces the motion of charged residues (R1 to R4) in the S4 helix, aplha helices in the voltage sensor slide against each other which leads to the bending of the S6 helix and to channel gating. E1 and E2 in S1 would then be important for the stabilization of the closed or opened state (see also section 2.3.1 for a description of a similar role for the phospholipid phosphodiester group).

Note that the conformational changes at the interface between the channel and the membrane could thus be significant. We will discuss the possible implications of these changes in section 2.3.1.

2.1.2.5 Inactivation

Inactivated state is the non conductive state that prevents the back propagation of action potentials. As discussed in section 2.1.1.3, it allows the action potential to propagate only one way down the axon. It is also important to limit the change of ion concentrations in and out the cell.

Two inactivation mechanisms have been studied so far and are still debated. The first one occurs rapidly after pore opening and involves plugging the pore with the channel N terminus. This mechanism is thus called N term or ball and chain inactivation [17].

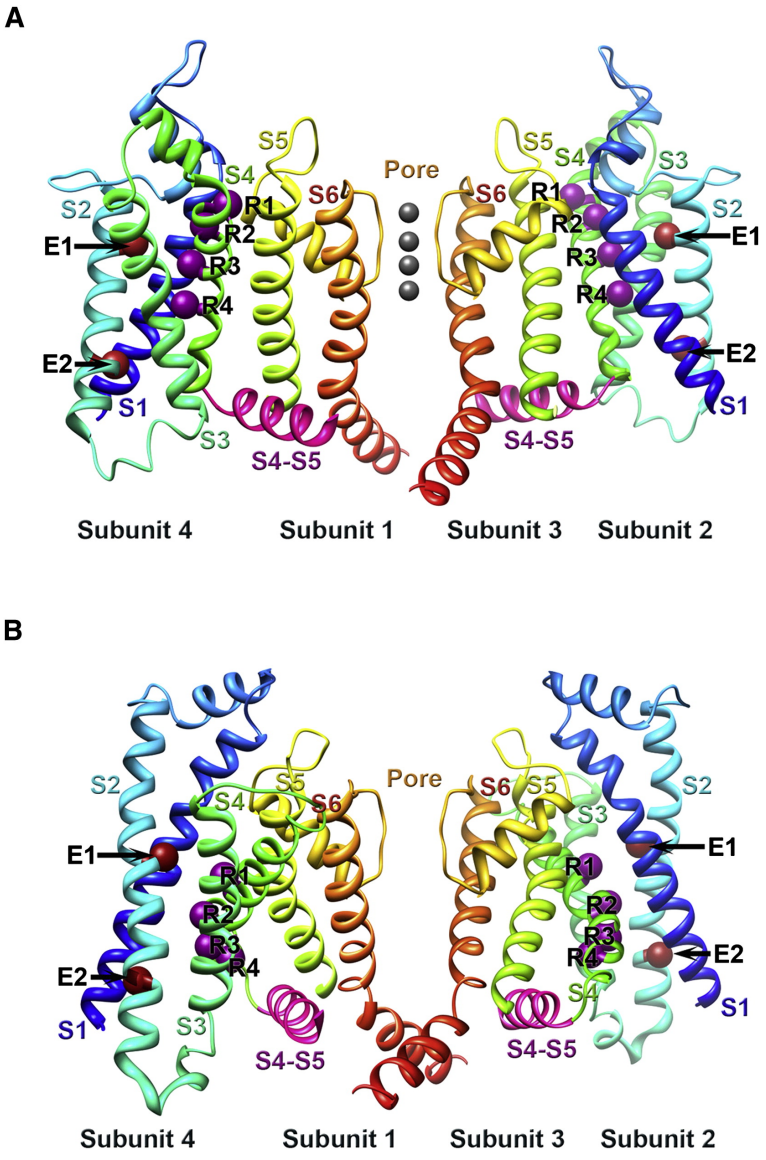

Figure 2.8: A) Structure of Kv1.2 in the open state as determined by X-ray crystallography [15]. Only two of the 4 monomers constituting the channel are shown. B) Resting state structure as predicted by the Rosetta software. From [16].

The second is still under debate but seems to involve a change of conformation in the pore [18].

2.1.2.6 Voltage gated channel diversity in cells

Cells have many different channel subtypes with diverse gating kinetics. Kv channels can form heteromers, and many channels can interact with additional subunits [19] and be further regulated by phosphorylation [20] and palmitoylation [21] for example. This

leads to an important variability of biophysical properties. Furthermore, channels with specific characteristics need to be in specific locations in the neuronal membrane in order to accomplish their specific function [22] (see chapter 5 for details of channel localization). All this complexity is important for setting the shape and speed of the action potential, but also for signal integration in a neuron [19].

Finally, membrane characteristics such as lipid composition, membrane tension and neuron geometry, are also crucial parameters that can affect channel activity and localization, and consequently information coding in the brain. These parameters are discussed in the next section.

2.2 Biophysics of membranes

2.2.1 Biological and model membranes

2.2.1.1 Cell membrane

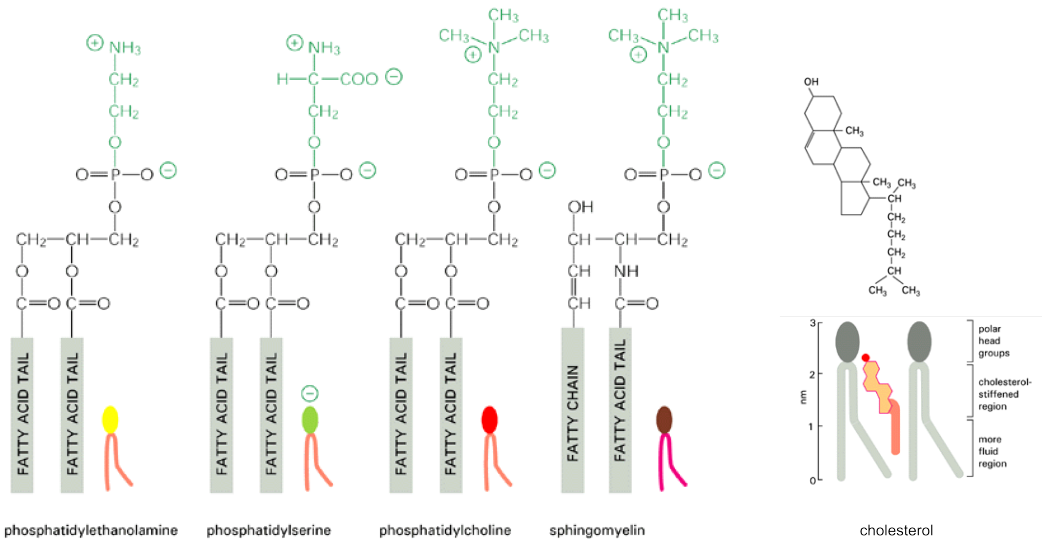

Figure 2.9: Some lipids present in cell membranes [23]. Note that they all have a hydrophilic head group and two hydrophobic tails (except for cholesterol).

The primary role of cell membranes is to isolate the internal content of the cell and its organelles from the external medium. These membranes are composed of a large variety of amphiphilic molecules that form a bilayer with a hydrophobic core. This includes many different lipids (a few examples are shown in figure 2.9), cholesterol and fatty acids, but also many membrane proteins (typically 50% in mass) [26]. The precise lipid composition depends on the organelle. For instance, the cholesterol and the sphingolipid concentration increases along the secretary pathway from the endoplasmic reticulum to the plasma membrane. In addition, the composition is asymmetric between the two leaflets of the bilayer.

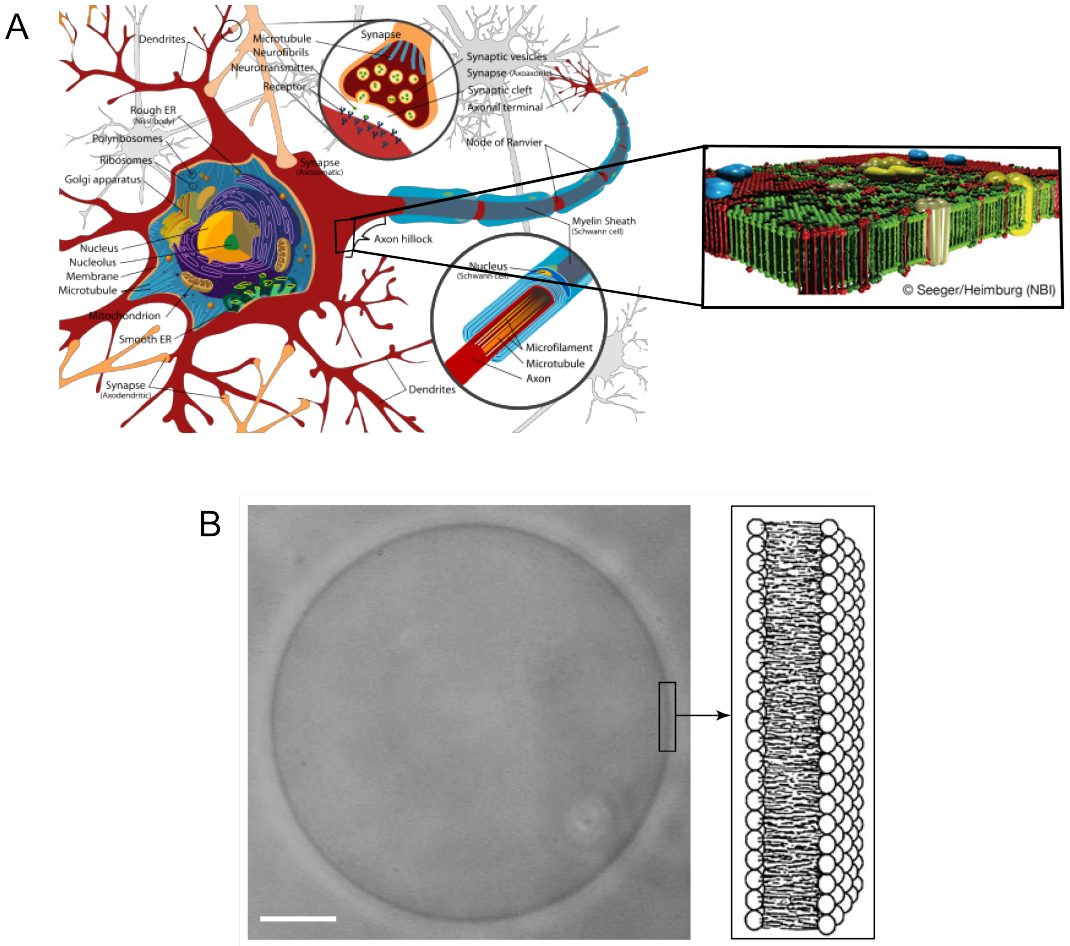

Figure 2.10: A) Sketch representing the complexity of a neuron and the cell membrane. From http://en.wikipedia.org/wiki/Neuron and [24]. B) Phase contrast image of a GUV and detail of the bilayer. Bar: 10 microns. From [25].

Cell membranes also exhibit lateral heterogeneities (see figure 2.10A, top right). Among them, lipid rafts are small dynamic membrane domains enriched in cholesterol and sphingomyelin (see section 2.2.2.5), which play an important role in protein signalling and trafficking [27].

Finally, membrane composition is dynamically adjusted by endocytosis and exocytosis, as well as by chemical transformations by enzyme proteins. Membrane tension and membrane shape are also controlled by the cell [28, 29]. Because of these active regulations, it difficult to externally control membrane parameters in order to study their effects on cell functions. It is thus useful to use model membrane systems in which relevant parameters can be scrutinised.

2.2.1.2 Model membranes

Several model systems can be used depending on the specific biophysical question [30] (see figure 2.11).

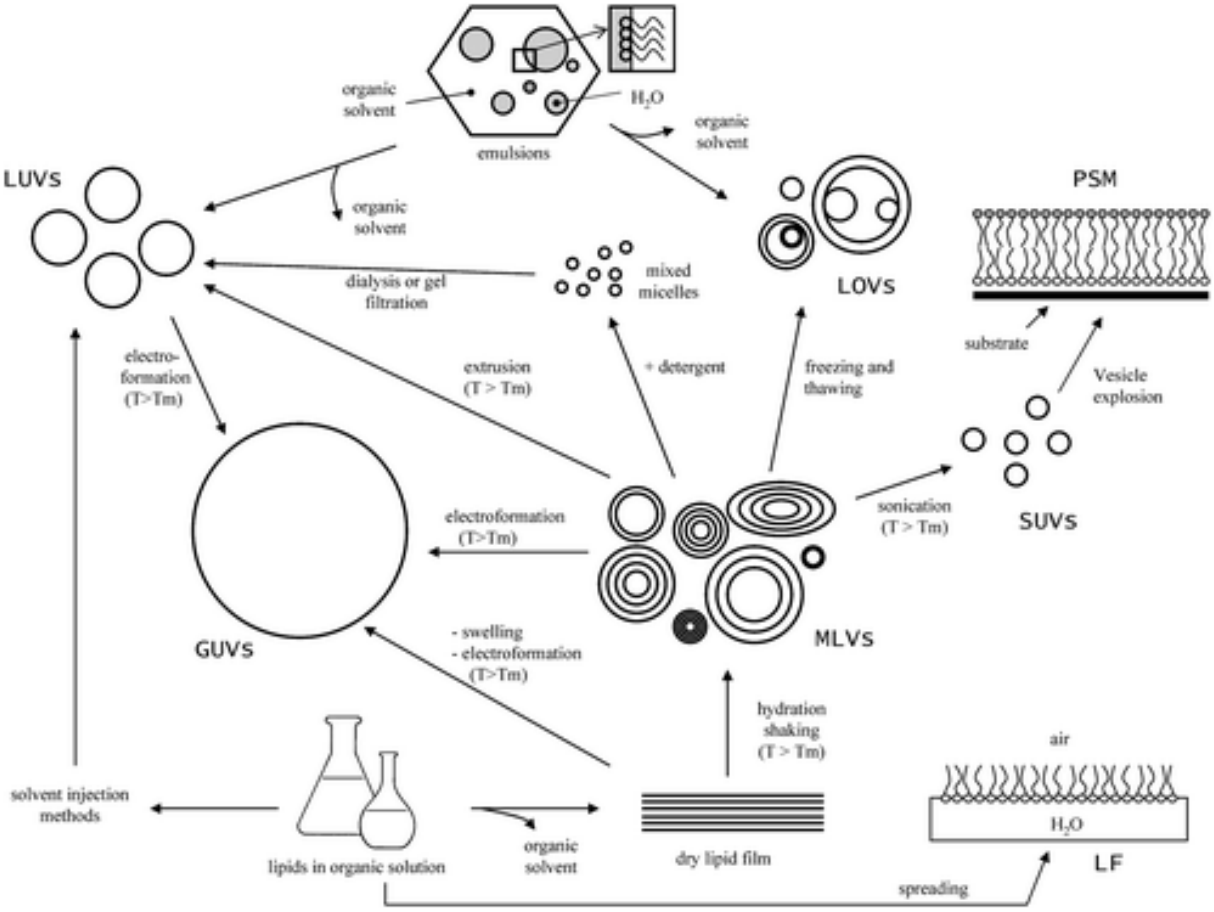

Figure 2.11: Different model systems to study membrane properties. From [31].

SUVs (Small Unilamellar Vesicles with a diameter below 100 nm) and LUVs (Large Unilamellar Vesicles ranging between 100 nm and 1 micron), nanodiscs, free standing bilayers, supported bilayers or monolayers, lipid monomolecular films at the air/water interface also called Langmuir films, are model membrane systems that have been extensively used to study some membrane properties. However, due to their size or geometry, these systems are in general not well suited to study the mechanical properties of membranes.

For this purpose, Giant Unilamellar Vesicles (GUVs) are better systems. They are vesicles made of a single lipid bilayer, with a size similar to cell size, typically ranging between a few microns up to 100 microns (see Figure 2.10B).

They have been extensively used as models to study membrane mechanics and electric properties, membrane phase separation, as well as budding and fission mechanisms to mimic endo/exocytosis for example.

First experiments on GUVs were done in the 80s' using GUVs composed of simple

lipids. Since then, many groups have worked with systems of increased complexity such as complex lipid composition or reconstituted membrane proteins in the GUVs membrane, or a cytoskeleton reconstituted inside the GUV. For details and references for GUVs preparation methods and applications see [30].

2.2.2 Physics of the membrane

The seminal theoretical work of Helfrich [32] and Canham [33] is the 70s' is widely used to describe the energy needed to deform lipid membranes. They originally considered the pure lipid membrane as a 2D liquid film. Thus, shear deformations could be ignored. In the following, we will describe the other elementary deformation modes of lipid membranes.

2.2.2.1 Microscopic model of membrane elasticity

Membrane elastic deformations are summarized in figure 2.12.

2.2.2.1.1 Curvature

The free energy per unit area required to bend a lipid membrane is given by the Helfrich hamiltonian [32]:

$$H_{curv} = \frac{1}{2}\kappa(c_1 + c_2 - c_0)^2 + \kappa_G c_1 c_2 \tag{2.3}$$

Where c_1 and c_2 are membrane principal curvature as introduced in figure 2.12A right [33].

c_0 is the membrane spontaneous curvature. It corresponds to the energetically peferred curvature. A non zero c_0 can be related to an asymmetry of composition between the two leaflets of the bilayer. This parameter will be discussed in detail in chapter 5.

κ is the bending rigidity modulus which represents the energy required to bend the membrane from its prefered curvature. It ranges between a few kT to 100 kT for typical membranes [34].

κ_G is the gaussian bending rigidity modulus. It is constant for an homogeneous membrane of constant topology (Gauss-Bonnet theorem). Furthermore, in all the membrane geometries considered in this thesis (tube and giant sphere), at least one of the curvature is close to zero so $c_1 c_2 = 0$. It will therefore be ignored in the remaining of the thesis. Note nevertheless that, as the protein is a tetramer with a cruciform shape, it would be interesting to study the effect of $(c_1 - c_2)^2$ which would be related to the torsion of the channel along one direction as compared to the other.

2.2.2.1.2 Stretch and thickness

As shown in figure 2.12B, microscopic membrane tension σ is the stress associated with a change of membrane area.

The energy $H_{stretch}$ per unit area needed to increase by ΔA the area A_0 of a microscopic piece of membrane is given by:

$$H_{stretch} = \frac{K}{2}(\frac{\Delta A}{A})^2 \tag{2.4}$$

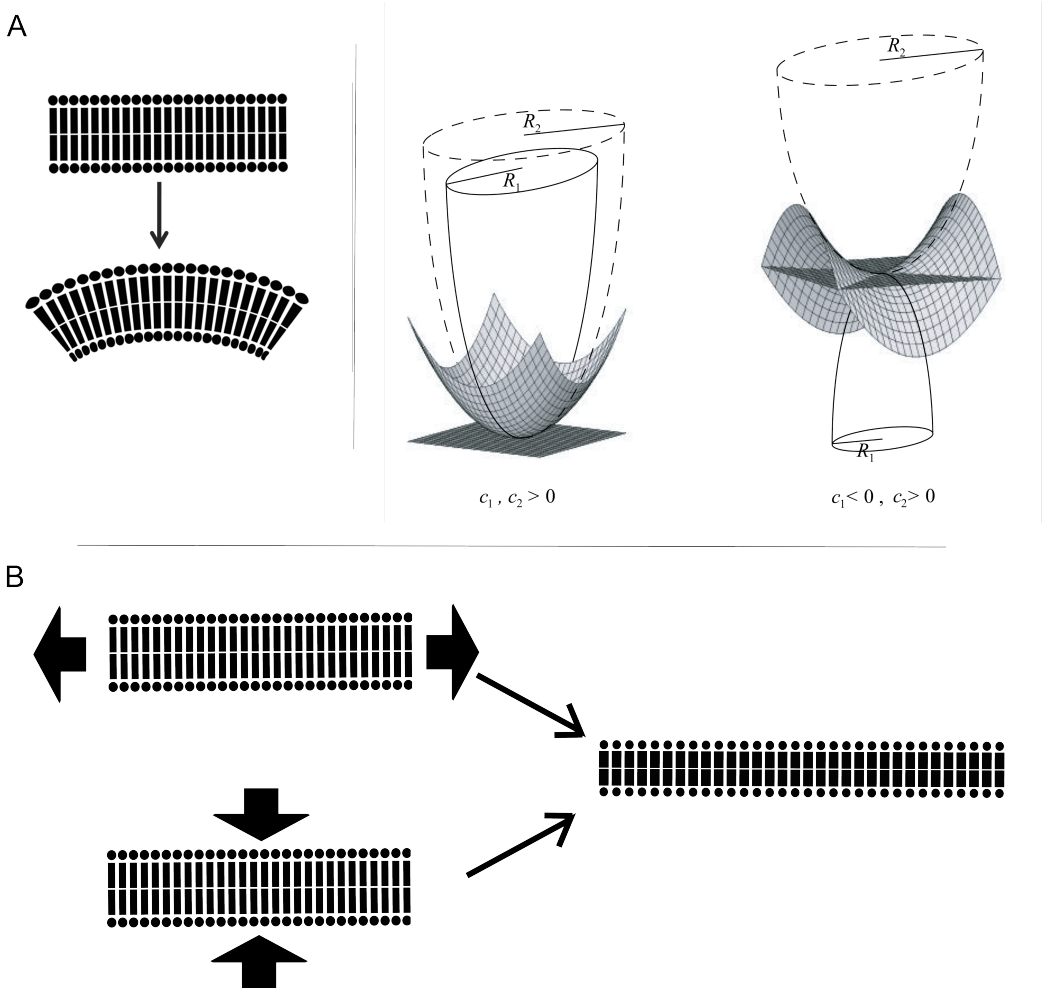

Figure 2.12: Microscopic membrane deformations. A) Membrane bending. Left, bending the membrane requires to stretch one leaflet and compress the other. Right) Local membrane bending is caracterized by the two principal curvatures (c_1 and c_2). From [33]. B) Membrane stretching. Note that increasing membrane microscopic tension leads to a decrease of thickness because the lipid tails are mostly incompressible, and an increase in the distance between lipid headgroups.

where K is the area-stretching modulus which is approximately 60 k_bT/nm^2 (or 250 mN/m) [35].

If we define membrane tension σ so that

$$H_{stretch} = \sigma(\frac{\Delta A}{A}) \tag{2.5}$$

we find using 2.4 that

$$\sigma = \frac{K}{2}(\frac{\Delta A}{A_0}) \tag{2.6}$$

As shown in figure 2.12B, since membrane is incompressible, a change in area is linked to a change in membrane thickness Δh [36]. The corresponding free energy per unit area is then:

$$H_h = \frac{K_t}{2}(\frac{\Delta h}{h})^2 \tag{2.7}$$

where, K_t is approximately the same as the area-stretching modulus K introduced in equation 2.4.

2.2.2.2 Fluctuations and macroscopic tension

Membrane tension is more complicated to define at the macroscopic level [37]. Indeed, unlike a simple elastic sheet, the microscopic membrane area and its optically detected area can be different. Because of brownian motion of the water molecules, lipid membranes are submitted to constant kicks and fluctuate around their equilibrium position. Membranes are thus crumpled at different scales as shown in figure 2.13A [38] . The macroscopic area (or projected area A_p) change thus comes from unfolding these small fluctuations. As it corresponds to a reduction of the number of conformations of the membrane, this regime is called "the entropic regime".

However when the tension is large enough (typically above 10^{-4} N/m), membrane fluctuations are small (membrane is mostly flat) and increasing the tension leads only to stretch the membrane at a molecular scale. This regime is called the enthalpic regime.

Increasing tension in the enthalpic regime is limited. A pure lipid membrane can only stretch by few percent before lysis. This corresponds to membrane tension of the order of $\sigma = 10^{-3} N/m$ [39].

2.2.2.3 Controlling membrane tension in GUVs

It is possible to impose a membrane tension in GUVs using the micropipette aspiration method which was initially developed by E. Evans [40]. This method is illustrated in figure 2.14.

Tension is then given by

$$\tau = \frac{P_{ext} - P_{pip}}{2(\frac{1}{R_{pip}} - \frac{1}{R_{ves}})} \tag{2.8}$$

Where τ is the experimentally imposed macroscopic tension, P_{ext} (P_{pip}) is the pressure outside (respectively inside) the pipette, R_{pip} (R_{ves}) is the radius of the pipette (respectively the vesicle). Note that $\tau - \sigma <$ when both are above approximately 10^{-5} N/m [37].

Micropipette aspiration can be used to control GUV membrane tension over a wide range ($\sim 10^{-7}$ N/m to $10-^{3}$ N/m) [**?**], which includes biologically relevant tensions (see figure 4.3 of chapter 4).

Note that with this type of experiment, it is also possible to measure the change in projected area A_p of the vesicle as a function of the imposed tension τ. Indeed the macroscopic area difference is then given by

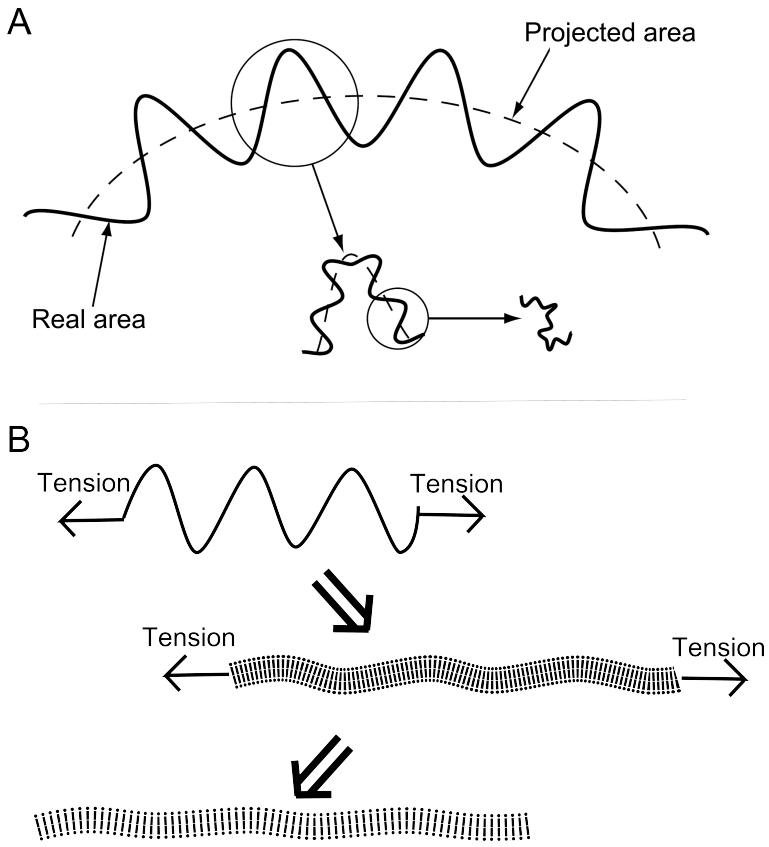

Figure 2.13: A) Illustration of membrane fluctuations at different scales [thesis P. Girard]. B) Tension in the entropic and in the enthalpic regimes.

$$\frac{\Delta A_p}{A_p} = \frac{k_b T}{8\pi\kappa} ln \frac{\tau}{\sigma_0} + \frac{\tau}{K} \tag{2.9}$$

It is thus possible to distinguish the different regimes (entropic -first term- and enthalpic -second term-)[**?**].

This method has been extensively used in particular by E. Evans to measure the compressiblity moduli, the bending rigidity and the lysis tension of many types of lipid membranes.

2.2.2.4 Controlling membrane curvature using GUVs

It is possible to produce a membrane of controlled curvature using GUVs, by extracting a cylindrical membrane tube ("tether") by locally exerting a force f on a vesicle as shown in figure 2.15A [41, 42].

The tube free energy F_{tube} depends upon the energy needed to bend the membrane (term containing the bending rigidity κ), that tends to increase the tube radius r_t and on the vesicle tension σ (supposed to be equal to τ) that tends to minimize its surface area [43], and thus to reduce the tube radius:

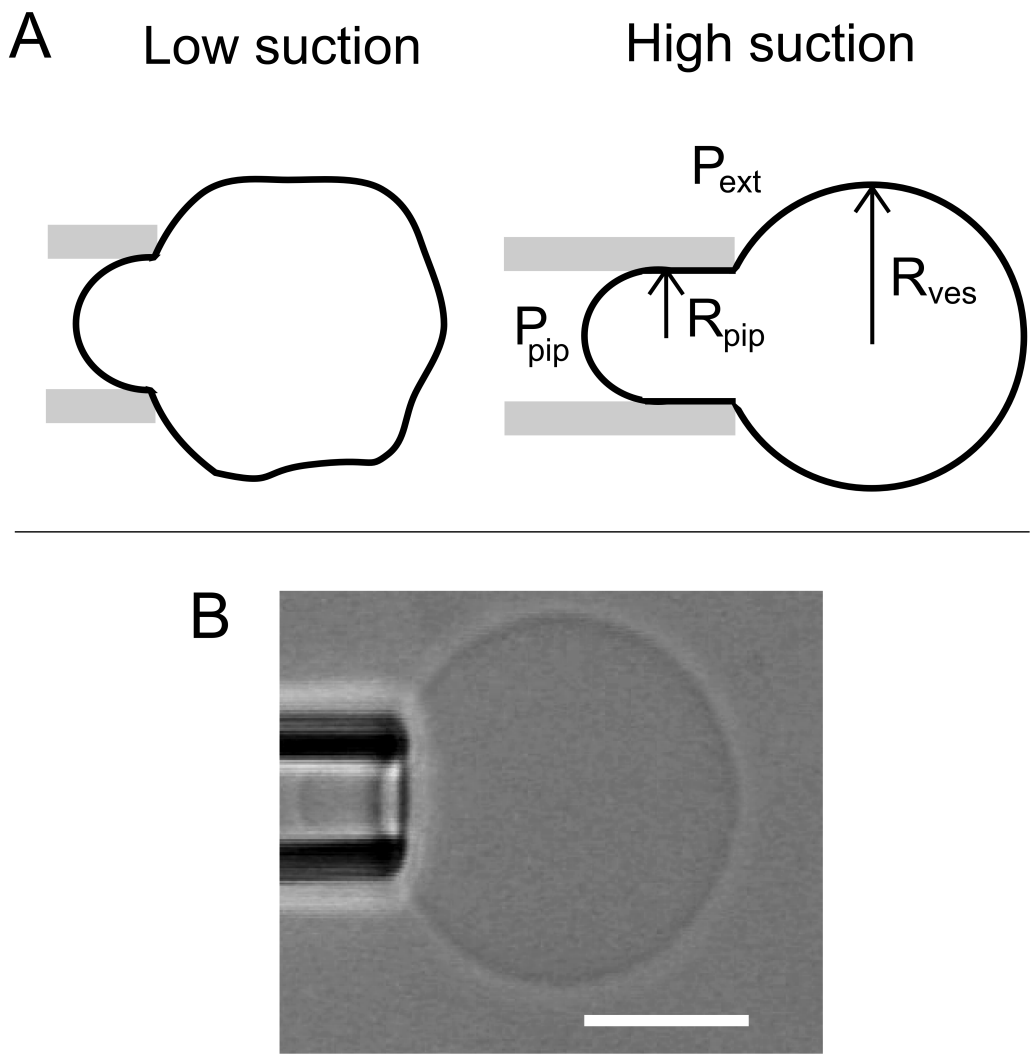

Figure 2.14: A) Scheme of a vesicle aspirated in a micropipette. Membrane fluctuations amplitude decreases while membrane tension increases upon aspiration. Parameters used for eq. 2.8 are also shown. B) Image of a vesicle aspirated in a micropipette. Scale bar is 10 microns.

$$F_{tube} = \frac{\pi\kappa l_t}{r_t} + 2\pi r_t l_t \sigma - f l_t \tag{2.10}$$

where l_t is the tube length, r_t is the tube radius and f is the force necessary to hold the tube.

Minimizing this free energy versus radius r_t provides the tube equilibrium radius r_0:

$$r_0 = \sqrt{\frac{\kappa}{2\sigma}} \tag{2.11}$$

The tube radius can hence be controlled by adjusting the tension using the micropipette aspiration presented in section 2.2.2.3 (see figure 2.15B).

Minimizing the free energy versus the tube length l_t provides the equilibrium force f_0 necessary to hold the tube:

$$f_0 = 2\pi\sqrt{2\kappa\sigma} \tag{2.12}$$

and thus the measure of the force can be used to determine κ. Note that even though the stress tensor in the vesicle is isotropic, it is not the case for the tube, where the stress in the direction parallel to the tube is 2σ, whereas it is nearly zero for the direction perpendicular to the tube [44].

Pulling tubes from a GUV aspirated in a micropipette allows one to control the tube radius over a biologically relevant range of membrane curvatures (R $\sim$ 10nm to 200nm) [45]. It has already been used in many in vitro studies and will be used for experiments presented in chapter 5 and 6.

2.2.2.5 Coexisting membrane phases

As any other physical systems, a membrane made of only one lipid type can exist in different phases depending on physical parameters such as temperature. At high temperature, the tails are disordered and membrane is in a fluid state (liquid disordered or Ld state). At low temperature, lipid tails are ordered and the membrane is like a gel (liquid crystal state also called "solid state" in the literature). The phase transition temperature T_m (also called the melting temperature) is characteristic of the lipid (and depends mostly on the tail length and the number of double bonds) and varies from -60°Cto 80°C. When cholesterol is added, the interaction between the head groups and the cholesterol molecules leads to another organization type, where the lipid tails are more ordered than in the Ld phase but the membrane is still fluid. In this phase (called the liquid ordered or Lo phase), membrane is thicker than the Ld phase (see figure 4.26A). When lipid mixtures are used, phase co-existence can be observed.

Motivated partly by the debate on rafts in cell biology (see section 2.2.1.1), an important work has been made in the past years on the physics of multi-component membranes. Phase diagrams of various lipid mixtures have been studied [31] and the shape of GUVs containing domains analyzed both experimentally and theoretically (see for example [47]). As shown in figure 4.26B left, a GUV made of a mixture of phosphatidilcholine, sphingomyelin and cholesterol exhibits domains for some particular compositions, corresponding to a Ld/Lo phase co-existence. It is also possible to obtain similar domains with GUVs prepared from native membranes (figure 4.26B right). This suggests that in the absence of active processes and of the underlying cytoskeleton, cell membranes have composition close to phase separation [27].

2.2.3 Models describing coupling between trans-membrane proteins and membrane physical parameters

Cell membranes contain a large amount of membrane proteins. It has thus been important to understand the effect of proteins, that are in general large and rigid inclusions, on

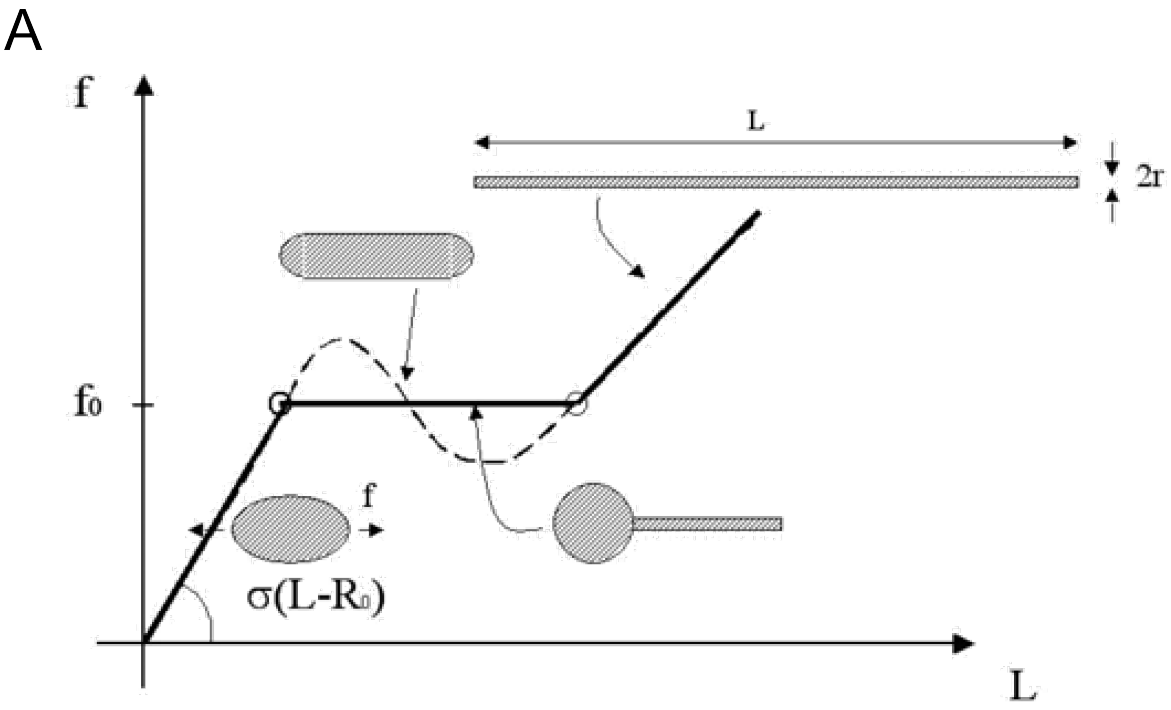

Figure 2.15: A) Pulling on a point of the vesicle deforms a spherical GUV into an ellipsoid at low forces but at high forces, the configuration with a spherical vesicle connected to a thin tube is more stable. From [42]. B) Tube extrusion technique used in chapter 5 and 6 of this thesis. The vesicle is aspirated in a micropipette which sets membrane tension. A bead is attached to the GUV and trapped in optical tweezers for example. When moving the GUV away from the bead, a membrane tube is formed. The force necessary to hold the tube can be measured with the displacement in the optical tweezers The bending rigidity can be deduced from this force. Tube radius can be obtained from these two quantities according to 2.11. From [46].

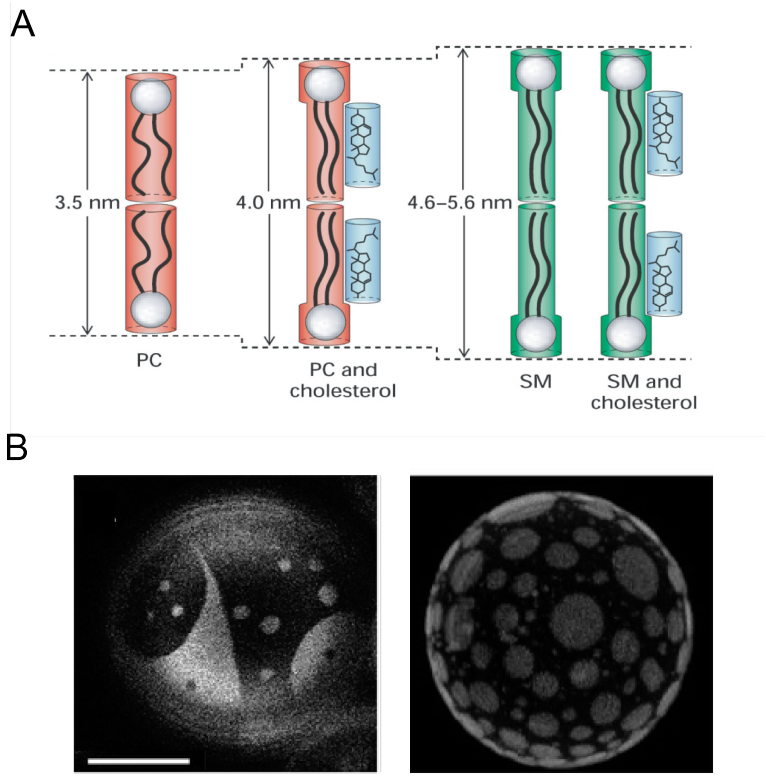

Figure 2.16: A) Effect of cholesterol on lipid tail organization and membrane height [48]. B) Liquid ordered/Liquid disordered phase coexistence in GUVs. Left) sphingomyelin/DOPC/cholesterol 1/1/1 mol and Right) native porcine pulmonary surfactant. bar: 15 μm. From [31].

membranes physical properties.

In this part, I will discuss how membrane proteins pertubate lipid membranes.

2.2.3.1 Mesoscopic modelling

As a first step to describe the effect of conformational changes or the presence/absence of transmembrane proteins, one can use the membrane elasticity model described above in section 2.2.2 and add boundary conditions imposed by the protein. This approach supposes that membrane is enslaved to protein conformation which is reasonable as proteins are much more rigid than lipids and as some specific sites in proteins can bind to lipids [49].

The protein can deform the membrane using three major deformation modes (see figure 2.17) related to the elasticity model described above [50].

- Midplane bending

  The protein can impose a tilt to the membrane midplane and produce a local membrane curvature.

  Note that the energy of membrane deformation imposed by the protein will thus be lower if the membrane is already curved. In a seminal work, Stanislas Leibler

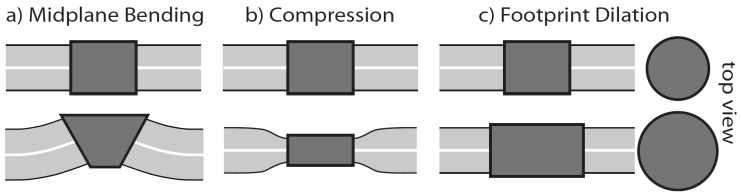

Figure 2.17: Three classes of membrane deformation induced by a membrane protein. From [36].

showed that this effect can lead to a redistribution of the protein in membranes with curvature gradients [51]. This problem will be reviewed in more detail in chapter 5.

For a membrane that is flat far from the protein, the characteristic length after which the deformation has relaxed is given by [50] :

$$\lambda_{bending} = \sqrt{\frac{\kappa}{\sigma}} \approx 5 - 500nm \tag{2.13}$$

Where κ is the membrane bending rigidity and σ is the membrane tension.

- Compression deformation

  This mode is caused by a hydrophobic mismatch between the protein and the preferential membrane thickness.

  This also produces a membrane deformation over a typical length $\lambda_{compress}$ given by [50]:

$$\lambda_{compress} = \sqrt[4]{\frac{\kappa h_0^2}{K}} \approx 1nm \tag{2.14}$$

  where κ is the membrane rigidity, h_0 is membrane thickness and K is the area-stretching modulus.

- Footprint dilation
  This deformation mode corresponds to the change in cross sectional area of the protein, so a global change for membrane area.

Calculation of orders of magnitudes of the membrane deformation energies associated with those conformational changes for realistic parameter values show that they all could be above kT [50]. Proteins could hence have a significant effect on membrane mechanics while membrane mechanical proterties could have an effect on the protein conformational change.

2.2.3.2 Microscopic approaches for modelling trans-membrane protein/membrane interactions

Several levels of complexity can be added in order to mimic molecular interactions.

One can first consider the attractive interactions at the level of the lipid heads and the repulsion at the tails. This has been included in the "lateral pressure profile" approach that models the attraction or repulsion by a "pressure" along a membrane section [52].

The elasticity model as well as the pressure profile model have successfully described the effect of membrane tension, composition and curvature on the gating of mechanosensitive channels [53] , which are ion channels that open in the presence of a high membrane tension.

One limitation of these approaches is that they do not take into account the fact that boundaries between the membrane and a protein are usually not neat and that lipids and proteins can be entangled. Studying these effects is possible using numerical simulations and molecular dynamics [54]. Nevertheless, even with these methods, coarse grained approaches are necessary due to the high number of atoms.

All those studies show that membrane mechanical properties should play an important role in membrane protein conformational changes.

However, even when including fine details of the lipid and protein structures, these models usually include only one or few types of lipids. In reality, cell membranes are composed of many coumpounds with different biophysical properties (for example fatty acids and phospholipids that have very different head and tail sizes). Thus, any energetic frustration in the membrane due to membrane protein as described above can be partially relieved by adjusting the local composition. However, this reorganization will be balanced by entropic and kinetic effects. Indeed, entropy tends to disfavor local heterogeneities and redistribute different components. For example, as will be presented in chapter 5, membrane curvature is usually not sufficient to lead to reorganisation of lipids in the membrane because mixing entropy is too high. In addition, if the protein undergoes conformational changes faster than membrane species diffuse, this reorganization will not have time to occur.

2.2.3.3 Membrane-mediated protein/protein interactions

The deformations imposed by proteins to the membrane can lead to membrane-mediated protein/protein interactions as shown in figure 2.20. For example, two proteins changing membrane thickness could be effectively attracted to each other in order to minimize the total deformation of the membrane (figure 2.20, top left). By way of contrast, two different protein types producing opposite effect on membrane thickness can repeal (figure 2.20, bottom left). This is also true for similar conical inclusions with identical insertion directions (figure 2.20, bottom right).

Combining the two kinds of deformations, proteins can also form a 2D crystal as described by [56]. That could occur for example if a protein imposes the same tilt on lipids in both leaflets of the membrane (which would induce repulsion) while affecting membrane thickness (which would lead to attraction).

Another mechanism leading to protein/protein interaction is the Casimir effect where the boundary conditions imposed by the protein restrict membrane fluctuations and thus decreases entropy. Proteins will thus form clusters to keep the number of possible membrane configurations as high as possible [55].

Note that these protein/protein interactions must take place in cells as the typical

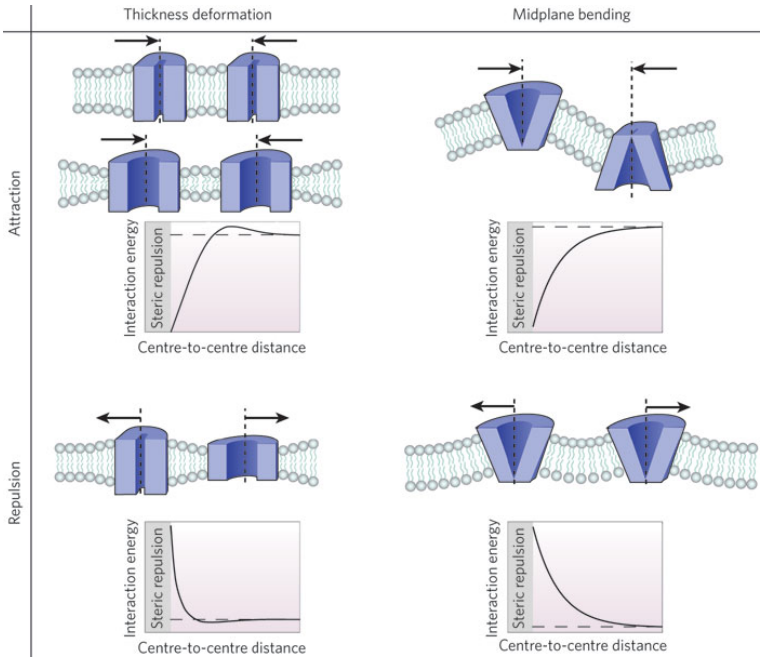

Figure 2.18: Protein-protein interactions induced by membrane deformations. From [55].

distance between protein is of the order 10 nm [55] (which is the same order of magnitude as the decay length of membrane deformations imposed by proteins seen in section 2.2.3.1).

Although a large amount of theoretical work has been made on the presence of inclusions in lipid membranes, the experimental work is still extremely limited, probably due to the difficulty to reconstitute membrane proteins and to further perform mechanical measurements.

2.2.3.4 Active membranes

An important and non-trivial contribution of membrane proteins to mechanical properties of membrane is to consider the effect of non-equilibrium activity of proteins. Indeed, proteins can change conformation using some energy source (ATP hydrolysis, electric potential, light or mechanical stretch for instance). For a review, see [57].

To go further in the description of the effect of membrane proteins on membrane mechanical properties, one can consider membranes containing proteins constantly and randomly changing conformation, thanks to a energy source (that can be ATP, an electric field or a ion gradient accross the membrane for example).

Prost and Bruinsma in 1996 have developed a pioneer model of these "active membranes" [58]. They first considered the effect of ion channels and calculated the consequences of their activity on the membrane fluctuation spectrum. They have used the elasticity theory described above to account for the effect of the channels, and added a force due to the ions crossing the membrane. The value and the application point of this force was stochastic (shot noise); nevertheless, the effect of this force was not a white noise but was spatially correlated due to protein diffusion in the membrane. As this random

force acted in addition to termal kicks from the solvent molecules on the membrane, it is expected in a first approximation that the properties of the membrane should follow the same power laws as a membrane without the proteins, but that the effective temperature should be higher. Prost and Bruinsma have shown that the effect can be more subtle and interestingly, that the fluctuation spectrum of the membrane should be changed.

Other theoretical models were later developed to take into account the coupling between protein curvature and activity [59, 60]. They included the effect of protein shape and insertion direction in the initial model. The protein changes the midplane bending when changing its conformation as in figure 2.17a. The same kind of model based on the elastic theory led to an effective decrease of membrane rigidity. These models even predicted that a strong coupling between protein activity and curvature can lead to shape instabillities. They also predicted the existence of travelling waves in the membrane .

More elaborated models were derived to describe the effect of ion pumps on membranes. The ion flux through pumps is 3 orders of magnitude lower than for ion channels, but they have very large conformational changes during ion transfer [61]. Their contribution was modeled by adding a higher term in the model, a dipolar force, which turned to be dominant for this protein type [60, 62, 63, 64, 65]. They also predicted complex changes in the fluctuation spectrum and in a first approximation, a higher effective temperature of the membrane. In addition, changes of the effective membrane tension and of the bending rigidity were predicted [65, 66]. So far, these models have been tested with 2 types of ion pumps. A strong increase of the effective membrane temperature has been measured for the bacteriorhodopsin [60] and the Ca^{2+}+ATPase[67]. In addition, from the measurement of the flickering of GUV containing Bacteriorhodopsin, El Alaoui et al [68] have shown that bacteriorhodopsin pumping can reduce the effective membrane tension. These models have recently been used to reanalize the fluctuations of red blood cells [69]. Nevertheless, experimental data on active membranes are still scarse, and nothing has been done so far on membranes containing ion channels.

2.3 Role of membranes in cell excitability

After having described general results on the coupling between membrane mechnics and trans-membrane proteins, we will discuss more specifically the interactions between membranes and voltage gated-ion channels.

2.3.1 Influence of membrane on voltage-gated channel function and localization

As shown in structure of Kv1.2 in membranes (figure 2.19), the voltage sensor is surrounded by lipids. It would thus not be surprising that membrane composition, tension and geometry affect voltage gated channel activity. I will prese,t some evidences of these effects in the following section.

2.3.1.1 Effect of specific lipids

First, specific lipids have been shown to affect voltage gated channel function.

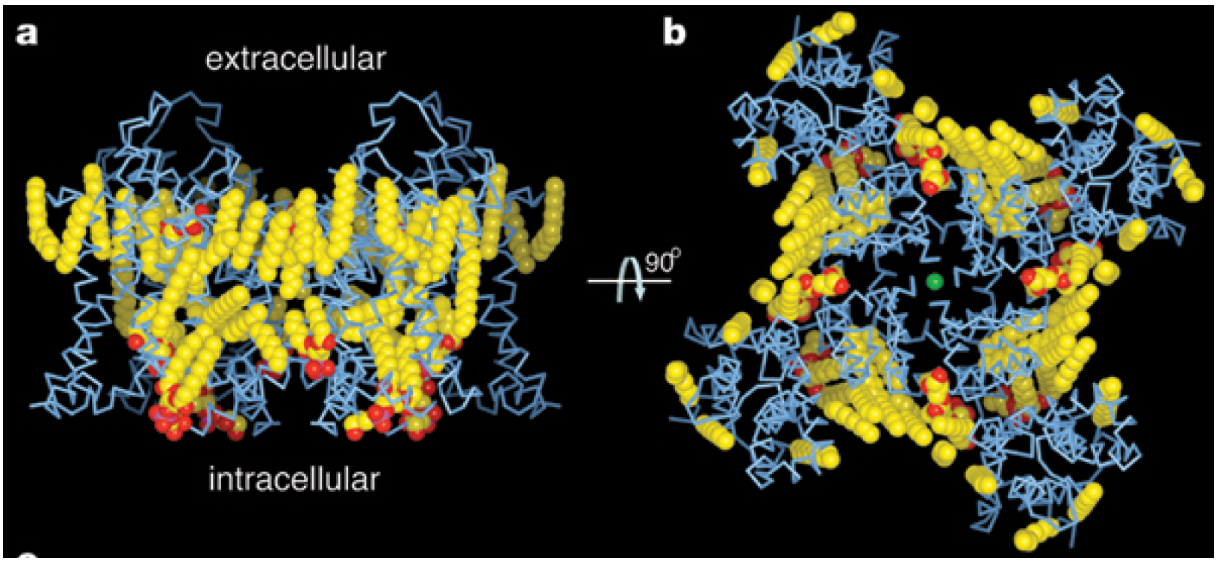

Figure 2.19: Kv1.2 structure embedded in lipids. a) side view, b) top view. From [1].

A very strong effect was shown in [70], that demonstrated that the specific interaction between KvAP and the phosphodiester group in phospholipids is necessary for voltage gating. Indeed, when reconstituted in DOTAP (a lipid containing no phosphodiester group) KvAP was not showing any activity while the function was recovered when some phospholipids (containing the phosphodiester group) were added to the membrane.

Furthermore, it has been shown in native membranes that Kv2.1 channels were activated in membranes in which sphingomyelin was converted to ceramide-1-phosphate [71], which suggests that the negative group of the ceramide-1-phosphate stabilizes the channel. On the other hand, removing also the phosphate group from the sphygomyelin stabilized the closed state [72]. Furthermore, phosphatidylinositol-4,5-bisphosphate (PIP2), was reported to activate Kv7 channels [73].

These studies indicate that interactions between the channels and the phosphate groups of lipids are important for their function. Indeed, the phosphate groups could be implied in the stabilization of the voltage sensor conformation as shown in figure 2.20. The interaction details are still a matter of active research [74, 75].

2.3.1.2 Effect of membrane elasticity on channel activity and distribution

In addition to specific protein-lipid interactions, the physical properties of the membrane (tension, thickness, curvature, etc.) may influence channel function with the same mechanisms as those described in section 2.2.3[36].

For example, Lundbaek et al.[77] review the effect of amphiphilic molecules on channel function. They show that these molecules do not affect channel function in a specific way but rather by changing the bilayer stiffness. Another study confirmed this view showing that alkanols in BLMs affect single KvAP conductance with a gradual effect of concentration, suggesting that these compounds act on membrane global mechanical properties more than on specific sites that would block the pore or the voltage sensor [78].

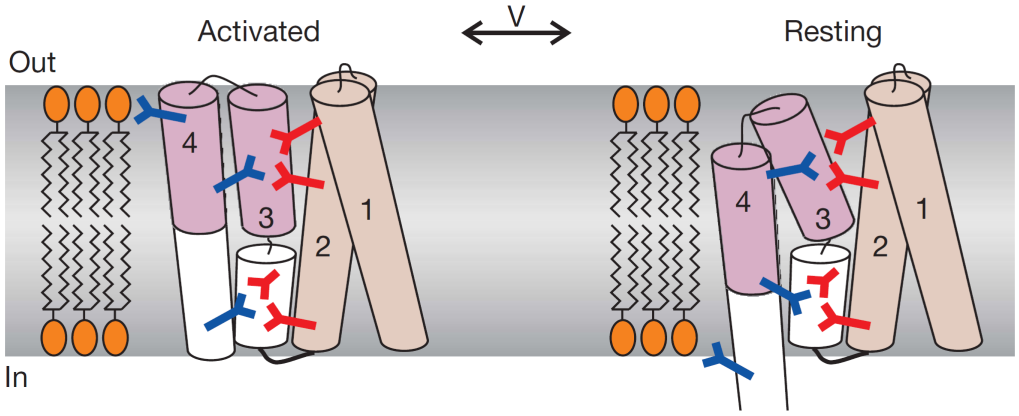

Figure 2.20: Voltage sensor stabilization by interactions with lipid headgroups and . Blue residues are positively charged arginines, acidic residues are in red and lipid head groups are in orange. From [76].

Similarly, it has been suggested that membrane tension is responsible for the functional difference of the same voltage gated potassium channels recorded using different electrophysiology techniques (BLM, patch clamp and whole cell) see figure 2.21 [79].

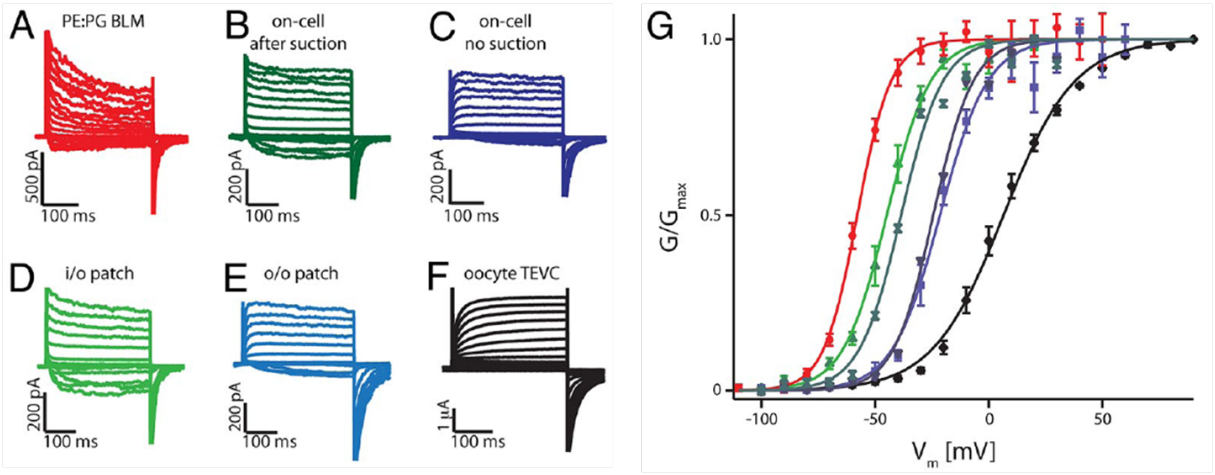

Figure 2.21: Effect of membrane environment on KvCh activity. The activity of the same channel (the Kv1.2/Kv2.1 chimera) was recorded with different experimental systems with different membrane tension. From [79].

Some groups have also studied the direct effect of membrane tension on voltage-gated ion channel function.

For example, in [80], the mechanosensitivity of NavCh overexpressed in oocytes was measured by cell-attached patch clamp upon changing the pressure in the patch pipette. The authors showed that activation and inactivation are accelarated by stretching. This

type of effect has been also demonstrated for Kv channels [81, 82] and Cav channels [83].

The specific interactions of the channel with lipid headgroups as described in previous section could lead to a local deformation of the membrane as described in section 2.2.3.1. Indeed, even though neutron diffraction experiments and molecular dynamics simulations have shown that voltage sensor only causes a thinning of 3 Angstroms [84, 85], other simulations (with the full Kv1.2 chimera for example[86]) show a more significant thinning of the membrane. Note that the importance of membrane deformation should depend on the preferential membrane thickness which would depend on the local membrane composition in cells.

Because of these membrane deformations, collective effects could occur by membrane mediated protein/protein interactions through the membrane. For example, if a channel changes membrane thickness when it opens, this would increase the gating probability of other channels next to it [50, 87, 88].

Note that as described in section 2.2.3.4 conformational changes of channels could also have an effect on membrane mechanics, changing effective temperature, bending modulus or even membrane tension.

2.3.1.3 Influence of the membrane on voltage-gated channel localization

Proper localization of voltage gated channels in neuronal membranes is crucial for functional communication in neuronal networks (see section 2.1.2.6).

Targetting of these channels to the proper location can be mediated by intracellular trafficking, but physical mechanisms such as heterogeneities in membrane composition, mechanical properties and shape could also contribute. For example, biochemical and functional data [89] have been used to infer the localization of several Kv channel types in "lipid rafts" described in section 2.2.1.1. Furthermore, many voltage gated channels have been shown to form clusters in cell membranes [90]. This could be explained by interactions with the cytoskeleton and other proteins but also by membrane-mediated interactions [87].

Effect of membrane curvature on channel distribution will be discussed in detail in chapter 5.

2.3.2 Role of membrane shape in action potential propagation

The membrane geometry of neurons can have an effect on signal integration (by changing the geometry of the dendritic tree) [91], but also on action potential propagation in the axon [92].

First, axon diameter affects the velocity of the action potential. Indeed, for non myelinated axons, the velocity increases as the square root of the diameter [93].

Changes of membrane geometry are also important as the presence of varicosities at the level of synaptic boutons can lead to changes in action potential speed and amplitude and branch points in the axon can create delays and and even failure in the action potential that are important for information coding and learning [92].

Finally, as presented in section 2.2.3.4, conformational changes due to changes of membrane potential could also produce a propagative membrane deformation upon action potential propagation.

2.4 Model system proposed to study the role of the membrane in cellular excitability

Studying the effects of membrane physico-chemical properties on channel function and localization in vivo is challenging as the composition and physical state of the membrane are highly regulated by the cell itself. Consequently, an important piece of work has been performed to isolate membrane proteins and reconstitute them in membranes of controlled composition as described in section 4.1.1 of chapter 4. For electrophysiological studies of ion channel activity, several in vitro systems have been developed including black lipid membranes (BLMs) and patch-clamp on multilamellar vesicles. However, as we will see in detail in chapter 4 each technique has distinct limitations concerning the control of membrane tension, shape or composition.

2.4.1 GUVs for voltage gated channel biophysics

Giant Unilamellar Vesicles (GUVs) are a promising alternative in vitro system. As described above 2.2.1.2 and in chapter 4, these cell-sized unilamellar liposomes can be prepared from a wide range of lipid compositions (see chapter 4) while both membrane tension and curvature can be controlled (as described in section 2.2.2).

The protein distribution between the GUV and the membrane nanotube can be monitored with fluorescence confocal microscopy, while channel activity can be measured with electrophysiology techniques as will be presented in detail in chapter 4.

Thus, GUVs offer the possibility to study channel activity and distribution while controlling membrane composition, tension and curvature at once in order to check predictions from the elasticity theory and more elaborate models.

2.4.2 Model action potential

My PhD work is part of a larger project aiming at creating a minimal axon where the parameters underlying action potential propagation can be controlled and investigated.

2.4.2.1 Previous experimental models of action potential

A few attempts have already been made to create experimental models of electical propagations of signals on membranes.

For example, P. Fromherz's group has studied the propagation of electrical signals along a planar membrane suspended over a groove [94]. They were able to check the validity of the cable equation in this system. They also incorporated an ion channel, gramicidin (which is not voltage gated) to study the effect of heterogeneous changes of membrane conductance on signal propagation.

Another similar approach was to coat nanowires with lipid bilayers [95]. Here also, some simple peptide pores (gramicidin and alameticin) could be incorporated in the membrane.

Finally, one last approach was developped in the group of Owe Orwar in Sweden. They created a network of vesicles separated by tubes and showed that they could apply electric fields inside the tube that could make charged species move [96].

All these strategies are very promising but they all lack an essential component of an active signal propagation which is the presence of voltage gated ion channels. It is thus necessary to develop a method for a proper reconstitution of these channels in membranes that could then be used in all those devices.

2.4.2.2 Our model system for action potential propagation

As we have seen in section 2.2.2, membrane tension and geometry can a priori be controlled in GUVs. It sounds thus appealing to use a tube extracted from a GUV containing reconstituted ion channels as a model for neuronal axon and soma as shown in figure 7.3. Electrophysiology would then be used to set electrical potential and measure "action potential" propagation.

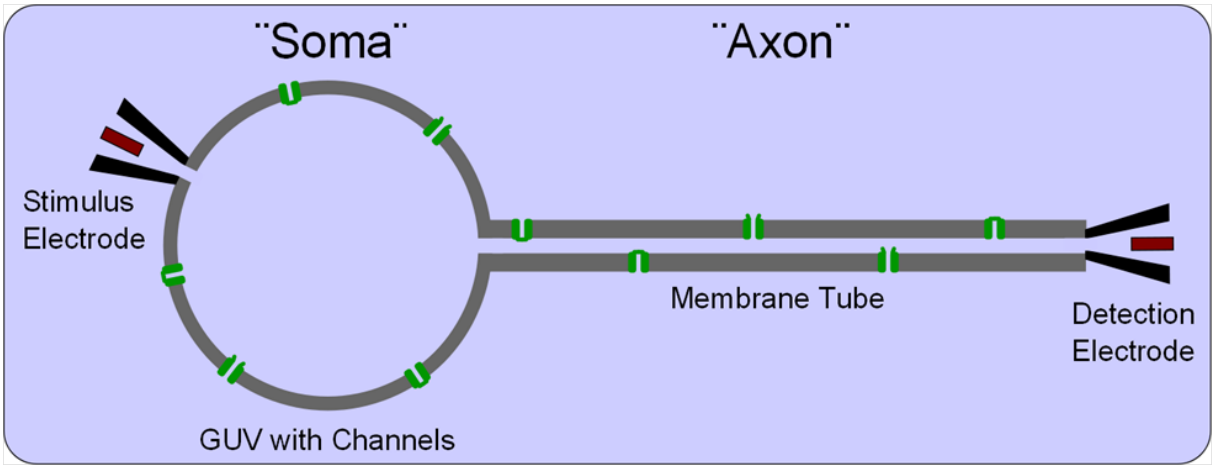

Figure 2.22: The model system developed in our prject to investigate action potential propagation.

In such a system, it is a priori possible to control

- Lipid composition and channel density: using the appropriate reconsitution technique (see chapter 4)
- Membrane tension and "axon" radius: using the micropipette aspiration technique (see section 2.2.2)
- Temperature
- Membrane electical potential

Chapter 3

KvAP biochemistry

3.1 Introducing KvAP

KvAP was discovered in an hyperthermophilic archaebacterium [97]. We chose to use it as a model voltage gated channel because, as a bacterial channel, it is easy to express and purify and it has high homology and strong functional and structural similarities to eukaryotic Kv channels. Furthermore, its structure is known, allowing better understanding of interactions between the channel and the membrane.

3.1.1 Sequence and structure

As shown in figure 3.1, the KvAP sequence has high homologies with other voltage gated potassium channels (including mammalian channels). A KvAP monomer consists of six transmembrane segments (noted S). Furthermore, some amino acids are highly conserved in those segments. In particular, the pore region (P in the figure), contains the characteristic TVGYG sequence corresponding to the transit zone for potassium ions. The four arginines (positive amino acids) in S4 (in red) that are a signature of the channel voltage sensor are also present in KvAP.

The tertiary structure, shown in figure 3.2, is also very close to the structure of eukaryotic Kv channels (see the structure of Kv2.1 in the chapter 2). Indeed, like the other members of the Kv family, the channel consists of a central pore surrounded by four voltage sensors, with each monomer contributing with 2 helices (S5, S6) to the central pore, while the remaining 4 helices (S1-S4) form a voltage-sensing domain [10].

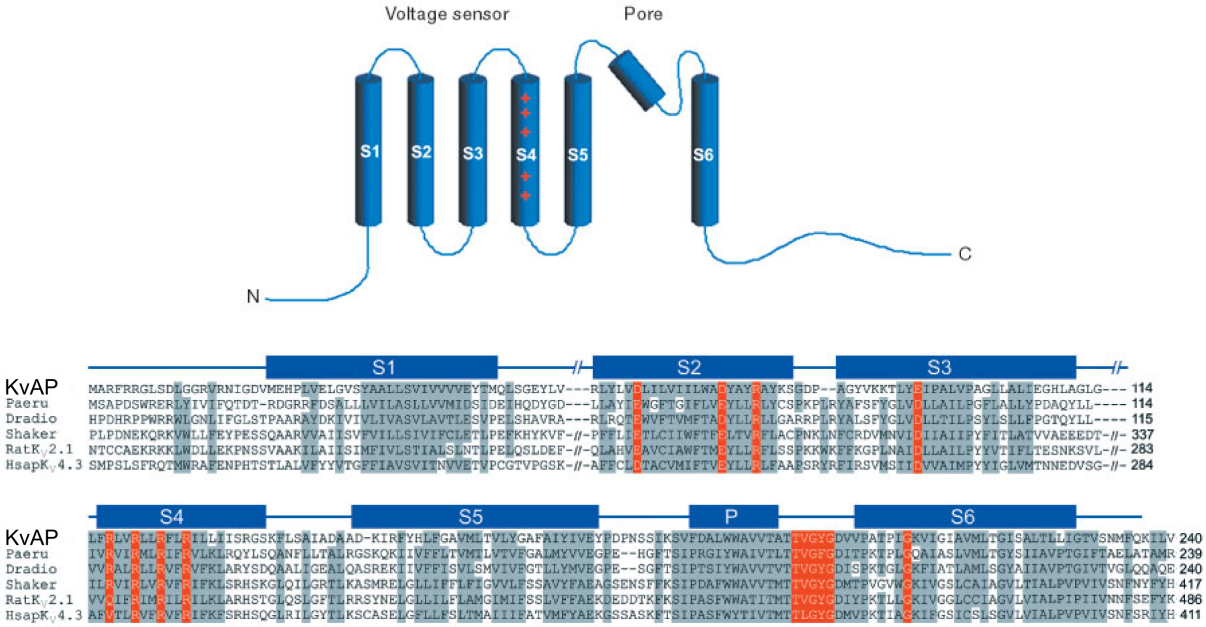

Figure 3.1: Sequence of Kv channels from different species. S1 to 6 are transmembrane spanning segments. Sequence regions of high homology are colored in grey and functionally important residues are colored in red. The K+ channels are: KvAP from *Aeropyrum pernix* (GI: 5104624); Paeru, *Pseudomonas aeruginosa* (GI: 15596693); Dradio, *Deinococcus radiodurans* (GI: 15805856); Shaker, *Drosophila melanogaster* (GI: 13432103); RatKV2.1, *Rattus norvegicus* (GI: 24418849); HsapKV4.3, *Homo sapiens* (GI: 5059060). Figure adapted from [97].

3.1.2 Functional characterization

The KvAP channel function also exhibits similar characteristics to the eukaryotic voltage gated channels presented in chapter 2. Ruta et al.[97] have studied KvAP activity using black lipid membranes, a technique described later in this chapter. Briefly, the channel is incorporated in a suspended membrane, and the current going through the membrane is recorded as a function of the applied voltage.

These measurements have shown that KvAP is highly selective for potassium as expected considering that the sequence and structure of the pore are very close to other Kv channels. Similarly to eukaryotic channel, KvAP is also voltage gated and inactivates (as will be discussed in details in section 3.5).

Finally, KvAP pore is blocked by charybdotoxin, a toxin from a scorpion venom that specifically block potassium channels at the entrance of the pore.

3.2 Purification procedure

I will present here the principles of the purification procedure. A detailed protocol is given in the annex A.

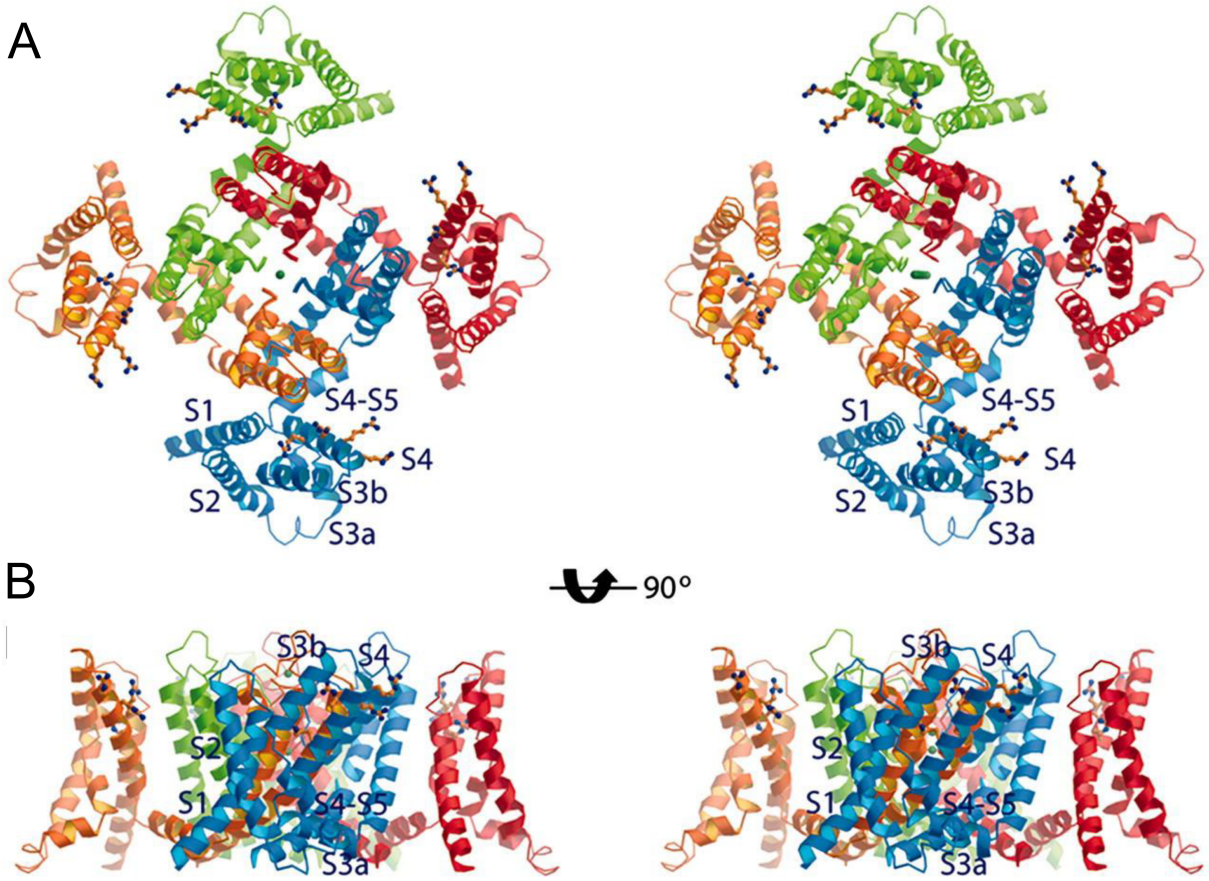

Figure 3.2: Stereo view of of a model of KvAP structure in the open conformation. The channel is shown in the top-down view A) and in the side view B). Each subunit is colored blue, green, gold, and red. Figure from [10]. S5 and S6 (not noted on the figure) form the central pore region.

Protein purification and reconstitution in Small Unilamellar Vesicles (SUVs) were performed following a procedure that was developed in the group of Rod MacKinnon at Rockefeller University [97]. I collaborated with Daniel Schmidt from this group to learn the method.

First, note that the plasmid I used contains the gene for wild-type KvAP, thus with the endogenous cysteine C247. It also carries a HIS tag coding sequence, thus allowing the protein to bind to a nickel column (see below). The plasmid was incorporated in XL1-Blue cells (an *E coli* strain). Bacteria were grown at 37 ℃and protein expression was induced with IPTG, that triggers the transcription of the lac promoter, upstream of the KvAP gene. 10mM $BaCl_2$ was added to block K^+ permeation. Bacteria were then mixed with 40 mM DM (DecylMaltopyranoside, a non ionic detergent) for 3h to solubilize cell membranes. Un-dissolved material was removed via ultra-centrifugation.

All the following steps were done in 5 mM DM. Note that Alice Berthaud in our laboratory has shown that it is possible to use DDM (Dodecyl Maltopyranoside) instead

of DM. The first purification step was to bind the protein to a nickel column via its His-tag (polyhistidine-tag affinity chromatography). We then washed the column to remove any unspecifically bound molecules before eluting the protein with imidazole, a molecule that has stronger affinity for nickel than the protein His-tag, and thus detaches it from the column.

The His-tag was cleaved from the protein by incubation overnight with thrombin.

Before the last purification step, 1mM TCEP (tris(2-carboxyethyl)phosphine) was added to reduce cysteines for 1h.

To remove any leftover impurities and check that the channel did not form aggregates, final purification was done on a Superdex 200 10/300 GL size exclusion column which sorts the molecules as a function of their size. An example of an elution profile is shown in Figure 3.3. A single peak in the FPLC is important at this stage to show that the purification was successful. Note that I suspect the cysteine reduction step to be critical to obtain a one peak FPLC profile (at least for wild type KvAP). A multi-peak FPLC profile could also result from a bad handling of detergent (to keep very dry and in -80 ℃).

Finally, we have checked that the protein was pure using coomassie stained SDS PAGE (see the signle band in the acrylamide gel in figure 3.4).

Note that we used the same protocol to express and purify several KvAP mutants. For the one that contained no cysteine (C247S), the protein yield in the end was high (approximately 0.5 mg per liter of culture), but for the same protein with an additional cysteine (G52C), the protein was highly unstable and the final protein yield was 10 times lower.

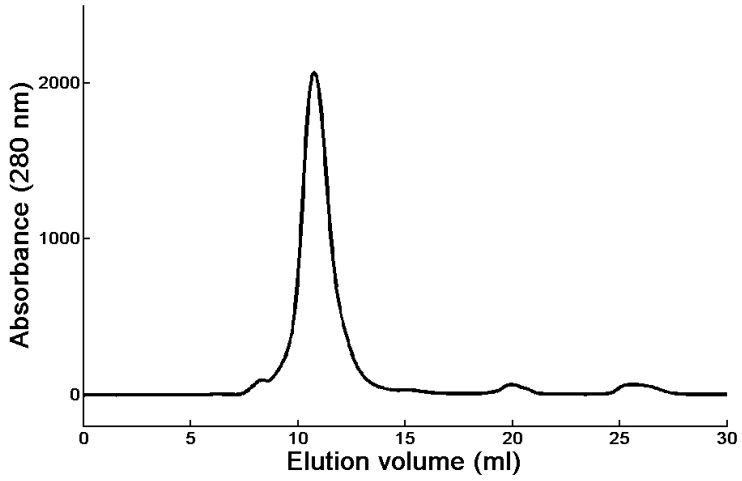

Figure 3.3: Size exclusion column profile of KvAP. The peak at 11 ml corresponds to KvAP.

3.3 Reconstitution in SUVs

The reconstitution in SUVs was done following a well established procedure [70]. Details are given in annex A.

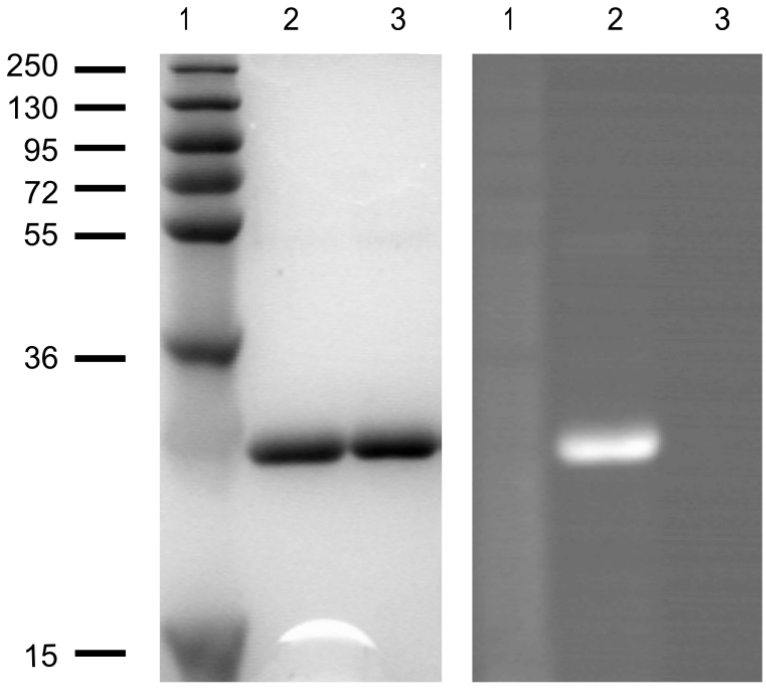

Figure 3.4: SDS PAGE of purified KvAP. The left image shows the gel stained with Coomassie Blue while the image on the right image shows fluorescence (under UV illumination) from the same gel (prior to staining). (Lane 1: protein ladder; Lane 2: KvAP after labeling with Alexa 488; Lane 3: unlabelled KvAP). Samples were run on a 12 % SDS-PAGE gel and approximately 50mM of beta-mercapto ethanol was added to samples to reduce disulfide bonds.

As shown in figure 3.5, the principle is to prepare small unilamellar vesicles and partially solubilize them [98]. For that, SUVs were prepared by sonicating an aqueous solution of lipid (at 10 mg/ml) using a tip sonicator. This solution was then incubated for 30min with 10 mM of DM. The purified protein was then added to these liposomes, 7.5 mM of DM were supplemented and the mixture was left agitating for approximately 1h for a good incorporation of the protein in the lipid/detergent micelles. The last step was detergent withdrawal via dialysis for 3 days at room temperature. Note that for KvAP, it is not advisable to use the fast biobeads (few hours) method (Daniel Schmidt, private communication) that was used previously in the group for the reconstitution of other membrane proteins. The proteoliposomes were then flash-frozen in liquid nitrogen and kept at -80 ℃. In these conditions, no degradation of the protein was detected over at least one year.

We used two different lipid mixtures for the reconstitution:

- DPhPC (1,2-diphytanoyl-sn-glycero-3-phosphocholine): which makes stable membranes suitable for electrophysiology.
- EPC (Egg L-α-phosphatidylcholine):EPA (Egg L-α-phosphatidic acid)(9:1 w:w),

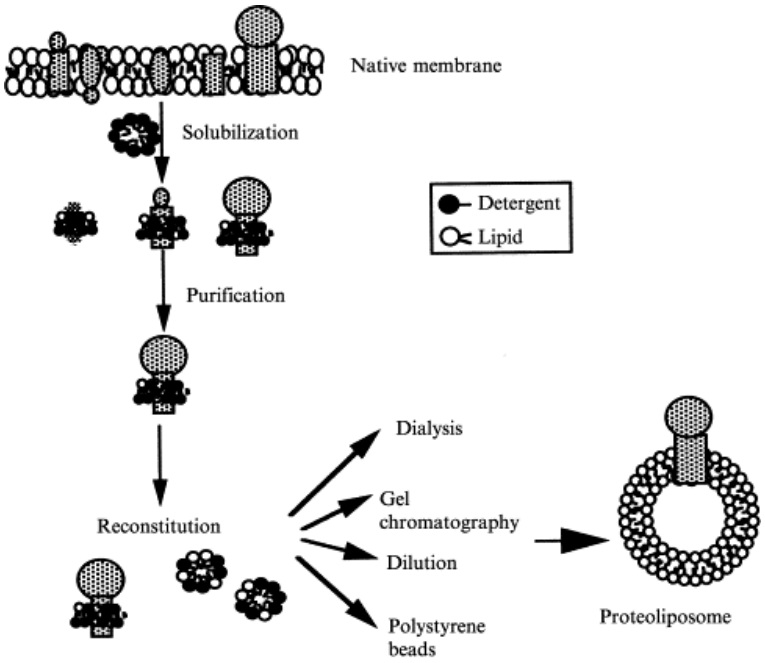

Figure 3.5: Principle of the reconstitution method: the purified proteins (in detergent) are mixed with pre-solubilized vesicles. Removing the detergent (by different possible methods) then leads to the formation of proteoliposomes. From [98].

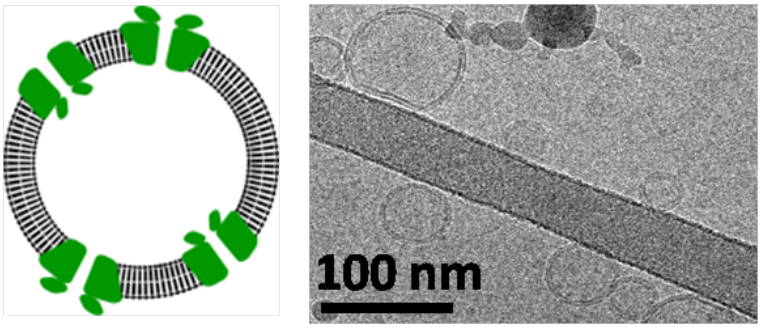

Figure 3.6: Left image) Cartoon of KvAP reconstituted in a small unilamellar vesicle. Right) Electron microscopy image of small vesicles produced after KvAP reconstitution. Image taken by Aurélie Di Cicco (Daniel Levy group in the Curie Institute).

mixtures of different lipids with different chain lengths which were believed to increase the chances of successful reconstitution.

The final SUV concentration was approximately 10 mg/ml in a relatively low-salt buffer (5mM KCl, 1mM HEPES pH7.4), except for BLM experiment (200mM KCl, 10mM HEPES pH7.4).

Proteoliposomes were then like those presented in figure 3.6.

3.4 Labeling

It was necessary to fluorescently label the channel, in order to monitor its incorporation in the membrane and for future experiments involving channel distribution.

3.4.1 Principle and method

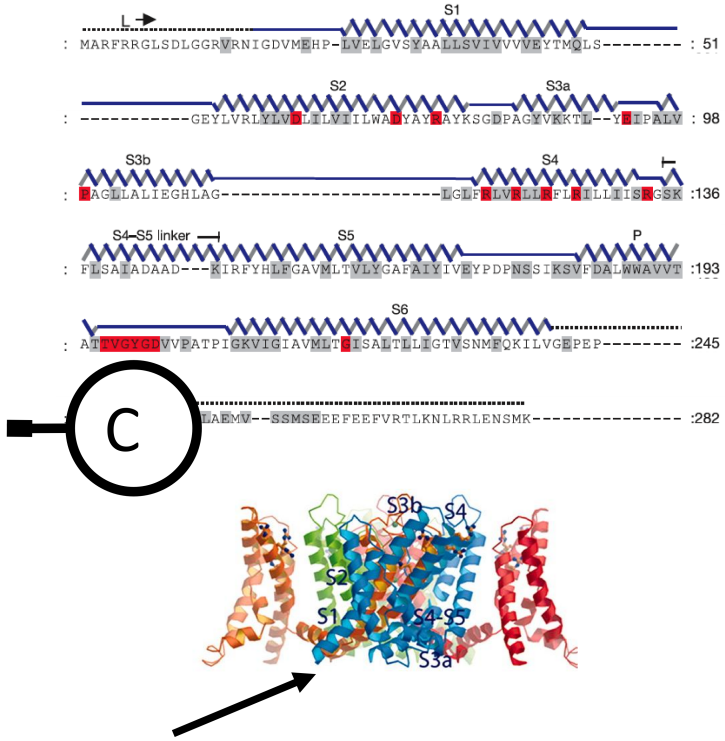

Figure 3.7: Position of the wild type cysteine in the channel. The arrow points to the approximate location of the orange monomer cysteine. Adapted from [14] and [99]

The protocol is also detailed in annex A. Briefly, labeling was done by attaching a fluorophore linked to a maleimide (Alexa Fluor 488 maleimide) to the unique cysteine of wild type KvAP, on the intracellular part of the channel (see figure 3.7).This was performed prior to reconstitution in SUVs. The excess of fluorophores was removed via dialysis along with the detergent.

As shown by the fluorescent band on the SDS PAGE gel of figure 3.4, the channel was successfully labeled. Note nevertheless that we suspected that some unspecific labeling occurred. Indeed, when prepared with low quantities of reducing agent, the protein formed dimers that could be observed in the SDS PAGE gel. This second band was not observed when using the mutant without cysteines. These observations strongly suggest that this dimer is formed by a disulphide bond between cysteines. Then, if the Alexa 488 maleimide was binding specifically to the cysteine, the labeled protein should not form dimer. This was nevertheless the case which indicates that the protein was probably not

labeled specifically on the cysteine.

3.4.2 Number of fluorophores per protein

The number of fluorophores per protein was measured via absorbance spectroscopy. Samples were prepared by solubilizing a solution of proteo-SUVs (at approximately 1 mg/ml of protein and 10 mg/ml of lipids) in 50mM DM followed by dialysis to remove any free dye that may have been trapped inside the SUVs.

Note that to avoid the dialysis step, it could be useful to separate the free dye from the protein prior to reconstitution (for example when it is bound to the nickel column).

The concentrations of the protein and of Alexa-488 were then measured with a Nanodrop spectrophotometer, and the number of fluorophores per monomer F_m was determined using:

$$F_m = \left(\frac{A_{494}}{A_{494,Alexa}}\right) \times \left(\frac{A_{280,KvAP}}{(A_{280} - (A_{Alexa,494} \times 0.11))}\right) \tag{3.1}$$

where $A_{494,Alexa} \approx 71000 mol^{-1} cm^{-1}$ and $A_{280,KvAP} = 37360 mol^{-1} cm^{-1}$. $A_{280,KvAP}$ was determined using the number of tryptophans and tyrosines of the protein (http://encorbio.com/protocols/Prot-MW-Abs.htm).

The labeling ratio ($F = 4 \times F_m$ because the protein is a tetramer) was measured for each preparation and was typically 1 to 2 fluorophores per channel. The uncertainty in F was dominated by the difficulty to measure protein concentration in the presence of a high absorption background due to the presence of lipids and detergent. This difficulty could in principle be avoided by measuring the number of fluorophores per protein prior to protein reconstitution into SUVs.

3.5 BLM experiments

To verify that the channel was functional after reconstitution and after labeling with Alexa 488 (which had never been done before), we performed BLM (Black Lipid Membrane) electrophysiology measurements. This technique has already been used extensively to study KvAP function in different membranes; it was thus the perfect tool to check the channel activity.

3.5.1 Principle and method

As described in figure 3.8, the principle is to fuse small SUVs containing reconstituted KvAP (see section 3.3) to a suspended bilayer (Black Lipid Membrane). After their incorporation in the membrane, it was possible to measure channel activity by measuring changes in conductance when channels open or close.

I also learned the protocol from Daniel Schmidt in the group of Rod MacKinnon [100] and reproduced it in the Curie Institute in collaboration with Gilman Toombes.

The experimental set up is presented in figure 3.9. A 200 microns hole separating two compartments was painted with a mixture of POPE:POPC (3:1) and decane using a glass wand. The cup in grey in figure 3.9 was filled with 15 mM KCl, 10 mM Hepes pH 7.2 and

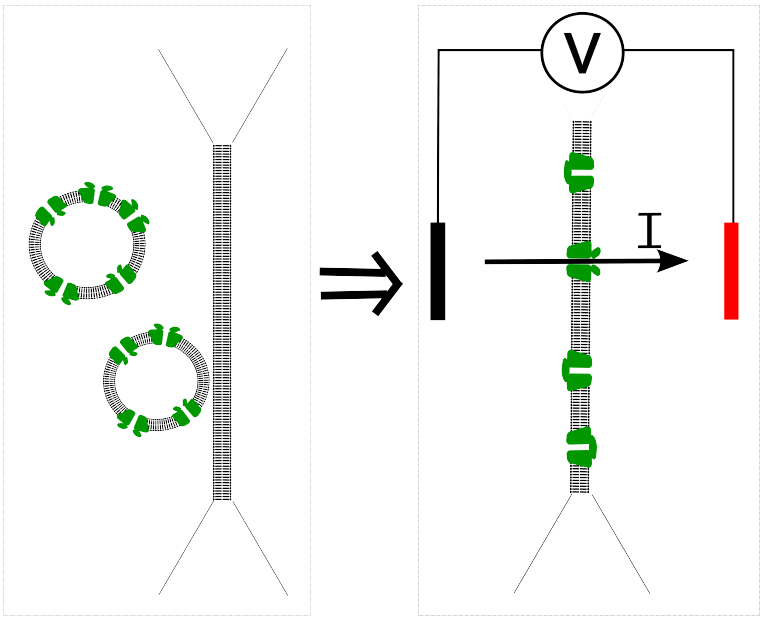

Figure 3.8: Cartoon representing BLM experiment principle. Small unilamellar vesicles are fused with a suspended membrane. Then current through the membrane is measured as a function of the applied voltage.

the other compartment (next to the cup) with 150 mM KCl, 10 mM Hepes pH 7.2. This asymmetrical concentration is known to help the SUV fusion to the membrane [101]. The SUVs were injected just above the hole. After fusion of the vesicles to the membrane, the concentration of the buffer in the cup was adjusted to get a symetrical configuration.

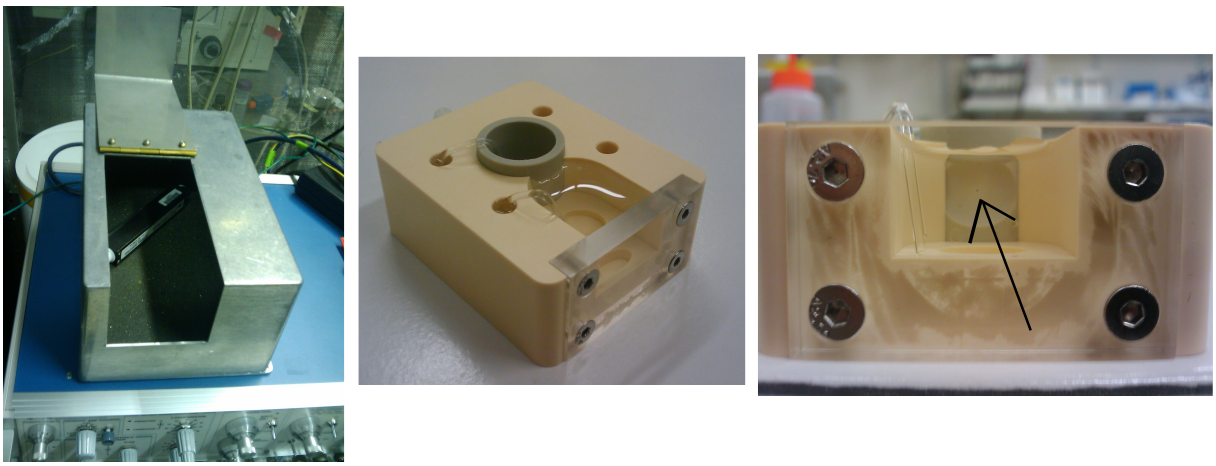

Figure 3.9: Pictures of the BLM set up. Left) Faraday cage containing the headstage. Middle) image of the BLM chamber. Right) Front view of the BLM chamber. The arrow points at the hole. Chlorinated silver electrodes were placed in the holes next to the saline bridges.

After the incorporation of the channel in the membrane, the membrane was maintained at a negative voltage. A voltage step was then applied (see figure 3.10) and current going through the membrane was recorded.

3.5.2 Results

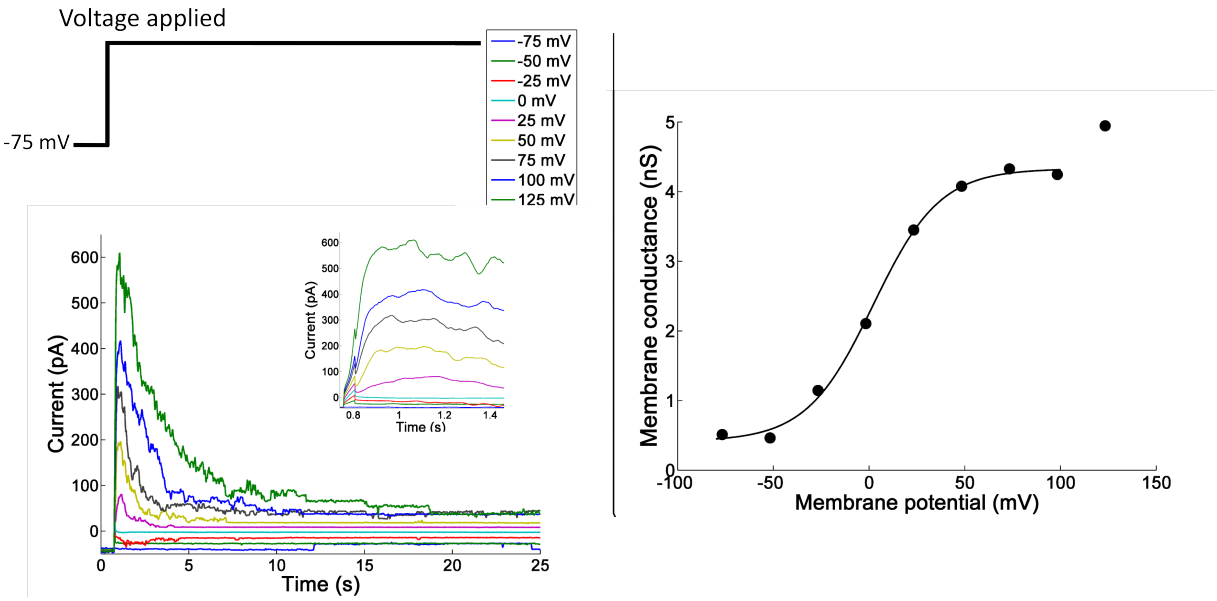

Figure 3.10: BLM experiments. SUVs containing Alexa labeled KvAP where fused with a suspended membrane containing POPE:POPC lipids at a mass ratio of 3:1. Left figure shows current traces corresponding to a pulse protocol shown above. The inset is a zoom of the opening period. The figure on the right corresponds to the peak conductance as a function of applied voltage. A Boltzmann curve fits the data if last point is excluded.

Figure 3.10 shows current responses after different voltage steps for the labeled channel. For both the labeled and the non-labeled channels, we found that the channel opened in approximately 100 ms after the voltage step. The current then decreased in a few seconds as channels progressively inactivated, until one could detect step-like currents characteristic of single channel closing (see the end of the trace in green for exemple). Furthermore, the peak conductance increased as a function of the voltage step applied, showing that the channel is voltage-gated.

My results are not significatively different from previously published data [70] shown in figure 3.11 for the same membrane composition. Indeed, the half opening probability voltage is also close to zero and the activation and inactivation times are similar. Note nevertheless that it is still possible that all the channels observed here correspond to the unlabeled fraction. However, this seems unlikely, as the current amplitude I obtained is of the same order of magnitude for the labeled and the non labeled channel.

In summary, labeling does not significantly alter KvAP function in BLM which presents the same kinetics and voltage dependence as in the literature.

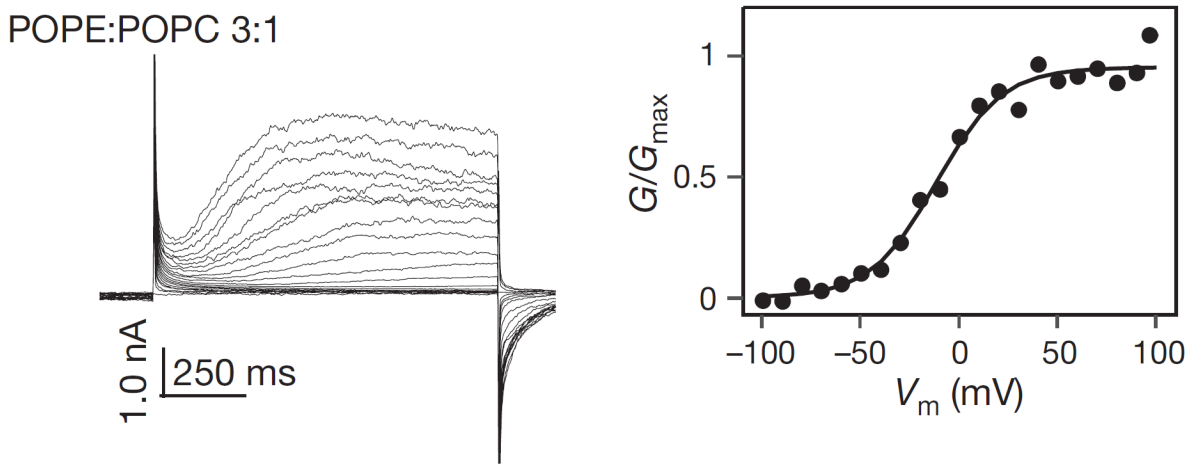

Figure 3.11: Previously published measurement for the same membrane composition with unlabeled KvAP. Note that there is no obvious difference from figure 3.10 with KvAP labeled with Alexa 488. From [70].

In this chapter, I have shown that:

- KvAP was successfully expressed, purified and reconstituted in SUVs of different lipid compositions.
- KvAP could be labeled with Alexa 488 (although not at a specific site).
- KvAP was still functional after labeling and reconstitution in SUVs as determined with BLM experiments.

Chapter 4

Reconstitution of KvAP in Giant Unilamellar Vesicles

The results presented in this chapter were published in [102].

4.1 Introduction

The interactions between voltage gated ion channels and membranes are difficult to study in cells because cells actively regulate membrane state (see details in the chapter 2). It is thus useful to reconstitute the channel in a system where membrane parameters (voltage, composition, tension, curvature) can be accurately controlled.

4.1.1 Existing techniques for reconstitution of channels in model membranes

For electrophysiological studies of ion channel activity, several in vitro systems have been developed, including fusion of SUVs with planar membranes and patch-clamp on multilamellar vesicles, both presented in the following paragraphs. However, as we will see, each technique has distinct limitations concerning the control of membrane tension, shape or composition.

4.1.1.1 Planar membranes

The different methods developed to reconstitute channels in planar membranes are summarized in figure 4.1.

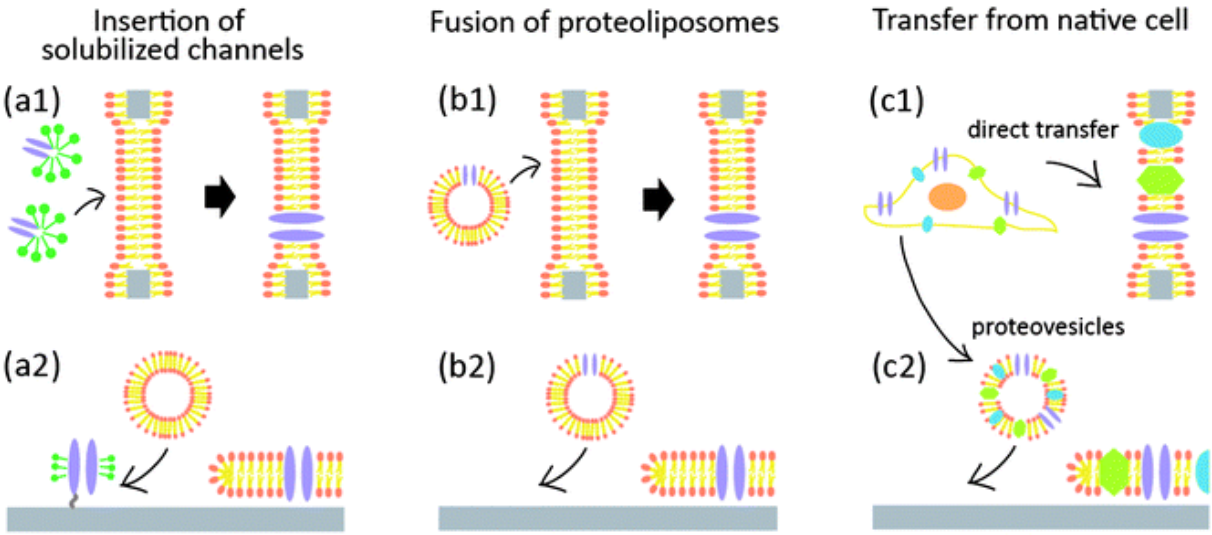

Figure 4.1: Procedures for ion channel incorporation into bilayers: integration of ion channels in preformed free-standing bilayers suspended in micro- or nanopores is achieved (a1) from solubilized membrane proteins (b1) from proteoliposomes or (c1) directly from native cells. On surfaces, (a2) the protein is either first immobilized and the space is filled up with lipids by liposome fusion, or (b2) proteoliposomes with reconstituted channels or (c2) proteovesicles from native cells are produced and form a proteobilayer on surfaces. Figure and caption are from [103].

The classical Black Lipid Membrane technique has already been presented in section 3.5 of chapter 3. Briefly, a mixture of lipids and solvent (usually decane) is applied to a small aperture (approximately 300 microns in diameter) to form a suspended film. The lipids get at the interface between the solvent and the air. Because of curvature of the interface due to the imposed contact angles, Plateau-Gibbs border suction occurs and the film gets thinner. London-Van der Waals attraction between the aqueous phases separated by the film makes the film thinner and a membrane composed of mostly lipids is formed in the middle of the film. Small vesicles can then be fused to the membrane, or channel solubilized with detergent can be directly incorporated in the membrane (a1), b1) and c1) of figure 4.1) before electrophysiological measurements.

However in this system, many membrane parameters are poorly controlled. First, remaining solvent in the membrane, necessary for membrane stability [104], could affect channel activity in uncontrolled ways. Indeed, it has been suggested that the effects of membrane composition changes (by adding alkanol for example) on the channel function will be dramatically altered by the presence of decane in the bilayer. A mecanism for this effect is that small decane molecules can fill the gaps in the membrane and thus relax the pressure profile in the membrane [78] (see figure 4.2).

Another parameter difficult to control is the protein density. Indeed, the fusion of small liposomes to the BLM strongly depends on many parameters, including the precise location and flow rate at which the vesicles are injected by the experimenter, and the number of channels per vesicles which are difficult to control. These drawbacks make it

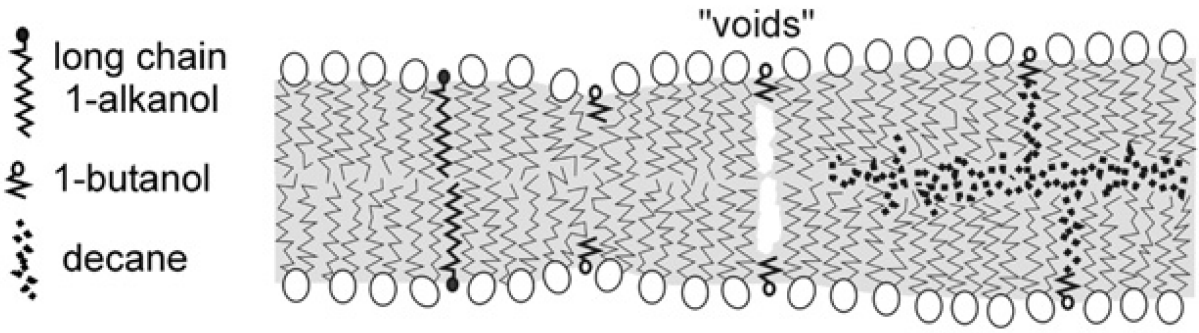

Figure 4.2: Effect of an alkanol on the membrane with and without decane. From [78]

difficult to determine the proportion of active channels for example.

Furthermore, in those experiments, the membrane tension is set by the equilibrium with the oil annulus which should depend on the biochemical properties of the lipid, the solvent and the substrate [104]. The tension is thus mostly impossible to adjust for a given lipid composition and is high as compared to cells (see figure 4.3). Finally, some groups have pulled tubes from BLMs [105, 106]. However here it is difficult to control the tube radius (because membrane tension is fixed).

Another method to incorporate ion channels in planar membranes is to prepare solid supported bilayer (sSLMs) as presented in figure 4.1 a2) b2) and c2). The principle is to make the small vesicles fuse to a substrate. A major drawback of this technique is that the membrane must tightly adhere to the substrate to create a good electrical seal. The small gap between the membrane and the surface can lead to an accumulation of ions, and can also affect trans-membrane protein conformation. An interesting alternative is to explode giant vesicles on nanoporous surfaces. However, for those strategies, membrane tension is set by the adhesion energy with the substrate and is usually high as compared to typical membrane tension in cells (see figure 4.3). Membrane geometry is also given by the substrate geometry which is planar in most experiments. Nevertheless, some groups have prepared bilayers containing channels supported on silicon nanowires (down to 20 nm in diameter) [107].

4.1.1.2 Multilamellar Vesicles

A second strategy is to form giant liposomes by fusing together SUVs that already contain the protein, either by applying freeze-thaw cycles [111] or drying SUVs and then rehydrating the fused membranes [112]. This produces multilamellar vesicles of approximately 10 microns. The addition of magnesium leads to the detachment of unilamellar blisters from the multilamellar vesicles, as presented in figure 4.4. A glass pipette can be stuck on these blisters to make patch-clamp measurements (for details see section 4.5).

Note that these experiments are done routinely with asolectin lipids (a mixture of many different lipids) or cell extracts in different group. The same experiment using purified lipids has been difficult to perform in our hands, suggesting that lipid composition matters. Another drawback of this method is that the tension in the patch is set by the adhesion energy of lipids on the glass in the pipette and is again really high as compared to cell

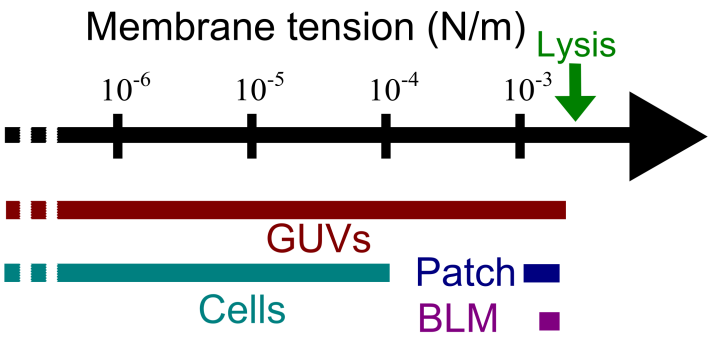

Figure 4.3: Summary of membrane tension in different membranes. Data from [108, 109, 79, 110]. Note that the values for the high cell tensions can be misleading as the tension measurements method reflects the interactions of the membrane with the cytoskeleton as well.

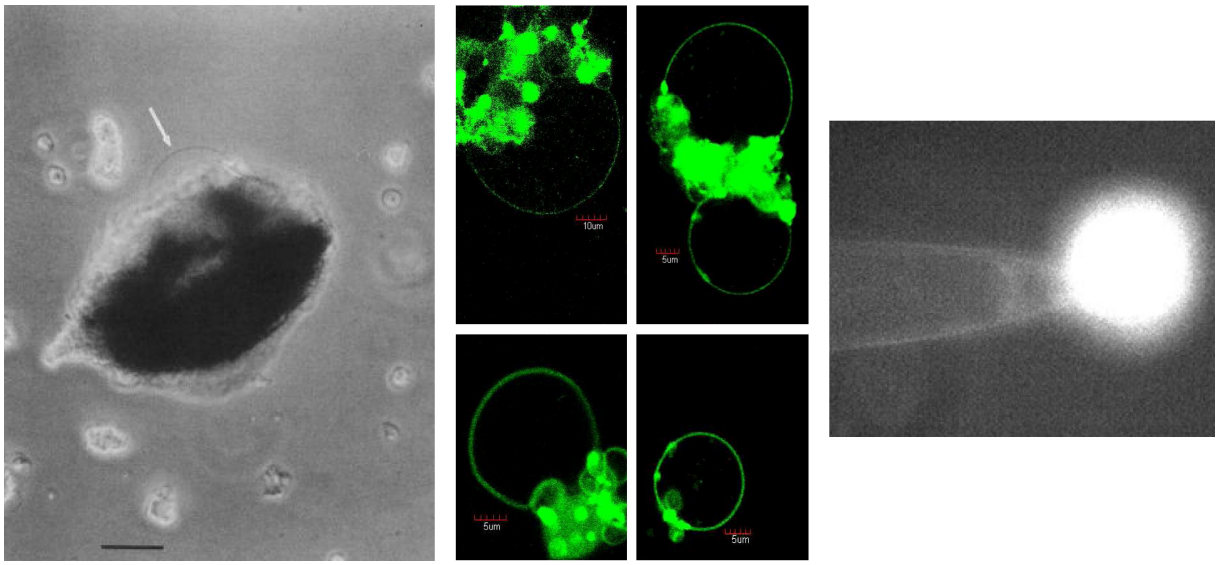

Figure 4.4: Typical liposomes for patch-clamp experiments. Left) Blisters from native membrane (*E Coli*) liposomes [111]. Bar 50 microns. Middle) Asolectin liposomes containing fluorescent MscL (top panel) and MscS (bottom panel). From [113]. Right) Patch-clamp on a multilamellar vesicle.

membranes. Finally, the area of the patch being small, it is usually difficult to record from a large number of channels.

4.1.2 Existing techniques for reconstitution of trans-membrane proteins in GUVs

4.1.2.1 Strategies to incorporate functional trans-membrane proteins into GUVs

In contrast with the methods described in the last paragraph, membrane parameters (composition, tension and curvature) can all be readily controlled in physiologically relevant ranges in GUVs as described in the introduction chapter. Thus, several groups have already put some efforts in the reconstitution of trans-membrane proteins into GUVs.

Classically, GUVs have been prepared using a lipid film deposited from organic solvent [30], a procedure likely to damage all but the toughest proteins [114]. Thus, one difficulty was to find conditions that preserve protein activity while still allowing a high yield of GUVs.

To date, two main strategies have been employed. In the first approach, lipid-only GUVs are first prepared and the protein is then incorporated afterwards. Efforts have been made to introduce the protein by mixing GUVS with protein-detergent micelles [115], and by fusing proteo-SUVs to GUVs either spontaneously [116], or with the aid of charged lipids and fusion peptides [114]. While this strategy protects the protein from extreme conditions, the final density of proteins in GUVs has typically been quite low and difficult to control, while conditions must be finely tuned to avoid destroying the GUVs when they are exposed to the detergent or fusion-enhancing charged lipids or peptides [114].

In the second approach, GUVs are formed directly from a membrane film that already contains the protein [117]. The membrane stack has typically been formed by partial dehydration of a solution of proteo-SUVs, while applying an AC electric field during rehydration (electroformation) can greatly boost the yield of unilamellar defect-free vesicles [118]. An obvious drawback of this approach is the difficulty of forming a membrane film without damaging the protein, although sugars (e.g. sucrose or trehalose) can be added to stabilize the protein during the dehydration step [119]. Thus, the electroformation approach has already been applied for a variety of membrane proteins, usually with a very low salt content (for examples see [119], [120], [121]). We chose to use the electroformation method because a high yield of defect-free unilamellar vesicles is usually required for most of the applications (see chapter 2).

A third exotic approach has been to use jetting across a bilayer [122] or using the inverse emulsion technique [123] for producing GUVs with reconstituted membrane proteins together with encapsulating proteins in the lumen of GUVs. However this technique works for a single transmembrane domain like syntaxin or a really tough protein like KcsA but should be incompatible with the reconstitution of a complex trans-membrane protein. Furthermore, the process involves the use of oil which can remain as a trace in the membrane (Campillo et al. in preparation) which might affect the channel function.

4.1.2.2 Trans-membrane proteins previously reconstituted in GUVs

The SUV dehydration/electroformation approach has been successfully used to reconstitute a number of membrane proteins into GUVs, for studies including the affinity of pro-

teins for lipid rafts (PLAP, syntaxin, synaptobrevin, bacteriorhodopsin et caet. [124]), the effect of pump activity on membrane fluctuations (Ca^{2+}-ATPase [125], bacteriorhodopsin [68]), the effect of membrane composition and thickness on protein mobility (GltT, LacY [126]), and a model for cell adhesion kinetics (Integrins [127])).

Some simple ion channels have also been reconstituted into GUVs, including the bacterial mechanosensitive channel MscL [119], several porins ([115], [116], [128]), an unidentified chloride channel [129], the potassium channel, KcsA[123], and Connexin-26 [130].

However, the incorporation of a complex membrane protein (containing several domains and subunits) into GUVs while retaining protein activity remains challenging.

4.2 Reconstitution method

I will first summarize the protocol that we developed. It is based on partial dehydration/electroformation protocol [131] modified to allow a wider range of salt concentrations in the GUV interior [132]. Then I will present the characterization of the reconstitution.

4.2.1 GUVs preparation principle

GUVs containing reconstituted KvAP were prepared using a protocol based upon a SUV fusion/electro-formation method developped previously in the group [131]. In this approach, a solution of SUVs containing the protein is deposited onto electrodes. The controlled partial dehydration of this solution causes the SUVs to fuse together to form a protein-lipid film consisting of membranes stacked parallel to the film surface. When buffer is then added, the membrane stack swells and in the presence of an applied alternating voltage, individual membranes detach from the stack to form GUVs. These steps are summarized in the schematic shown in Figure C.3.

The challenge is to efficiently transform proteo-SUVs into GUVs while still maintaining the protein in a functional state. The GUV yield and state of the protein depend upon multiple parameters including the composition of the SUV solution, the level of dehydration, the salt concentration of the GUV growth buffer, and the frequency and amplitude of the applied electric field. During the trials used to refine the protocol, the growth of GUVs on the electrodes was followed with phase contrast microscopy (see figure 4.6) on a Zeiss axiovert 135 microscope (LWD Zeiss achroplan 40x air objective, 0.65 Na), while the incorporation of protein into GUVs was monitored using fluorescently labeled KvAP. Conditions which provided consistent GUV yields are described in detail in Annexe B.

As shown in figure 4.6 and 4.7, the SUV fusion/electro-formation strategy allowed to produce defect-free GUVs.

4.2.2 Membrane and buffer compositions

To confirm the method was suitable for different biophysical applications, GUVs were prepared with several different membrane compositions and different buffers encapsulated inside the GUVs.

Clearly, the GUV internal solution is especially important for studies of ion channels. For a relatively "low-salt" buffer (5mM KCl, 1mM HEPES pH 7.3, 400 mM sucrose), useful

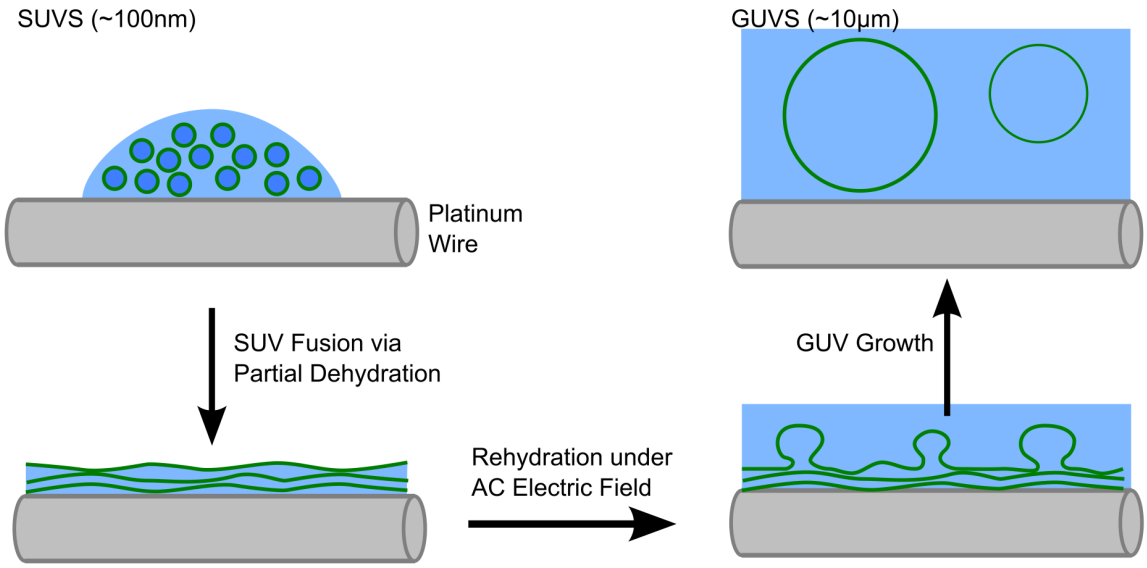

Figure 4.5: Schematic of the electro-formation process. Droplets containing SUVs are deposited on the electrode. Partial dehydration of the solution causes the SUVs to fuse to form a stack of membranes. Buffer is then added and an AC electric field applied. as the film swells, individual membranes detach from the stack to form GUVs.

GUV yields could be obtained by applying a sinusoidal voltage of 0.7V (RMS) and f=10Hz for approximately two hours. Preparing GUVs with "physiological" salt concentrations (typically 100 mM) has traditionally been more difficult as salt can have a significant effect on the rehydration/swelling step of GUV formation [133]. However, it was recently reported that a higher frequency voltage ($\backsim$500Hz) allowed the efficient electroformation of GUVs containing 100mM salt [132]. For such a growth buffer (100 mM KCl, 10 mM Hepes pH 7.3, 200 mM sucrose), GUVs containing KvAP could be formed using a voltage of 0.3V (RMS), f=500Hz overnight. Several lipid compositions were also tested. Both DPhPC and EPC:EPA (9:1 by mole) proteo-SUVs allowed the production of a high yield of GUVs. Confocal images of labeled KvAP in these vesicles, showed that the protein was homogeneously distributed in the membrane (see for example figure 4.7).

To control GUV composition, protein-containing SUVs were mixed with SUVs containing the red fluorescent lipid, Texas Red 1,2-dihexadecanoyl-sn-glycero-3-phosphoethanolamine (TR-DHPE; Invitrogen), 1,2-dioleoyl-sn-glycero-3-phosphoethanolamine-N-[methoxy(polyethylene glycol)-2000] (PEG-DOPE; Avanti Polar Lipids), or other lipids. 2-10mM trehalose (generously provided by Pr. Lorenzo Cordone, Palermo, Italy) was added to the solution to protect the protein during the partial dehydration step [119]. The final lipid concentration of the SUV mixture was typically 3mg/ml. Droplets of the SUV solution ($0.35\mu L/cm^2$) were deposited onto two parallel platinum wires (diameter=0.5 or 0.8mm; edge to edge distance = 2.5mm) in a custom-made Teflon chamber (see figure in AnnexeB), and the SUVs then allowed to dry for approximately 30 min under atmospheric conditions. GUV formation buffer was then added to the chamber and an

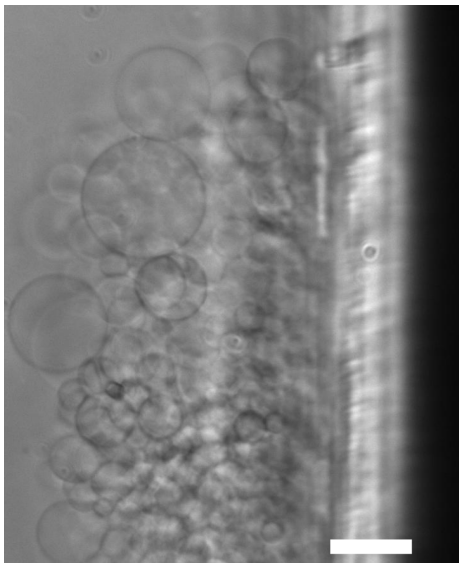

Figure 4.6: Phase contrast image showing GUVs growing on the platinum electrode. GUVs were grown from an EPC:EPA proteo-SUV solution (lipid concentration of 2 mg/ml; 1:10 protein to lipid mass ratio; 10mM trehalose). The growth buffer was 100mM KCl, 10mM HEPES (pH7.4), 2 mM EDTA, and 200mM sucrose. GUVs were formed by growth overnight with an applied voltage of 0.8 V_{RMS}, f=500Hz. The scale bar is 20 microns.

electric field applied during the rehydration of the film. For a "low salt" GUV formation buffer (5mM KCl, 1mM HEPES pH 7.3, 400 mM sucrose), the lipid film was rehydrated for approximately 2 hours under an applied AC voltage of 0.7V RMS (Root Mean Square), 10Hz. For a more physiological buffer (100 mM KCl, 10 mM HEPES pH 7.3, 200 mM sucrose), a voltage of 0.3V RMS, 500 Hz was applied overnight. Further details of the GUV formation process are given in AnnexeB.

As summarized in table 4.1, it was thus possible to produce GUVs containing KvAP with different buffers and lipid composition.

Lipids
EPC:EPA 9:1
POPC:POPG 9:1
DPhPC

Protocol	High salt	Low salt
Buffers	100 mM KCl	5mM KCl
	10 mM HEPES pH 7.3	1mM HEPES pH 7.3
	200 mM sucrose	400 mM sucrose
Frequency	500 Hz	10 Hz
Voltage	0.3V RMS	0.7V RMS
Time	o/n	2h

Table 4.1: Summary of the different conditions tested

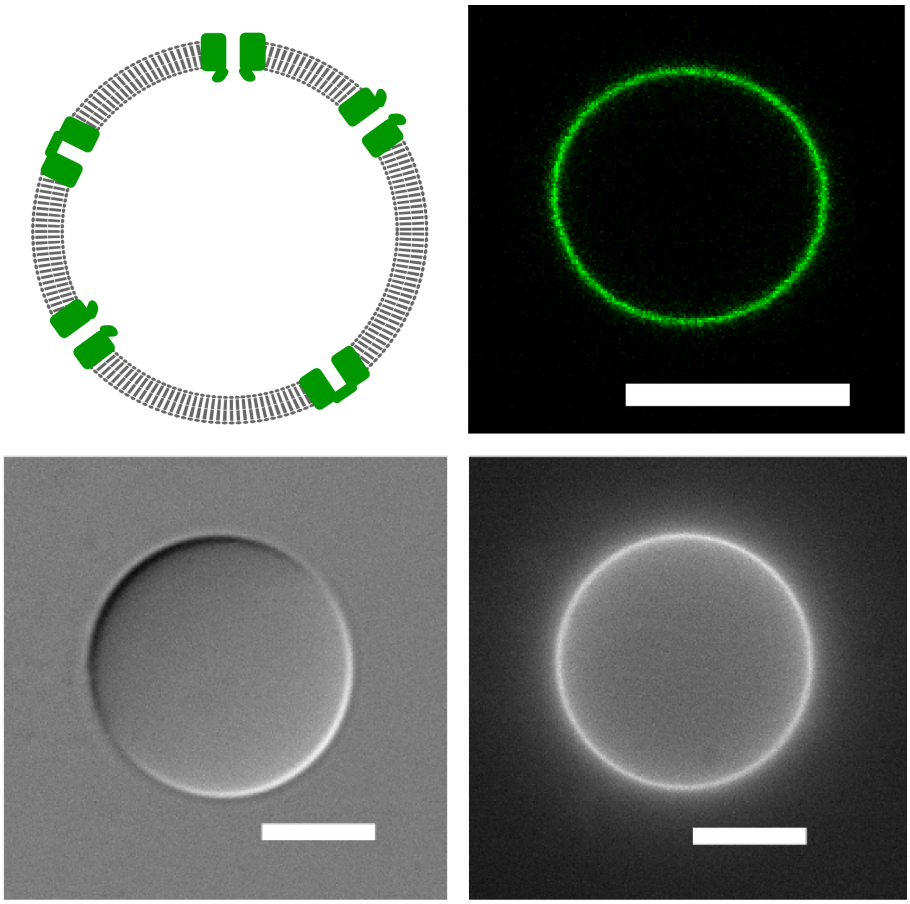

Figure 4.7: Giant unilamellar vesicle containing reconstituted KvAP. Top left: Cartoon of ion channels (green) inserted into the lipid bilayer (gray) of a GUV (not at scale). Top right: Confocal image of a representative GUV containing KvAP labeled with Alexa 488. Bottom: DIC (left) and epifluorescence (right) images of another typical vesicle containing KvAP labeled with Alexa 488. Scale bars: 10 μm.

4.3 GUV characterization

4.3.1 Confocal imaging

For more detailed observations of vesicle morphology and fluorescence quantification, GUVs were transferred to a chamber containing a solution of glucose, NaCl or KCl and HEPES (pH 7.4) with the same osmolarity as the GUV formation buffer. The difference in density between sucrose and glucose should in principle allow the vesicles to settle at the bottom of the observation chamber and the index difference should help observing the vesicles with phase contrast microscopy. However, when the density of proteins was high (typically more than a hundred of proteins per square microns), vesicles lost contrast in few minutes, making them more difficult to find in the chamber. A possible explanation for this effect would be that few porins (not detectable on electrophoresis gels) remain

with the protein after purification or that a small fraction of the protein was misfolded enough to create some pores in the membrane.

Nonetheless, vesicles could be found for all protein densities tested and confocal images of GUVs equatorial plane were taken to study vesicle unilamellarity, determine vesicle size and measure the protein density in the GUV membranes . This was done using a Nikon Eclipse TE 2000-E microscope with a D-Eclipse C1 confocal head with two laser lines (λ=488 nm;λ=543 nm) and a Nikon Plan Fluor 100x oil objective (1.3 NA).

Several factors were important for achieving quantitative comparison of fluorescence intensities. Firstly, all relevant confocal parameters (PMT gain and offset, pixel dwell, pixel size, laser power, pinhole size, and position of GUV in the confocal field) were either held constant, or the effect of any changes was corrected for. For example, a calibration was performed to allow comparison of images obtained with different PMT gains using the equation, $I_1 = I_0 \times exp(\beta \times (Gain_1 - Gain_0))$, where β describes the scaling of the PMT gain ($\beta \approx 0.068$ for red channel). To obtain reliable results, confocal parameters were adjusted so that the fluorescent signal strength was significantly larger than the PMT noise but not so strong as to saturate the detector.

To avoid bleaching of the fluorophores (alexa 488, Bodipy-HPC), care was taken to avoid exposure of the GUVs to bright light before the measurement. For typical imaging conditions (pixel size of approximately 100 nm and a dwell time per pixel of $1.68\mu s$), the fluorescence intensity diminished by less than a few percent per image. As only one image was taken for fluorescence measurements, the bleaching was negligible. Clearly, the measured fluorescence intensity depended upon excitation intensity and detector efficiency. Changes in fluorescence intensity were observed over a time-scale of weeks to months, probably due to misalignment or aging of the laser. These variations were accounted for by regularly measuring the intensity of a solution of known fluorophore concentration (e.g. $10\mu M$ of Alexa 488).

4.3.2 Quantitative image analysis

GUV images were analyzed using a Matlab (Mathworks, Ma) program (see Figure 4.8). For each GUV, the membrane contour was fitted to the form of an ellipse and the intensity profile was then determined by averaging along the contour. In cases where part of the contour could not be used (e.g. when two GUVs were too close together for example), the average was taken on the section of the contour where the membrane of the GUV could be clearly isolated. The fluorescence intensity of the membrane, I, was defined to be the maximum of the intensity profile minus the background fluorescence level.

Along with the careful image acquisition described above, this analysis technique allowed to determine the size, unilamellarity and protein density in the GUVs containing KvAP.

4.3.3 Yield and size distribution

Although the yield and size of GUVs depended on the exact parameters used, GUV formation was generally quite efficient with hundreds of GUVs per electro-formation chamber. The size distribution of proteo-GUVs was evaluated using confocal images of the proteo-GUVs. Each GUV was analysed as described in section 4.3.2 and the GUV diameter

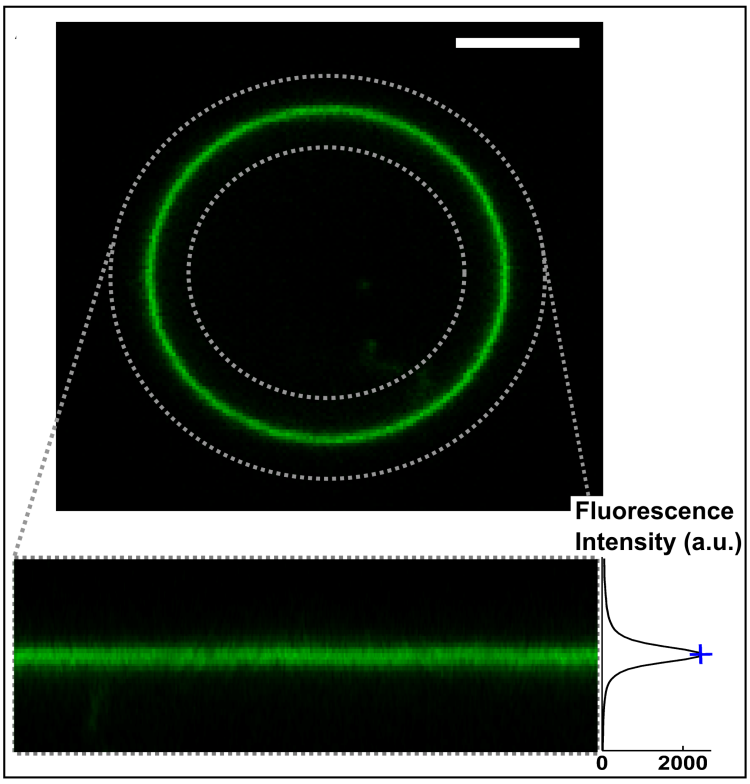

Figure 4.8: Determination of membrane intensity from images of the vesicle equatorial plane. Confocal images of the equatorial plane of GUVs containing Bodipy-HPC (top) were transformed into a coordinate system centered on the membrane contour (bottom) in order to calculate the membrane intensity profile (right). Membrane fluorescence intensity was characterized by the profile maximum (blue cross). Scale bar : $5\mu m$.

calculated from the width of the GUV contour. As shown in figure 4.9, proteo-GUVs with EPC/EPA lipids were approximately 10 microns in diameter. Note that increasing voltage and electroformation duration seemed to increase GUV size. Also DPhPC seemed to form larger vesicles.

4.3.4 Vesicle Unilamellarity

As the vesicle unilamellarity is crucial for most applications described in section **??**, it was important to verify that the reconstitution technique allows to produce a high yield of unilamellar vesicles.

To distinguish between unilamellar and multilamellar objects, proteo-GUVs were prepared containing a fluorescent lipid. Membrane fluorescence should then be proportional to the number of bilayers in the vesicle. To establish the fluorescence signal of a single membrane, reference GUVs were prepared using a classical electro-formation protocol known to produce a high yield of unilamellar vesicles [134]. Proteo-GUVs were prepared following the protocol described in Annexe B, from a SUV mixture with a molar composi-

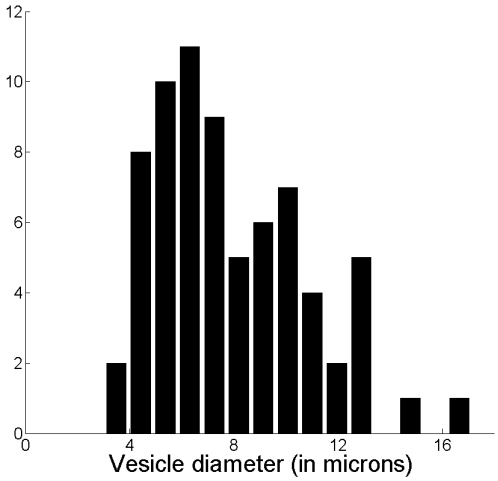

Figure 4.9: Histogram of proteo-GUV diameters. GUVs were formed using a low salt buffer (5 mM KCl, 1 mM HEPES, 400 mM sucrose), and a histogram of GUV protein density for the same population is show in Figure 4.15. The GUVs have a mean diameter of 7.9 microns and standard deviation of 2.9 microns (N=71).

tion of 89% EPC, 9.5% EPA, 0.5% TR-DHPE.1% PEG-DOPE was added as this has been reported to help produce defect-free GUVs [127]. Reference GUVs (99.5 % EPC, 0.5% TR-DHPE) were prepared using the protocol described in Annexe B. The same stock solution of TR-DHPE was used for both types of GUVs. After preparation, proteo-GUVs were collected using a 200μL pipette tip cut so the end formed a V shape. The pipette tip was scraped along the wires while aspirating, thereby collecting almost all the lipid material on the wire. Note that this especially aggressive harvesting method was used in an effort to collect everything produced during the growth.

The GUV solution was transferred into an observation chamber containing an isoosmolar solution and the GUVs were imaged via confocal microscopy. Figure 4.10 shows a typical field of view. Note that like many GUV preparation methods, the protocol produced a fraction of multi-lamellar objects. However, most GUV experiments manipulate or at least analyze GUVs individually so multi-lamellar objects can be readily detected (and excluded) by fluorescence microscopy. With our protocol, at least half the objects transferred into the observation chamber were spherical and surrounded by a membrane that presented a single line (within the limits of the optical resolution of the microscope).

These objects thus appeared to be GUVs. To determine if the membrane fluorescence intensity of these "apparent GUVs" was consistent with a single lipid bilayer or had several membranes stuck closely together, confocal images of vesicle equatorial plane were analysed as described in section 4.3.2. As shown in figure 4.11, the membranes of the reference GUVs (notionally unilamellar), proteo-GUVs prepared with low salt and proteo-GUVs prepared with 100mM salt all had very similar mean lipid fluorescence ($2000 \pm 260(a.u.)$). Indeed, of the 142 vesicles analysed, only 2 were obviously bi-lamellar (vesicles with an intensity of 4500 for low salt preparation). Thus, the intensity of lipid fluorescence from "apparent

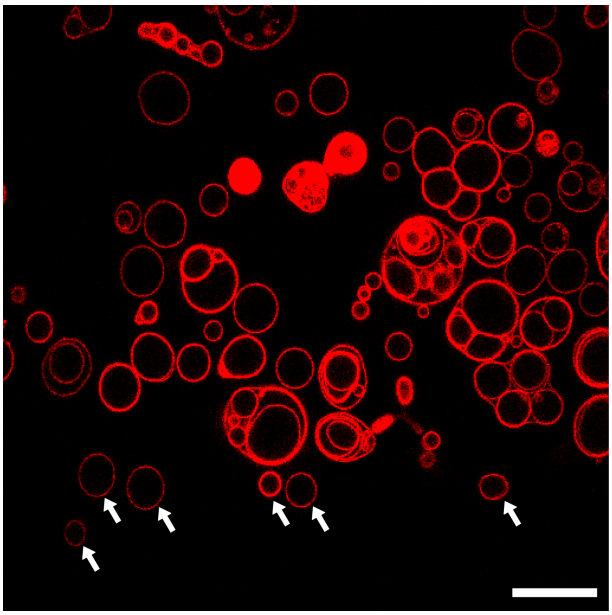

Figure 4.10: Representative image of objects harvested from the GUV growth chamber. White arrows identify examples of round vesicles with a single membrane. The fluorescence intensity of these "apparent GUVs" was then analyzed for unilamellarity. Note that the fluorescence intensity is brighter in the center of this image because the extremely large field of view. Scale bar: 20 microns.

GUVs" containing protein is entirely consistent with a membrane consisting of a single bilayer.

Our protocol thus allows to produce a high number of unilamellar vesicles.

4.3.5 Rare Oddities

In some preparations, a few vesicles (less than 10%) exhibited an inhomogeneous protein and fluorescent lipid distribution as shown in figure 4.12. Such vesicles somewhat resemble a phase-separated GUV in which one domain is enriched in both TR-DHPE lipid and KvAP. However, the lipid fluorescence in the "enriched domain" is essentially two times the level in the low intensity region, as if the bright region consisted of two bilayers. Micropipette aspiration suggests that these vesicles are not simple, unilamellar objects. as shown in Figure 4.13, the vesicle forms two "tongues" inside the pipette with the green fluorescence signal concentrated in the outer "membrane". This outer "membrane" can even be stripped off suggesting the vesicle really did possess locally 2 bilayers. We have not observed similar objects in lipid-only GUVS. How such structures form and remain stable remains a mystery, and it is important to stress that they represent a tiny (but very curious) fraction of the objects formed.

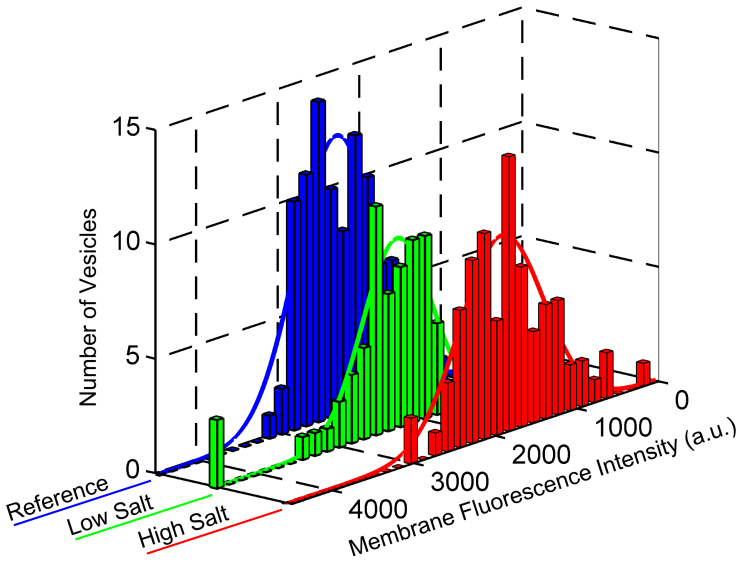

Figure 4.11: Vesicle unilamellarity. Histograms of membrane fluorescence intensity for GUV prepared with lipids only (ITO), proteins in low-salt buffer, and proteins in high-salt buffer. Each distribution was fitted to a gaussian function to determine the mean and standard deviation (pure lipid GUVs - Mean = 2331, std = 487,N=96; low salt proteo-GUVs -Mean = 2291, std = 422,N=67; 100mM salt proteo-GUVs - Mean = 1884, std = 511,N=75).

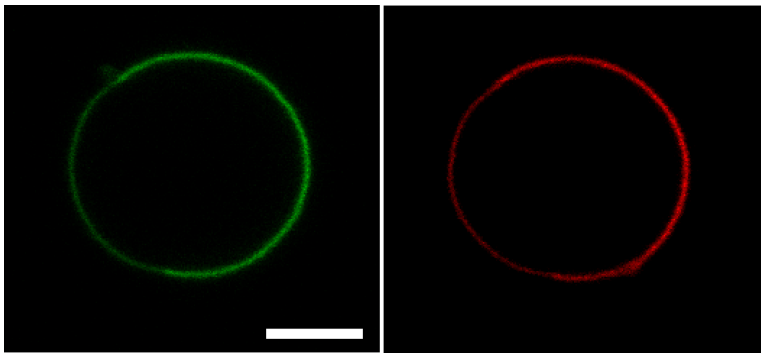

Figure 4.12: Example of a weird (and rare) vesicle exhibiting inhomogeneous fluorescence. Left: lipid fluorescence, right: protein fluorescence. Scale bar: 5 microns.

4.4 Density quantification

4.4.1 Method principle

The density of fluorescently labeled proteins in GUVs was measured via confocal microscopy. In principle, the molecular concentration per square micron, D, and the fluorescence intensity, I, should be related by the equation,

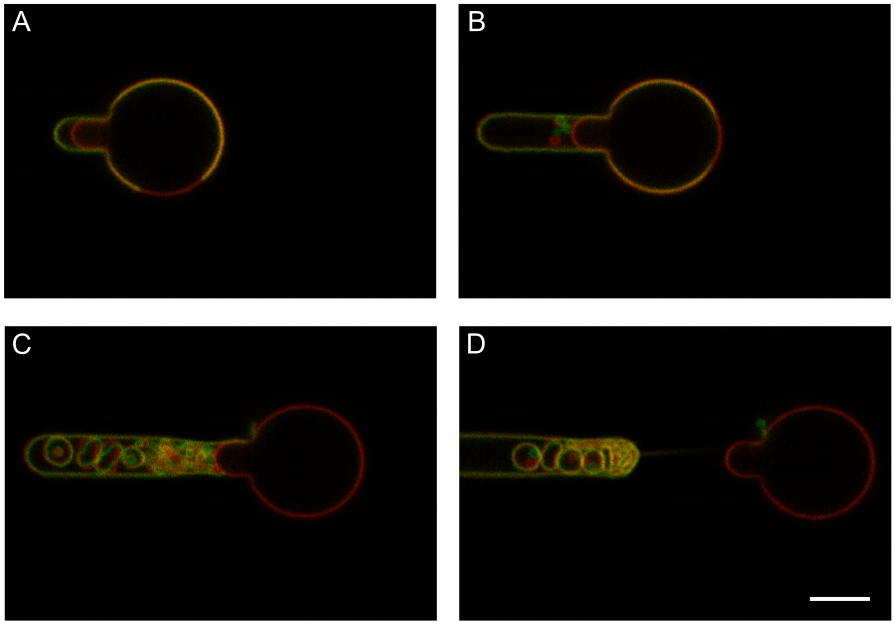

Figure 4.13: Micropipette aspiration of a weird (and rare) vesicles. Panels a to D present a sequence of confocal images taken as the vesicle was progressively aspired into the pipette. It appears as if the green fluorescence is concentrated in an outer "membrane"that can be stripped off while the inner"membrane" stays in place. Scale bar: 5 microns.

$$D = I/(N_f \times a \times I_0) \tag{4.1}$$

where N_f is the number of fluorophores per molecule, a is the effective membrane area in the confocal volume, and I_0 is the intensity per fluorophore. Thus, in addition to measuring the fluorescence intensity, I, one must also determine the product of N_f, a and I_0. The number of fluorophores per molecule, N_f, can be directly determined via absorbance spectroscopy. In contrast, a and I_0 depend upon many factors including the orientation of the membrane (horizontal, vertical, etc.), the nature and environment of the fluorophore, the intensity of the fluorescence excitation source and the efficiency of the detector. Recently, [135] introduced an elegant method to determine the product, $a \times I_0$, through the use of a reference fluorophore (e.g. fluorescent lipid) that can be incorporated into membranes at known density. Adapting this approach to confocal images of GUV membranes, the calibration is performed by measuring the effects of:

- Geometry
  Measurements of the fluorescence intensity, I_{ref}, of similar GUVs containing a reference fluorophore (lipid with 1 fluorophore per lipid) at known density D_{ref}, are used to determine the product,

$$M_{ref} = a \times I_{(0,ref)} = I_{ref}/D_{ref} \tag{4.2}$$

- Relative fluorescence intensity
  Measurements of fluorescence from bulk solutions (SUVs or detergent micelles) are

used to compare the intensity of the protein fluorescence $I_{(0,protein)}$ relative to the reference fluorophore $I_{(0,ref)}$,

$$F = I_{(0,protein)}/I_{(0,ref)} \tag{4.3}$$

Combining these two measurements then gives

$$D = I/(N_f \times (a \times I_{(0,ref)}) \times (I_{(0,protein)}/I_{(0,ref)})) = I/(N_f \times M_{ref} \times F) \tag{4.4}$$

The following sections describe the measurement of

- Membrane fluorescence
- Effect of geometry
- Fluorescence yield

and their final application to determine the density of proteins in GUVs.

4.4.2 Effect of geometry

Fluorescence intensity measurements were calibrated using GUVs prepared with a classic electroformation protocol [134]. These GUVs contained known concentrations (0.008 % to 0.5 % by mole) of the green fluorescent lipid Bodipy-HPC (2-(4,4-difluoro-5,7-dimethyl-4-bora-3a,4a-diaza-s-indacene-3-pentanoyl)-1-hexadecanoyl-sn-glycero-3-phosphocholine, Molecular Probes). The concentrations of Bodipy-HPC solutions were determined by measuring the absorbance at 509 nm ($\approx 70000 mol^{-1} cm^{-1}$; Invitrogen) of a sample that had been resuspended at a concentration of 0.02mg/ml in a solution of 100mM NaCl, 200mM glucose, 10mM Hepes (pH 7.4), and 50 mM of detergent (DM). EPC and EPA stock solutions were prepared by weighing the lipid in powder form before dissolving them in chloroform. The number of fluorophores per square micron was then calculated by assuming a lipid head size of 0.7 ± 0.1 square nanometer (corresponding to the size of Egg PC lipids [136] which gives $(2 \times 10^6)/0.7 = (2.9 \pm 0.4) \times 10^6$ lipids per micron square. This range of Bodipy-HPC concentrations was large enough to effectively test the linearity of the detector over the intensity range studied while still avoiding fluorophore saturation [135]. For each fluorophore density, approximately 10 vesicles were scanned. Confocal images of the GUV equatorial plane were analyzed as described above. As shown in figure 4.14, the fluorescence intensity depended linearly on the fluorophore concentration and the slope of the plot was equal to $M_{ref} = a \times I_{0,ref}$. To expand the range of the calibration, measurements were performed at several PMT gain settings.

4.4.3 Fluorescence yield

To compare the relative fluorescence intensity of Bodipy-HPC and KvAP-alexa 488, the fluorescence from homogenous solutions of these two fluorophores was measured with the confocal microscope.

SUVs containing Bodipy-HPC or the fluorescent protein were prepared as described in section A.4 of Annexe A. Several solutions with different fluorophore concentrations (1 to

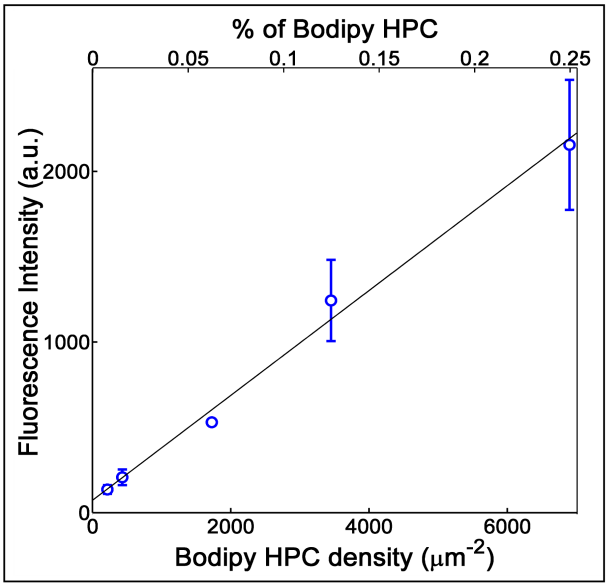

Figure 4.14: Membrane fluorescence intensity as a function of Bodipy-HPC density. Each point represents $\backsim$ 10 vesicles (except for the third point (density $1800\mu m^{-2}$) which represents a single vesicle) and error bars show the sample standard deviation.

20 μM) were then obtained by diluting the SUVs in the external buffer solution (200mM glucose, 150mM NaCl, 10mM HEPES at pH 7.3). The absorbance of the solutions containing DM was measured with a Nanodrop (Thermo Scientific) to determine fluorophore concentration ($A_{509} \approx 70000 mol^{-1} cm^{-1}$ for Bodipy-HPC and $A_{494} = 71000 mol^{-1} cm^{-1}$). Each solution was then loaded into a chamber on the microscope and images taken at 3 different places in the chamber. To match the GUV imaging conditions, the objective was focused at a height of 10 microns above the coverslip. The mean intensity of the fluorescence was then measured in a region near the optical axis of the microscope where the intensity was most uniform.

Although the SUVs in solution should have been much smaller than the optical resolution of the microscope, bright saturated spots in the images suggested the presence of lipid aggregates. As these spots saturated the PMT, they could have introduced a non-linearity into the measurements and attempts were made to eliminate them. Additional sonication of the solutions produced more homogenous images, but also reduced the overall fluorescence suggesting that sonication can damage fluorophores. Dissolving the SUVs in detergent (50 mM DM) also produced a homogeneous solution, but the presence of detergent may affect the fluorophore environment and yield. However, the fluorescence intensity of SUVs and SUVs dispersed in detergent were quite similar, suggesting that aggregates did not strongly influence the measurements.

For both Bodipy-HPC and KvAP-alexa488, the fluorescence intensity was proportional to fluorophore concentration. The ratio of fluorescence intensity in bulk for Alexa 488 on KvAP and per fluorophore was found to be $F = 0.94 \pm 0.10$.

Note that this measurement is for an isotropic solution. In contrast, in GUVs the

fluorophores can have a net orientation relative to the bilayer normal. If the reference fluorophore and protein fluorophore have different net orientations, the fluorescence yield ratio in GUVs may be altered by a polarization factor.

4.4.4 Protein density in GUVs

GUVs were prepared using the low salt protocol described in Annexe B. Briefly, for this experiment, proteo-SUVs were diluted in 2 mM trehalose down to 2 mg/ml. The rehydration buffer was sucrose 400 mM, KCl 5 mM, Hepes 1 mM pH 7,3, EDTA 2 mM. For the data shown in figure 4.15, the SUVs had a lipid/protein mass ratio of 10.5±2.5. For a mean lipid molecular mass ($770 \times 0.9 + 697 \times 0.1 = 763$ g/mol for our EPC:EPA 9:1 mix) and channel mass of $4 \times 30860 = 123440$ Da, this corresponds to $(1,8 \pm 0,4) \times 10^3$ lipids per protein. The protein density in the SUVs should then be $(1,6 \pm 0,4) \times 10^3$ proteins per square micron. The fluorescence intensity of GUVs was measured as described in section 4.3.2. Interestingly, GUVs containing a high concentration of protein did not sediment rapidly and had low contrast when imaged in DIC. These observations suggest that sucrose/glucose was able to exchange across the membrane, which might result from a failure to completely eliminate bacterial porins during the purification or a bacterial contamination in the proteo-SUVs. However, any contamination by porins must be minor as they were not observed during patch-clamp recordings of GUVs. To allow as many GUVs as possible to sediment to the bottom, measurements were only started one hour after transferring GUVs to the observation chamber.

For each vesicle, the protein density was calculated using $D = I/(N_f \times F \times M_{ref})$ Where F is the protein labeling ratio determined in section 3.4. The results for N=72 vesicles are shown in figure 4.15.

The distribution is fairly broad but the average GUV protein density of 1000 ± 700 proteins/μm^2 is comparable to the protein density of the SUVs from which they were prepared. While a few GUVs did not contain detectable level of channels, KvAP was detectable in the vast majority with some containing well in excess of 1000 proteins/μm^2.

To summarize, protein density in GUVs was measured using the fluorescence of labeled KvAP. A calibration using vesicles containing a controlled amount of a reference fluorophore was used to relate membrane intensity to fluorophore density. The fluorescence yield ratio between the reference fluorophore and protein was then used to directly relate membrane fluorescence intensity to protein density.

In general, the average density of channels in GUVs could be controlled by adjusting the protein-to-lipid ratio of the SUVs allowing to get as low as few channels per square micron up to thousands of channels per square micron, so in the same range as density of channels in cells [5].

4.4.5 Effect of growth protocol on channel density in GUVs

In general, GUVS prepared with low-salt buffer had a narrower distribution of protein densities than GUVs prepared with "physiological" salt buffer. Figure 4.16 presents protein density histograms for two extreme cases. The very homogeneous distribution shown in the upper histogram corresponds to a batch of proteo-GUVs prepared using electroformation in low salt buffer. The extremely broad distribution shown in the lower histogram

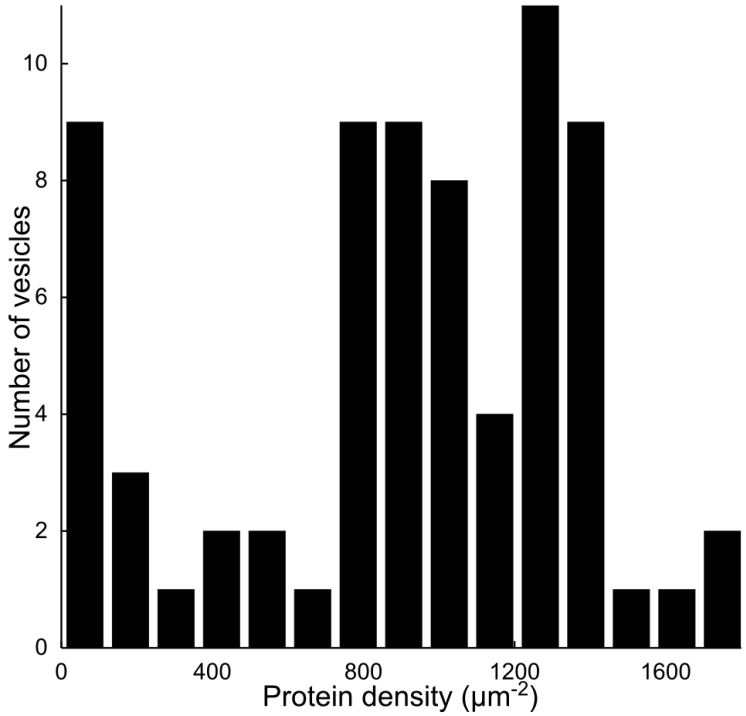

Figure 4.15: Histogram of protein density in GUVs. GUVs were formed using a low salt buffer (5 mM KCl, 1 mM HEPES, 400 mM sucrose) and protein density measured via quantitative confocal fluorescence. The average protein density of the GUVs (1000 ± 700 proteins/μm^2) is comparable to the protein density of the (EPC:EPA) SUVs from which they were formed (1600 ± 400 proteins/μm^2).

corresponds to a batch of GUVs prepared via a long electroformation in "physiological" salt buffer. For this batch of GUVs, many vesicles contained nearly no protein and a few contained a high protein density.

It is important to note that even though the protein density was greatly different between GUVs, the protein was still homogeneously distributed within each GUV. To exclude the possibility that vesicles highly enriched in protein were in fact multilamellar, protein density was measured for GUVs containing TR-DHPE grown using the "physiological" salt buffer. For these GUVs, lipid fluorescence could be used to detect multilamellar objects. As shown in figure 4.17, the wide protein density distribution is not due to multilamellar objects.

4.5 Activity measurements: patch clamp on GUVs

The fluorescent measurements described in the previous section showed that the channel was well incorporated in GUVs. To determine if these channels were functional, their activity was studied using the well-established patch-clamp technique [8] (see section 2.1.2.1 of chapter 2). This technique has been routinely used to study ion channels in

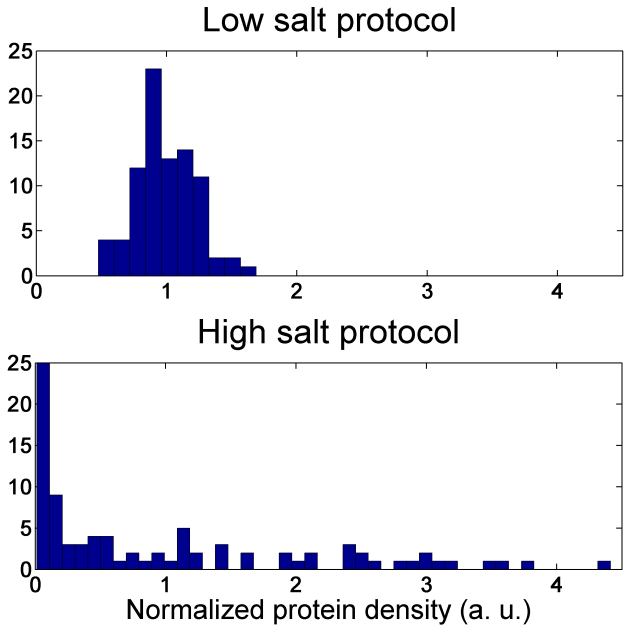

Figure 4.16: Dependence of protein density on GUV preparation method. Histograms of protein density for batches of GUVs prepared in low salt buffer (upper, N=86) and high salt buffer (lower histogram, N=88). Note these batches are extreme cases of homogenous and heterogeneous distributions. Low-salt GUVs are not always so uniform (e.g. 4.15) while high-salt GUVs are not always so disperse (e.g. Figure 4.17).

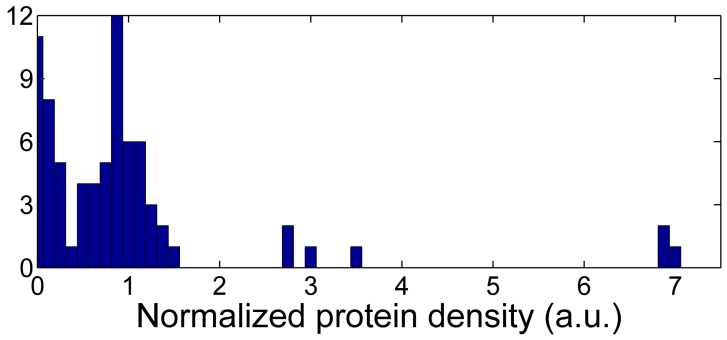

Figure 4.17: Variability of protein density in "high salt" GUVs is not due to multilamellarity. Protein density histogram (N = 75) of the population of high salt proteo-GUVs presented in Figure S10 (which were shown to be unilamellar). although the GUVs are unilamellar, the protein density still varies between GUVs with very high protein densities in a couple of GUVs.

cells, but have also been used with reconstituted systems (MLVs see 4.1.1.2). Only a few studies have shown its use with GUVs (see for exemple [119].

The experiments in this section have been done by Gilman Toombes.

4.5.1 Patch-clamp on GUVs

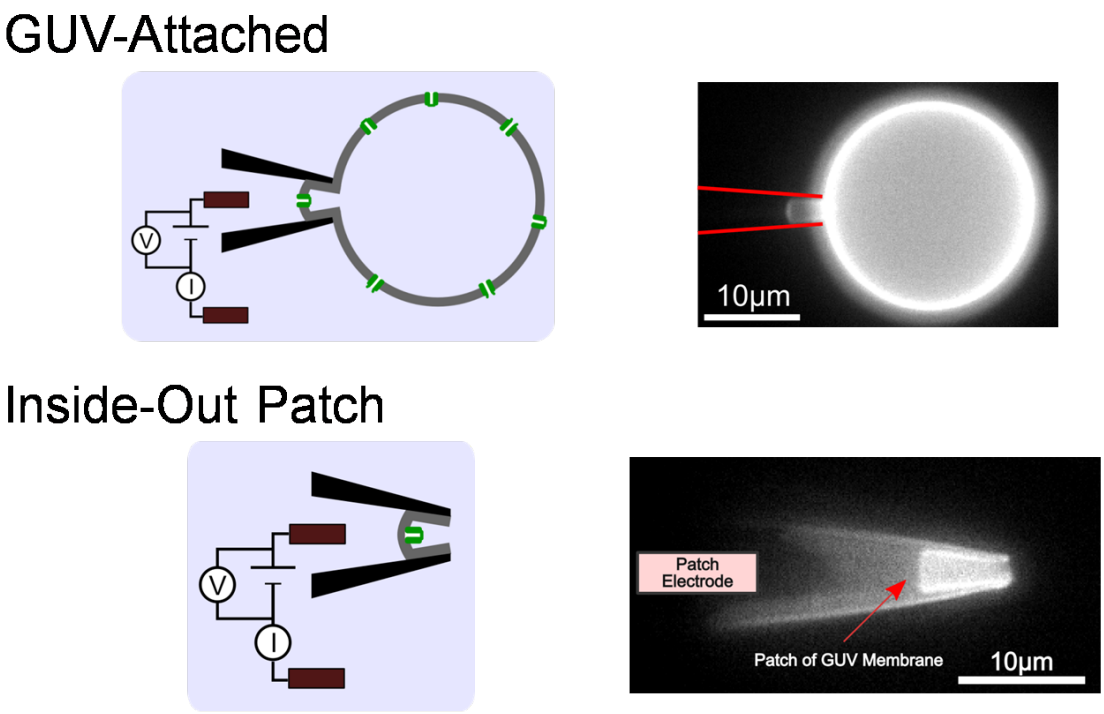

Figure 4.18: Summary of patch-clamp configurations.Top, GUV-attached configuration. A glass pipette containing an electrode is stuck on a vesicle. Another electrode is in the bath. The current going from one electrode is recorded for a given applied tension. Bottom, the patch has been separated from the vesicle (inside-out configuration).

As shown in figure 4.18, the principle is to stick a small and very clean pipette to the vesicle. The current going from one electrode in the pipette, through the membrane, and towards the other electrode in the bath is then recorded. In practice, this is done by approaching the vesicle while blowing with the pipette (to keep it really clean) and then aspirating (10-500 Pa) when really close to the vesicle to have a piece of the GUV membrane stuck into the patch pipette. That allows a good contact between the membrane and the glass; the resistance is then the order of a gigaohm (this tight seal is thus called a "Gigaseal"). The good seal thereby permits measurements of the current through the patch (down to single channels) at a fixed voltage (voltage-clamp mode). Measurements were then made either in the GUV-attached or the "inside-out" geometry as shown in figure 4.18.

Patch pipettes were pulled from borosilicate glass (KIMaX 51, I.D. = 0.7mm, O.D. = 1mm, Catalog number 46481-1, Kimble Chase Corp., NJ) using a P-2000 puller (Sutter Instrument Company, Novato, Ca). Tip diameters were typically between 1-4 microns with

a resistance between 2-5 MOhms. The acquisition of the signal was done with an axon Multiclamp 700B Microelectrode amplifier (Molecular Devices, St Gregoire, France), and a PCI-6221 DaQ Card (National Instruments, Nanterre, France) controlled via LabView (National Instruments). Current traces were filtered at 1kHz (4-pole Bessel) and sampled at 5kHz. Membrane currents and voltages are presented with respect to the GUV interior (i.e. V = -Vpipette; I = -Ipipette). Epi-fluorescence images of the GUV and patch pipette were taken with a ProSilica GC1380 camera (t_{exp}=50 or 100ms; allied Vision Technologies, Stadtroda, Germany) to measure the distribution of the protein (marked with alexa Fluor 488) and membrane (TR-DPPE, 0.125% by mol).

4.5.2 Single channel currents

Figure 4.19 shows an example of a current trace recorded from a DPhPC proteo-GUV membrane patch under symmetric conditions (100mM KCl in patch pipette and bath). Upon jumping to +100mV, rapid transitions between distinct current levels were observed, consistent with the opening and closing of individual channels with a conductance of 100pS. In general, membrane patches showed far more channel events at +100mV than at -100mV (see figure 4.23, for example). This suggests that the channels in the patch membrane are both voltage-gated (as described in detail below) and preferentially oriented. Because the open probability of KvAP increases with voltage [97], the opening of channels at more positive voltages implies that they are inserted "physiologically" (i.e. with their intra-cellular domain facing into the GUV interior as shown in figure 4.25).

For figure 4.20, the same electrical protocol was applied to a vesicle prepared using the low salt protocol in EPC:EPA, thus showing that the GUV formation protocol or the membrane composition didn't notably affect the channel activity.

4.5.3 Selectivity for potassium

To characterize ionic selectivity, experiments were conducted in which 90 % of the KCl in the pipette solution was substituted with NaCl. A potassium channel would block the diffusion of Na+ ions out of the pipette ($[Na^+]$pipette = 90mM $\gg$ $[Na^+]$bath), while allowing the diffusion of K^+ into the pipette($[K^+]$bath/GUV = 100mM, $[K^+]$pipette = 10mM, V_{Nernst} = -58mV see equation 5.6) as schematized in figure 4.21. Thus, even when the voltage across the membrane is zero, current should flow through a potassium channel as K+ ions diffuse into the pipette.

To measure the channel selectivity, patch-clamp experiments were performed in these buffer conditions (patch pipette was filled with 10mM KCl, 90mM NaCl, 4mM HEPES (pH 7.2) whereas bath was 100mM KCl, 4mM HEPES (pH 7.2)). Sections of current traces consistent with single channel gating events (like the one in figure 4.22A) were identified by eye, and a histogram of the current was fitted to two gaussian functions representing the "open" and "closed" current levels. The mean single-channel current and standard error of the mean were calculated for each membrane voltage.

As shown in Figure 4.22, the K+ gradient drove current through the channels even when opposed by a small negative voltage (-4mV). The dependence of mean single-channel current on applied voltage is shown in 4.22B. The combination of a positive voltage and the concentration gradient drives large currents, while at negative voltages the current

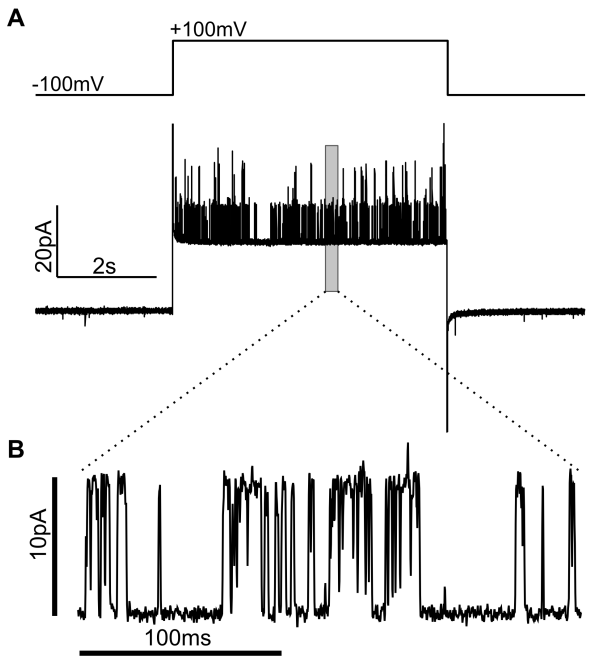

Figure 4.19: Activity of GUV Membrane Patches. a) GUV membrane patch current in response to an applied voltage step. Patch and bath solutions were both 100mM KCl, 4mM HEPES, pH 7.2, and the patch was formed from a DPhPC containing KvAP. B) Section of the trace showing distinct jumps in conductance (100pS) that are consistent with the opening and closing of individual channels.

reduces as the potential opposes diffusion. A sufficiently negative voltage should reverse the current, but this was challenging to observe as channel events became increasingly rare at more negative voltages (consistent with voltage-dependent gating). However, the channels must be strongly selective as outward channel currents were observed at fairly negative voltages (e.g. V $\sim$ -50mV). A linear fit for the range, V <0, yielded a conductance of $93 \pm 2pS$. This value is comparable with the conductance measured in BLM (170 pS for 150 mM of KCl) [97]. The reversal voltage of $-57 \pm 3mV$ (figure 4.22B), which is within experimental error of the Nernst potential for potassium.

These observations imply that KvAP in GUVs is highly-selective for potassium, consistent with its earlier characterization in BLMs [97].

4.5.4 Voltage dependence

Voltage-gating was tested by holding the membrane voltage at -100mV (30 seconds per cycle) before applying a transient voltage step (5.5 seconds duration) to a more positive voltage. The mean current during the interval from 0.5s to 1s after the beginning of the voltage-step was used to estimate the peak patch current and conductance. To characterize the ensemble behavior, these experiments were performed using larger patch pipettes (diameter of 3-4 μm) so as to obtain membrane patches containing more channels. Patch

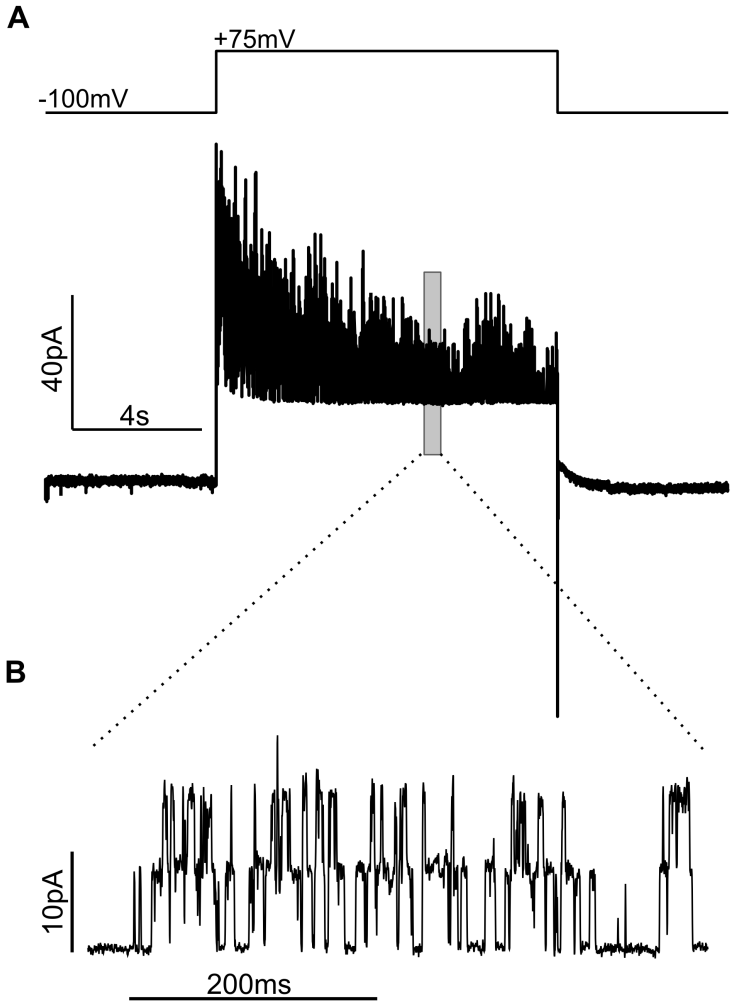

Figure 4.20: Activity of Membrane Patch from a GUV formed with low-salt buffer. a) GUV membrane patch current in response to an applied voltage step. Patch and bath solutions were both 100mM KCl, 4mM HEPES, pH 7.2, and the patch was formed from a EPC:EPA (9:1 by mole) GUV formed using low-salt buffer (5mM) B) Section of the trace showing distinct jumps in conductance that are consistent with the opening and closing of individual channels.

and bath solutions both contained 100mM KCl, and the patch was held at -100mV between voltage steps.

As shown in Figure 4.23A, stepping to a positive voltage caused channels to open rapidly. The moderate decrease in current during the step is consistent with some channels entering the inactivate state [100]. Finally, channels rapidly closed at the end of the step as the voltage returned to -100mV. The tendency for more channels to open with increasing voltage is clearly evident in the dependence of peak membrane conductance on applied voltage (Figure 4.23B). For V $<$ -25mV, very few channels were open and the

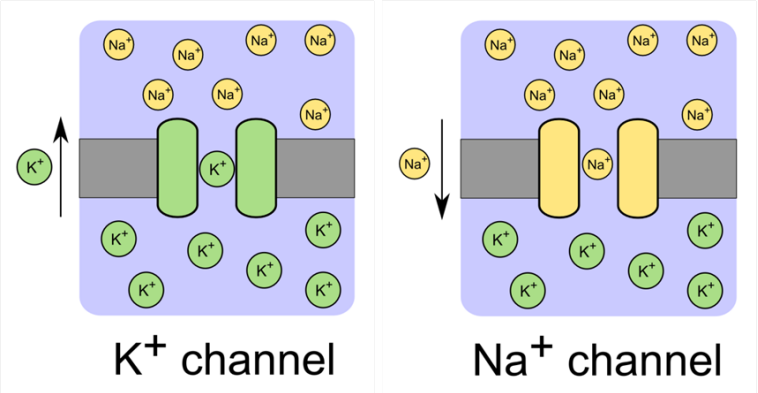

Figure 4.21: Ionic selectivity. If 0 mV are applied to the membrane but the salts are different on both sides, a potassium selective channel would let potassium diffuse against its concentration gradient whereas a sodium channel would lead to a sodium current in the opposite direction. The sign of the measured current in these conditions thus gives information about the selectivity of the channel for a specific ion.

conductance was dominated by the leak current of patch. In contrast, at very positive voltages (V $\geq$ 100mV), approximately 50 channels were open on average (assuming a channel conductance of $\sim$ 100pS).

These results implies that the channel is still voltage gated after its reconstitution in GUVs.

4.6 Discussion

4.6.1 Advantages (and disadvantages) of the reconstitution method

4.6.1.1 Yield and cleanness

The results presented in this chapter indicate that the SUV dehydration/electro-formation method is an effective method to reconstitute KvAP into GUVs. Starting with a modest amount of material ($\sim 10\mu g$ of SUVs), the method yielded hundreds of GUVs per chamber. The size of GUVs was similar, although slightly smaller, to that obtained via classical electro-formation (diameter $\sim$ 10 microns). Like many GUV preparation methods, the protocol produced a fraction of multi-lamellar objects. However, most GUV experiments manipulate or at least analyze GUVs individually so multi-lamellar objects can be readily detected (and excluded) by fluorescence microscopy. Note also that changing the method to detach the vesicles from the wire and transfer them to another chamber could improve the final unilamellar/multilamellar ratio a lot. For example, applying a square electric field at the end of the electroformation could help to detach the GUVs from the remaining lipid stacks on the wire [121]. Yet, note that further caracterisation would be needed to make sure that currents induced by the square wave wouldn't damage the protein.

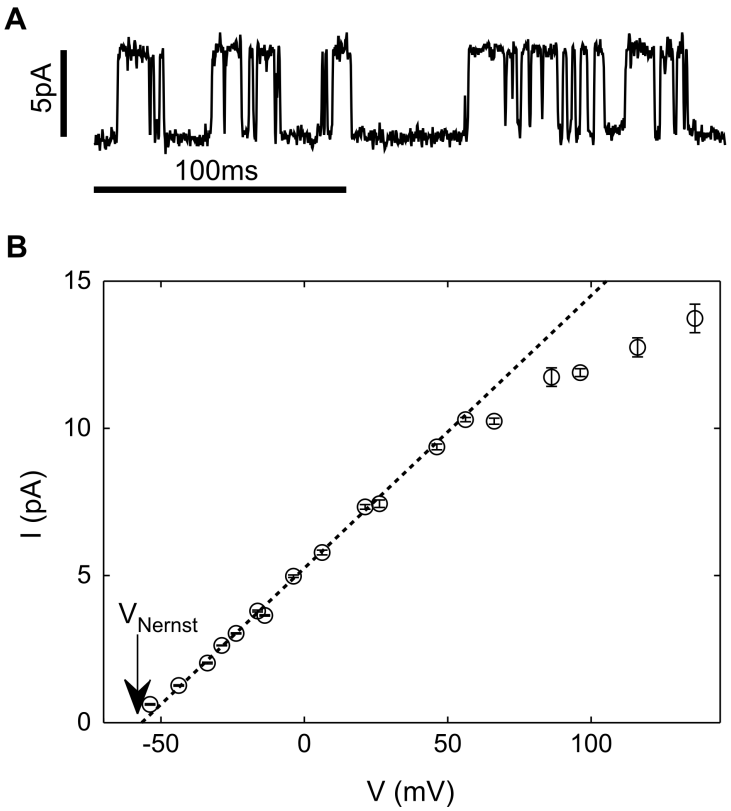

Figure 4.22: Ionic selectivity. A) Single channel current driven by ionic diffusion ([K^+]bath = 100mM, [K^+]pipette = 10mM, V_{Nernst} = -58mV) overcome a small negative applied membrane potential (V = -4mV). C) Dependence of single channel current, I, on membrane voltage, V. a linear fit for negative voltages (dotted line) gives a conductance of $93 \pm 2pS$ and reversal voltage of $-57 \pm 3mV$.The experiments were carried out at room temperature (20 ℃) using fluorescently labeled KvAP reconstituted into DPhPC GUVs grown in 100mM KCl.

4.6.1.2 Membrane and buffer compositions

Importantly, the protocol does not require any specific membrane components (e.g. charged lipids, peptides, etc.), and GUVs were grown with several different membrane compositions simply by changing the composition of the initial SUV solution. This ability to vary membrane composition is very important for studies of protein-membrane interactions. Furthermore, even though electro-formation has traditionally been applied using low-salt buffers, GUVs could be effectively prepared in buffers containing physiological salt concentrations by applying a voltage with a higher frequency (∼500Hz) [132]. Thus, this approach allows the formation of GUVs without imposing serious constraints either on GUV composition or internal solution.

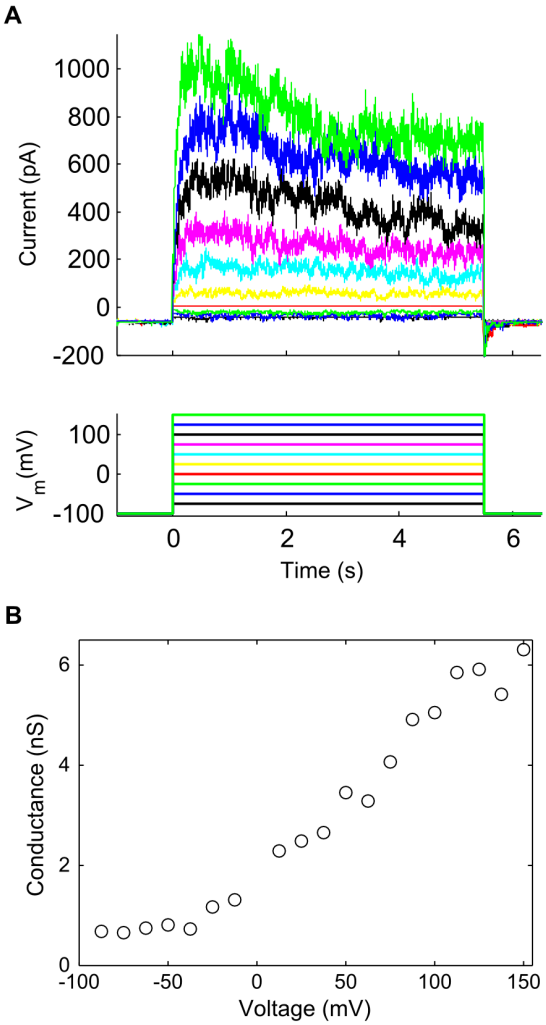

Figure 4.23: Voltage-dependent gating. A) Response of patch membrane current (top) to a transient step in voltage (bottom). Pipette and bath solutions both contained 100mM KCl, and the membrane was held for 30 seconds at -100mV between successive voltage steps. Membrane current was filtered at 500Hz. B) Peak conductivity as a function of voltage. Experiment carried out at room temperature ($\sim$ 20°C) using fluorescently labeled KvAP reconstituted into DPhPC GUVs grown in 100mM KCl.

4.6.1.3 Density and state of the protein

A calibration method was developed to allow quantitative measurements of the protein density in GUVs using only a confocal fluorescence microscope. Images of the labeled channel in GUVs showed that the protein was homogeneously distributed at optical length-scales, while measurements of protein diffusion were also inconsistent with the formation of large aggregates (see chapter 6). However, the protein incorporation depended on whether GUVs were grown using "low-salt" or "physiological" buffer. For GUVs prepared using a

low salt buffer, the average protein density in GUVs was comparable to the density of the SUVs from which they were formed. Furthermore, some batches of GUVs had a very small variation in the concentration of protein in individual GUVs. Thus, under these conditions the protein density in GUVs could readily be controlled by varying the density in SUVs. In contrast, GUVs formed in "physiological" buffer exhibited a very broad distribution of protein densities with some GUVs containing practically no protein while others contained densities higher than the initial concentration in SUVs. Such compositional heterogeneity has previously been observed in GUVs formed from immiscible lipid mixtures when either the film deposition or electroformation is performed at too low a temperature [137]. As both low and "physiological" salt GUVs are prepared from the same protein-lipid film, it seems likely that the heterogeneity occurs during the growth of GUVs from the film rather than during the deposition. Practically, the compositional heterogeneity of GUVs formed with physiological buffer can even be advantageous, as an experimenter can select GUVs with different protein densities from a single GUV batch. While more work is required to better understand and control protein incorporation, the present protocol produces GUVs with protein densities up to $\sim$1000 channels/μm^2. The density of voltage-gated ion channels in cell membranes varies widely from close to zero ($\sim$ 1 channel/μm^2) to several thousand channels per square micron in specialized regions such as the nodes of Ranvier in the axon [5]. The channel density in the GUVs is comparable to this range and high enough to permit a wide range of biophysical measurements.

Furthermore, with this technique, we could use different lipid compositions but no specific species, such as charged lipids or peptides were necessary to produce the proteo-GUVs. For a long time, it was thought that the electroformation technique was incompatible with the use of solutions containing physiological (e.g.$\sim$ 100mM) salt concentrations. However, it was recently shown that this limitation could be overcome by using a higher frequency for the applied electric field [132]. Thus, this approach allows the formation of GUVs without imposing serious constraints on GUV composition or internal solution. A concern could be that the electrical field could alter KvAP conformation as the channel has a charged domain sensitive to changes of electric potential. Confocal images and diffusion measurements were also inconsistent with the formation of large aggregates. More importantly, activity measurements showed that there were well-folded voltage gated potassium channels in the GUV membrane.

4.6.2 Preliminary comparison of protein activity between BLM and GUVs

The activity of the reconstituted protein was tested via patch-clamp. These measurements showed that the channels in the GUV membrane were both selective for potassium and voltage-gated.

However, the observed voltage-dependent gating is not identical to the reported KvAP gating in DPhPC BLMs [100]. In particular, the increase in channel opening probability occurs both more gradually and at more positive voltages for our channel, while channel inactivation is both markedly slower and incomplete in GUVs as compared to BLMs (see figure 4.24).

Several factors could account for the interesting differences between KvAP dynamics

in our DPhPC GUVs and in DPhPC BLMs from the literature [138] as well as in our POPE:POPC BLMs. Amphipathic agents such as alcohols and anesthetics that are known to insert in the membrane have been reported to modulate KvAP gating in BLMs [78], suggesting that the protein is sensitive to the membrane environment. Thus the difference in membrane tension between the GUV membrane patch and BLM, or the presence of residual alkane in the BLM, could modify channel inactivation.

Additionally, the Alexa 488 label could have an effect. Indeed, a recent study of KvAP-DNA chimera in which ssDNA was attached to a site near the native cysteine (V240C) found that channel opening shifted to much more positive voltages with a less sharp voltage response [139]. While further work is required, the ability to use GUVs to study the ensemble behavior of channels while controlling membrane parameters should help greatly in understanding membrane/channel interactions.

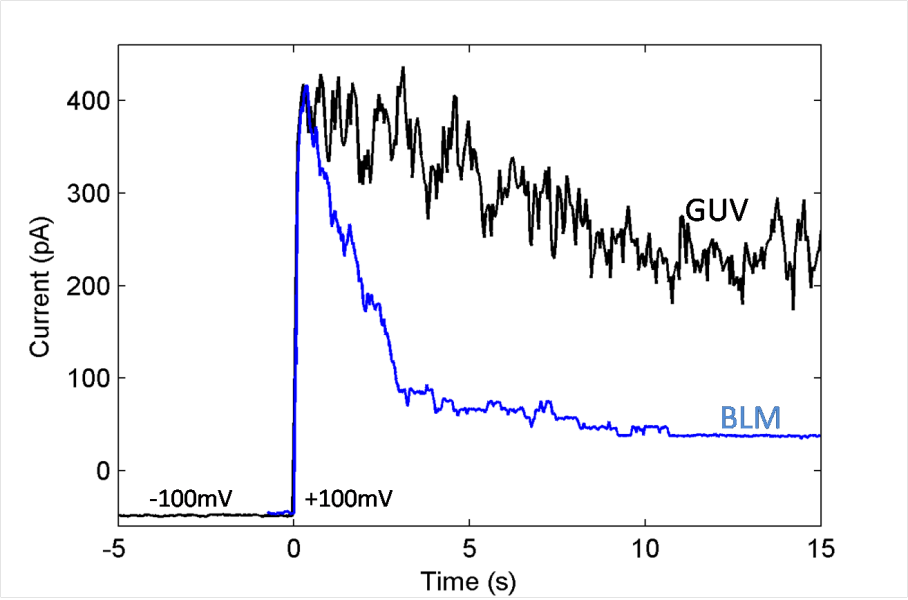

Figure 4.24: Difference in activation in the BLM and in the GUV. For the same channel (KvAP labeled with alexa 488) and the same protocol (but different lipids), channel inactivation is much faster in the BLM than in the GUV patch.

4.6.3 Proportion of active channels

While it is tempting to compare the number of active channels in a membrane patch to the density of channels in the GUVs, studies have shown that the composition of the cell and patch membrane can differ[140]. To compare the composition of patch and GUV membranes, patch-clamped GUVs were imaged via epi-fluorescence as shown in Figure4.25. Fluorescence from the channels (green) and membrane (TR-DHPE ; red) were scaled to be equal on the GUV body so as to permit direct comparison of the fluorescent protein/lipid concentration. The protein concentration in the patch membrane is clearly lower as it cannot be observed using protein fluorescence yet lipid fluorescence can be

easily resolved. Epi-fluorescence is not ideal for making a quantitative estimate due to the strong fluorescent signal from the GUV, but the protein/lipid concentration must be at least 10 times lower in the patch membrane. This observation suggests that channels are strongly excluded from the patch membrane and prevents a simple comparison of patch and GUV membranes. This observation illustrates just how different the composition and tension of the patch membrane can be from the source membrane [140], and this very different environment must be considered when comparing the behavior of channels in membrane patches and cells.

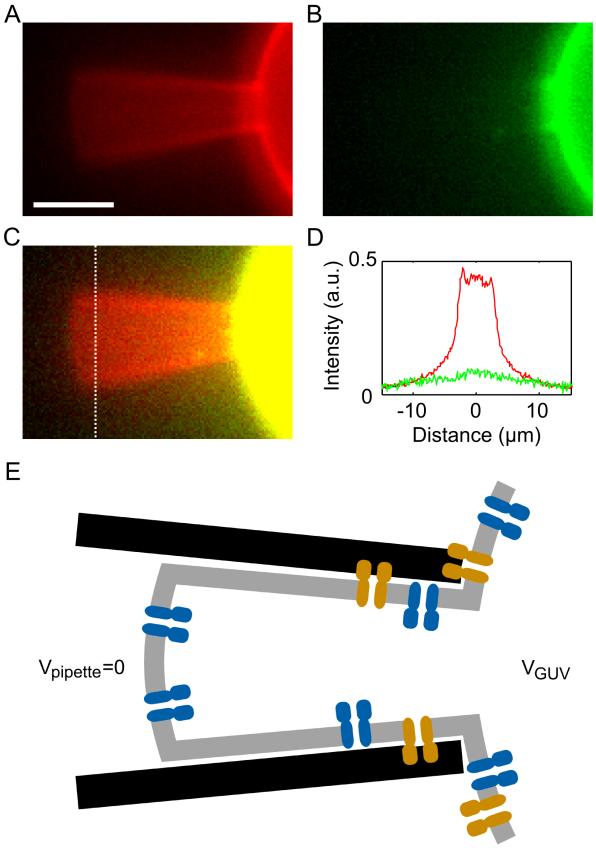

Figure 4.25: Protein concentration in the patch membrane. A-B) Epi-fluorescence image of the patch pipette and GUV showing the lipid (A, red) and KvAP (B, green). Red and green channels are scaled to be equal on the GUV body. C) Merged image with contrast increased to show the absence of protein (green) fluorescence in the patch. Scale Bar : $5\mu m$. D) Fluorescence intensity across the patch membrane (dotted line in C) of lipid (red) and KvAP (green). E) Schematic illustrating how adhesion between the membrane and pipette could favor the "correct" (blue; intracellular domain facing into the GUV interior) insertion over the "reverse" insertion (orange). The larger intracellular domain of the "reverse" insertion may stick more easily to the patch pipette walls, thereby excluding it from the patch membrane.

4.6.4 Channel insertion

It was somewhat unexpected that the active channels in the patch membranes were inserted almost exclusively in the physiological orientation (e.g. cytoplasmic domain facing into the GUV interior). Although membrane proteins reconstituted into SUVs can have a net orientation, it seems likely that this would be scrambled during the SUV fusion and that GUVs would contain approximately equal amounts of both insertions [141]. Interestingly, previous patch-clamp studies of KcsA [142] [143] and KirBac [144] reconstituted into MLVs also reported that channels were predominantly oriented with this same orientation (cytoplasmic domain facing into the MLV interior). Figure 4.25E illustrates how this orientation could result from interactions between proteins and the patch pipette. During the formation of a "giga-seal", the membrane tightly adheres to the patch pipette [140]. After adhesion to the glass, lipids remain quite mobile while proteins are effectively immobilized. In crystal structures of KvAP [99], KcsA [145], and KirBac [146], the channel does not project very far out from the extra-cellular side of the membrane, while the C-terminal tails of Kcsa and KirBac form comparatively large intra-cellular domains (in available crystal structures of KvAP the C-terminal tail is disordered or truncated). Thus, the channels oriented with the intra-cellular domain facing out ("non physiological" orientation) may stick easily to the glass, while a low fraction of channels with the "physiological" orientation may be able to more easily enter/stay in the patch membrane. Although channels may be preferentially oriented in MLVs and GUVs, this adhesion-based mechanism would account both for the reduced density and preferred orientation of channels observed in the patch membrane.

4.7 First application of the reconstitution method: KvAP distribution in inhomogeneous membranes

In neurons, biochemical and functional data [89] have been used to infer the localization of several Kv channel types in so-called "lipid rafts", dynamic small membrane domains enriched in cholesterol and sphingomyelin [27]. Furthermore, some studies have shown that

In our vesicles, studying the partitioning of Kv channels between domains could probe protein-membrane interactions and test whether lipid interactions contribute to the localization of Kv channels in cells.

As a proof of principle, SUVs were mixed to have a final composition of DPhPC:DPPC(1,2-dipalmitoyl-sn-glycero-3-phosphocholine) :Chol (6:2:2 by mole), with KvAP (protein:lipid 1:20 mass ratio) and 0.5 percent of TR-DHPE. GUVs were then prepared using a low salt buffer. To avoid phase separation of this mixture during the GUV formation, the deposition of SUVs, drying and electroformation were all performed at 50 ℃. Note that exposing this mixture to elevated temperatures is not expected to lead to significant lipid oxidation [147]. DPhPC:DPPC:Chol has a well characterized phase diagram [148], and membranes with this composition (6:2:2) exhibit liquid ordered and liquid disordered domains at room temperature. TR-DHPE has been shown to preferentially segregate into liquid disordered phases [149]. Figure 4.26 shows a confocal image of a GUV containing co-existing domains. The protein (green) colocalizes with the TR-DHPE,

which is consistent with enrichment of the channel in the liquid disordered phase.

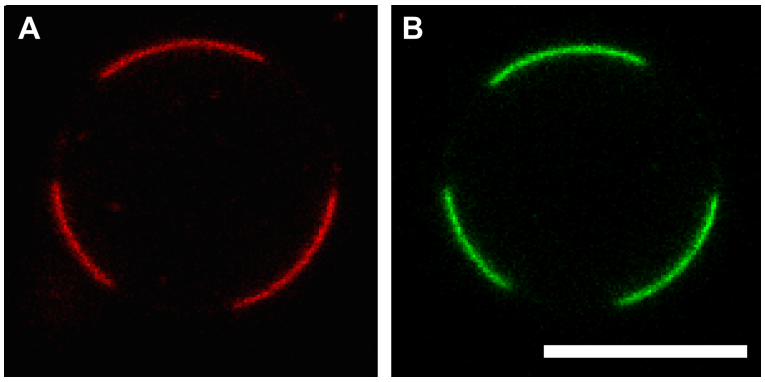

Figure 4.26: Co-existing liquid domains in GUVs containing KvAP. a) Confocal fluorescence image of TR-DHPE, a red fluorescent lipid that preferentially segregates into the liquid disordered phase. B) KvAP (green) is enriched in the same membrane domains. The GUV was formed from a lipid mixture of DPhPC, DPPC, and Chol (6:2:2 by mole with 0.25 % of TR-DHPE) and KvAP was included at a protein to lipid ratio of 1:14 (by weight). The gain has been adjusted to show the membrane more clearly. Scale bar : 5 μm.

Note that it is difficult to conclude about the affinity of the channel for rafts from this experiment at this point as even proteins known to have a strong affinity for rafts in vivo have been observed in Ld domains in similar in vitro experiments.

Nevertheless the next step would be to use different lipids (in particular phospholipids, sphingomyelin and ceramide-1-phosphate) to see whether some specific interactions between the channel and those lipids could change the repartition of the channel between the liquid ordered and the liquid disordered phase. These effects could in principle be studied in detail by tuning composition of the different phase and temperature. Quantitate image analysis of reconstituted 3D images of vesicles [150] would then allow measuring partition coefficients which would give informations about the protein-lipid interactions.

4.8 Conclusion

To conclude, we have presented a method to reconstitute KvAP into optically defect-free spherical Giant Unilamellar Vesicles (mean diameter $\sim$ 10 microns). GUVs could be formed from membranes with different compositions and the protein density was quantitatively characterized. Furthermore, patch clamp measurements of GUVs confirmed that after reconstitution the channel remained potassium-selective and voltage-gated.

As will be discussed in the conclusion chapter, GUVs containing functional voltage-gated ion channels should prove a powerful tool for studying channel/membrane interactions so as to understand how the membrane influences ion channel activity, distribution and diffusion and modulates cellular excitability.

In this part I have shown that:

- KvAP was successfully reconstituted in GUVs
- Membrane composition (several lipid tested), buffers (high and low salt) and protein density (<1 to few thousands proteins/μm^2) could be controlled
- Channels were still selective for potassium and voltage gated after reconstitution
- It is possible to use those vesicles to study the affinity of the channel for different membrane compositions (by doing heterogeneous GUVs and looking at the channel distribution)

Chapter 5

Enrichment of KvAP in curved membranes

As presented in the chapter 2 (and will also be detailed in this chapter), membrane protein lateral distribution can depend upon membrane geometry. Indeed, if membrane proteins locally curve the membrane around them, we expect they will also be preferentially localized in an already curved membrane [51].

In chapter 3 and chapter 4, I have described the experimental steps to reconstitute KvAP in Giant Unilamellar Vesicles. I will now show how we can use this model system to measure KvAP distribution as a function of membrane geometry.

5.1 Motivation

5.1.1 Membrane curvature in cells

Cell membranes have a large distribution of curvatures. As shown in figure 5.1A, the plasma membrane is relatively flat at a large scale (curvature radius of approximately 10 microns) but they also contain many endocytotic or exocytotic vesicles with radii ranging typically between 30 and 100 nm. Another example of curved plasma membrane is the neuronal membrane with neurite radii that can be as small as 20 nm [151]. The internal organelles of the cell can have highly curved membranes too. See for example the Golgi apparatus, endosomes and mithochondrion shown in figure 5.1 (B, C and D respectively) and the Endoplasmic Reticulum.

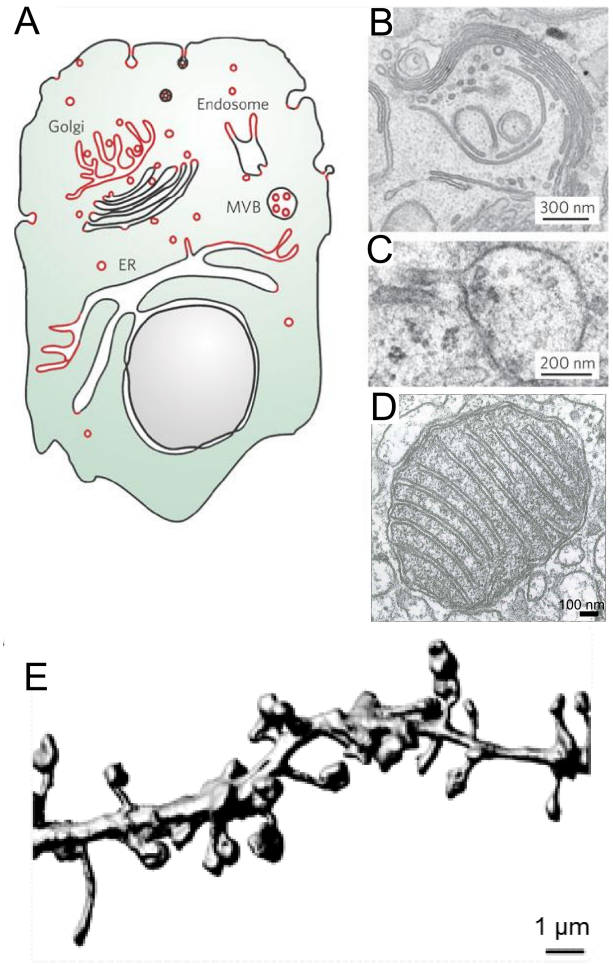

Figure 5.1: Membrane shape in the cell. A) Curved and flat membranes in a typical cell. Membranes of high positive curvature are highlighted in red. MVB, multi-vesicular body; ER, endoplasmic reticulum. Right, electron micrograph of B) Golgi C) Endosome D) Mithochondrion. A), B) and C) are from [152] while D) is from [23]. E) 3D reconstruction of a neurite imaged with STED (Stimulated Emission Depletion microscopy) (from [153]).

5.1.2 Coupling membrane composition and curvature

5.1.2.1 Lipid sorting in curved membranes

Lipid membrane composition highly depends on organelles [154]. However, there is a constant exchange between organelles via vesicle trafficking which should produce in principle a homogeneous lipid distribution. It was proposed that lipid sorting occurs when a trafficking vesicle is formed [155]. The vesicles could be formed from preexisting lipid domains in the membrane (the "rafts" presented in section 2.2.1.1 of chapter 2), and proteins binding to the membrane could also induce membrane reorganization [27].

Another possible mechanism could be a coupling between lipid composition and mem-

brane curvature, so that membrane composition would change when membrane geometry changes in order to reduce the mechanical energy (see figure 5.2).

As described in chapter 2 the energy to bend an homogeneous membrane of area A is given by

$$E_{curv} = \frac{1}{2}\kappa(C - C_0)^2 A \tag{5.1}$$

where C is the mean curvature, C_0 is the spontaneous curvature and κ is the bending rigidity. Two membrane reorganization mechanisms could thus lead to a decrease of the energy of the curved membrane:

- Lipids can locally reorganize between the two leaflets to have lipids with a large head group and a small tail on the exterior and lipids with a small head group and a large tail in the interior (figure 5.2A). This leads to a local change of membrane spontaneous curvature (C_0).
- The species producing a softer membrane can be enriched in the curved part (figure 5.2B) which leads to a local decrease in bending rigidity (κ).

Note that on the other hand, entropy will tend to disperse any concentration heterogeneity, as will be discussed in detail in section 5.4.

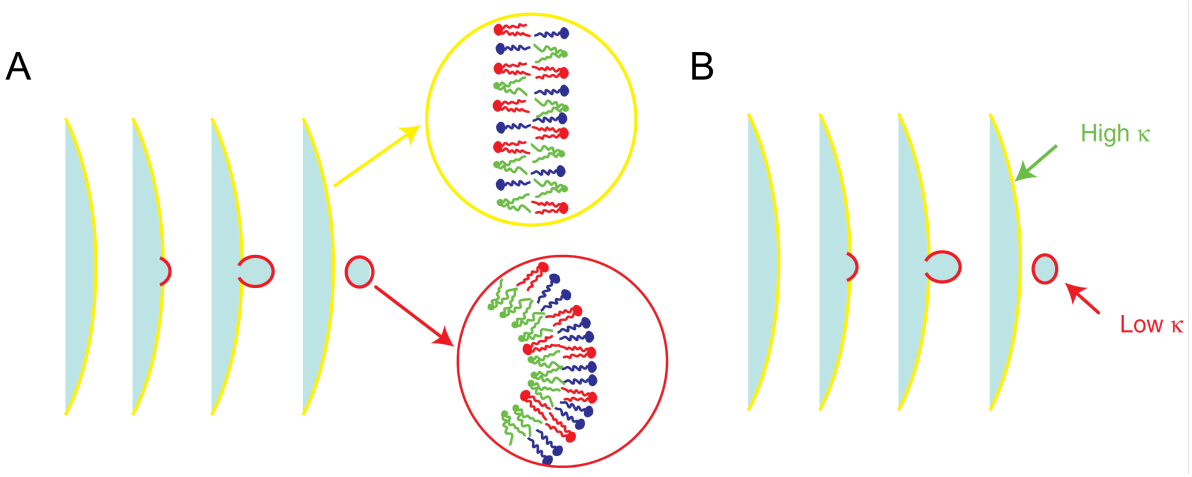

Figure 5.2: A) Lipid sorting due to a local change of spontaneous curvature. This mechanism is associated with an asymmetric distribution of lipids with conical shapes between leaflets. B) Lipid sorting due to a local change in bending rigidity. This change is due to a lateral redistribution of the lipids producing a softer membrane in the curved part. Scheme from [156].

Experiments with model systems have been done to determine if lipid sorting can be observed in simple lipid mixtures. Both types of sorting principle have been tested **??**. Kamal and collaborators have used small unilamellar vesicles of various radii to determine the coupling between lipid shape and leaflet curvature [157]. They show that an enrichment can be measured but is weak (inf 25%).

Furthermore, in our group, Benoît Sorre has pulled tubes from GUVs made of cholesterol, sphingomyelin and DOPC, using the technique described in section 2.2.2.4 of chapter 2 and in following sections. By measuring the partitioning of fluorescent lipid phase markers between the GUV and the tube, and by measuring the force on the tube, he has shown that in general, lipid sorting due to bending rigidity minimization is a very weak effect [158]. This can be predicted by a simple order of magnitude calculation as described in [156]. Assuming a typical bending rigidity difference of $\Delta\kappa = 40 k_B T$ between a stiff Lo and a soft Ld phase, a tube radius R of 20 nm and a lipid surface of $a \approx 0.5\ nm^2$, the gain in mechanical energy upon lipid sorting would be (if the interactions are neglected):

$$\Delta F = \frac{1}{2}(\frac{\Delta\kappa}{R^2})a = \frac{1}{40}k_B T \tag{5.2}$$

which is much smaller than $k_B T$. Entropy is thus expected to be dominant due to the small size of lipids.

However, for a composition and temperature close to demixing in the GUV (see section 2.2.2.5 of chapter 2), lipid-lipid interactions become dominant (see section 5.4) and a significant sorting up to a factor of four can occur[158].

Moreover, interactions with a protein enriched in curved membranes can also help lipid sorting. For example, Shiga toxin binding to GB3 glycolipids can contribute to sphingomyelin enrichment in curved membranes [159], [160], because of favorable interactions between the glycolipids and the sphingomyelin. On the other hand, if the protein is depleted from the tube, the sphingolipids are also depleted from the curved structures [161].

To conclude, lipid sorting due to coupling between membrane composition and membrane curvature cannot occur in ideal lipid mixtures but only with the aid of some lipid/lipid or lipid/protein interactions.

5.1.2.2 Protein sorting in curved membranes

Proteins have a much larger size than lipids (a membrane protein area is typically 10 times larger than the area of a lipid head group). In principle, enthalpic effects could therefore overcome entropy (see equation 5.2) independently of other interactions.

Main possible mechanisms of coupling between membrane proteins and membrane curvature are illustrated in figure 5.3. The scaffolding mechanism shown in figure 5.3a, is used by proteins like BAR domain proteins (such as amphiphysin for example) that locally impose a shape to the membrane [162]. Another mechanism is hydrophobic insertion (see figure 5.3b), in which amphipatic helices insert in the membrane creating a wedge (like epsins [152] or Arf-GAP1 [163] for instance). These effects can be enhanced by oligomerization (see figure 5.3c). Dynamin is known to form helical structures upon dimer oligomerization for example[164]. Finally, a local overconcentration of proteins on one side of the membrane could also curve it via steric repulsion between the proteins [165](see figure 5.3d).

Note that at high concentrations, these proteins change the membrane shape over large scales (curvature generation) whereas at low concentrations, coupling between protein and

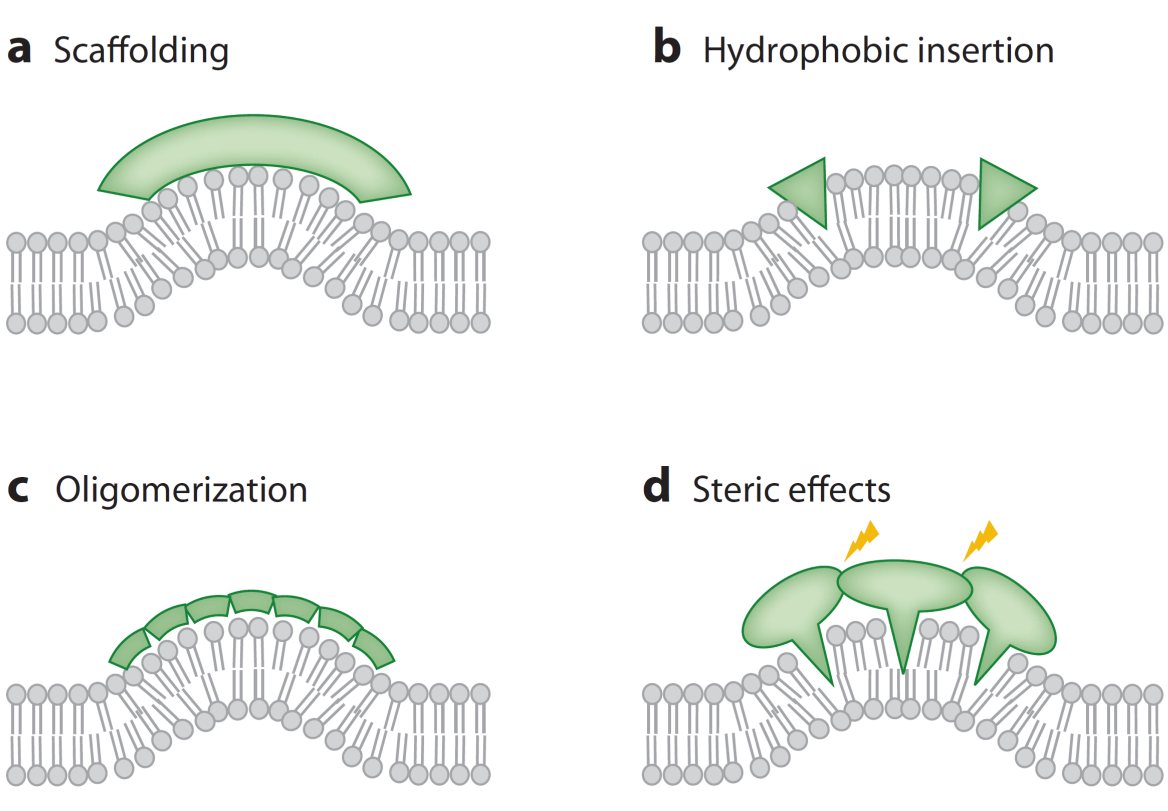

Figure 5.3: Mechanisms for membrane curvature/proteins coupling. From [166].

membrane curvature will be macroscopically detectable by an enrichment of the protein in curved part of the membrane [167].

The effect of transmembrane proteins on curvature has been less studied. The shape of the protein could in principle impose an tilt to the membrane as described in chapter 2. An example of wedge shaped proteins that could impose a curvature are reticulon and DP1/Yop1p that could be involved in shaping the endoplasmic reticulum [168] by creating tubular structures or stabilizing those formed by molecular motors moving on microtubules[169]. Similarly, the F1F0-ATP synthase could be involved in shaping mitochondria membrane [170].

5.1.2.3 Physics of coupling between membrane composition and curvature

Many theoretical studies for coupling of membrane composition and curvature (for reviews see [156, 166, 171]) have been developed.

Three main approaches have been used, all based on the theory of elasticity developed in section 2.2.2 of chapter 2:

- One of the first models coupling curvature and density of inclusions in the membrane was done by Stanislas Leibler in 1986. The principle was to add a free energy to the

Helfrich hamiltonian shown in equation C.1, coupling protein density to curvature:

$$\mathcal{F}_c = -\Lambda\phi CA \tag{5.3}$$

where Λ is the coupling constant between membrane mean curvature C and inclusion density ϕ and A is the membrane area.

He also added a term to take into account the interaction between particles

This theory predicted enrichment of the inclusions in curved membrane, a reduction of the bending rigidity, a change of the spontaneous curvature and even membrane shape instabilities for high insertion densities.

- Another widely used strategy is to use only the Helfrich hamiltonian but to add a dependence of bending rigidity and/or spontaneous curvature on the protein density. This type of theory will be developed in section 5.4.
- Finally, another approach models the effect of inclusions as local forces exerted by the proteins on the membrane. This was used for example to explain the budding mechanism in cavaolae [172].

Note that measuring the protein density in a membrane with a curvature gradient thus gives microscopic information such as the spontaneous curvature imposed by the protein to the membrane.

5.1.3 Voltage gated channels and curvature in cells

As shown in figure 5.4, voltage gated ion channels are distributed inhomogeneously in neurons. This has important functional implications. For example it is crucial that voltage-gated sodium channels are concentrated at the "entrance" of the axon (the axon initial segment -AIS-) or at Ranvier nodes between myelin sheets, in order to produce an efficient action potential initiation and propagation. It is also important that voltage-gated potassium channels with different biophysical characteristics are located in specific membrane subparts to control signal integration in the neuron[22, 19].

The targeting of voltage-gated channels to specific neuron parts is a field of active research [22, 173]. For instance, it is known that some specific motifs in the channel interacting with other proteins (like scaffolding proteins involved in endocytosis and exocytosis for example) are involved in targeting, trafficking and clustering of channels. However, much still needs to be understood.

Importantly, the effect of membrane curvature on voltage-gated ion channel distribution has not been studied so far to my knowledge. Yet, a coupling between membrane curvature and channel distribution (with mechanisms described in section 5.1.2) could have an important effect on trafficking of those channels via endocytosis or exocytosis, by affecting the number of channels per vesicle but also by changing the energy necessary to form them.

Note for curiosity that it has been shown in endocrine cells that only 2 % of Kv2.1 channel do conduct[174]. This suggests that these voltage-gated channels have another function than the control of membrane potential. Furthermore, some other studies have

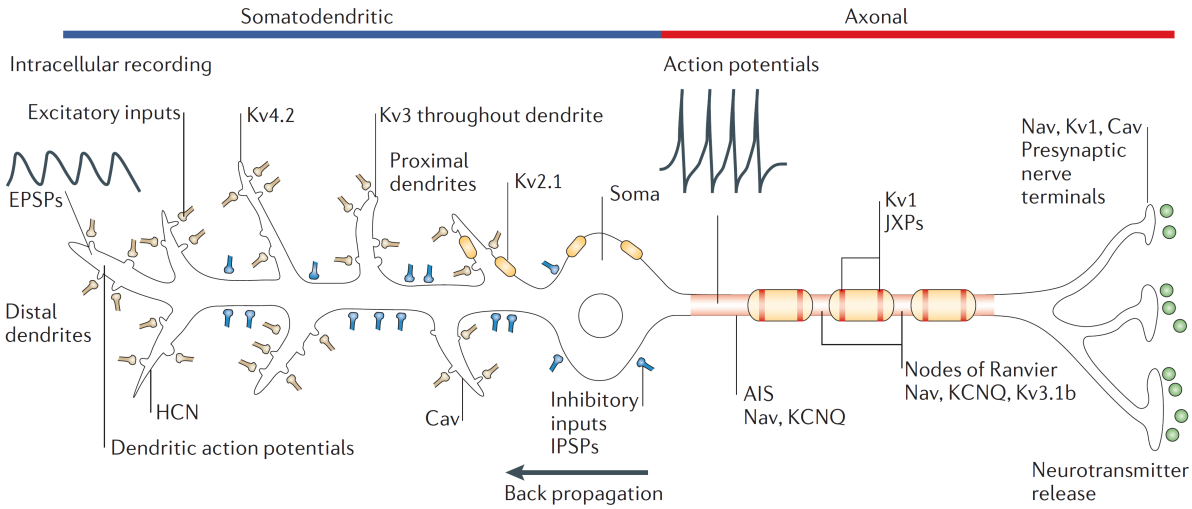

Figure 5.4: Distribution of potassium voltage gated channels sub-types in a typical neuron (from [22]).

shown that these channels facilitate exocytosis upon membrane depolarization [175]. It would thus be tempting (even though completely hypothetical at this stage), to attribute this to a change of Kv2.1 channel conformation with voltage that would bend the membrane and thus help exocytosis.

Finally, coupling with membrane curvature could be involved in the enrichment or the depletion of channels in curved part (distal dendrites for example) as compared as flat part (like the soma) of the neuronal membrane.

We have therefore used in vitro experiments to evaluate quantitatively the coupling between KvAP lateral distribution and membrane curvature.

5.2 Experimental approach

To measure channel distribution as a function of membrane curvature (see figure 5.5), I have pulled tubes from GUVs as described in section 2.2.2.4 of chapter 2 and shown in figure 5.5. Briefly, by sticking a streptavidin coated bead on a vesicle containing a very small fraction of biotinylated lipids, and then moving the vesicle away, a membrane tube is created. Changing the tension makes it possible to change the tube radius ($R = \frac{f}{4\pi\sigma}$ for an homogeneous membrane as detailed in chapter 2). Finally, fluorescence measurements allow characterizing the enrichment of the protein in the tube as compared to the GUV as a function of membrane curvature.

To make these experiments, I used a custom built set up described in figure 5.6. It combines the possibility to make fluorescence measurements using the confocal microscope (a Nikon Eclipse), while controlling membrane tension using a micropipette linked to a water tank, and measuring the force necessary to hold the tube thanks to optical tweezers.

I will now go into the details of a typical experimental procedure.

The pipette and the chamber were incubated for approximately 20 minutes in a solution

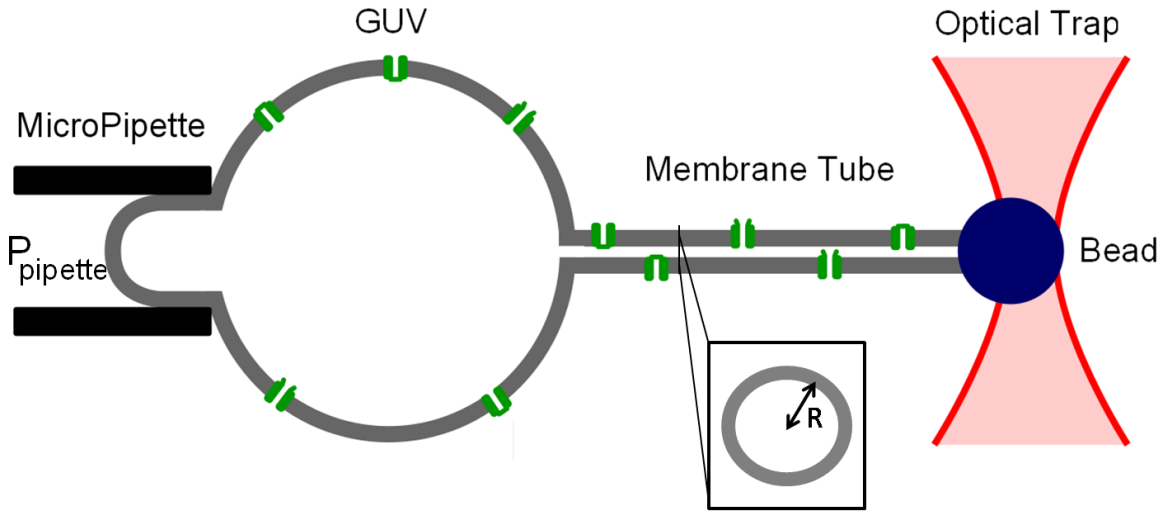

Figure 5.5: Experimental principle. A membrane tube is pulled from a GUV containing channels. Controlling the pressure in the pipette sets the membrane tension. The force necessary to hold the tube is measured by the displacement of the bead in the optical trap.

containing casein (5 mg/ml) to prevent the vesicle from sticking to the glass. GUVs containing reconstituted KvAP labeled with Alexa 488, Texas red DHPE (0.2 to 0.5%) and EPC:EPA 9:1 and sometimes PEG2000-PE (up to 1% to ensure that vesicles were unilamellar) were injected in the observation chamber containing a solution of NaCl, glucose, Hepes (pH 7.2) and casein (0.5 mg/ml) at the same osmolarity as the vesicles.

To be able to impose a tension using the pipette aspiration method, it is necessary to have GUVs with an initally low tension. This can be achieved by waiting for at least half an hour to slowly increase the osmolarity of the solution in the chamber by evaporation. The solution outside the GUV is thus at higher osmolarity than the inside which leads to a deflation of the vesicle and a decrease of its tension. However, for my vesicles, some pores in the membrane led to an equilibration of the osmolarity without a tension decrease. It was thus necessary to include in the external solution large osmolites (PEG 1500 from Roche) that don't cross the membrane to obtain vesicles of low tension. Note that the pores were probably due to a few porins remaining from the purification or to a few misfolded channels. Nevertheless, these impurities were probably at very low density as they were rarely detected in patch-clamp experiments (see chapter 4).

Note also that a difference of density between the internal and the external solution (sucrose and glucose respectively) is usually used so that GUVs sediment to the bottom of the chamber. In the presence of these pores in the membrane, it was also more difficult to have vesicles sediment, so it was necessary to wait a longer time before starting the experiment.

When the tension was low enough, a vesicle was aspirated in the micropipette, and a bead was trapped in the optical trap (IR laser with a power of approximately 150 mW)).

The vesicle was then pushed against the bead so that a small patch of membrane would stick and pulled away to create a membrane tether of approximately 5 microns in

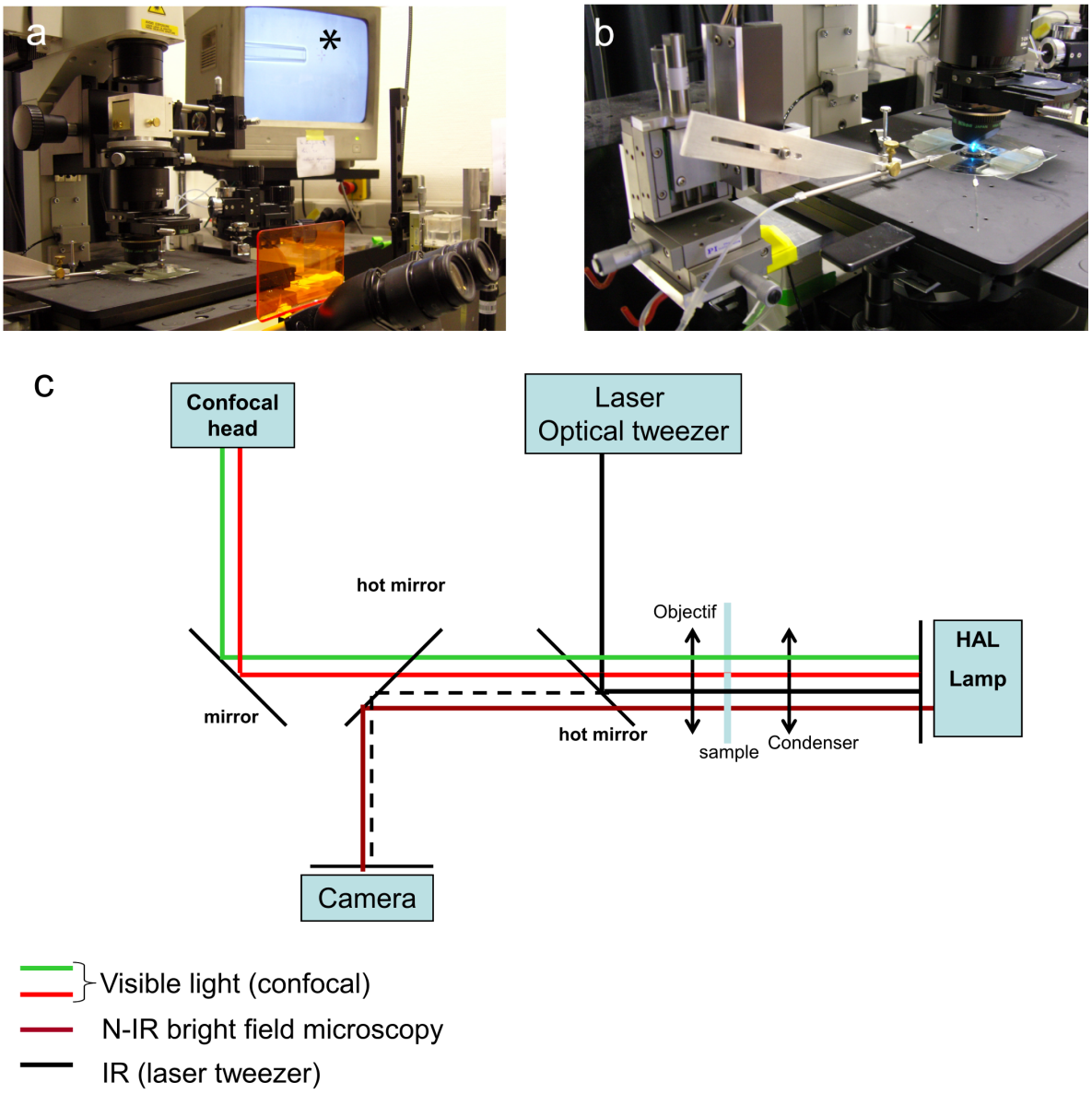

Figure 5.6: Experimental set up. a) Overview of the set up. b) The pipette and the micromanipulator to manipulate the GUV are on the left of the observation chamber. c) Optical path. Fluorescence images are taken using the confocal in visible light, bright field with near IR is used for imaging the pipette, the vesicle and the bead, while the optical trap uses mid-IR (λ=1064 nm). Adapted from [176].

length. The tension of the vesicle was then adjusted by changing the height of a water reservoir linked to the pipette. The membrane tension was increased (and thus the radius decreased) step by step. After waiting for at least one minute to let the system equilibrate, the force f necessary to hold the tube was measured by video tracking the displacement

Δx of the bead and by using

$$f = k\Delta x \tag{5.4}$$

were the trap stiffness k was approximately 40 pN/μm and was regularly calibrated by using a known Stokes drag force [177, 176].

The fluorescence data were obtained by recording confocal images for both fluorophores: Texas Red DHPE (with the 543 nm laser) and KvAP labeled with Alexa 488 (with the 488 nm laser). Number of acquired images was limited in order to reduce bleaching effects (in the conditions I used approximately 1% of Alexa 488 and 0.05% of Texas red were bleached per image).

The confocal images were then analyzed using a Matlab program designed by Benoît Sorre to determine the intensity values in the tube for the two fluorophores (I_t^{KvAP} and I_t^{lipid}) and in the GUV (I_v^{KvAP} and I_v^{lipid}) as shown in figure 5.7.

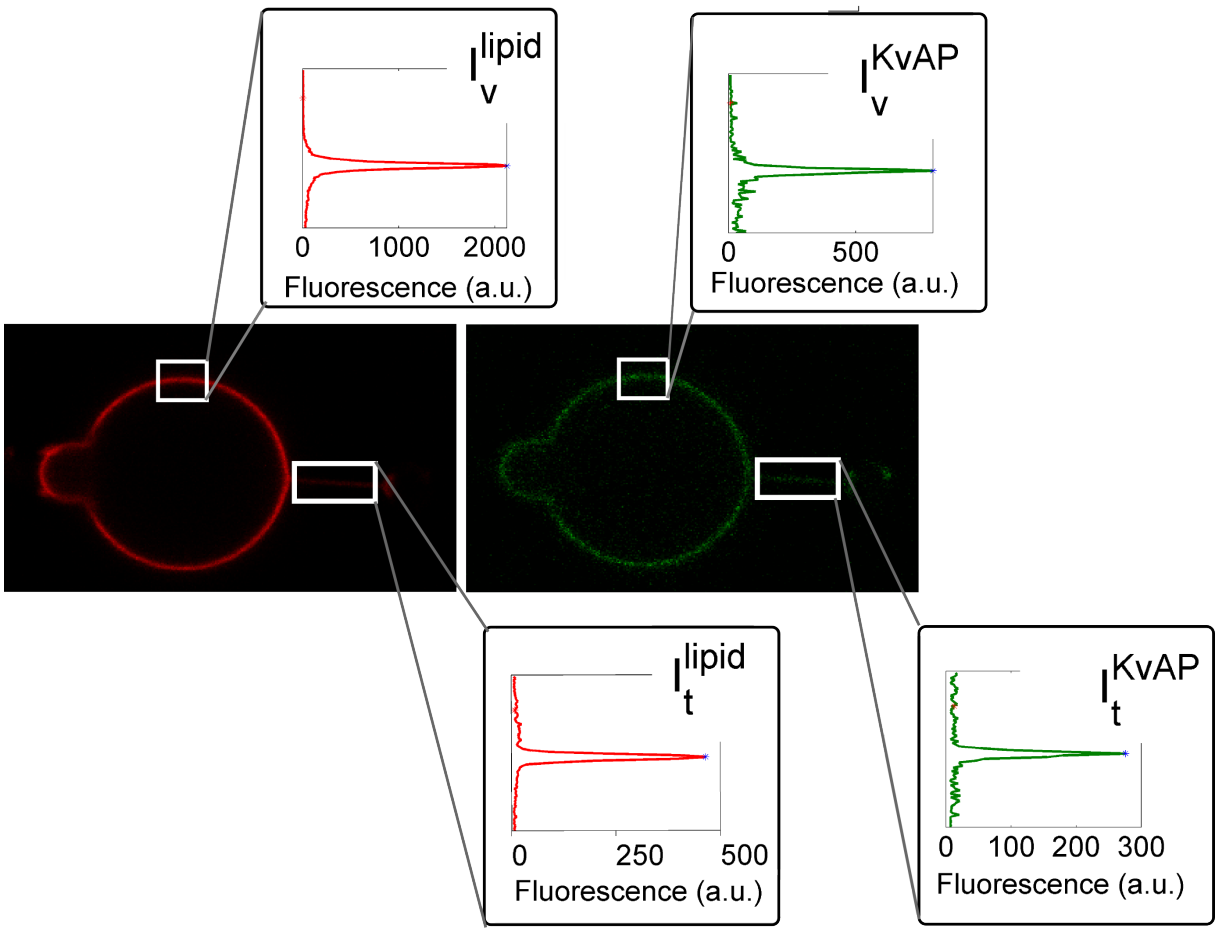

Figure 5.7: Confocal image analysis. For each image portion delimited by the white frames, the pixel intensity values were averaged along each line to create a profile perpendicular to the membrane. The maximum of this profile defines the intensity value.

The Sorting value of KvAP was then defined as [176]:

$$Sorting = \left[\frac{I_t^{KvAP}/I_t^{lipid}}{I_v^{KvAP}/I_v^{lipid}} \right] \tag{5.5}$$

A sorting larger than one should imply that KvAP is enriched in the tube as compared to the GUV. Note nevertheless that the sorting value is not necessarily equal to one even when the tube and the GUVs are the same composition because due to some polarization effects associated with the difference of geometry between the vesicle and the tube and to the orientations of dyes in the membrane. However, if this polarization effect is not negligible, it should be independent of the radius of the tube (provided that it is smaller than the illumination volume). Any relative change of the sorting value should not be affected and reflect a change in protein density in the tube as compared to the GUV.

5.2.0.0.1 Tube radius calibration

As described in section 5.2, for an homogeneous and symmetric membrane, the tube radius should be related to the force f and the tension σ by $R_t = \frac{f}{4\pi\sigma}$.
This equation might not be correct for vesicles containing proteins as membrane could be heterogeneous and asymmetric.

It is thus important to perform another measurement of the tube radius, independent of the force, using the ratio between the tube and the vesicle **lipid** fluorescence intensity. Indeed, as the tube radius is below optical resolution, the total fluorescence intensity of the tube per unit length should be proportional to the tube surface circumference $2\pi R_t$ and thus to its radius [176].

I calibrated this measurement using the radius deduced from the force with vesicles containing only lipids (EPC, EPA 10%, and Texas red up to 0.5%, biot-PEG2000-DSPE 0.01%). Note that the bending rigidity for these vesicles was 15 ± 1.5 kT as deduced from the force measurement (see figure 5.8A). The lipid fluorescence ratio $\frac{I_t^{lipid}}{I_v^{lipid}}$ was determined as shown in figure 5.7 for the red fluorescence, and $\frac{f}{4\pi\sigma}$ corresponds to radius measured from the force (see figure 5.8B). The slope was 0.009 +/- 0.002 nm^{-1} (4 vesicles). This value is in agreement with other experiments previously done by Benoit Sorre in the group using the same set up and without Egg PA in the membrane [176]. The measure of fluorescence thus allows a direct measurement of the tube radius.

5.3 Results

5.3.1 KvAP is enriched in curved membranes

A tube was pulled from a vesicle containing KvAP channels. A confocal image was taken after approximately 1 minute. The fluorescence of the lipids and proteins were homogeneous in the vesicle and along the tube as shown in figure 5.9(note that there was no enrichment of the protein at the neck of the tube). Fluorescence intensities of KvAP (labeled with Alexa 488) and the lipid dye (Texas red DHPE) were then measured in the vesicle and in the tube by analysing the confocal images and the sorting ratio was determined.

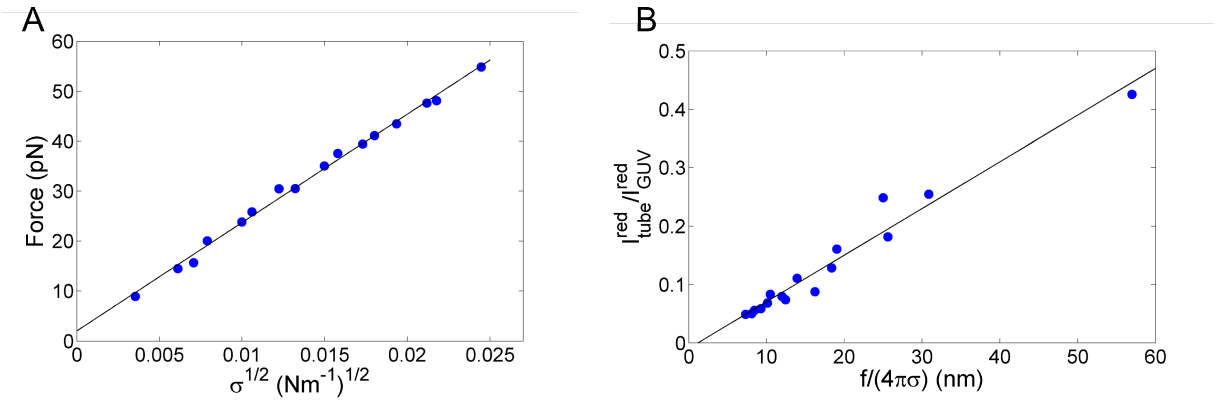

Figure 5.8: Calibration of the lipid fluorescence to determine the tube size. A) Force necessary to hold the tube as a function of square root of sigma. Note that the slope of the curve is $p = 2\pi\sqrt{2\kappa}$ leading to a bending rigidity of $\kappa = 14,7kT$ for this vesicle. B) Calibration curve to measure the radius from the lipid fluorescence in the tube as compared to the lipid fluorescence in the vesicle. The fit is $y = 0.008x - 0.0095$.

The tube radius was estimated from the ratio of the tube lipid fluorescence over the vesicle lipid fluorescence as described in the previous section. As shown in figure 5.10A, the density of proteins in the tube relative to the density in the vesicle, and thus KvAP sorting, increased with curvature. The data points are consistent with a linear relationship between the enrichment and the tube curvature. This increase of protein density with curvature was observed for approximately 80 vesicles under various conditions including different lipid compositions (POPC/POPG 9:1, EPC:EPA 9:1), different GUV preparation methods (high salt and low salt protocols), different protein labeling methods (Alexa maleimide, maleimide-PEG-biotin linked to a fluorescent streptavidin) and different protein densities. The effects of these different parameters will be discussed below. As we will discuss in section C.3.2.2, the density in the tube can be as high as 12 times the density in the vesicle.

It is interesting to note that if we now plot the protein fluorescence intensity in the tube (which is proportional to the total number of proteins in the tube) as a function of curvature, we find a constant value as shown in figure 5.10B. This could be due to either a linear relationship between protein density and curvature or to a trapping of proteins in the tube. Indeed, when the tension is increased, lipids flow out of the tube to the GUV which decreases the tube radius. If the channels cannot cross the tube neck then and are trapped in the tube, the total number of channels remain constant and hence the channels will be enriched as compared to lipids.

5.3.2 KvAP freely diffuses at the neck of the tube

I used FRAP experiments (Fluorescence Recovery After Photobleaching) to check if the channels were trapped in the tube. Some of these experiments have been done in collaboration with Mathieu Pinot on the set up of Jean-Baptiste Manneville in the Curie Institute and some on the set up in the group (the same result was obtained on both

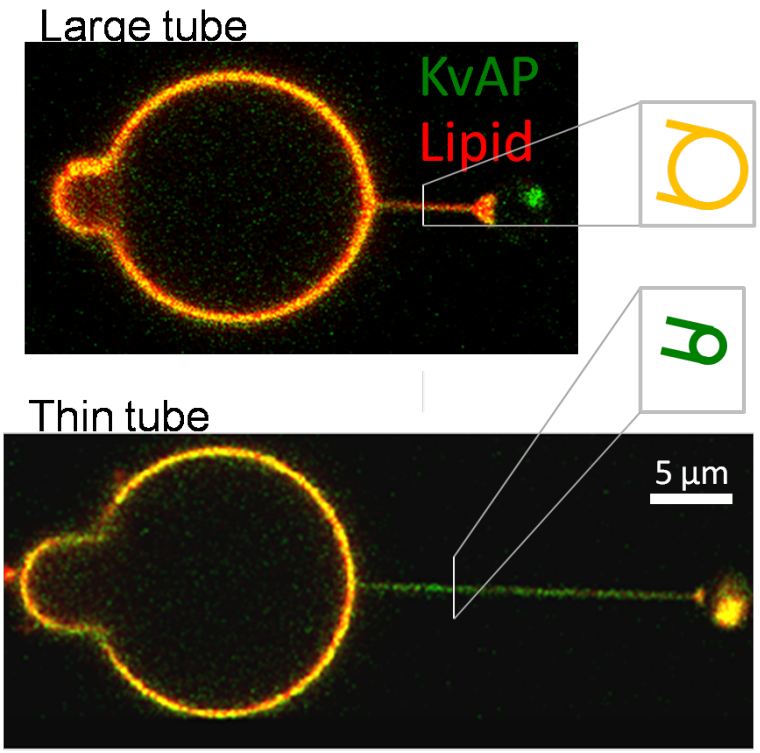

Figure 5.9: Example of a confocal image of a tube (on the right) pulled from a vesicle containing reconstituted KvAP and held in a micropipette (on the left). Red corresponds to lipids (Texas red DHPE) and green is the protein labeled with Alexa 488. The vesicle is yellow which means that fluorescence intensity is the same for green and red. For a large tube the fluorescence is also yellow (top image). In contrast, for the thin tube (bottom image), the tube is green which corresponds to an enrichment of the protein as compared to the vesicle. Bar: 10 microns. Note that typical experiments were done with smaller tube lengths.

setups). The principle was to completely bleach the Alexa 488 linked to proteins with a high laser intensity in the tube and measure the recovery of the fluorescence in the tube at low laser intensity. A recovery would indicate a diffusion of the proteins back in the tube while no recovery would show that they cannot cross the tube neck.

Figure 5.11 presents images of the vesicle before, a few seconds and a few minutes after photobleaching the protein in the tube. As you can see in the middle image, fluorescence recovery occurs from the tube region close to the GUV. It is complete after few minutes. This recovery was observed for the 10 vesicles tested on four different days, indicating that the protein can diffuse between the tube and the GUV.

I also checked that the sorting value was the same after photobleaching. Figure 5.12 presents sorting values for a typical experiment. The tube was first pulled with a large radius (approximately 100 nm) to a length of 9 microns. After 5 minutes, the sorting ratio indicated that the protein was not enriched in the tube (Figure 5.12 point 1). The tube

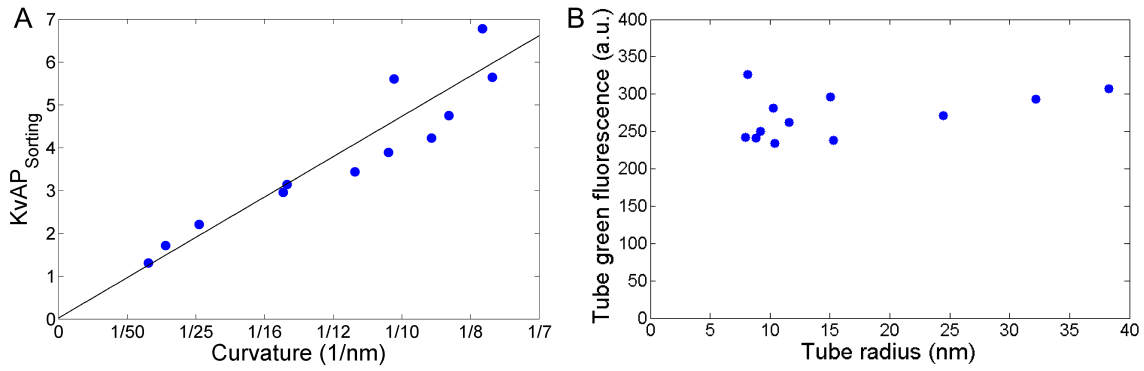

Figure 5.10: A) Change in KvAP sorting as a function of curvature for a chosen vesicle (200 $\pm$ 140 proteins/μm^2. The fit is $Sorting = 47 Curvature + 0.031$. B) Green fluorescence as a function of tube radius. Protein total quantity is constant in the tube. See figure 5.12 for an order of magnitude of the scattering of the data points.

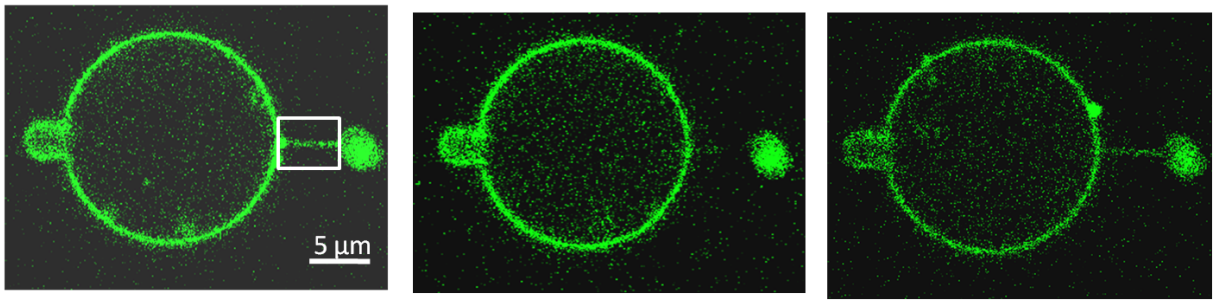

Figure 5.11: Fluorescence recovery after photobleaching. The zone in the white square is illuminated with high laser power to bleach the Alexa 488 on the protein. Middle image: Image of the vesicle and the tube few seconds after photobleaching. Right: Image few minutes after photobleaching. Some proteins with unbleached fluorophores have diffused in the tube.

radius was then decreased to a smaller value (approximately 30 nm) and the enrichment was measured after 5 minutes. The protein was then approximately 3 times denser in the tube than in the vesicle (Figure 5.12 point 2). The fluorophores linked to the protein in the tube were then bleached using the full power of the 488 nm laser. Note that the lipid fluorescence was not bleached. The decrease in the sorting ratio measured after 30 seconds reflects this decrease of the protein fluorescence in the tube (Figure 5.12 point 3). 10 minutes after photobleaching, proteins had diffused in the tube and the sorting value was back to its initial value (Figure 5.12 point 4) thus corresponding to its equilibrium state.

The kinetics of fluorescence recovery over the whole tube was measured as shown in figure 5.13. Berk and Hochmuth have calculated the recovery expression precisely for the same geometry as in our experiment [178], for insertions diffusing freely between the vesicle and the tube. As in our experiment the tube radius is small (approximately 10 nm

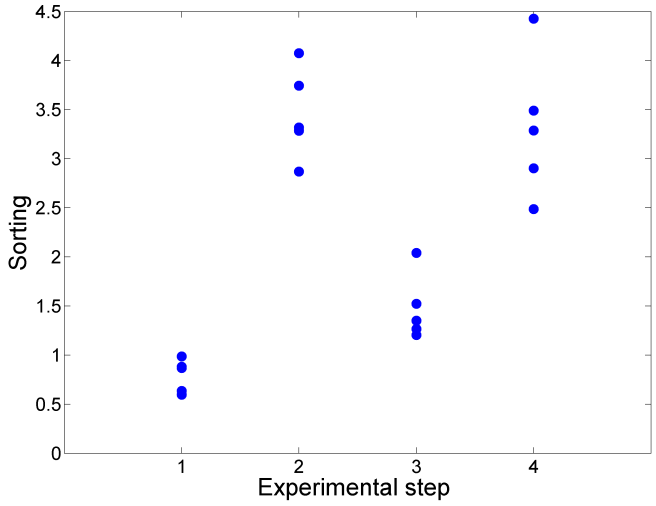

Figure 5.12: Sorting values in a typical FRAP experiment. 1) Tube radius 100nm (after 5min of equilibration). 2) Tube radius 30nm (after 5min of equilibration). 3) Tube radius 30 nm, 30 seconds after bleaching. 4) Tube radius 30 nm, 10 min after bleaching. The few measurements made for each condition show the scattering of the values.

for the experiment corresponding to figure 5.13) and the tube is long (5.7 microns), the fluorescence recovery curve should be given by:

$$Sorting = S_0 - \sum_k a_k exp^{-\frac{(\frac{(2k-1)\pi}{2})^2 D_t t}{L^2}} \approx S_0 - a_1 exp^{-\frac{\frac{\pi}{2}^2 D_t t}{L^2}} \tag{5.6}$$

Where a_k are constants that decrease quadratically with k, D_t is the lateral diffusion coefficient, L is the tube length. It was actually possible to fit the recovery curve with one term as shown in figure 5.13, leading to a lateral diffusion coefficient in the tube of $0.36\mu m^2/s$ which is in agreement with the diffusion measured with single particle tracking for this tube radius (see chapter 6).

5.3.3 No detectable effect of KvAP sorting on force

We have then investigated the effect of the protein enrichment in the tube on its mechanical properties. Indeed, it was already shown for an N-BAR protein (amphiphysin) that force and tube radius could be affected by protein enrichment in the tube at moderate protein density [176].

As discussed in section 2.2.2.4 of chapter 2, the force necessary to hold the tube is linked to the energy to bend the membrane. For an homogeneous membrane:

$$f = 2\pi\sqrt{2\kappa}\sqrt{\sigma} \tag{5.7}$$

The slope f as a function of $\sqrt{\sigma}$ should thus be related to the membrane bending rigidity.

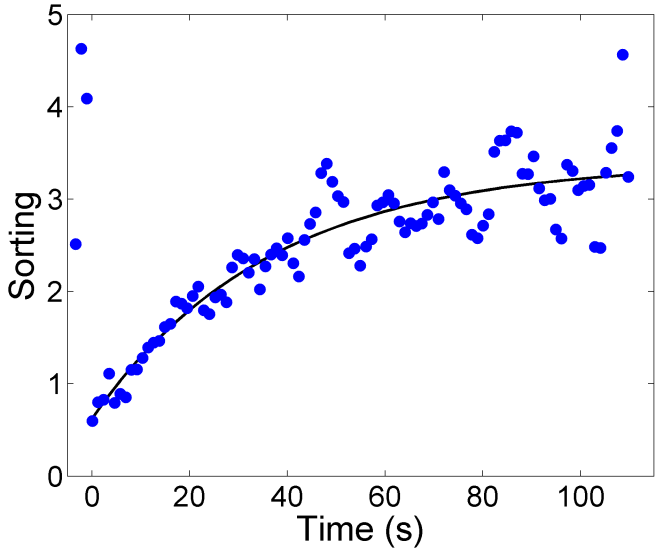

Figure 5.13: Recovery of KvAP fluorescence in the tube. The fluorescence of the whole tube was bleached at t=0. The data was smoothed over 5 points to reduce noise. The fit equation is $Sorting = 3.39 - 2.77exp(-0.027t)$.

Similar experiments have been done in the group with protein binding the membrane. The typical experiment was thus to measure the mechanical protperties of a vesicle before and after adding the protein. For amphiphysin, at moderate densities, a change of the slope and a shift of the curve were detected due to the spontaneous curvature imposed by the protein [167]. In other cases, for example with dynamin [179] or amphiphysin at high densities (above 1000 protein/μm^2), a linear relationship between f and σ was measured.

No clear signature of the protein on the force curve as compared with the curve in the absence of proteins were detected. An example of force curve for a vesicle containing protein is shown in figure 5.14. Bending rigidity of vesicles containing proteins was 16 $\pm$ 7 kT (18 vesicles) whereas for vesicles without protein 17 $\pm$ 4 kT (30 vesicles). Note that the variability in force curves from vesicle to vesicle was important, probably due to the presence of PEG lipids and Texas red in the membrane, but also because of the important asymmetry of buffers inside and outside the vesicle.

The absence of detectable effect of the protein on the membrane mechanics could be explained by the low protein density in the membrane (few percent of area at the maximum). Indeed, the higher density value for these experiments was $\Phi_v = 2000$ protein/μm^2. This corresponds to a protein area fraction of $\phi_v < 10\%$ assuming a KvAP area of 7 nm $\times$ 7 nm, as determined from the crystal structure [99].

5.3.4 Effect of protein density in the vesicle on protein enrichment in the tube

Even though KvAP enrichment as a function of curvature can be observed in most experiments, the enrichment intensity highly depends on the density of proteins in the GUV

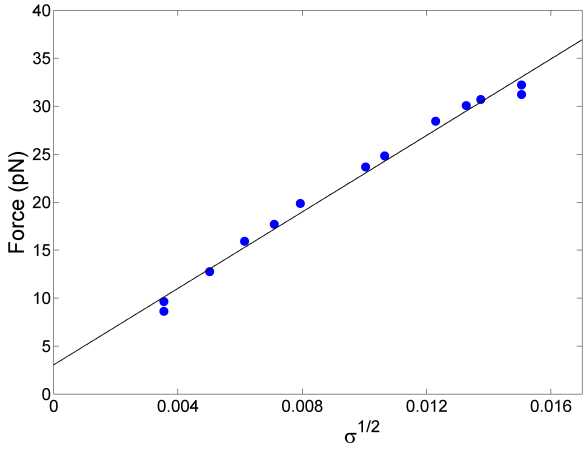

Figure 5.14: Variation of the force to maintain the tube as a function of $\sqrt{\sigma}$ for the same vesicle as that used for figure 5.10. Data are fitted to $f = 2120\sqrt{\sigma} + 1.6$ corresponding to $\kappa = 14.4kT$. The lipidic composition is the same as for the purely lipidic vesicle shown in figure 5.8.

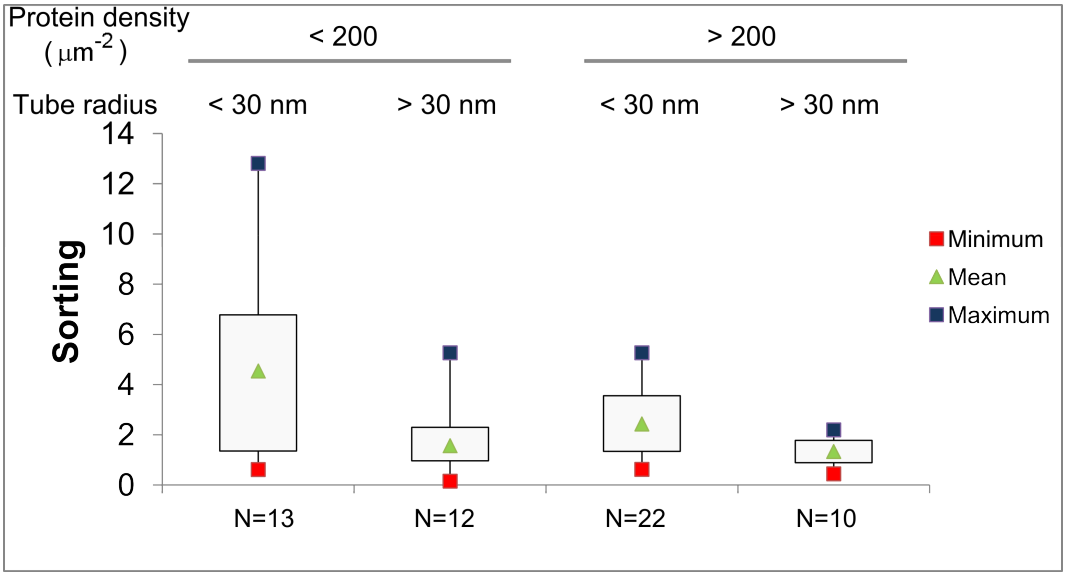

Figure 5.15: Boxplot of the sorting values for different protein densities and tube radii. The box comprises data between the first and the third quartile. N is the number of vesicle.

(Φ_v). Figure 5.15 summarizes the different sorting values obtained. Figure 5.16 presents the sorting strength which is the slope of the sorting curves as deduced from figure 5.10 for example. The sorting strength is plotted as a function of protein densities in the vesicle, measured from the protein fluorescence intensity as described in chapter 4.

The sorting strength and variability strongly decrease with the density on the GUV.

These effects will be compared to a theoretical model and discussed below.

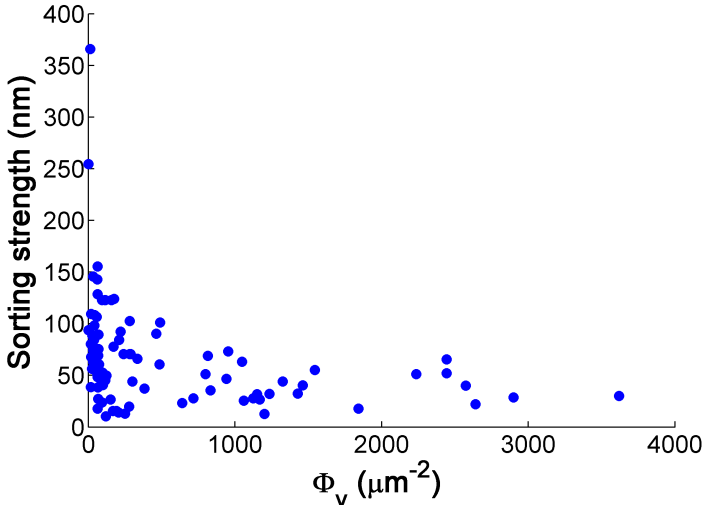

Figure 5.16: Slope of the sorting curves (as shown in figure5.10) as a function of protein density in the vesicle.

5.4 Theoretical model

A theoretical model was developed by Andrew Callan-Jones (now in the Coulomb laboratory in Montpellier) to describe the sorting of transmembrane proteins in nanotubes and their effect on membrane mechanical parameters. The membrane is divided in three parts: the tongue in the pipette, the GUV and the tube. In this model, the two possible orientations for the protein insertion are considered and noted + and -.

The free energy of this system is written as

$$F = F_p + F_v + F_t - PV_{\text{tot}} + \sigma A_{\text{tot}} - \mu_+ N_+ - \mu_- N_- \,, \tag{5.8}$$

where F_p, F_v, and F_t are the free energies of the pipette-aspirated tongue, the vesicle, and the tube. The quantities P, σ, μ_+, and μ_- are Lagrange multipliers introduced to keep the total volume, V_{tot}, the total area, A_{tot}, and the total number of both orientations of proteins, N_+ and N_-, constant.

The free energy of each part of the membrane is described by the Helfrich energy and the protein mixing entropy:

$$F_p = P_p V_p + A_p \left\{ \frac{\kappa}{2} \left[\frac{1}{R_p} - C_0(\phi_{p+}, \phi_{p-}) \right]^2 + f_m(\phi_{p+}, \phi_{p-}) \right\} \tag{5.9}$$

$$F_v = P_0 V_v + A_v \left\{ \frac{\kappa}{2} \left[\frac{2}{R_v} - C_0(\phi_{v+}, \phi_{v-}) \right]^2 + f_m(\phi_{v+}, \phi_{v-}) \right\} \tag{5.10}$$

$$F_t = P_0 V_t + A_t \left\{ \frac{\kappa}{2} \left[\frac{1}{R_t} - C_0(\phi_{v+}, \phi_{v-}) \right]^2 + f_m(\phi_{t+}, \phi_{t-}) \right\} - f L_t. \tag{5.11}$$

where R_p is the pipette radius, L_p is the tongue length, R_v is the vesicle radius, R_t is the tube radius, L_t is the tube length, ϕ_{p+}, ϕ_{p-}, ϕ_{v+}, ϕ_{v-}, ϕ_{t+}, and ϕ_{t-} are the protein area fractions on the tongue (p), vesicle (v), and tube (t). P_0 is the pressure outside the vesicle and f is the force exerted on the free end of the tube.

f_m is the mixing free energy given by

$$f_m(\phi_+, \phi_-) = k_B T \rho_l \left[\frac{\phi_+}{x} \ln \phi_+ + \frac{\phi_-}{x} \ln \phi_- + (1 - \phi_+ - \phi_-) \ln (1 - \phi_+ - \phi_-) \right], \quad (5.12)$$

where k_B is Boltzmann's constant, T is the temperature, ρ_l is the inverse area per lipid, and x is the number of lipids corresponding to the same total area as a single protein. Furthermore, $\rho_l \approx 2$ nm^{-2} and $\rho \approx 1/25$ nm^{-2}, $x \approx 50$.

The effect of the protein is modelled by a spontaneous curvature C_0 imposed by KvAP to the membrane. We suppose a linear dependence of the membrane spontaneous curvature with the protein density, and the two orientations of the protein in the membrane have opposite effects. We thus have:

$$C_0(\phi_+, \phi_-) = \bar{C}_0(\phi_+ - \phi_-), \quad (5.13)$$

where $\bar{C}_0$ is the intrinsic spontaneous curvature of the protein.

Minimizing the free energy thus gives the equilibrium equations for protein density and tube mechanics. The tube force is then given by:

$$f = 2\pi \left[\kappa H - \kappa \overline{C}_0 \left(\phi_{t+} - \phi_{t-} \right) \right] . \quad (5.14)$$

It was then possible to solve the equilibrium equations numerically to find the curves for the sorting:

$$S = \frac{\phi_{t+} + \phi_{t-}}{\phi_{v+} + \phi_{v-}} . \quad (5.15)$$

and compare it with the value from the fluorescence experiments.

The curve in figure 5.17 represents the sorting value as a function of the tube curvature rescaled by $1/\sqrt{\rho}$. The parameters are $\kappa = 10 k_B T$,$\rho \approx 1/25$ nm^{-2}, $x \approx 50$ and $\overline{C}_0/\sqrt{\rho} = 1$.

Note that for this graph, the orientation of the channel in the vesicle is supposed to be random ($\frac{\phi_{v+}}{\Phi_v} = \frac{\phi_{v-}}{\Phi_v} = 0.5$). As a result, at linear order in the tube curvature (hence for low curvatures), there is no sorting, since an enrichment of one type of protein in the tube is exactly opposed by a depletion of the other type. One must consider larger curvatures to see a sorting effect, in which depletion slows down (there are very few proteins left in the tube to remove) but enrichment from the vesicle to the tube continues to increase. Note also that this mechanism predicts a high dependence of the sorting on protein orientation in the membrane as only the orientation "up" is enriched in the tube.

The model also predicts the strong effect of protein density on sorting strength that we have observed. This is shown by the difference of the blue curve (0.5% of surface coverage) and the red curve (5%) of surface coverage in figure 5.17. It is also illustrated in figure 5.18 that has to be compared with the experimental curve 5.16 as will be discussed below. Note that a similar dependance was also predicted by [180] for the enrichment of lipids (asymmetrically distributed betwen the two leaflets) as a function of membrane curvature.

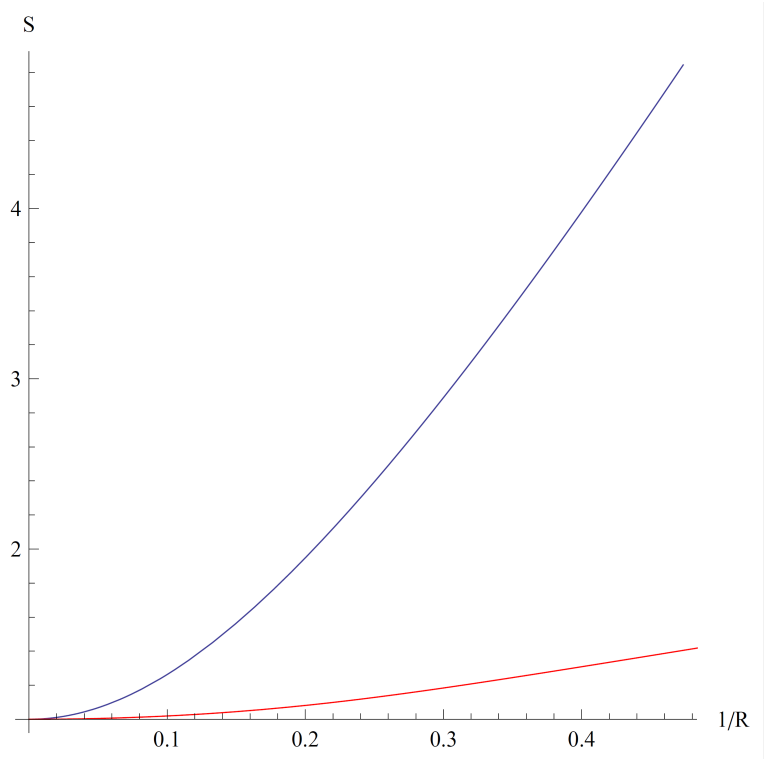

Figure 5.17: Sorting versus rescaled tube curvature. Blue: $\phi_{v+} = \phi_{v-} = 0.005$. Red: $\phi_{v+} = \phi_{v-} = 0.05$. $x = 50$.

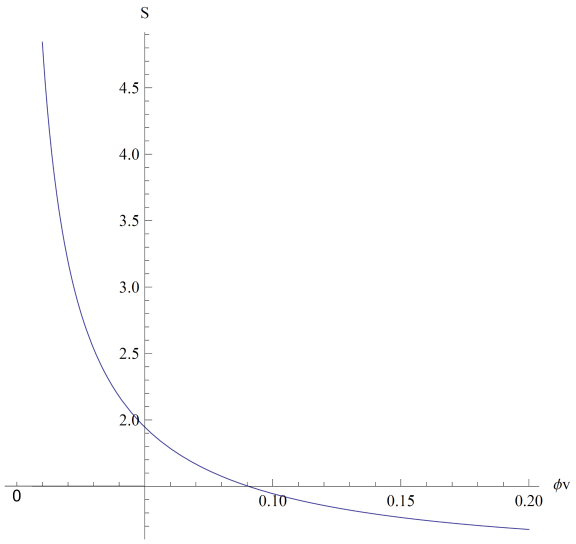

Figure 5.18: Sorting versus total protein area fraction on the vesicle, $\phi_v = \phi_{v+} + \phi_{v-}$.

Finally, figure 5.19 presents the force rescaled by $k_BT\sqrt{\rho} \approx 1pN$, as a function of $\sqrt{\tilde{\sigma}}$, where $\tilde{\sigma}$ is the tension imposed by the experimenter rescaled by $k_BT\rho \approx 2.10^{-4}N.m^{-1}$. The model predicts weak effects on the force for typical protein densities used in the experiments (see figure 5.14).

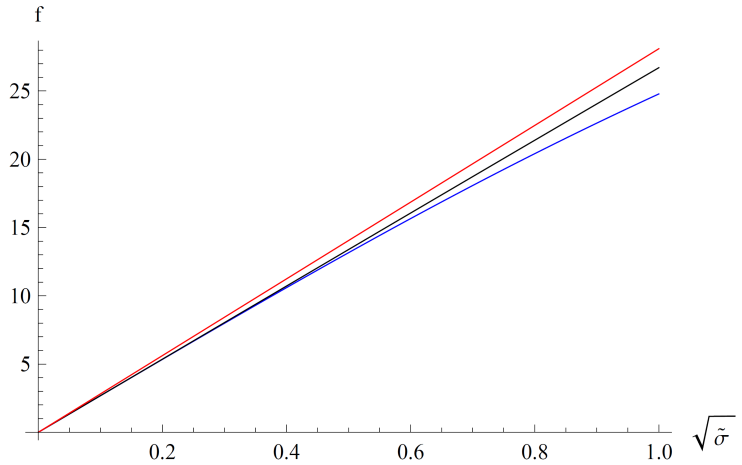

Figure 5.19: Rescaled tube force as a function of rescaled $\sqrt{\tilde{\sigma}}$. Red curve: force for a bare vesicle. Black curve: force for $\phi_{v+} = \phi_{v-} = 0.005$ for $x = 50$. Blue curve: force for $\phi_{v+} = \phi_{v-} = 0.005$ for $x = 1$.

5.5 Discussion

We have shown that KvAP is enriched in curved membranes and that the proteins diffuse freely in and out of the tube. That implies that after enough time for the proteins to diffuse along the tube (few minutes as in our measurements presented in this chapter), the membrane is at equilibrium and an equilibrium theory is valid.

Measurements of protein density as a function of membrane curvature have shown that the sorting varies approximatively linearly as a function of curvature. The model from Andrew Callan-Jones reproduces nicely this result, with a deviation for low curvatures that can be interpreted considering that both insertions are present in large tubes. When the tube radius is decreased, the insertion locally imposing a negative curvature to the membrane is depleted while the other insertion is enriched. For high sorting values, the insertion present in the tube is mostly the one imposing a positive spontaneous curvature to the membrane.

We also found that the sorting highly depends on the protein density in the vesicle. This can be understood in terms of an entropic pressure preventing high increase of protein density in the tube. It is thus easy to enrich the protein in the tube when it is at low density, but more and more difficult as the density is already higher in the vesicle.

Finally, no effect can be detected on the membrane mechanics even for the range of densities studied. This is also predicted by the theory and is probably due to the low

protein area fraction that is always below 10 % in our experiments.

Thus, a simple theory based on spontaneous curvature allows reproducing the experimental data, suggesting that this description is correct.

Note that the effect is surprisingly strong. Indeed, the orders of magnitude for the sorting are the same as those measured for a BAR-protein which is implicated in clathrin-mediated endocytosis and is suspected to sense or impose membrane curvature in cells [167]. The high effect we find for KvAP is difficult to link to the structural data right now and will need to be further investigated.

5.6 Perspectives

5.6.1 Control of protein orientation

One main difference between curve 5.16 and curve 5.18 is the large scattering of the data in the experimental curve. Note that an important parameter that is not yet controlled experimentally is the orientation of the protein e.g. Φ_+ and Φ_-. Indeed, it is possible to measure the total protein density Φ_v by quantifying vesicle fluorescence, but the relative fraction of the two insertions is not known. Because of the method to form the GUVs which involves fusing small liposomes, there should be in principle a random orientation of the proteins in the membrane. Nevertheless, the discrepancy between the experimental curve and the theory could be explained by a variability of the orientation of the proteins from one vesicle to the other. It would thus be useful to find a method to experimentally discriminate between the two insertions.

5.6.1.1 Single protein insertion

The next obvious step is therefore to separate the effects of the two insertions (Φ_+ and Φ_-). For that, the best would be to reconstitute directly the protein with only one insertion. This could be done in principle by adding the protein in detergent to the GUVs. Indeed, this process have been shown to produce a highly preferential orientation in supported bilayers [181]. However, preliminary experiments done in collaboration with Manuela Dezi in the group of Daniel Levy in the laboratory have shown that this strategy was difficult to implement with KvAP.

5.6.1.2 Invert the tube geometry

Some preliminary experiments have been done to invert membrane curvature by pulling a tube inside the GUV instead of outside as shown in figure 5.20. This should help determining if there is an asymmetry between insertions as the sorting could be changing depending on if the tube is pulled inside or outside the GUV. Note that the difficulty here was first to move the bead inside the vesicle. Indeed, when the bead is pressed towards the interior of the GUV, the membrane coats the bead. This induces an increase in the tension of the vesicle. To have enough excess membrane to start with, large vesicles were used, and the bead was moved inside the vesicle before its aspiration in the micropipette to have the lowest tension possible. Finally, as this geometry is less stable than the tube

outside the GUV, the tube should be small and exactly at the level of the vesicle equatorial plane.

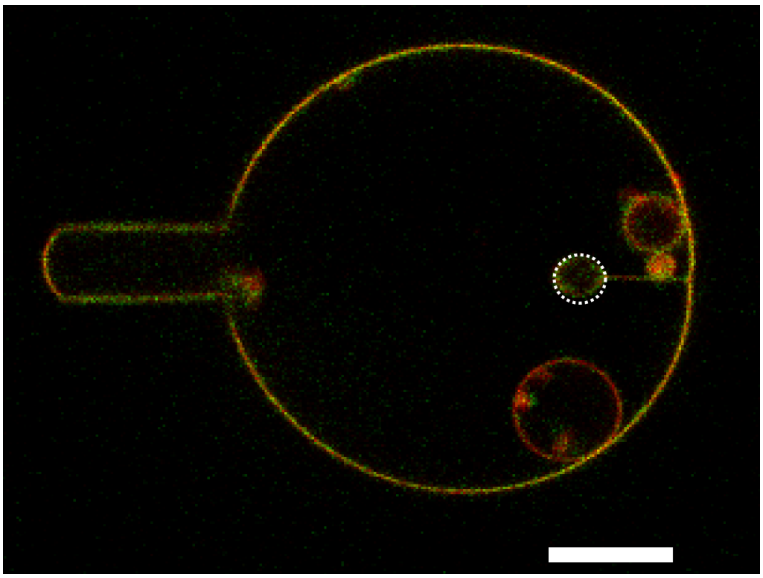

Figure 5.20: Tube pulled inside the vesicle. Bar 10 microns.

5.6.1.3 Strategies to label only one insertion

The most promising strategy to separate protein orientation in fluorecence measurements is to label the protein on a specific site after its reconstitution in GUVs. The main difficulty here is to find a label that does not penetrate inside the GUV which is challenging with these vesicles as they are slightly porous (see section 5.2).

Up to now, the best method was to use a biotin linked to the single cysteine residue on the protein. The protein can then be labeled after reconstitution in GUVs by adding fluorecent streptavidin in the bulk outside of the GUV. Thus, only the insertion with the cysteine on the external side should be labeled.

In a preliminary experiment shown in figure 5.21, an increase of the sorting value up to 6 for a 20 nm tube was observed for the protein while no significant sorting was observed under the same conditions for biotinalted lipids also labeled with the same fluorescent streptavidin.

Note that, unfortunately, we found later on that the biotin-maleimide was not specifically bound to the cysteine. Indeed, with our labeling protocol (involving a PEG-biotin-maleimide), the mutant containing no cysteine was labeled at the same level as the mutant with a cysteine. Preliminary experiments using a iodoacetyl-PEG-biotin showed that it could be a promising alternative. In the future, it would be useful to have mutants with cysteins at different places to measure the sorting for the different insertions in the membrane.

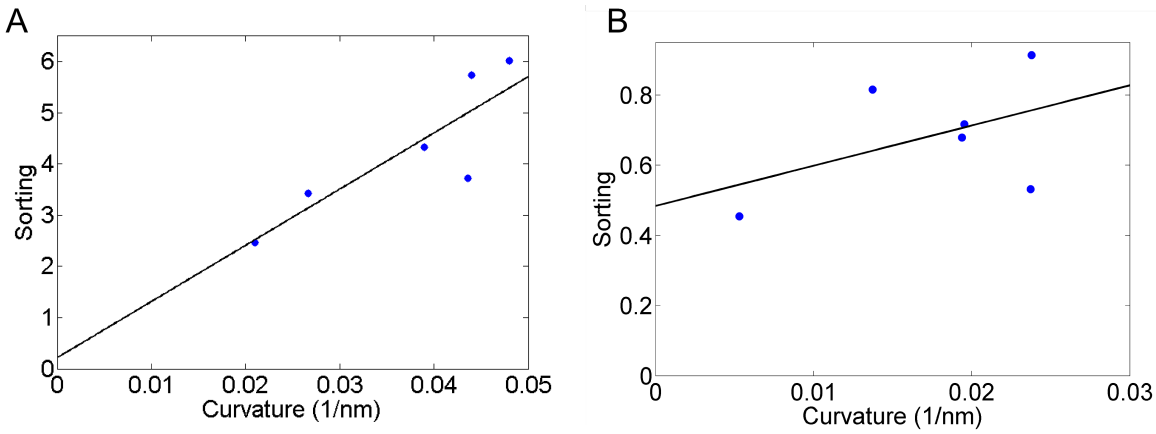

Figure 5.21: Sorting experiments with KvAP (A) and a lipid (B) labeled with a PEG biotin and with a fluorescent streptavidin in the GUV. The fit ewpression is $110\frac{1}{R}+0.22$ for the protein and $11\frac{1}{R}+0.48$ for the lipids. The slight increase in the sorting ratio is not significant for lipids while it is for the protein.

5.6.2 Other perspectives

5.6.2.1 Protein state in the membrane

A serious concern remaining is that the proteins could be partially misfolded. Indeed, if some transmembrane segments (for example if the S3-S4 helices) are misfolded and span only part of the membrane, this could result in a higher affinity for curvature (as for amphipatic helices: see section 5.1.2). Yet, even though some active channels were detected in patches, it was impossible to measure the fraction of active proteins in the membrane because the composition of the patch is different than the composition of the GUV as described in chapter 4. Protein unfolding might result from the electroformation process. However, in my experiments, sorting didn't increase with the duration and voltage of the electroformation step which seems to indicate that electroformation was not responsible for protein misfoding and further coupling with curvature. Note also that as this protein has been cristallized after a similar purification process by other groups [10], and measurement of the channel conformation have been done after reconstitution in SUVs and fusion to BLMs [182], no denaturation should occur during these steps. Furthermore, diffusion experiment presented in chapter 6, and FRAP experiments shown in this chapter show that the diffusion coefficient is consistent with a single protein diffusing in the membrane so the protein didn't form aggregates that could result from protein misfolding.

It would nevertheless be useful in the future to use very different reconstitution techniques (like the freeze-thaw technique to fuse small liposomes for example that should have a different effect) that would impose different constraints on the protein, and measure portein affinity for curvature with these reconstituted systems.

5.6.2.2 Mutating the amphipatic helix

The affinity of the channel for curvature could be explained by the presence of the amphipathic helix S0 at the beginning of the channel sequence [74]. By partially inserting in the membrane, this helix could locally curve it (see section 5.1.2.2). It would thus be interesting to make a mutant of the protein without this amphipatic helix and measure the sorting in this condition.

5.6.2.3 Control of membrane potential

Other interesting experiments could involve a better control of membrane potential to study how the affinity for the curvature changes with protein conformation. Indeed, here, because of the pores in the membrane, it is difficult to control the membrane potential using potassium concentration. It could thus be useful to understand the origin of these pores or to control the voltage using electrophysiology techniques as described in chapter4.

Eventually, an ambitious goal is to measure the spontaneous curvature imposed by the channel to the membrane as a function of channel conformation to understand the interplay between channel activity and distribution, and membrane properties.

5.6.2.4 Changing boundary conditions between the membrane and the protein

As presented in chapter 2, the spontaneous curvature imposed by the protein to the membrane should highly depend on the boundery conditions at the edge of the protein. This could be achieved for example by changing the lipid shapes (for example using some wedge shaped lipids such as PE or lysolipids and changing phospholipids chain length) or adding a toxin (such as the Voltage Sensor Toxin -VSTx- that interacts with the voltage sensor in the membrane) could change the enrichment of the protein as a function of curvature, which would provide a measure of the intrinsic spontaneous curvature and eventually some information on the channel conformation.

5.6.2.5 Sorting experiments with other trans-membrane proteins

To confirm that the method can indeed give information on trans-membrane proteins conformation, it would interesting to measure be some proteins will well characterized conical structure like MscS[55] or KcsA for example.

Preliminary experiments in collaboration with Alice Berthaud in the group with the aquaporin 0, which is a protein with a cylindrical shape in first approximation, have shown that this protein is not enriched in the tube. Furthermore, when visiting our group, Ivan Lopez Montero has measured a depletion of the Acetylcholine receptor from tubes, in agreement with the presence of this protein in only the flat region of the neuromuscular junction.

Hence, the enrichment versus depletion in curved membranes depends complitely on the protein studied and is a priori consistent with mesoscopic data.

5.6.2.6 Experiments on cells

Finally, it would be interesting to study the relevance of these mechanisms in cells. One approach would be to pull tubes from cells and see if some membrane proteins are enriched or depleted in these tubes.

In this perspective, I pulled tubes from RPE1 (Retinal Pigmented Epithelial) cells that had a receptor SSTR3-GFP (type III somatostatine) that was endogeneously highly enriched in cilia. This study was done in collaboration with Rania Ghossoub and Alexandre Benmerah from the Cochin Institute.

We found that the receptor was not enriched in the pulled tube whereas it was enriched in the endogeneous cillia. This means that membrane curvature alone is not responsible for the receptor enrichment in the cilia, and that other active mechanisms are necessary.

In this chapter, I have shown that:

- KvAP is enriched in curved membranes and the enrichment increases with curvature consistently with a linear behavior.
- There is no diffusion barrier at the neck of the tube.
- The enrichment has no significant effect on membrane mechanics in the density range studied.
- The sorting strength is higher at low protein densities. It also exhibits more variability from one vesicle to the other.
- These experimental results are in agreement with a theory using a coupling between membrane curvature and protein density based upon the spontaneous curvature imposed by the protein on the membrane.

Chapter 6

Effect of confinement on diffusion

In this chapter, I present a study of the effect of membrane geometrical confinement on lipid and membrane protein diffusion. For this, we used single particle tracking to follow the diffusion of lipids and KvAP in membrane tubes as a function of membrane curvature. This work has been done in collaboration with Yegor Domanov, a post doc of the group. The results presented in this chapter were published in [183].

6.1 Introduction

I will first present an example of the relevance of membrane confinement for protein diffusion in a biological system. I will then introduce an hydrodynamic model for protein diffusion in membranes and an adaptation of this model for the tube geometry.

6.1.1 Biological motivation

Diffusion of lipids and membrane proteins in cell membranes play an important role in the kinetics of biomolecular processes in the membrane [184]. It is thus necessary to study which parameters can influence this diffusion.

As will be discussed in the next paragraphs, one parameter that could affect diffusion is membrane geometry because it affects membrane confinement. In particular, this effect could be important in neuronal dendrites where the membrane can be highly curved (see paragraph 5.1.1 of chapter 5). For example, Ashby et al. [185] have performed fluroescence recovery after photobleaching experiments on dendritic spines. They found that the diffusion of AMPA receptors and membrane-targeted green fluorescent protein into and out of dendritic spines is slower if the neck of the spine is thin (mushroom) as presented in figure 6.1.

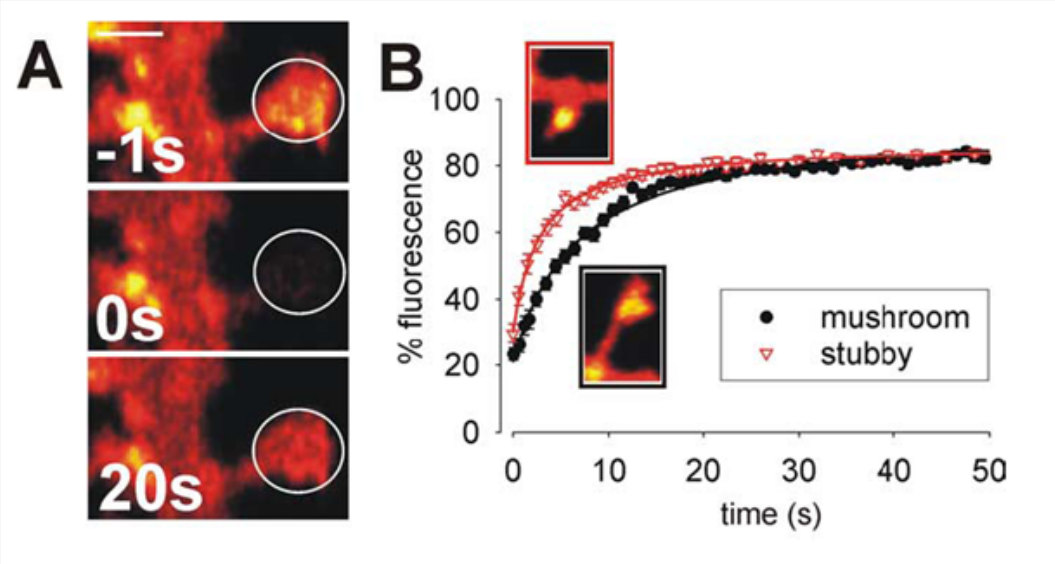

Figure 6.1: FRAP experiment on dendritic spines of different geometries: mushroom with a thin neck or stubby with a wide neck. The fluorescent protein is membrane-targeted green fluorescent protein (GFP) [185].

Furthermore, experiments from Marianne Renner in the group of Antoine Triller (ENS) using single particle tracking on a lipid, a peptide with one trans-membrane segment and a membrane receptor also showed a dependence of the protein diffusion coefficient as a function of the neurite radius as shown in figure 6.2. A reduction of the diffusion is also observed for thinner neurites [183].

Using our reconstituted system, we wanted to investigate whether this diffusion reduction results only from the membrane geometry, or from membrane lateral organization and interactions with the underlying cytoskeleton or other proteins.

6.1.2 Physics of membrane protein diffusion

I will now present a physical model for the diffusion of inclusions in the membrane, that can be used for trans-membrane proteins.

6.1.2.1 The model of Saffman and Delbrück

In a seminal work, Saffman and Delbrück introduced a hydrodynamic model for the diffusion of proteins in membranes. The basic is illustrated in figure 6.3 [186].

The protein is modeled as a cylinder of radius $R_{protein}$ moving laterally in a membrane of thickness h made of an homogeneous fluid of low Reynolds number and of viscosity μ. The membrane is surrounded by water.

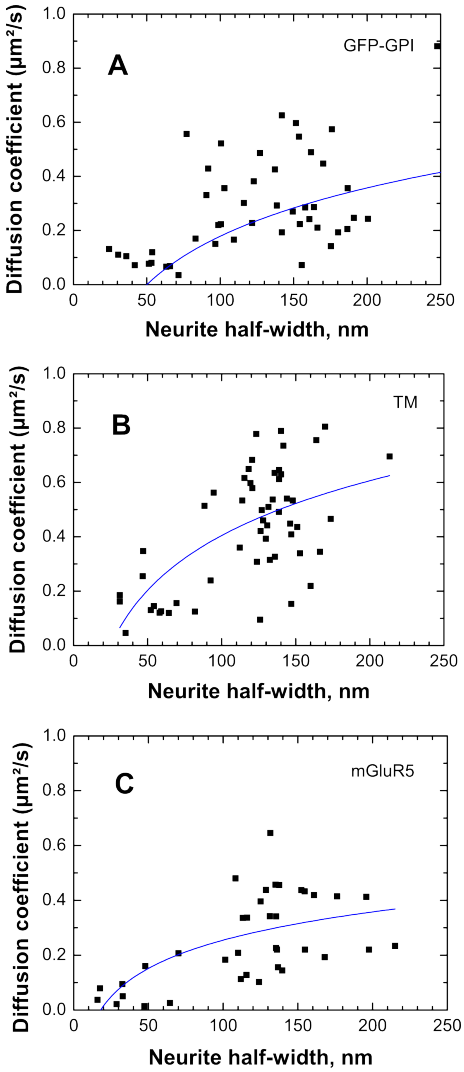

Figure 6.2: Mobility of tracers of different sizes in live neurons as a function of neurite size. The diffusion coefficients were measured by SPT in cultured hippocampal neurons of rats with QDs attached via specifiac antibodies to: (A) glycosylphosphatidylinositol-anchored green fluorescent protein, GFP-GPI, (B) super-ecliptic phluorin chimera with one transmembrane segment, TM, or (C) glutamate receptor with 7 transmembrane segments, mGluR5.From supplementary informations of [183].

6.1.2.2 Effect of membrane confinement

Saffman and Delbrück found that the protein diffusion coefficient for a membrane of finite size $R_{Membrane}$ is given by[186]:

$$D = \frac{k_b T}{4\pi\mu h} ln \frac{R_{Membrane}}{R_{Protein}} \tag{6.1}$$

Where μ is the membrane viscosity, h is membrane height, $R_{Membrane}$ is the radius of

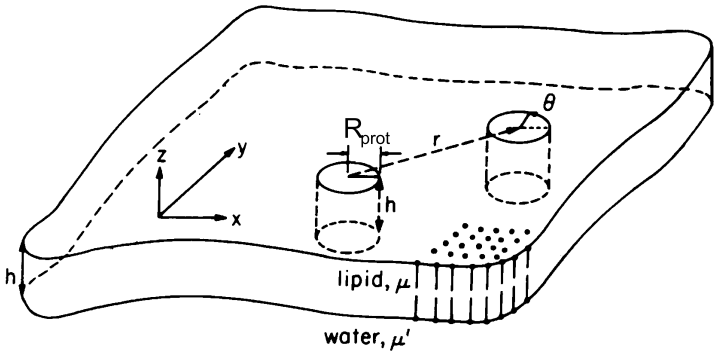

Figure 6.3: Saffman and Delbrück hydrodynamic model. From [186].

the circular sheet surrounding the protein and $R_{Protein}$ is the protein radius.

An intuitive explanation for the decrease of the membrane protein diffusion coefficient as a function of membrane size is presented in figure 6.4. As the protein moves in the membrane, the lipids must flow around the protein to fill the gap left behind the protein. If the membrane is geometrically confined, it will be more difficult for the lipids to flow around the protein which will impair its movement.

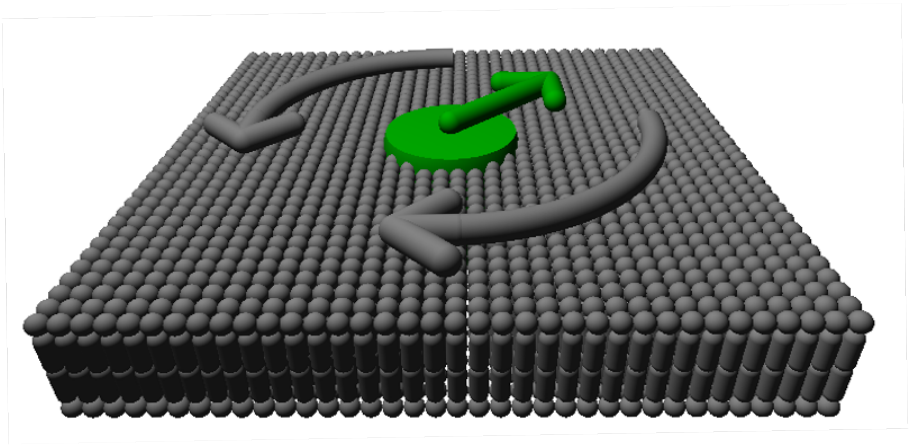

Figure 6.4: Cartoon explaining the effect of confinement on membrane protein diffusion. As the protein moves, the lipids must flow around it, which is more difficult if the membrane is small.

6.1.2.3 Adaptation of the Saffman and Delbrück model for the tube geometry

Daniels and Turner [187] have adapted this theory to the case of a membrane tubular geometry. The confinement of the membrane is then due to the geometry of the tube.

They found that the lateral diffusion coefficient should be given by:

$$D = \frac{k_b T}{4\pi\mu h} ln \frac{R_{Tube}}{R_{Protein}} \tag{6.2}$$

Note that the diffusion coefficient is expected to decrease logarithmically with the radius of the tube R_{Tube}.

6.2 Experimental system

To test Daniels and Turner's theory, we measured the diffusion coefficient of a lipid and of KvAP as a function of membrane curvature.

6.2.1 Measurement principle

The experimental principle is presented in figure 6.5. As for experiments in chapter 5, a vesicle is held in a micropipette to set membrane tension. A bead trapped in an optical trap is then stuck to the vesicle. The vesicle is then pulled away to create a membrane nanotube. Quantum dots attached to KvAP or to a lipid (biotin-phosphatidylethanolamine) are then followed using an EMCCD camera (Andor) with a 1 to 4 ms exposure time. The movement of the quantum dots are then analyzed to extract the diffusion coefficient parallel to the tube axis (see details in the article at the end of the chapter).

6.2.2 KvAP labeling and GUV preparation

My main experimental contribution to this project was to label KvAP with a biotin so that a streptavidin-coated quantum dot could bind to it. I also prepared GUVs containing the channel.

KvAP was purified and reconstituted in small unilamellar vesicles as described in chapter 3. To label the protein, I proceeded as described in section 3.4 of chapter 3 except that I used an EZ-Link maleimide-PEO11-biotin (Pierce) in place of the Alexa 488 maleimide. Briefly, the protein was incubated in 1 mM TCEP (Invitrogen) for one hour and further purified in a size exclusion chromatography column (Superdex 200 GL, GE Healthcare). The protein was labeled for 2 to 4 hours at room temperature in a 600 μM solution of EZ-Link Maleimide-PEO11-Biotin (Pierce, Rockford, IL). The labeled protein was then mixed with small unilamellar vesicles (SUVs) of EPC:EPA (9:1 molar ratio) pre-solubilised with decylmaltopyranoside (anagrade, Affymetrix, Maumee, OH). The free label and the detergent were removed during the dialysis.

GUVs were then prepared as described in section 4.2.1 of chapter 4. EPC/EPA SUVs containing proteins labeled with maleimide-PEG-biotin were unfrozen and mixed with pure EPC/EPA SUVs to achieve a final lipid/protein weight ratio between 8 and 200. Then GUVs were formed using the protocol in high salt buffer as described in section 4.2.2 of chapter 4.

Prior to the single particule tracking experiments, the GUV suspension was diluted with a buffer solution of matching osmolarity containing 20 mM Hepes, 50 mM NaCl, 75 mM glucose and 0.04 g/L casein at pH = 7.0. A small amount (~10 pmol) of QD625-streptavidin conjugate (Invitrogen, Cergy Pontoise, France) was added. These quantum

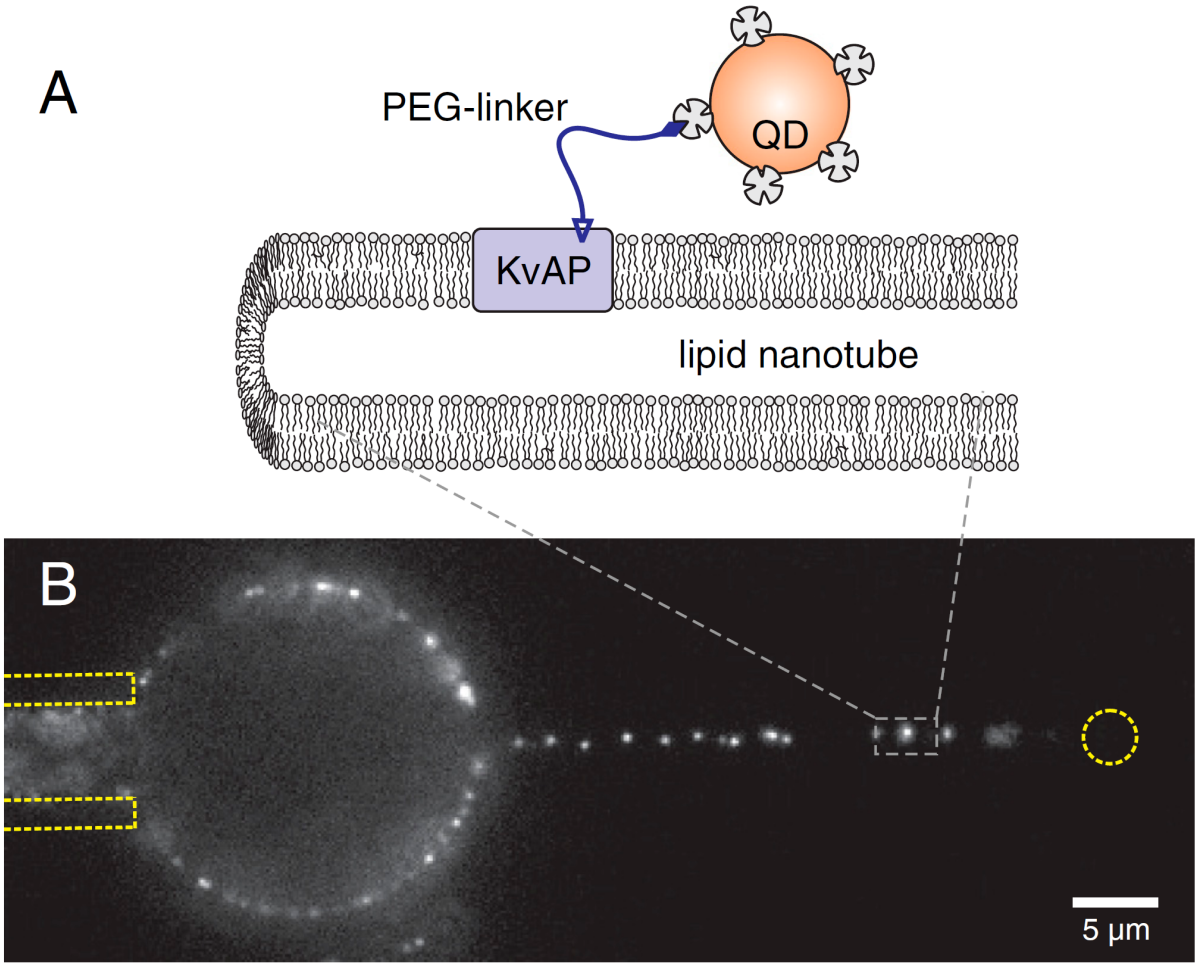

Figure 6.5: Single particle tracking experiments with KvAP. A vesicle is held in a micropipette (on the left). A tube is then pulled using a bead trapped in an optical tweezer (on the right). The diffusion of KvAP is then measured by following a quantum dot attached to it using an ultra fast camera.

dots have a maximum of emission at 625 nm and have (as all quantum dots), a very large absorption band in the UV range. After 1-2 min incubation, the GUVs were washed with the same buffer solution 3 times for 1 min at 1000g in a mini-centrifuge to get rid of the free quantum dots in solution. Note that, in proportion, more vesicles containing proteins than purely lipid vesicles were lost during this washing step. This might be due to a higher probability of vesicles containing proteins to become permeable and thus a higher difficulty to sediment.

6.3 Results and discussion

6.3.1 Compatibility with the Daniel and Turner model

The lateral diffusion coefficients of KvAP and biotin-phosphatidylethanolamine were measured for tube radii between 10 and 250 nm. The main result we obtained was that lipid and KvAP lateral diffusion coefficients both decrease by approximately 3 folds with tube radii in this range. Furthermore, as shown in figure 6.6, the curves were fitted with the relation 6.2, using the diffusion coefficient on the GUV as a reference for zero curvature (3.3 μm^2/s for the lipid and 2.3 μm^2/s for the protein). The fit from the lipid curve gives a lipid radius of 0.7 nm which is in good agreement with lipid size values from the literature [136]. The fit from the protein curve gives a protein radius of 3.0 $\pm$ 0.5 nm which is reasonable when considering KvAP structure (see figure 3.2 of chapter 3, in which the hydrophobic thickness is approximately 3,5 nm and the protein radius is between 2.5 nm -pore radius- and 5 nm). Furthermore, the membrane viscosity values from the fit ($\eta = 5.5 \times 10^{-10} Jm^{-2}s$ from the lipid and $\eta = 7.3 \times 10^{-10} Jm^{-2}s$ from the protein) are close to each other and to those found in the literature [188]. The lateral diffusion coefficient dependence with the tube radius is thus consistent with the model of Daniels and Turner.

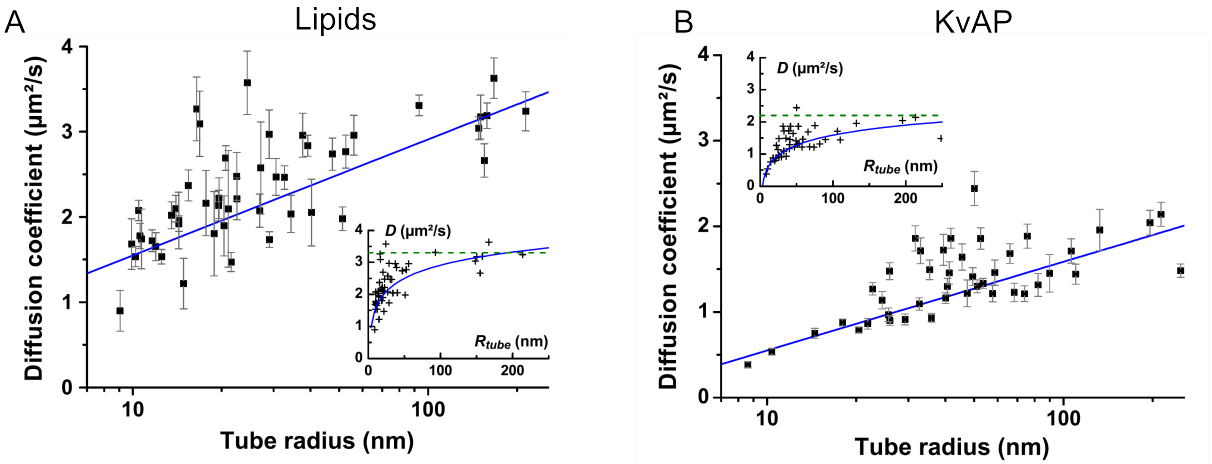

Figure 6.6: A) Lipid lateral diffusion coefficient. B) KvAP lateral diffusion coefficient. Semilogarithmic plots of longitudinal diffusion coefficient as a function of the tube radius. (Insets) The same data in linear coordinates.

6.3.2 Other factors possibly affecting the diffusion as a function of tube radius

The main other factors that are changed along with the confinement during the experiment are membrane curvature and membrane tension.

As presented in section 2.2.2 of chapter 2, membrane tension should increase the area per lipid and thus the distance between lipid headgroups. This should in principle

increase the diffusion coefficient and thus counteract the effect of membrane geometry. Furthermore, measurement of the diffusion coefficient on the GUV were not significantly affected by tension.

Similar arguments can be used for the effect of membrane curvature. Indeed, for the lipid experiments, the quantum dot only labels the external leaflet of the tube. The positive curvature should thus increase the area per lipid headgroup in this leaflet and thus also increase the measured diffusion coefficient. Note also that a transmembrane protein such as KvAP should be affected differently as it spans the full bilayer. This was not not the case as a good agreement with Daniels and Turner's model was found for both the lipid and the protein.

One last point to note here is that the diffusion coefficient values are consistent with the diffusion of a single protein. The protein is thus not aggregating because of denaturation for example. Furthermore, the protein does not form clusters as could be expected if in the presence of protein-protein interactions. It was thus reasonable to neglect protein-protein interactions as a first approximation in the theory developed in chapter 5 that describes the enrichment of KvAP with membrane curvature.

In this chapter, I have shown that:

- The lateral diffusion coefficient of a membrane protein (KvAP) and a lipid (biotin-phosphatidylethanolamine) decreases three fold with tube of radii ranging from 250 nm down to 10 nm.
- The decrease in diffusion coefficient is consistent with a hydrodynamic model of diffusion in confined membranes.

Chapter 7

Conclusion

In this thesis I have shown that it is possible to reconstitute KvAP in giant unilamellar vesicles while conserving the channel function. Furthermore, the system could be used to measure an enrichment of KvAP in curved membranes, and a decrease of KvAP diffusion coefficient with membrane confinement.

In this last part, I will recapitulate the results and highlight the many perspectives that are now opened and that I would dream to do myself if I had time to.

In chapters 3 and 4 I have presented the preparation and characterization of the model system. In chapter 3 I have shown that KvAP was successfully expressed, purified, labeled with Alexa 488, and reconstituted into small liposomes. With black lipid membranes experiments, I have also shown that the protein was still functional after labeling. In chapter 4, I have presented the successful reconstitution of KvAP into GUVs. With the protocol I developed, membrane composition (several lipid tested), buffers (high and low salt) and protein density (a few proteins to a few thousands proteins/μm^2) can now be controlled. We also showed that channels were still selective for potassium and voltage-gated after reconstitution.

In principle, GUVs containing functional voltage-gated ion channels should now open the way to a range of new biophysical experiments. These GUVs are very suitable for microscopy techniques because they have diameter of the order of tens of microns and their membrane is defect-free and because they are unilamellar. As I have presented in section 4.7 of chapter 4, one interesting application that I started to study is the interaction between channels and lipids by observing the lateral distribution of ion channels in GUVs containing co-existing domains. In a first experiment, KvAP was strongly segregated in Ld domains. Even though these experiments probably do not reflect directly the organization in cells, quantitatetive image analysis of reconstituted 3D images of vesicles [150] could

allow measuring the partition coefficients and thus provide a measurement of protein-lipid interactions. For example, it should be possible to prepare GUVs with lipid mixture of phospholipids, cholesterol and sphingomyelin and with reconstituted KvAP, that should exhibit coexisting domains. Specific interactions between the channel and those lipids could change the repartition of the channel between the liquid ordered and the liquid disordered phase but also affect the phase diagram as compared to the vesicles without KvAP. It could then be possible to use sphingomyelinase C to expose the phosphate group by removing the choline, or to also remove the phosphate using sphingomyelinase D [71, 72], and see the effect of these membrane composition changes with on the channel distribution and the vesicle phase diagram.

One could also consider combining electrophysiology and micromanipulation. It should thus be possible to measure effects of mechanical tension (as done for gramicidin by [189]) (using the micropipette aspiration technique) and curvature (by pulling nanotubes) on the channel activity. It would also be interesting to study the effects of specific membrane composition at physiological tensions which was not possible using previous techniques with reconstituted channels. Finally, the measure of channel lateral distribution (by confocal microscopy), but also clustering (by diffusion measurements) could be done as a function of the channel activity.

For these last perspectives it will be necessary to control the voltage in the whole GUV. This has been challenging so far because the GUV has no cytoskeleton and is thus more sensitive than a cell to differences of pressure between the pipette and the external buffer. The GUV membrane can also adhere more easily to the patch pipette and then crawl inside the pipette. This also leads to the disappearance of the vesicle and prevents electrophysiological measurements. However, some recent progress have been done in by Matthias Garten and Gilman Toombes in our group and the "whole GUV" geometry can now be achieved (see for example figure 7.1). By measuring the channel fluorescence in the vesicle, this technique will also allow checking if activity has an effect on channel distribution and clustering.

As presented in section 2.2.1.2 of chapter 4, it is possible to control membrane curvature by extracting nanotube of controlled radii from GUVs.

In chapter 5, I showed that KvAP is enriched in curved membranes and that the enrichment increases apparently linearly with curvature. Furthermore, FRAP experiments showed that there is no diffusion barrier at the neck of the tube so the enrichment corresponds to an equilibrium state. Even though in principle the protein could stabilize the tubes, no significant effect on membrane mechanics was observed in the density range I studied. Another non expected result was that the sorting strength is higher at low protein densities. All these experimental results are in agreement with a theory based a spontaneous curvature imposed by the protein to the membrane that was developed in collaboration with Andrew Callan-Jones. The large variability observed from one vesicle to the other for a given protein density is consistent with a variability in protein insertion, but could also be explained by other variable parameters such as the non controlled membrane voltage.

Many perspectives have already been presented in chapter 5, so I will not go into details here. Briefly, one major step will be to discriminate between both insertions (either by

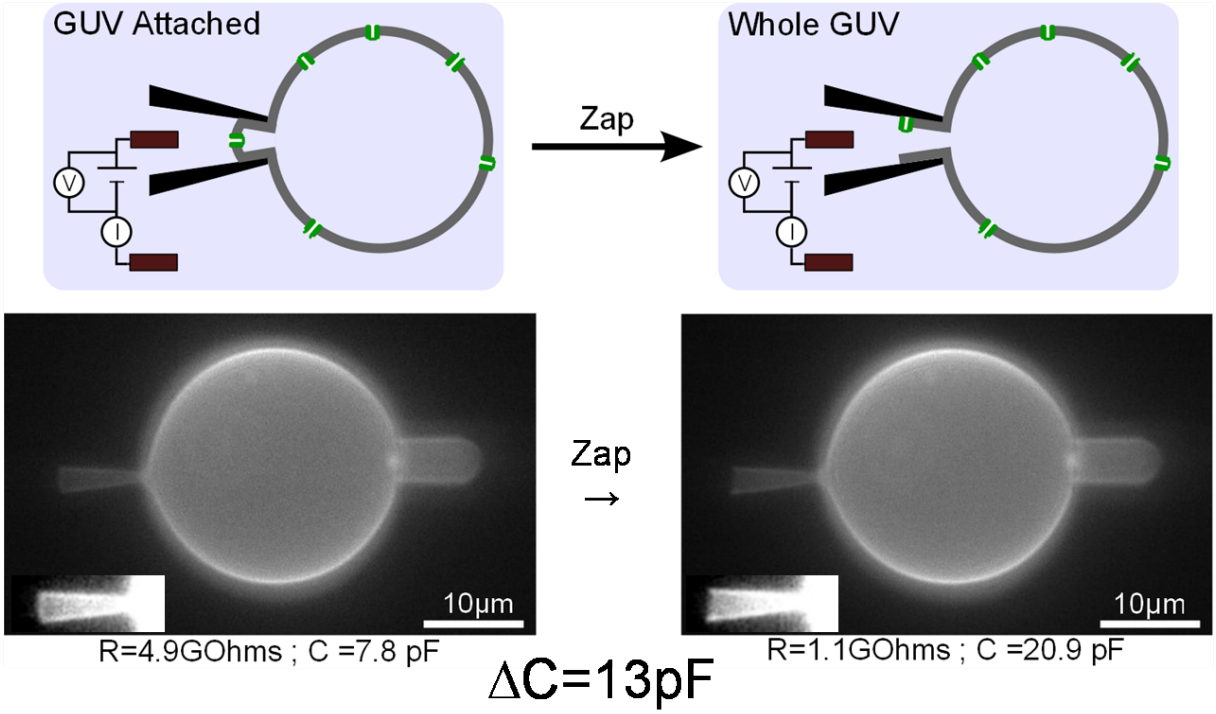

Figure 7.1: "Whole GUV" experiment. In oder to control the voltage of the whole vesicle membrane, the patch must be disrupted as shown in the drawing at the top. The two bottom images show a successfull access to the whole GUV body as seen with the capacitance increase. Experiment done by Gilman Toombes in the group.

changing the reconstitution protocol or by labeling only one insertion in the GUV) in order to validate the theory based on spontaneous curvature. Another range of possible experiments would involve changing channel conformation (either by changing membrane potential, by changing the channel interactions with the membrane e. g. by changing membrane composition or by mutating the channel). The channel distribution could also be studied in geometries other than a simple tube. For a example, a Y shape can be created by pulling two tubes from a vesicle [190] that could mimic the same geometry in axons. Finally, it would be interesting to test the coupling between protein density and curvature in vivo by pulling membrane nanotubes from cells.

In chapter 6, I have summarized the analysis of the diffusion of KvAP and a lipid as a function of the tube radius using single particle tracking. We found that the longitudinal diffusion coefficient of a membrane protein (KvAP) and a lipid (biotin-phosphatidylethanolamine) decreases three folds with tube radii ranging from 250 nm down to 10 nm. This decrease in diffusion coefficient is consistent with a hydrodynamic model of diffusion in confined membranes proposed by Daniels and Turner. It was the first experimental evidence of the confinement effect in the Saffman Delbrück theory. The obvious experiment to do now is to measure the effect of tension on the diffusion independently of membrane curvature. On the top diffusion coefficient increase due to the increase of area per head groups, there should be some interesting effects due to mem-

brane fluctuations and coupling of the protein to curvature [191, 192]. This experiment is already in progress in the group on the same GUVs.

One important aspect of the effect of trans-membrane proteins on membranes has been eluded during this thesis: their effect on membrane dynamics. When changing membrane shape, the two monolayers of the membrane need to slide against each other. The presence of insertions such as trans-membrane proteins could thus impair this relative flow (i.e. add a friction between the two leaflets) and thus resist to membrane deformation. This effect can be measured by monitoring the force necessary to hold the tube when changing the tube length, as the membrane needs to go from an effectively flat geometry (in the vesicle) to a really curved geometry (in the tube). As described in section 2.2.2 of chapter 2, at equilibrium, the force necessary to hold a tube should be independent of the tube length ($f = 2\pi\sqrt{2\kappa\sigma}$). However, this force should change when changing the tube length if there is friction between the two leaflets [193]. With pure lipids, this effect is negligible for extrusion velocities of the order of 1 to 10 $\mu m/s$. In cells, a force increase was detected but was attributed to the interactions between the cytoskeleton and the membrane [29]. Clement Campilo in the lab [194] has shown that the presence of oil between the leaflets could markedly increase the friction. Similarly, the presence of transmembrane objects could also radically change the ability of the two leaflets to slide on the top of each other. Tube extrusion experiments on GUVs containing KvAP should allow determining the respective contributions of transmembrane proteins and the cytoskeleton to the force increase observed in cells.

In preliminary experiments, I pulled tubes from a vesicle containing reconstituted KvAP and changed the tube length. While changing the tube length had no effect on the force for a purely lipid vesicle, the resulting force change could be dramatic with GUVs containing KvAP as shown in figure 7.2. I found also that the force relaxed with time scales depending on the tube radius. These experiments should be further continued to obtain clear results and to ensure for example that the vesicles used in this study were unilamellar.

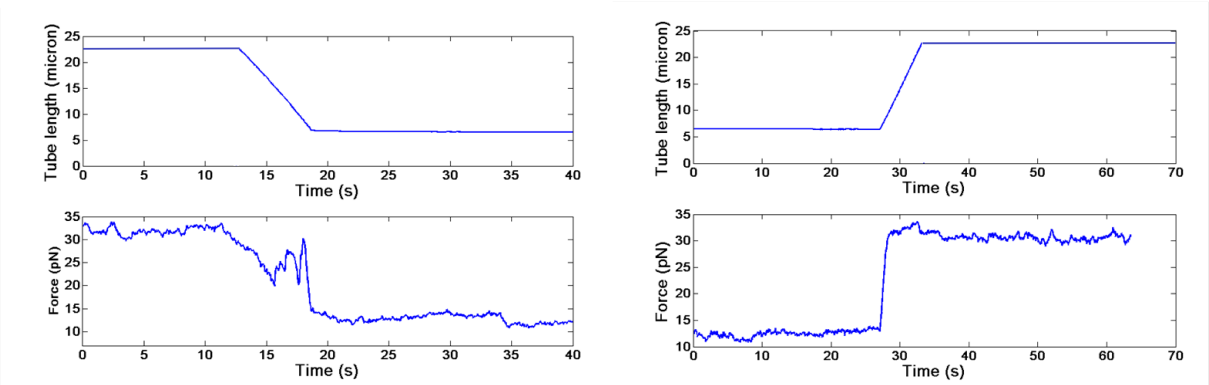

Figure 7.2: Effect of tube length change on the force necessary to hold a tube. Left: retraction, right: extension.

Finally, the long term goal of the project is to produce an in vitro model action potential

as shown in figure 7.3. A tube would be pulled from a vesicle containing reconstituted channels, thus mimicking the soma/axon geometry. A ion concentration difference is required between the inside and the outside of the GUV. When exciting the "soma" with an electrode, ion channels would open and let ions go through the membrane, which would in turn change the membrane potential. Channel in the close vicinity would then open and this process would propagate further. It would thus be possible to propagate a simplistic "action potential".

Preparing such system would allow studying the propagation of this signal as a function of membrane parameters. We could thus investigate the parameters that affect the signal propagation velocity, the effect geometry changes (i. e. branching points or pearling), the minimum density of channels for action potential triggering, the role of channel noise and how it is related to other parameter such as the "axon" length and diameter... And finally is it really necessary to have ion channels for the propagation of an action potential or can phase transitions in the membrane be sufficient as proposed by Thomas Heimburg [195]?

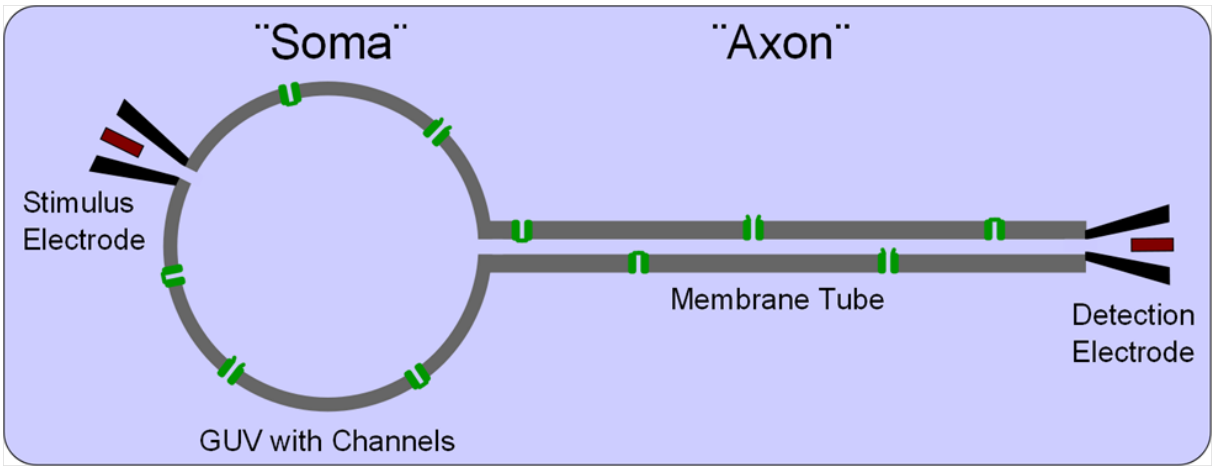

Figure 7.3: The model system developed in our project to investigate action potential propagation.

To conclude, an application at very long term of such systems would be to build "soft" interfaces (like our model neuron) between neurons and transistors to connect the brain to electronic devices... But I should probably stop there and leave the rest to your imagination.

Chapter A

Detailed purification protocol

A.1 Expression and Solubilization

The protocol for purifying KvAP was based upon the work of [97]. Pr. R. MacKinnon (Rockefeller University, NY) generously gave us the wild-type KvAP cDNA inserted into the pQE60 vector (Qiagen). This plasmid included the endogenous cysteine, C247, a C-terminal hexa-histidine tag and the T5 Promoter. For each purification, 100 μL of XL-1 Blue competent cells were transformed with the plasmid (100 ng) and incubated in 500 μL of SOC medium (Invitrogen) for 30 min at 37 °C. The bacteria were then plated onto 6 LB/ampicillin agar plates and left overnight at 37 °C. The following morning, all the colonies on the plates were transferred into 200 ml of LB containing 200 mg/L (0.6mM) ampicillin and this small culture was incubated for 1h at 37°C. The bacteria were then diluted into 6 baffled flasks (2L Nalgene Shake Flasks, Thermo Fisher Scientific) containing 1L of LB, 200 mg/L ampicillin and 10 mM BaCl2 and grown at 37 °C under vigorous shaking (240 RPM). After 4 to 5 hours, the culture reached an OD600 of 0.8-0.9 and protein expression was then induced by the addition of 0.4mM isopropyl-b-D-thiogalactopyranoside (IPTG, Euromedex). Following 4 hours of expression, cells were harvested via centrifugation (15 min, 8000 g) and the pellets stored overnight at 4°C. The following day, the cells (30 g wet mass) were resuspended in 100 ml of a buffer containing 100 mM KCl, 50 mM Tris (pH8), 6 tablets of EDTAfree proteinase inhibitors (Roche), 1 ml of 100 mM phenylmethylsulfonyl fluoride (PMSF, Fluka) and a small spatula of DNAse I (Roche diagnostics). Cells were broken by tip sonication on ice (8 cycles each consisting of 60 seconds of sonication (1 second on, 1 second off) followed by a pause, XL 2020 Sonicator, Misonix). 40mM n-Decyl-maltopyranoside (DM, Anagrade, Affymetrix, Maumee, OH) was then added to solubilize the cell membranes and the solution was gently agitated for three hours at room temperature. After solubilization, un-dissolved material

(such as inclusion bodies) was removed by ultracentrifugation (30000g, 20 min, 10 °C) and the resulting supernatant filtered (0.2 micron) in preparation for purification.

A.2 Purification

Initial purification of the protein was achieved via IMAC (Immobilized Metal ion Affinity Chromatography). Using an AKTAbasic system (GE Healthcare), a His-tag affinity column (1mL volume, HiTrap chelating column charged with Ni2+, GE Healthcare) was equilibrated with buffer A (5 mM DM, 100 mM KCl, and 20 mM Tris pH 8) and the lysate then loaded at a flow rate of 1ml/min. To remove non-specifically bound proteins, the column was washed first with 5 ml of buffer A, and then with 10 ml of buffer A + 15 mM imidazole. For each wash, absorbance at 280 nm was monitored and the wash was stopped when the absorbance returned to the baseline. KvAP was then eluted using buffer A + 400 mM imidazole. The most concentrated protein fractions were selected using the measured absorbance at 280nm. The typical yield after pooling these fractions was 5 mg of protein at a concentration of 2 mg/ml. To remove the hexa-histidine tag, 2 units of thrombin (Roche diagnostics) were added and the solution left overnight at room temperature. The following morning, disulfide bonds were reduced by adding 1mM TCEP (Invitrogen). After allowing the reaction to proceed for 1 hour at room temperature, the protein was re-concentrated to 10 mg/ml using a 10 kDa cutoff concentrator (Amicon) and filtered using a 0.2 micron Spin-X filter (Sigma). The final purification was achieved in 5 mM DM, 20 mM TRIS (pH 8), 100 mM KCl using a Superdex 200 10/300 GL (GE Healthcare) size exclusion column. After selecting the most concentrated fractions, the protein concentration was determined by measuring the absorbance with a Nanodrop UV-Vis absorption spectrometer(NanoDrop Spectrophotometer, Thermo Scientific, Illkirch, France) (A280 = 37000 M-1cm-1). The final yield of the purification was typically around 3 mg protein.

A.3 Fluorescent labeling

Before reconstitution, the protein was fluorescently labeled with Alexa 488 maleimide (Invitrogen) at a final ratio of 0.2mg Alexa-488 per 1 mg of KvAP. After allowing the reaction to proceed for 2-4h at room temperature, the un-reacted free label was removed (along with the detergent) via dialysis during the reconstitution process. The protein and fluorophore concentrations then measured by absorbance spectroscopy using the Nanodrop.

A.4 Reconstitution in small liposomes

The protein was reconstituted in small liposomes following a protocol from [70]. EPC (L-α-phosphatidylcholine), EPA (L-α-phosphatidic acid), DPhPC (diphytanoylphosphatidylcholine),POPC (1-palmitoyl-2-oleoyl-sn-glycero-3-phosphocholine)and POPG (1-hexadecanoyl-2-(9Z-octadecenoyl)-sn-glycero-3-phospho-(1'-rac-glycerol)) were purchased from Avanti Polar Lipids (Alabaster, AL) and stock solutions were prepared by weighing

lipids before dissolving them in chloroform. Three lipid compositions were used for reconstitution: EPC:EPA (9:1 w:w), POPC:POPG (9:1 w:w), and DPhPC. Lipids in chloroform were dried under argon and any remaining solvent was then removed by placing the samples under a vacuum for 3-12h. The lipid was then suspended at 10mg/ml in a low-salt buffer (5 mM KCl and 1 mM HEPES pH 7.4). Small Unilamellar Vesicles (SUVs) were then formed by tip sonication (1sec on/1sec off for 30 sec, 5 times; XL 2020 Misonix). Note that solutions with DPhPC did not fully clarify after sonication. The SUVs were then pre-solubilized by adding 10 mM decylmaltopyranoside (DM) for 30 min at RT. The protein was concentrated up to approximately 10 mg/ml in a 15 ml 30 kDa cutoff oncentrator (Amicon) and was added to the pre-solubilized SUVs to achieve a protein:lipid ratio of 1:10 by mass. More DM was then added (final concentration of 17.5mM) and the resulting mixture was gently agitated for approximately 1h. Detergent was then removed at room temperature by dialysis (12-14K tubing, Spectrum Laboratories, The Netherlands). The external buffer was changed every 6 to 12 h for 3 days, and after dialysis the resulting vesicles were aliquoted, flash-frozen in liquid nitrogen and stored at -80 °C. These small proteoliposomes were used as stock for GUV preparation.

Chapter B

Production of GUVs with and without reconstituted KvAP

The protocol to prepare GUVs containing KvAP was based upon that of Girard et. al. [32], with modifications to allow the use of physiological buffers [33]. Figure S3 illustrates the key steps of the electro-formation process. Droplets of a solution of SUVs containing the protein are deposited on wire electrodes. Partial evaporation of the solution leads to the formation of a lipidprotein film through the fusion of SUVs. GUVs then form when this film is rehydrated under an applied AC electric field. The protein-to-lipid ratio and lipid composition of the initial SUV solution was adjusted by combining a solution of the proteoliposomes (preparation described in Supporting Text S1) with other SUV solutions. For example, SUVs containing TR-DHPE were frequently added (final concentration of up to 0.5was homogenized by vortexing for approximately 1 min. Sonication of the SUV solution did not appear to produce GUVs with more uniform fluorescence. Because the salt concentration increases significantly during the partial dehydration step, SUVs were always prepared in a low-salt buffer (5mM KCl, 1mM HEPES pH7.4). In addition, 2 to 10 mM of trehalose (generously given by Prof. Lorenzo Cordone, Palermo, Italy) was added to the SUV solution to further protect the protein during the partial dehydration step[61]. The final lipid concentration in the SUV mixture was typically 3 mg/ml.

As shown in Figure B.1, the electro-formation chamber was made from a Teflon block containing three wells (diameter 10mm). The electrodes consisted of two parallel platinum wires (0.5mm or 0.8 mm in diameter, Goodfellow, UK) separated by a edge-to-edge distance of 2.5 mm. Tests showed that GUVs could also be formed using titanium wires in place of the platinum wires. Before each GUV growth, the wires were typically cleaned by rubbing with Kimwipe tissues (Kimberly-Clark), washes with water, ethanol and chloroform and bath sonication in these same solvents. Electrolysis of a 1M NaCl solution

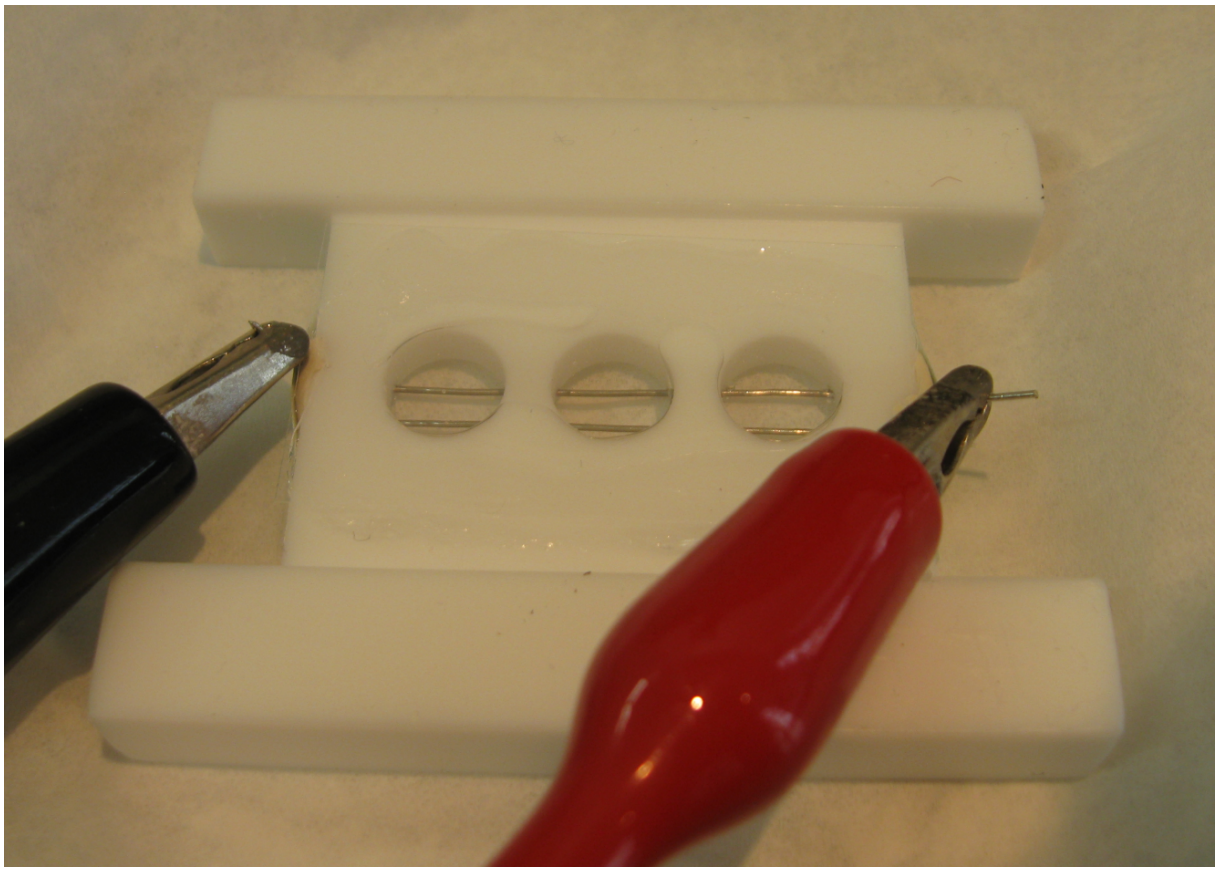

Figure B.1: GUV electroformation chamber. The two platinum electrodes are mounted in a teflon block with 3 wells. The top and bottom of the wells are sealed with microscope coverslips, and the two platinum wires are connected to a signal generator via alligator clips.

(V=7V RMS; f=1Hz) for 60 seconds was found to clean the wires very effectively and helped ensure a good yield of vesicles afterwards. To form the protein-lipid film on the platinum wires, the proteoliposome mixture (5 μl of solution per 8 cm of platinum wire) was applied using a 10μl glass syringe (Hamilton, Bonaduz, Switzerland). Small droplets of the SUV solution were spread along the wire while taking care not to touch droplets to each other (to avoid merging droplets). The droplets were left to dry under room atmosphere for approximately 30 minutes: no liquid could be detected by eye after approximately 5 to 10 minutes and evaporation was typically allowed to continue for an extra 20 minutes. Insufficient dehydration of the SUV solution resulted in GUVs with non uniform membranes or even a dispersion of SUVs in solution during the rehydration. The use of a SUV solution with a high osmolarity (e.g. 100mM KCl) only further exacerbated such problems. In principle, excessive dehydration could damage the protein, so the shortest period of dehydration consistent with a good GUV yield was used. After the deposition of the SUVs, the chamber bottom was sealed with a glass coverslip held in place by grease (Silicon Paste P4, Wacker). The wells were then carefully filled with GUV

hydration buffer and the top of the chamber was then sealed with a second glass coverslip. To apply a sinusoidal voltage, a signal generator (TG315 or TG215, TTi, or GFG 2004, Iso-tech) was connected to the two electrodes by alligator clips and the voltage across the two electrodes measured with a multi-meter. The voltage applied during GUV growth was chosen according to the GUV rehydration buffer. To grow GUVs in a "physiological" buffer of 200mM sucrose, 100mM KCl, 10mM Hepes pH 7.4, a voltage of 0.35V RMS (Root Mean Square) and 500Hz was applied overnight. For GUVs grown in low-salt buffer (5mM KCl, 1mM HEPES (pH 7.4),400mM sucrose) a 10 Hz voltage was used. The voltage was slowly stepped up to the maximal value of 0.7 V RMS over 30 minutes before continuing the growth for approximately 2 hours. Because the electric field could potentially affect protein conformation, efforts were made to use the lowest voltage/shortest time that gave a useful GUV yield. The growth of GUVs on the electrodes could be followed via phase-contrast microscopy as shown in Figure S5. Note that GUVs typically formed in bunches along the wires. Curiously, when using DPhPC SUVs a surprising number of extremely large GUVs formed at the ends of each well where the wires made contact with the Teflon block. As PEG lipids are thought to help produce defect-free GUVs [41], growth was tested with up to 1divalent ions cross-linking the dehydrated membranes stacks, GUV growth was also tested in the presence of 2 mM of EDTA. However, the presence of trehalose, EDTA or PEG lipids did not significantly affect GUV growth and the effects of trehalose, EDTA or PEG lipids on channel function were not studied. Preparation of GUVs containing co-existing liquid domains To prepare SUVs containing DPPC:Cholesterol (1:1 by mole), lipids in chloroform were mixed, dried at 50 ℃for several minutes, and then kept under vacuum overnight. The lipid film was then rehydrated in a solution of 2 mM trehalose and sonicated as described in Supporting Text S1. SUVs containing DPhPC and TR-DHPE were prepared in the same way. To prepare vesicles with domains, DPhPC proteo-SUVs were mixed with these DPPC:Cholesterol SUVs to achieve a final lipid molar composition of 6:2:2 (DPhPC:DPPC:Cholesterol) plus 0.5This composition has been reported to produce GUVs with co-existing liquid domains at room temperature[34]. 10 mM trehalose was then added to the SUVs mixture. To try to prevent de-mixing of the lipids during the GUV growth, the SUVs were dried at 50 ï¿½C, rehydrated at 50 ℃in low-salt buffer (5mM KCl, 400mM sucrose, 2mM HEPES (pH 7.3)). During rehydration, a voltage of 0.5V RMS (10Hz) was applied for 30 min. For imaging, the resulting GUVs were then transferred into a buffer of 200mM glucose, 100mM NaCl, and 10mM Hepes (pH 7.3) at room temperature. Production of pure lipid GUVs GUVs containing only lipids were prepared using a standard electro-formation protocol[62]. The stock solution for unilamellarity measurements was prepared by adding TR-DHPE (0.5 % by mole) to a solution of EPC in chloroform (0.5mg/ml). For membrane fluorescence quantification, Bodipy-HPC was added to a solution of EPC in chloroform to form stock solutions with concentrations between 0.008% and 0.5 % by mole. 25ul of the lipid solutions (0.5 mg/ml) was spread with a Hamilton syringe onto two ITO slides (Prazisions Glas & Optik, Iserlohn, Germany). Residual solvent was removed by placing the slides under vacuum for 2 hours to overnight. The slides were then assembled into a chamber (1mm thickness) using sigillum wax (Vitrex Medical, Herlev, Denmark), a 200mM sucrose buffer added, and an alternating voltage of 1.1 V RMS and 10 Hz applied for approximately 1 hour.

Chapter C

Résumé

C.1 Introduction

C.1.1 Excitabilité des cellules

Certaines cellules ont la capacité de générer et de propager des signaux électriques. Dans le cas des neurones, ces signaux sont responsables de la propagation de l'information dans le cerveau par exemple. Des protéines trans-membranaires nommées canaux voltage-dépendants sont à la base de ce processus [5], comme je vais le détailler ci-dessous.

C.1.1.1 Potentiel de la membrane et potentiel d'action

Toutes les cellules sont entourées d'une membrane avec un coeur hydrophobe qui sépare le milieu intracellulaire de l'extérieur et empêche les molécules hydrophiles comme les ions de traverser. Cependant, des protéines présentes dans cette membrane (les pompes) font activement passer certains ions à travers la membrane, ce qui produit une différence de concentration ionique entre l'intérieur et l'extérieur de la cellule. Par exemple, la concentration en potassium est typiquement de 5 mM à l'extérieur de la cellule et de 150 mM à l'intérieur, alors que la situation est inversée pour le sodium (150 mM à l'extérieur et 10 mM à l'intérieur).

Si la membrane devient sélectivement perméable à l'un de ces ions, une dfférence de potentiel électrique va s'établir. Par exemple, si la membrane devient sélectivement perméable au potassium, le potassium va diffuser du milieu le plus concentré vers le milieu le moins concentré et va donc sortir de la cellule. Comme le potassium est chargé positivement, cela se traduit par un potentiel négatif de l'intérieur de la cellule par rapport à l'extérieur. Dans les cellules, la membrane est en général un peu perméable au potassium

mais pas au sodium, ce qui implique qu'elles ont un potentiel de repos d'environ -70 mV.

Dans les années 50, Hodgkin et Huxley ont proposé que des changements de conductivité de la membrane sont responsables de la propagation du signal électrique dans les neurones. Ils ont étudié l'axone géant du calamar et trouvé que lors du passage du signal électrique (appelé potentiel d'action), la perméabilité de la membrane pour le sodium augmente et ce d'autant plus que la membrane est éloigné de son potentiel de repos. Le sodium rentre alors dans la cellule ce qui la dépolarise d'autant plus. La perméabilité pour le sodium diminue alors tandis que la perméabilité pour le potassium augmente. Le potentiel de membrane se met à diminuer jusqu'à retourner au potentiel de repos. Pour cette découverte, Hodgkin et Huxley eurent le prix Nobel en 1963.

C.1.1.2 Canaux ioniques voltage-dépendants

Les protéines responsables du changement de perméabilité de la membrane ont été découvertes plus tard. Il s'agit des canaux voltage-dépendants. Ce sont des protéines transmembranaires qui permettent de laisser passer sélectivement des ions à travers la membrane en fonction du potentiel électrique appliqué.

Une technique importante pour leur mise en évidence a été inventée par Neher et Sakmann. Il s'agit de la technique de patch-clamp. Le but était de détecter le signal du à un canal ionique unique. Pour cela, il a fallu isoler électriquement un petit morceau de membrane en collant une pipette de verre contenant une électrode à la membrane d'une cellule, et mesurer le courant la traversant. Il ont ainsi pu observer de petits sauts de courant (de conductance égale à environ 10 pS) correspondant à l'ouverture et la fermeture de canaux uniques.

Plus tard, ces canaux ont pu être isolés et leur structure a été étudiée. Il s'agit de protéines transmembranaires constituées de quatre motifs identiques. Un exemple est présenté figure C.1.

Ces protéines sont constituées d'un pore central sélectif pour certains ions (potassium, sodium, ou calcium). Le pore est entouré par quatre domaines contenant des charges qui permettent à la protéine de changer de conformation lorsqu'un potentiel est appliqué à la membrane. Le canal a aussi la possibilité de s'inactiver après s'être ouvert, c'est-à-dire qu'il ne peut plus s'ouvrir avec le potentiel membranaire pendant une période variable d'un type de canal à l'autre.

C.1.2 Biophysique de la membrane

C.1.2.1 Membranes biologiques et membranes modèles

Comme mentionné au-dessus, le rôle principal des membranse cellulaires est d'isoler les milieux intracellulaires et extracellulaires en formant une barrière hydrophobe. Ceci est possible grâce à des molécules amphiphiles telles que les lipides par exemple. Ceux-ci possèdent une "tête" hydrophile et deux "queues" hydrophobes. Mais les membranes des cellules sont très héterogènes, de composition complexe et activement régulées par la cellule elle-même. Pour étudier leurs propriétés, il est donc utile de réaliser artificiellement des systèmes plus simples où les paramètres intervenant dans le problème à étudier peuvent être contrôlés.

Les Vésicules Unilamellaires Géantes (ou GUVs pour Giant Unilamellar Vesicle) sont des vésicules de quelques microns à 100 microns de diamètre, constituées d'une seule membrane lipidique. Leur taille permet notamment de les observer par microscopie optique mais aussi de les manipuler avec les mêmes outils que ceux utilisés pour les cellules.

C.1.2.2 Déformations de la membrane

Une approche fructueuse pour décrire les propriétés physiques des membranes a été d'utiliser la théorie de l'élasticité. Celle-ci a été adaptée au cas des membranes lipidiques notamment par Canham et Helfrich [32, 33] dans les années 70. L'hypothèse de base est de considérer la membrane comme un liquide bidimensionnel. L'énergie pour la cisailler est donc considérée comme négligeable.

Par contre, l'énergie pour la courber est donnée par la théorie de l'élasticité:

$$H_{curv} = \frac{1}{2}\kappa(C - c_0)^2 + \kappa_G C_G \tag{C.1}$$

où C est la courbure moyenne de la membrane, c_0 est la courbure spontanée (c'est-à-dire la courbure préférée énergétiquement), κ est la rigidité de courbure (valant typiquement de quelques kT à 100 kT), κ_G est la rigidité de courbure gaussienne, et C_G est la courbure gaussienne.

L'énergie pour étirer la membrane qui donnée en première approximation par

$$H_{stretch} = \sigma(\frac{\Delta A}{A}) \tag{C.2}$$

où σ est la tension membranaire. Il faut noter que comme la membrane est incompressible en première approximation, un étirement s'accompagne aussi d'un changement d'épaisseur.

Les membranes étant très flexibles, elles peuvent fluctuer sous l'action de l'agitation thermique.Une contribution entropique à la tension de membrane a également été calculée par Helfrich.

Cette tension peut être contrôlée dans des GUVs en les aspirant à l'aide d'une micropipette. En effet, suivant la loi de Laplace, plus la vésicule est aspirée dans la micropipette, plus la membrane est tendue.

Comme sera décrit dans la section C.4.2, il est aussi possible de contrôler la courbure de la membrane en formant un nanotube à partir de ces GUVs.

C.1.3 Rôle de la membrane dans l'excitabilité cellulaire

Dans le modèle de Hodgkin et Huxley, la membrane a pour seul rôle de faire barrière aux ions en l'absence de canaux ioniques ouverts. Cependant la membrane pourrait avoir d'autres rôles tant au niveau moléculaire (en agissant sur l'activité des canaux ioniques) qu'au niveau cellulaire (par exemple la géométrie de la membrane pourrait modifier la distribution des canaux).

La structure en croix des canaux ioniques voltage-dépendants (montrée dans la figure C.1) implique que l'interface entre ces protéines et la membrane est grande. En particulier, les domaines senseurs de voltage sont presque complètement entourés de membrane.

Tout d'abord, les lipides de la membrane peuvent interagir avec des sites spécifiques de la protéine. Cela a été montré pour les têtes phosphodiester des phospholipides [76], qui sont nécessaires pour stabiliser la conformation ouverte du canal. En effet, des expériences d'électrophysiologie en membrane suspendue ont montré que le canal ne s'ouvre pas quand ces groupes sont absents dans les lipides.

De plus, la conformation du canal pourrait être couplée à la courbure, à la tension ou à l'épaisseur de la membrane. En effet, la forme du canal et ses interactions avec les lipides de la membrane pourraient induire une courbure locale de la membrane. Il pourrait aussi changer localement l'épaisseur de la membrane. Enfin, si l'aire du canal dans la membrane change pendant un changement de conformation, l'activation pourrait être couplée à la tension de la membrane. Les propriétés mécaniques pourraient donc influencer l'activité du canal mais des hétérogénéités de courbure ou d'épaisseur membranaire pourraient également changer sa distribution dans les cellules. De plus, des déformations locales de la membrane pourraient induire des interactions canal/canal. Par exemple, si les canaux affinent localement la membrane, ils auront tendance à s'attirer pour minimiser la déformation totale de la membrane. Enfin, les changements de conformation des canaux pourraient influencer les fluctuations de la membrane ("membranes actives").

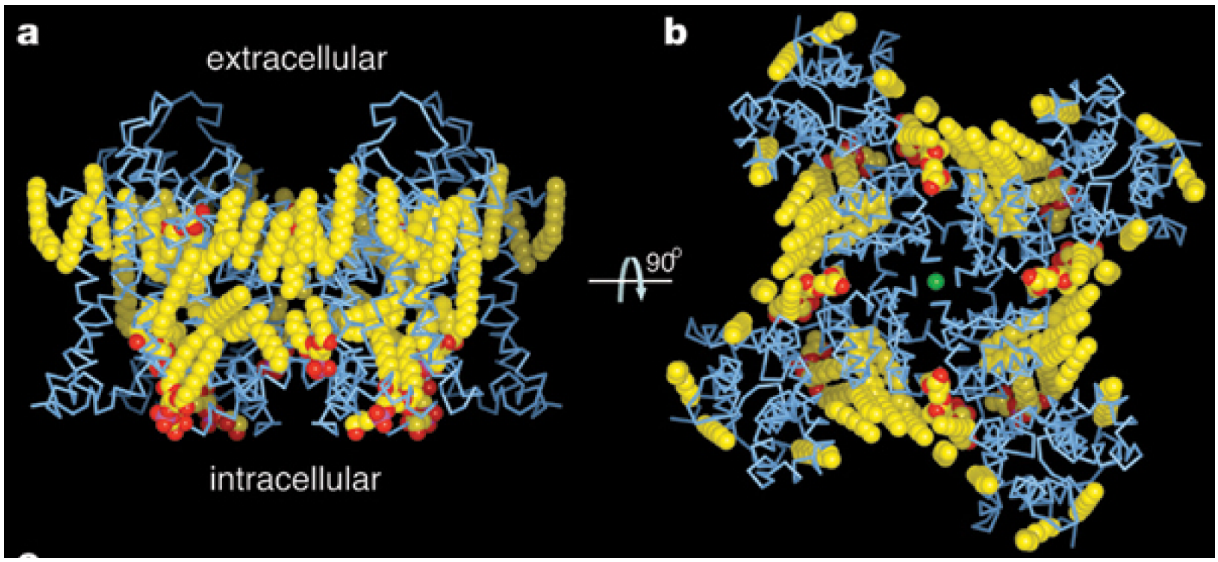

Figure C.1: Structure d'un canal potassium voltage-dépendant (Kv1.2) dans la membrane. a) vue de côté, b) vue de dessus. Tiré de [1].

Il est donc important de pouvoir étudier l'effet des propriétés des membranes sur le fonctionnement et la distribution de ces canaux.

C.1.4 Objectif de la thèse

Il est difficile d'étudier le rôle de la membrane dans l'excitabilité en utilisant des cellules car les paramètres pertinents (composition et état mécanique de la membrane, densité de canaux...) sont activement régulés par la cellule elle-même et donc difficilement ajustables. Nous avons donc choisi de réaliser un système simplifié et contrôlé, c'est-à-dire de

reconstituer des canaux voltage-dépendants dans des vésicules unilamellaires géantes dans lesquelles la composition lipidique, la tension, la courbure, la densité de canaux et le potentiel de membrane peuvent être contrôlés.

Ma thèse s'inscrit dans un projet plus vaste qui a pour but de développer un neurone minimal, dans lequel la propagation du potentiel membranaire pourrait être étudiée tout en contrôlant les paramètres de la membrane (voir figure C.2).

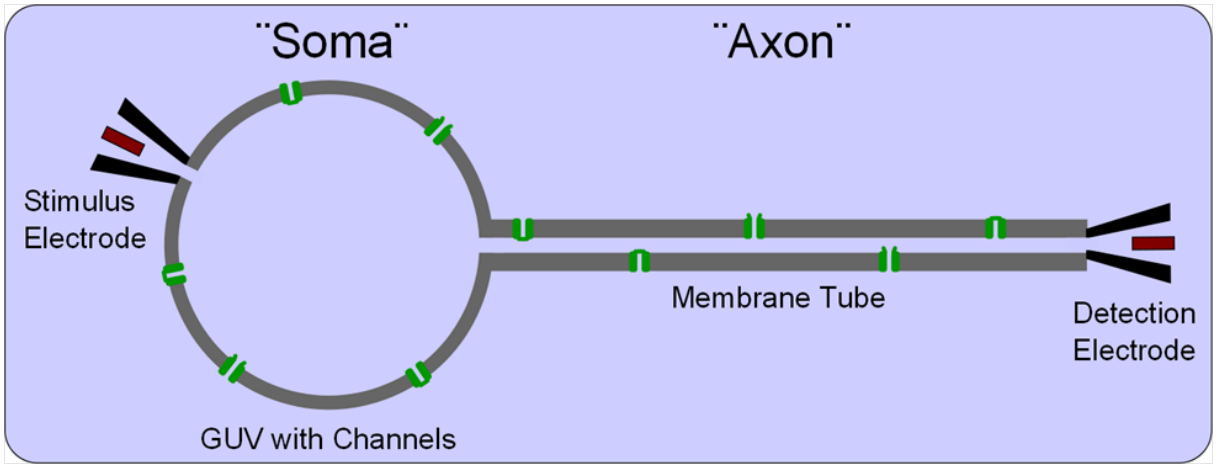

Figure C.2: Schéma du système que l'on souhaiterait réaliser dans le cadre du projet du "neurone minimal". L'excitation des canaux (en vert) est initiée dans le "soma" ou corps cellulaire (la GUV); un tube de membrane imite un axone (projection cellulaire permettant la propagation du potentiel d'action vers le neurone suivant). La propagation du signal dans ce tube sera détecté par une seconde électrode.

Dans ce qui suit, je vais d'abord présenter le canal que nous avons utilisé et le protocole pour le purifier, le marquer et le reconstituer en petits liposomes. Ensuite, je décrirai la méthode que j'ai développée pour le reconstituer dans des vésicules unilamellaires géantes. Le paragraphe suivant présentera une des questions que ces vésicules géantes contenant KvAP permettent d'étudier: l'affinité du canal pour la courbure membranaire. Je présenterai aussi une autre application: l'étude expérimentale de la diffusion du canal et d'un lipide dans une membrane confinée. Je finirai par une conclusion et un résumé des perspectives de mon travail.

C.2 KvAP

C.2.1 Un modèle pour les canaux voltage-dépendants

KvAP est un canal potassique voltage-dépendant découvert dans une archéobacterie thermophile [97]. Sa séquence est très proche de celle des autres canaux voltage-dépendants. De plus, sa structure est connue et ressemble également beaucoup à celle des autres canaux voltage-dépendants. En effet, la protéine est un tétramère et est formée d'un pore central sélectif pour le potassium et de quatre domaines senseurs de voltage entourant ce pore.

C.2.2 Purification, marquage et reconstitution en petits liposomes

La purification du canal a été réalisée dans l'Institut Curie en suivant un protocole développé dans le groupe de Rod MacKinnon à Rockefeller. Il s'agit d'abord d'exprimer la protéine en E Coli, de solubiliser les membranes avec du détergent et purifier la protéine grâce à une colonne se liant spécifiquement à la protéine (grâce à un his-tag). La deuxième étape de purification consiste en une chromatographie d'exclusion de taille pour éliminer les derniers contaminants et vérifier que la protéine ne forme pas d'agrégats.

Afin de pouvoir vérifier par la suite que la protéine est bien incorporée dans les GUVs, nous l'avons marquée avec un fluorophore (Alexa 488).

La protéine en détergent est ensuite mélangée à des petits liposomes présolubilisées. Le retrait du détergent par dialyse permet alors la formation de petits liposomes contenant KvAP.

C.2.3 Expériences d'électrophysiologie en membrane suspendue

La fonctionnalité de KvAP dans ces petits liposomes a été testée grâce à des expériences d'électrophysiologie en membrane suspendue. Le principe consiste à faire fusionner les petits liposomes avec une membrane suspendue séparant deux compartiments contenant des électrodes. Le courant traversant la membrane est alors mesuré en fonction du potentiel appliqué à la membrane.

Ces expériences ont été comparées à des expériences déjà publiées et réalisées dans les mêmes conditions mais sans marquage [70]. Ceci nous a permis de conclure que le canal est encore fonctionnel dans nos petits liposomes après marquage.

C.3 Reconstitution de KvAP en vesicules unilamellaires géantes

Comme je l'ai détaillé dans l'introduction, l'un des buts de ma thèse était de réaliser un système où les paramètres de la membrane sont contrôlés afin d'étudier leurs effets sur les canaux voltage-dépendants. Or, les techniques utilisées jusque-là pour la reconstitution des canaux ont toutes des limitations. Par exemple, les membranes suspendues présentées dans le paragraphe précédent contiennent toujours des traces d'huiles. De plus, la tension et la géométrie de la membrane sont difficiles à contrôler avec ce système. Par contre, tous ces paramètres peuvent être ajustés dans les vésicules géantes qui constituent donc un système bien adapté pour étudier les interactions entre les canaux et la membrane.

Dans les paragraphes qui suivent, je décris donc la méthode pour la reconstitution de KvAP en vésicules géantes ainsi que la caractérisation des vésicules formées.

C.3.1 Méthode de reconstitution

Le principe de la méthode est présenté dans la figure C.3. Dans une première étape, les petits liposomes (section C.2) sont partiellement déshydratés sur un fil de platine afin de faire fusionner les membranes. La solution qui constituera l'intérieur des vésicules est ensuite ajoutée et un champ électrique est appliqué. Ceci conduit au détachement

des films de membrane et à la formation de GUVs. Les paramètres d'électroformation (voltage, fréquence, temps) ont été ajustés afin de pouvoir utiliser des solution salines ou non, et différentes compositions membranaires.

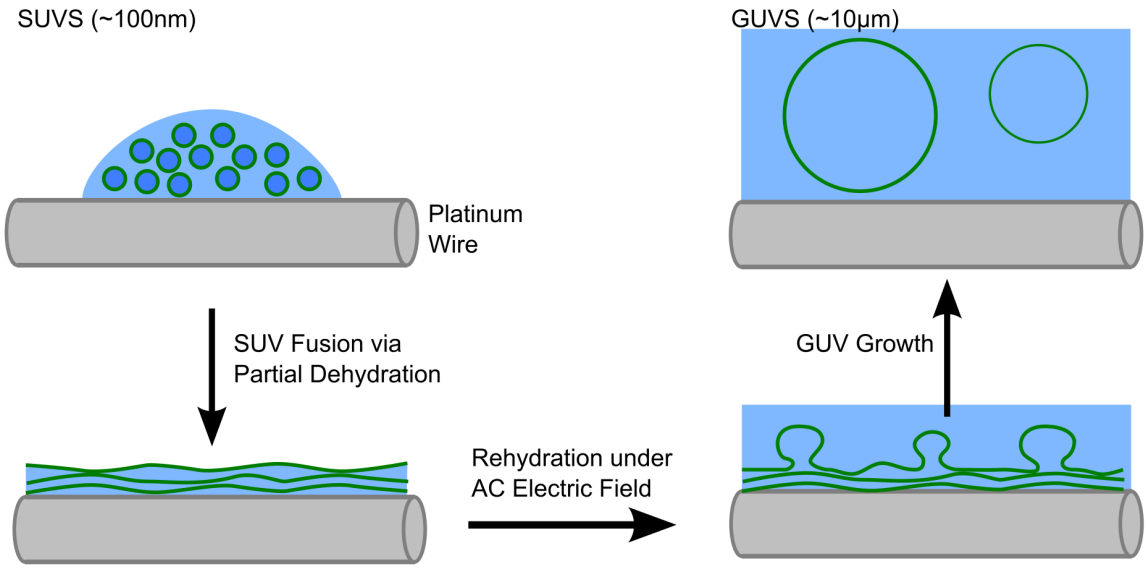

Figure C.3: Schéma du processus d'électroformation. Des gouttelettes contenant les petits liposomes sont déposées sur les électrodes. Une déshydratation partielle permet à ces liposomes de fusionner entre eux. La solution qui constituera l'interieur des GUVs est ensuite ajoutée et un champ électrique sinusoïdal est appliqué. Les films de lipides gonflent, ce qui conduit à la formation de VUGs.

C.3.2 Caractérisation de la reconstitution

C.3.2.1 Unilamellarité et taille des vésicules

Une vésicule typique obtenue par cette méthode est montrée figure C.4. En général, la méthode a permis d'obtenir des centaines de vésicules par chambre de pousse, de taille moyenne d'environ 10 microns. Des mesures de fluorescence ont de plus montré que les vésicules étaient bien unilamellaires.

C.3.2.2 Densité des protéines

Une méthode a été développée pour mesurer la densité de protéines à partir de la fluorescence de la membrane. Des vésicules contenant des densités contrôlées de lipides fluorescents à la même longueur d'onde (200 à 7000 par micron carré) ont été préparées et la fluorescence de leur membrane a été mesurée. La fluorescence des vésicules contenant KvAP a alors été comparée à ces vésicules, et, après mesure du rapport de fluorescence entre KvAP-Alexa 488 et ce lipide, nous avons pu déterminer la densité de KvAP dans les GUVs.

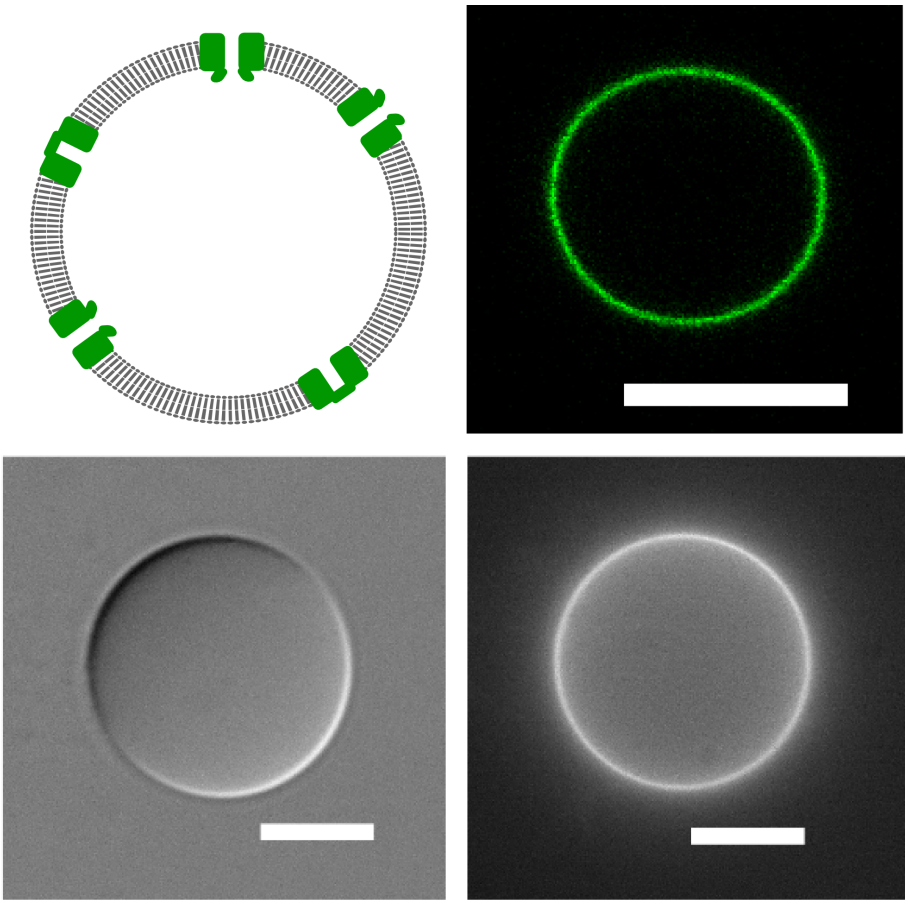

Figure C.4: GUVs contenant des KvAP reconstitués. En haut à gauche: Schéma représentant les canaux (en vert) reconstitués dans une GUV (les lipides sont en gris). En haut à droite: Image confocale d'une vésicule représentative contenant KvAP marqué avec Alexa 488. En bas: images en DIC (gauche) et épifluorescence (droite) d'une autre vésicule contenant KvAP marqué avec Alexa 488. Barres: 10 μm.

Nous avons trouvé que la densité de KvAP dans les GUVs est du même ordre de grandeur que dans les SUVs à partir desquelles elles sont formées. Nous avons donc pu préparer des vésicules contenant des densités variant de quelques à quelques milliers de protéines par micron carrés (ce qui est une gamme comparable à ce qui existe dans les membranes cellulaires).

C.3.2.3 Caractérisation de l'activité par des mesures d'électrophysiologie

Afin de vérifier que le canal est toujours fonctionnel après son incorporation dans les GUVs, Gilman Toombes, un post-doctorant du groupe a utilisé le patch-clamp pour mesurer leur activité.

Il a ainsi vérifié que le canal est toujours sélectif au potassium et également voltage dépendant. La seule différence marquante par rapport à l'activité mesurée en membrane

suspendue est que le canal semble s'inactiver beaucoup plus lentement dans le patch formé à partir de GUVs.

Pour conclure, la méthode que j'ai développée pendant cette thèse permet donc d'obtenir des vésicules unilamellaires géantes contenant un canal voltage-dépendant fonctionnel, à des densités physiologiques.

C.4 Enrichissement de KvAP dans les zones courbées de la membrane

Le premier problème que j'ai voulu étudier avec le système reconstitué est le couplage entre la courbure membranaire et la distribution des canaux.

C.4.1 Motivation

La membrane cellulaire peut être très courbée (par exemple au niveau des vésicules d'endocytose et d'exocytose, mais aussi au niveau des dendrites des neurones) et ou presque plate. Il a déjà été montré que certaines protéines se lient spécifiquement aux endroits courbées de la membrane. C'est le cas par exemple de protéines impliquées dans l'endocytose de vésicules synaptiques. Cependant, les études avec des protéines trans-membranaires sont beaucoup plus rares.

Des modèles (notamment celui de S. Leibler) utilisant la théorie de l'élasticité présentée dans le paragraphe C.1.2.2 prédisent une redistribution des protéines trans-membranaire si elles imposent localement une courbure à la membrane. La question était donc de savoir si cela est le cas pour les canaux volatges-dépendants, ce qui donnerait des informations sur la conformation des canaux dans la membrane mais pourrait aussi expliquer en partie la distribution non homogène des canaux dans les cellules.

C.4.2 Approche experimentale

Pour étudier cette question, j'ai utilisé le dispositif présenté dans la figure C.5. Une GUV contenant des canaux marqués avec Alexa 488 et des lipides fluorescents rouges (Texas red DHPE) est aspirée dans une micropipette. Une bille piégée dans une pince optique est collée sur la membrane et éloignée de la vésicule créant un tube de membrane. La force nécessaire pour maintenir le tube est mesurée grâce au déplacement de la bille dans le piège. Le rayon du tube est contrôlé par la tension de membrane qui est donnée par l'aspiration dans la micropipette.

La mesure du tri est effectuée par microscopie confocale. La quantification de l'intensité de fluorescence de KvAP dans le tube I_t^{KvAP} et dans la vésicule I_v^{KvAP} comparée à la même quantité pour le lipide fluorescent (I_t^{lipide} et I_v^{lipide}) permet de caractériser l'enrichissement en fonction de la courbure. On définie ainsi le tri T comme [176]:

$$T = \left[\frac{I_t^{KvAP}/I_t^{lipide}}{I_v^{KvAP}/I_v^{lipide}} \right] \tag{C.3}$$

La courbure est elle-même mesurée à partir du rapport entre la fluorescence des lipides dans le tube et dans la vésicule qui a été préalablement calibrée avec des GUVs sans

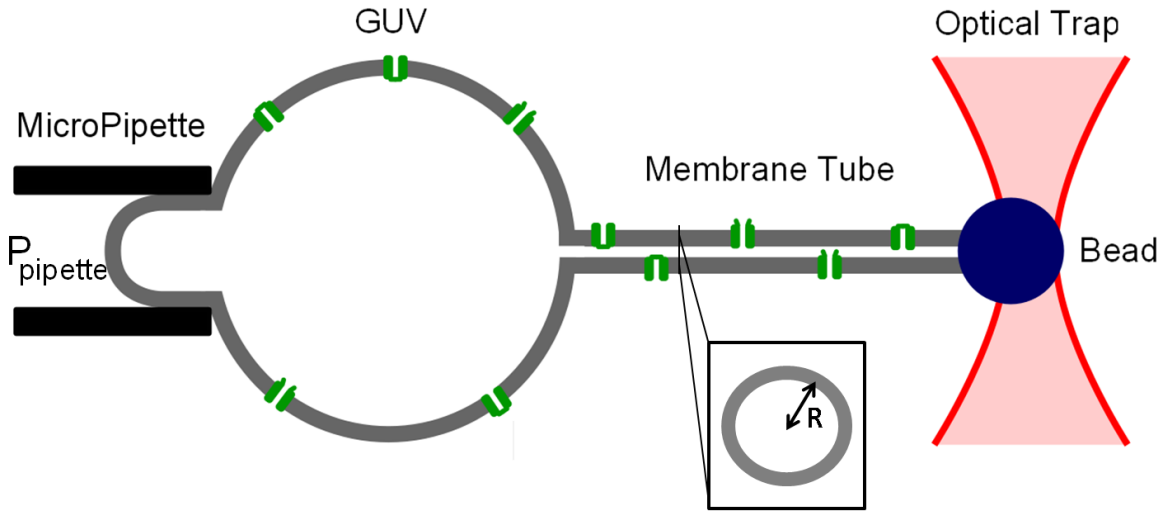

Figure C.5: Dispositif expérimental pour l'étude du tri de KvAP dans les membranes courbées. Un tube de membrane est tiré à partir d'une GUV contenant des canaux. Le contrôle de la pression dans la pipette par rapport au milieu extérieur permet d'ajuster la tension membranaire et donc de fixer le diamètre du tube. La force nécessaire pour maintenir le tube est mesurée grâce au déplacement de la bille dans la pince optique.

protéines pour lesquelles:

$$R = \frac{f}{4\pi\sigma} \tag{C.4}$$

où R est le rayon du tube, f est la force nécessaire au maintien du tube, σ est la tension membranaire.

C.4.3 Résultats

C.4.3.1 Enrichissement de KvAP dans le tube de membrane

Comme présenté dans la figure C.6, la protéine est enrichie (jusqu'à un facteur 10) dans le tube pour des courbures importantes (c'est-à-dire pour des rayons allant jusqu'à 7 nm). De plus, la relation entre l'enrichissement et la courbure semble linéaire en première approximation.

C.4.3.2 Diffusion libre au niveau du "cou" entre la vésicule et le tube

Une explication pour l'enrichissement de la protéine dans le tube pourrait être la présence d'une barrière de diffusion pour la protéine au niveau du cou entre la vésicule et le tube. En effet, pendant une expérience typique, je commence par tirer un tube de gros diamètre, puis diminue le rayon en modifiant la tension membranaire. Si la protéine reste bloquée dans le tube lorsque le rayon diminue, cela conduirait à une augmentation de la densité de protéines. Pour savoir si la protéine peut diffuser au niveau du cou, j'ai détruit les

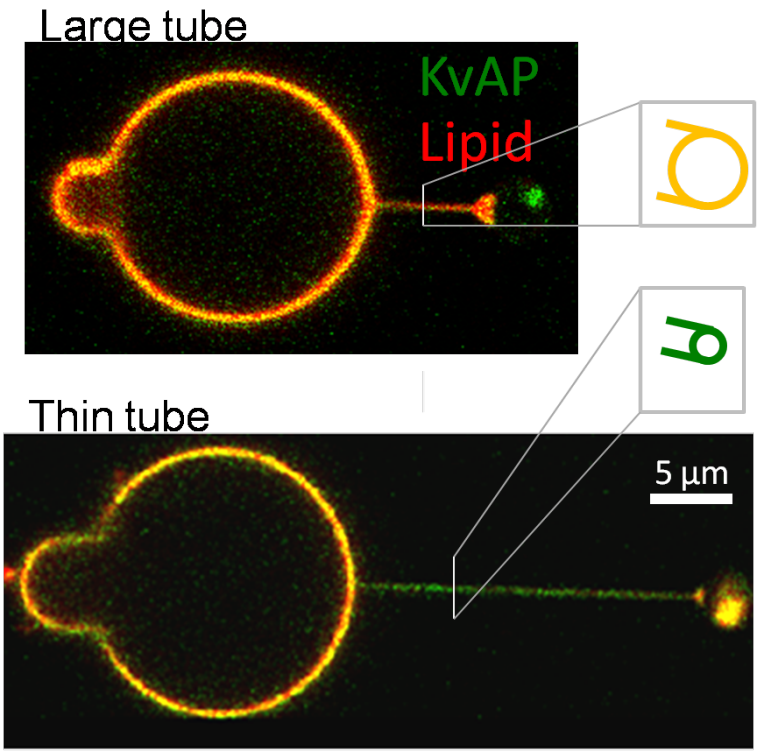

Figure C.6: Exemple d'image de microscopie confocale d'un tube tiré à partir d'une vésicule contenant KvAP marqué avec Alexa 488 (vert) et un lipide fluorescent (Texas red DHPE). Comme indiqué figure C.5, la vésicule est maintenue dans une micropipette, et un tube est tiré à partir de cette vésicule en collant une bille et en l'éloignant. En changeant la pression dans la pipette, on modifie la tension de la membrane et on diminue le rayon du tube. La vésicule est jaune ce qui correspond à une même intensité pour le vert et le rouge. Pour des tubes larges, le tube est aussi jaune mais pour des tubes fins, le tube est vert ce qui correspond à un enrichissement de la protéine par rapport aux lipides dans le tube en comparaison avec la GUV.

fluorophores liés à KvAP dans le tube grâce au laser du confocal à sa puissance maximale. J'ai ensuite observé un retour total de la fluorescence, en accord avec une diffusion libre au niveau du cou. Cela m'a permis de plus de mesurer un coefficient de diffusion de la protéine dans le tube très proche de la mesure en suivi de particule unique décrite dans le paragraphe C.5. Cela signifie que l'enrichissement de KvAP dans le tube est une propriété à l'équilibre du système.

C.4.3.3 Influence de la densité des protéines dans la vésicule

Même si l'enrichissement a été observé pour la plupart des 80 vésicules étudiées, l'intensité du tri est très variable d'une vésicule à l'autre. La mesure de la densité de protéines comme décrit dans le paragraphe C.3.2.2 a montré que le tri était plus important lorsque la protéine était peu dense dans la vésicule et qu'il décroît avec cette densité.

C.4.3.4 Modèle théorique

Andrew Callan-Jones a développé une théorie pour décrire l'enrichissement des protéines dans le tube. Le modèle est basé sur la théorie de l'élasticité présentée dans la section C.1.2.2. Les deux directions possibles pour l'insertion de KvAP dans nos GUVs sont prises en compte. Le couplage entre la densité de KvAP et la courbure de la membrane est introduit en écrivant que la courbure spontanée de la membrane C_0 dépend de la densité de la protéine dans les deux insertions ϕ_+ et ϕ_- suivant:

$$C_0(\phi_+, \phi_-) = \bar{C}_0(\phi_+ - \phi_-) \tag{C.5}$$

Cette théorie suffit à expliquer la dépendance quasi linéaire du tri en fonction de la courbure, l'effet de la densité des protéines, mais aussi un faible effet de la présence de la protéine sur la force nécessaire à maintenir le tube dans cette gamme de densités (que j'ai également observé expérimentalement).

C.4.4 Discussion et perspectives

L'enrichissement des canaux dans le tube peut donc s'expliquer par un couplage entre la courbure de la membrane et la densité des canaux à cause de la déformation locale de la membrane induite par le canal. Cependant un paramètre mal contrôlé pour le moment et qui mériterait de l'être dans le futur est l'insertion des protéines dans la membrane. En effet, la proportion de chaque insertion est un paramètre important dans le couplage (voir équation C.5) et pourrait être responsable de la grande variabilité dans l'intensité des tris observés.

Il sera aussi intéressant de relier le couplage observé à la conformation de la protéine dans la membrane. Par exemple, en appliquant un champ électrique à la membrane, il devrait être possible de déterminer si le tri change lorsque le canal est dans la conformation ouverte ou fermée.

C.5 Effet du confinement de la membrane sur la diffusion des lipides et des protéines membranaires

Une autre expérience intéressante qui a pu être effectuée grâce aux canaux reconstitués dans les GUVs est l'étude de l'effet du confinement de la membrane sur la diffusion d'espèces membranaires.

C.5.0.1 Motivation

La courbure des membranes cellulaires peut avoir des effets sur la distribution des protéines (comme décrit dans le paragraphe précédent) mais aussi sur leur diffusion. Par exemple, nos collaborateurs Marianne Renner et Antoine Triller de l'ENS ont observé que le coefficient de diffusion de plusieurs espèces membranaires diminue lorsque le diamètre de la neurite dans laquelle elle diffuse diminue.

Ceci peut s'expliquer par une théorie hydrodynamique développée par Saffman et Delbruck. Ils ont considéré que la membrane est un fluide bidimensionnel de bas nombre de

Reynolds, dans lequel une protéine de rayon R diffuse. Ils ont alors trouvé une dépendance logarithmique du coefficient de diffusion avec la taille de la membrane. La diminution du coefficient de diffusion peut s'interpréter de la façon suivante: comme montré dans le schéma C.7, lorsque la protéine diffuse dans la membrane, les lipides doivent la contourner pour remplir l'espace qu'elle a laissé derrière elle. Le flux de lipides est contraint si la membrane est confinée latéralement ce qui diminue la mobilité de la protéine.

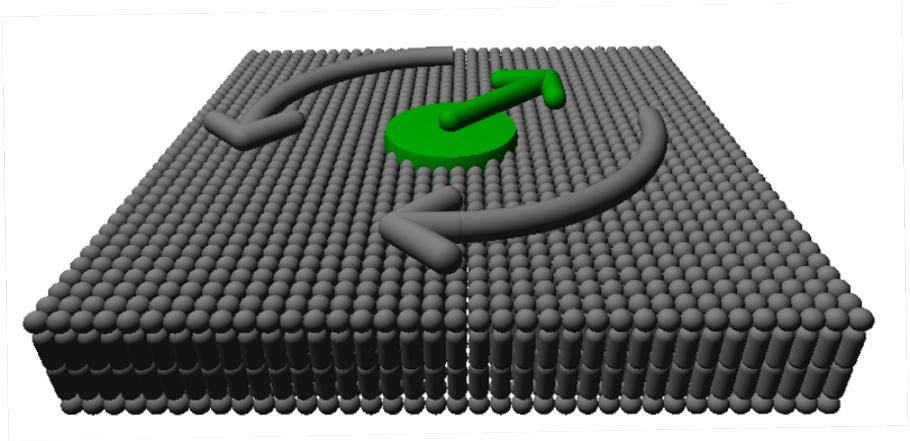

Figure C.7: Schéma expliquant l'effet du confinement de la membrane sur la diffusion des protéines trans-membranaires. Lorsque la protéine bouge, les lipides doivent la contourner pour remplir l'espace vide créé, ce qui est plus difficile si la membrane est confinée latéralement.

Daniels et Turner ont ensuite adapté la théorie de Saffman et Delbruck à la géométrie des tubes. Ils ont aussi prédit une dépendance logarithmique du coefficient de diffusion dans le rayon du tube.

C.5.0.2 Approche expérimentale

Pour tester la théorie de Saffman-Delbruck adaptée par Daniels et Turner, nous avons suivi la diffusion de KvAP d'une part et d'un lipide d'autre part dans des tubes de rayon contrôlé grâce à la technique de suivi de particule unique.

Pour cela, j'ai marqué le canal avec une molécule de PEG terminée par une biotine (figure C.8). Un quantum dot recouvert de streptavidine a alors été accroché à la biotine.

Le système pour former des tubes de membrane est le même que celui décrit dans la section précédente. Changer la tension de la membrane en changeant la pression d'aspiration de la vésicule permet de modifier le rayon du tube.

Les trajectoires des protéines ou des lipides marqués d'un quantum dot sont ensuite suivies grâce à une caméra ultra rapide.

C.5.0.3 Résultats et discussion

Les coefficients de diffusion du lipide et de la protéine en fonction du rayon du tube sont présentés dans la figure C.9. Nous avons trouvé que le coefficient de diffusion diminue de

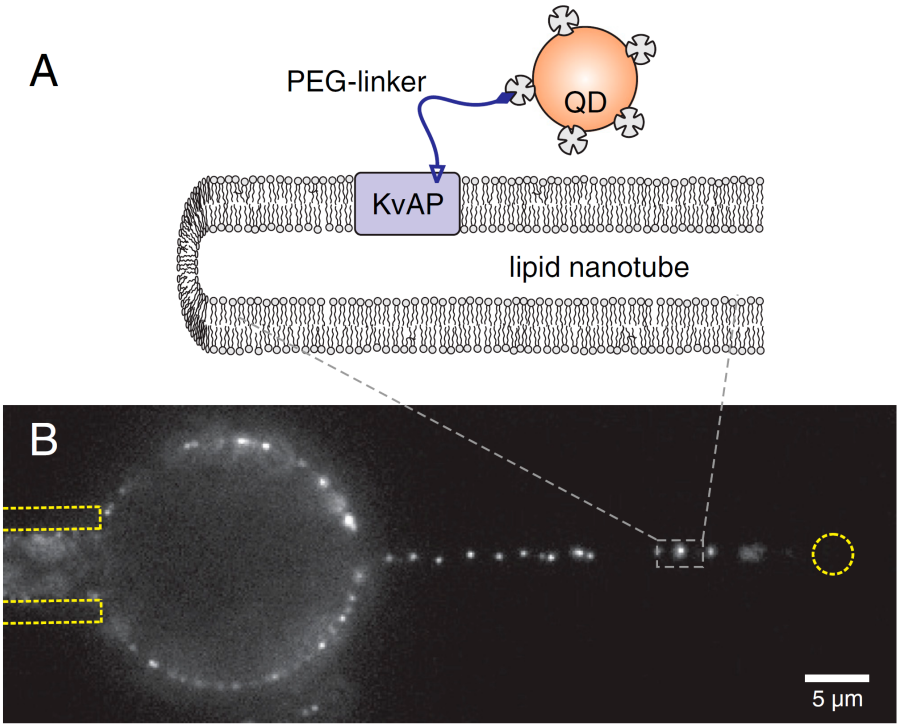

Figure C.8: Expérience de suivi de particule unique avec KvAP. Une vésicule est maintenue dans une micropipette (en pointillé sur la gauche). Un tube est tiré en utilisant une bille (en pointillé à droite) maintenue dans un piège optique. La diffusion de la protéine est ensuite mesurée grâce au suivi des quantums dots avec une caméra ultra-rapide.

plus d'un facteur trois lorsque le rayon du tube varie entre 250 nm et 10 nm. De plus, la courbe peut être ajustée grâce à l'expression du coefficient de diffusion dérivé par Daniels et Turner et avec des valeurs raisonnables pour la taille de la protéine et du lipide, et la viscosité de la membrane.

Ces résultats montrent donc que le confinement de la membrane pourrait avoir un rôle dans la diffusion des espèces dans les membranes cellulaires.

C.6 Conclusion

Pour conclure, j'ai d'abord pu montrer dans cette thèse qu'il est possible de créer un système reconstitué pour l'étude de l'effet de la membrane sur les canaux voltage-dépendants, dans lequel les paramètres de la membrane peuvent être contrôlés. J'ai en effet purifié et marqué KvAP, un canal potassique voltage dépendant, et l'ai reconstitué dans des vésicules unilamellaires géantes. Nous avons montré que la canal est encore fonctionnel dans ces GUVs.

J'ai de plus utilisé ce système pour mesurer l'effet de la courbure de nanotubes de membrane sur la distribution et la diffusion des canaux. J'ai ainsi montré que le canal est enrichi dans les parties courbées de la membrane. Ce résultat est en accord avec une théorie

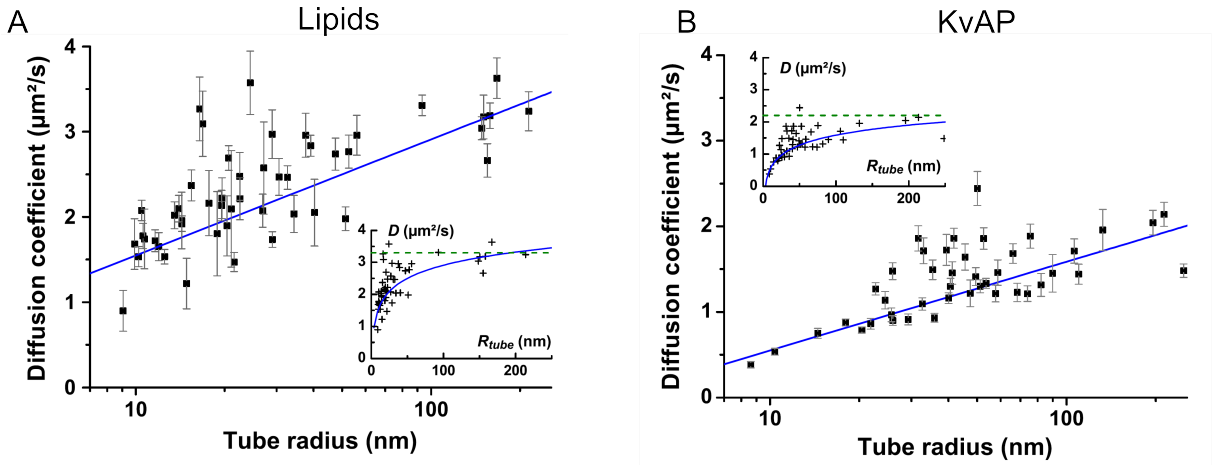

Figure C.9: A) Coefficient de diffusion des lipides parallèlement au tube. B) Coefficient de diffusion de KvAP parallèlement au tube. Courbe en coordonnées semi-logarithmiques du coefficient de diffusion en fonction du rayon du tube. (Encarts) Mêmes données en coordonnées linéaires.

de l'élasticité décrivant le couplage entre la densité de canaux et la courbure spontannée de la membrane. De plus, le coefficient de diffusion du canal le long du tube diminue logarithmiquement avec le rayon du tube, en accord avec une théorie hydrodynamique développée par Saffman et Delbruck et adaptée à la géometrie des tubes par Daniels et Turner.

Dans le futur, il sera intéressant d'utiliser ce système pour étudier d'autres questions comme l'influence de la tension et de la courbure membranaire sur l'activité des canaux par exemple. Il sera aussi possible de sonder les interactions entre les lipides et la protéine en produisant des vésicules hétérogènes et en regardant comment le canal interagit avec les différents domaines dans la membrane. Finalement, ce système minimal ouvre la voir pour l'étude quantitative des effets des paramètres membranaires sur la propagation du potentiel d'action, élargissant ainsi le modèle d'Hodgkin et Huxley.

Bibliography

[1] S. B. Long, X. Tao, E. B. Campbell, and R. MacKinnon, "Atomic structure of a voltage-dependent K+ channel in a lipid membrane-like environment.," *Nature*, vol. 450, pp. 376–82, Nov. 2007.

[2] J. M. Kralj, D. R. Hochbaum, a. D. Douglass, and a. E. Cohen, "Electrical Spiking in Escherichia coli Probed with a Fluorescent Voltage-Indicating Protein," *Science*, vol. 333, pp. 345–348, July 2011.

[3] W. Rawicz, B. a. Smith, T. J. McIntosh, S. a. Simon, and E. Evans, "Elasticity, strength, and water permeability of bilayers that contain raft microdomain-forming lipids.," *Biophysical journal*, vol. 94, pp. 4725–36, June 2008.

[4] S. Kaiser and H. Hoffmann, "Transport of Ions through Vesicle Bilayers," *Journal of colloid and interface science*, vol. 184, pp. 1–10, Dec. 1996.

[5] B. Hille, *Ion Channels of Excitable Membranes (3rd Edition)*. Sinauer Associates, 2001.

[6] A. L. Hodgkin and A. F. Huxley, "A quantitative description of membrane current and its application to conduction and excitation in nerve," *The Journal of Physiology*, vol. 117, no. 4, pp. 500–544, 1952.

[7] F. Bezanilla, "Ion channels: from conductance to structure," *Neuron*, vol. 60, no. 3, pp. 456–468, 2008.

[8] O. Hamill, A. Marty, E. Neher, B. Sakmann, and F. Sigworth, "Improved patch-clamp techniques for high-resolution current recording from cells and cell-free membrane patches," *Pflugers Archiv European Journal of Physiology*, vol. 391, no. 2, pp. 85–100, 1981.

[9] E. Neher, *Nobel lectures, Physiology or Medicine 1991-1995*. 1997.

[10] S. Lee, A. Lee, J. Chen, and R. MacKinnon, "Structure of the KvAP voltage-dependent K+ channel and its dependence on the lipid membrane," *Proceedings of the National Academy of Sciences of the United States of America*, vol. 102, no. 43, p. 15441, 2005.

[11] D. A. Doyle, J. Morais Cabral, R. A. Pfuetzner, A. Kuo, J. M. Gulbis, S. L. Cohen, B. T. Chait, and R. MacKinnon, "The Structure of the Potassium Channel:

Molecular Basis of K+ Conduction and Selectivity," *Science*, vol. 280, no. 5360, pp. 69–77, 1998.

[12] W. N. Zagotta, "Permutations of permeability," *Nature*, vol. 440, no. March, 2006.

[13] R. MacKinnon, "Potassium channels and the atomic basis of selective ion conduction," *Bioscience reports*, vol. 24, no. 2, pp. 75–100, 2004.

[14] Y. Jiang, A. Lee, J. Chen, V. Ruta, M. Cadene, B. T. Chait, and R. MacKinnon, "X-ray structure of a voltage-dependent K+ channel.," *Nature*, vol. 423, pp. 33–41, May 2003.

[15] S. B. Long, E. B. Campbell, and R. Mackinnon, "Crystal structure of a mammalian voltage-dependent Shaker family K+ channel.," *Science (New York, N.Y.)*, vol. 309, pp. 897–903, Aug. 2005.

[16] W. a. Catterall, "Ion channel voltage sensors: structure, function, and pathophysiology.," *Neuron*, vol. 67, pp. 915–28, Sept. 2010.

[17] R. W. Aldrich, "Fifty years of inactivation.," *Nature*, vol. 411, pp. 643–4, July 2001.

[18] L. G. Cuello, V. Jogini, D. M. Cortes, and E. Perozo, "Structural mechanism of C-type inactivation in K(+) channels.," *Nature*, vol. 466, pp. 203–8, July 2010.

[19] B. P. Bean, "The action potential in mammalian central neurons.," *Nature reviews. Neuroscience*, vol. 8, pp. 451–65, June 2007.

[20] O. Cerda and J. S. Trimmer, "Analysis and functional implications of phosphorylation of neuronal voltage-gated potassium channels.," *Neuroscience letters*, vol. 486, pp. 60–7, Dec. 2010.

[21] M. J. Shipston, "Ion Channel Regulation by Protein Palmitoylation," *The Journal of Biological Chemistry*, vol. 286, no. 11, pp. 8709–8716, 2011.

[22] H. C. Lai and L. Y. Jan, "The distribution and targeting of neuronal voltage-gated ion channels," *nature reviews neuroscience*, vol. 7, no. July, pp. 548–562, 2006.

[23] B. Alberts, *Molecular Biology of the Cell in Cell 4th edition*. Figure, 4rth ed., 2008.

[24] M. Eeman and M. Deleu, "From biological membranes to biomimetic model membranes," *Biotechnologie, Agronomie, Société et Environnement [= BASE]*, vol. 14, no. 4, pp. 719–736, 2010.

[25] P. Girard, *Membranes hors d equilibre : echanges et transport actif*. PhD thesis, 2004.

[26] D. M. Engelman, "Membranes are more mosaic than fluid.," *Nature*, vol. 438, pp. 578–80, Dec. 2005.

[27] D. Lingwood and K. Simons, "Lipid rafts as a membrane-organizing principle," *Science*, vol. 327, no. 5961, p. 46, 2010.

[28] V. Vogel and M. Sheetz, "Local force and geometry sensing regulate cell functions.," *Nature Reviews Molecular Cell Biology*, vol. 7, no. 4, pp. 265–275, 2006.

[29] M. P. Sheetz, "Cell control by membrane-cytoskeleton adhesion.," *Nature Reviews Molecular Cell Biology*, vol. 2, no. 5, pp. 392–396, 2001.

[30] P. Walde, K. Cosentino, H. Engel, and P. Stano, "Giant vesicles: preparations and applications.," *Chembiochem : a European journal of chemical biology*, vol. 11, pp. 848–65, May 2010.

[31] L. Bagatolli and P. B. Sunil Kumar, "Phase behavior of multicomponent membranes: Experimental and computational techniques," *Soft Matter*, vol. 5, no. 17, p. 3234, 2009.

[32] W. Helfrich, "Elastic properties of lipid bilayers: theory and possible experiments.," *Zeitschrift fur Naturforschung Teil C Biochemie Biophysik Biologie Virologie*, vol. 28, no. 11, pp. 693–703, 1973.

[33] P. B. Canham, "The minimum energy of bending as a possible explanation of the biconcave shape of the human red blood cell.," *Journal of Theoretical Biology*, vol. 26, no. 1, pp. 61–81, 1970.

[34] D. Marsh, "Elastic curvature constants of lipid monolayers and bilayers," *Chemistry and physics of lipids*, vol. 144, no. 2, pp. 146–159, 2006.

[35] W. Rawicz, K. C. Olbrich, T. McIntosh, D. Needham, and E. Evans, "Effect of chain length and unsaturation on elasticity of lipid bilayers.," *Biophysical Journal*, vol. 79, no. 1, pp. 328–339, 2000.

[36] D. Reeves, T. Ursell, P. Sens, J. Kondev, and R. Phillips, "Membrane mechanics as a probe of ion-channel gating mechanisms," *Physical Review E*, vol. 78, pp. 1–11, Oct. 2008.

[37] C. Barbetta, *Forces et fluctuations en membranes planes, sphériques et tubulaires.* PhD thesis, 2010.

[38] E. Evans and W. Rawicz, "Entropy-driven tension and bending elasticity in condensed-fluid membranes," *Physical Review Letters*, vol. 64, no. 17, pp. 2094–2097, 1990.

[39] E. Evans, V. Heinrich, F. Ludwig, and W. Rawicz, "Dynamic tension spectroscopy and strength of biomembranes.," *Biophysical journal*, vol. 85, pp. 2342–50, Oct. 2003.

[40] Kwok and Evans, "Thermoelasticity of large lecithin bilayer vesicles," *Biophysical Journal*, vol. 35, no. September, pp. 637–652, 1981.

[41] R. E. Waugh, J. Song, S. Svetina, and B. Zeks, "Local and nonlocal curvature elasticity in bilayer membranes by tether formation from lecithin vesicles.," *Biophysical Journal*, vol. 61, no. 4, pp. 974–982, 1992.

[42] O. Rossier, D. Cuvelier, N. Borghi, P. H. Puech, I. Derényi, a. Buguin, P. Nassoy, and F. Brochard-Wyart, "Giant Vesicles under Flows:Â Extrusion and Retraction of Tubes," *Langmuir*, vol. 19, pp. 575–584, Feb. 2003.

[43] I. Derényi, F. Jülicher, and J. Prost, "Formation and interaction of membrane tubes," *Physical review letters*, vol. 88, no. 23, p. 238101, 2002.

[44] J. Fournier, "On the stress and torque tensors in fluid membranes," *Soft Matter*, vol. 3, no. 7, pp. 883–888, 2007.

[45] V. Heinrich, B. Bozic, S. Svetina, and B. Zeks, "Vesicle deformation by an axial load: from elongated shapes to tethered vesicles.," *Biophysical Journal*, vol. 76, no. 4, pp. 2056–2071, 1999.

[46] S. Svetina, B. Zeks, R. E. Waugh, and R. M. Raphael, "Theoretical analysis of the effect of the transbilayer movement of phospholipid molecules on the dynamic behavior of a microtube pulled out of an aspirated vesicle.," *European biophysics journal : EBJ*, vol. 27, pp. 197–209, Jan. 1998.

[47] S. Semrau, T. Idema, T. Schmidt, and C. Storm, "Membrane-mediated interactions measured using membrane domains.," *Biophysical journal*, vol. 96, pp. 4906–15, June 2009.

[48] H. Sprong, P. Van Der Sluijs, and G. Van Meer, "How proteins move lipids and lipids move proteins.," *Nature Reviews Molecular Cell Biology*, vol. 2, no. 7, pp. 504–513, 2001.

[49] S.-Y. Lee and R. MacKinnon, "A membrane-access mechanism of ion channel inhibition by voltage sensor toxins from spider venom.," *Nature*, vol. 430, pp. 232–5, July 2004.

[50] R. Phillips, T. Ursell, P. Wiggins, and P. Sens, "Emerging roles for lipids in shaping membrane-protein function," *Nature*, vol. 459, no. 7245, pp. 379–385, 2009.

[51] S. Leibler, "Curvature instability in membranes," *Journal de Physique*, vol. 47, pp. 507–516, 1986.

[52] D. Marsh, "Lateral pressure profile, spontaneous curvature frustration, and the incorporation and conformation of proteins in membranes.," *Biophysical journal*, vol. 93, pp. 3884–99, Dec. 2007.

[53] E. Perozo, A. Kloda, D. M. Cortes, and B. Martinac, "Physical principles underlying the transduction of bilayer deformation forces during mechanosensitive channel gating.," *Nature structural biology*, vol. 9, pp. 696–703, Sept. 2002.

[54] E. Lindahl and M. S. P. Sansom, "Membrane proteins: molecular dynamics simulations.," *Current opinion in structural biology*, vol. 18, pp. 425–31, Aug. 2008.

[55] R. Phillips, T. Ursell, P. Wiggins, and P. Sens, "Emerging roles for lipids in shaping membrane-protein function.," *Nature*, vol. 459, pp. 379–85, May 2009.

[56] J. Fournier, "Microscopic membrane elasticity and interactions among membrane inclusions: interplay between the shape, dilation, tilt and tilt-difference modes," *The European Physical Journal B-Condensed Matter and Complex Systems*, vol. 11, no. 2, pp. 261–272, 1999.

[57] S. Ramaswamy and M. Rao, "The physics of active membranes," *C R Acad Sci Paris t 2 Série IV*, vol. 2, pp. 817–839, 2001.

[58] J. Prost and R. Bruinsma, "Shape fluctuations of active membranes," *EPL (Europhysics Letters)*, vol. 33, no. 4, p. 321, 1996.

[59] S. Ramaswamy, J. Toner, and J. Prost, "Nonequilibrium fluctuations, traveling waves, and instabilities in active membranes.," *Physical review letters*, vol. 84, pp. 3494–7, Apr. 2000.

[60] J.-B. Manneville, P. Bassereau, S. Ramaswamy, and J. Prost, "Active membrane fluctuations studied by micropipet aspiration," *Physical Review E*, vol. 64, pp. 1–10, July 2001.

[61] H. Luecke, H.-T. Richter, and J. K. Lanyi, "Proton Transfer Pathways in Bacteriorhodopsin at 2.3Å Angstrom Resolution," *Science*, vol. 280, no. 5371, pp. 1934–1937, 1998.

[62] H. Chen, "Internal states of active inclusions and the dynamics of an active membrane," *Physical review letters*, vol. 92, no. 16, p. 168101, 2004.

[63] N. Gov, "Membrane Undulations Driven by Force Fluctuations of Active Proteins," *Physical Review Letters*, vol. 93, pp. 1–4, Dec. 2004.

[64] D. Lacoste and A. Lau, "Dynamics of active membranes with internal noise," *EPL (Europhysics Letters)*, vol. 70, p. 418, 2005.

[65] M. A. Lomholt, P. L. Hansen, and L. Miao, "A general theory of non-equilibrium dynamics of lipid-protein fluid membranes," *The European Physical Journal E*, vol. 16, no. 4, pp. 439–461, 2005.

[66] M. A. Lomholt, "Mechanics of non-planar membranes with force-dipole activity," *Physical Review E - Statistical, Nonlinear and Soft Matter Physics*, vol. 73, no. 6 Pt 1, p. 061913, 2006.

[67] P. Girard, J. Prost, and P. Bassereau, "Passive or Active Fluctuations in Membranes Containing Proteins," *Physical Review Letters*, vol. 94, pp. 2–5, Mar. 2005.

[68] F. El Alaoui, D. Lacoste, J. Pécréaux, J. Prost, and P. Bassereau, "Membrane Tension Lowering Induced by Protein Activity," *Physical Review Letters*, vol. 038102, no. January, pp. 1–4, 2009.

[69] Y. Park, C. A. Best, T. Auth, N. S. Gov, S. A. Safran, G. Popescu, S. Suresh, and M. S. Feld, "Metabolic remodeling of the human red blood cell membrane.," *Proceedings of the National Academy of Sciences of the United States of America*, vol. 107, no. 4, pp. 1289–1294, 2010.

[70] D. Schmidt and Q. Jiang, "Phospholipids and the origin of cationic gating charges in voltage sensors," *Nature*, vol. 444, no. December, pp. 775–779, 2006.

[71] Y. Ramu, Y. Xu, and Z. Lu, "Enzymatic activation of voltage-gated potassium channels.," *Nature*, vol. 442, no. 7103, pp. 696–699, 2006.

[72] Y. Xu, Y. Ramu, and Z. Lu, "Removal of phospho-head groups of membrane lipids immobilizes voltage sensors of K+ channels.," *Nature*, vol. 451, pp. 826–9, Feb. 2008.

[73] N. Gamper and M. S. Shapiro, "Regulation of ion transport proteins by membrane phosphoinositides.," *Nature reviews. Neuroscience*, vol. 8, pp. 921–34, Dec. 2007.

[74] J. a. Butterwick and R. MacKinnon, "Solution structure and phospholipid interactions of the isolated voltage-sensor domain from KvAP.," *Journal of molecular biology*, vol. 403, pp. 591–606, Nov. 2010.

[75] M. Milescu, F. Bosmans, S. Lee, A. a. Alabi, J. I. Kim, and K. J. Swartz, "Interactions between lipids and voltage sensor paddles detected with tarantula toxins.," *Nature structural & molecular biology*, vol. 16, pp. 1080–5, Oct. 2009.

[76] K. Swartz, "Sensing voltage across lipid membranes," *Nature*, vol. 456, no. 7224, pp. 891–897, 2008.

[77] J. a. Lundbaek, "Lipid bilayer-mediated regulation of ion channel function by amphiphilic drugs.," *The Journal of general physiology*, vol. 131, pp. 421–9, May 2008.

[78] R. K. Finol-Urdaneta, J. R. McArthur, P. F. Juranka, R. J. French, and C. E. Morris, "Modulation of KvAP unitary conductance and gating by 1-alkanols and other surface active agents.," *Biophysical journal*, vol. 98, pp. 762–72, Mar. 2010.

[79] D. Schmidt and R. MacKinnon, "Voltage-dependent K+ channel gating and voltage sensor toxin sensitivity depend on the mechanical state of the lipid membrane.," *PNAS*, vol. 105, pp. 19276–81, Dec. 2008.

[80] C. Morris and P. Juranka, "Nav channel mechanosensitivity: activation and inactivation accelerate reversibly with stretch," *Biophysical journal*, vol. 93, no. 3, pp. 822–833, 2007.

[81] C. Gu, "Stretch-Activation and Stretch-Inactivation of Shaker-IR, a Voltage-Gated K+ Channel," *Biophysical Journal*, vol. 80, pp. 2678–2693, June 2001.

[82] U. Laitko and C. E. Morris, "Membrane tension accelerates rate-limiting voltage-dependent activation and slow inactivation steps in a Shaker channel.," *The Journal of general physiology*, vol. 123, no. 2, pp. 135–154, 2004.

[83] B. Calabrese, I. V. Tabarean, P. Juranka, and C. E. Morris, "Mechanosensitivity of N-type calcium channel currents.," *Biophysical journal*, vol. 83, pp. 2560–74, Nov. 2002.

[84] D. Krepkiy, M. Mihailescu, J. A. Freites, E. V. Schow, D. L. Worcester, K. Gawrisch, D. J. Tobias, S. H. White, and K. J. Swartz, "Structure and hydration of membranes embedded with voltage-sensing domains.," *Nature*, vol. 462, pp. 473–9, Nov. 2009.

[85] E. Schow, J. Freites, K. Gogna, S. White, and D. Tobias, "Down-state model of the voltage-sensing domain of a potassium channel," *Biophysical journal*, vol. 98, no. 12, pp. 2857–2866, 2010.

[86] P. Bjelkmar, P. S. Niemelä, I. Vattulainen, and E. Lindahl, "Conformational changes and slow dynamics through microsecond polarized atomistic molecular simulation of an integral Kv1.2 ion channel.," *PLoS computational biology*, vol. 5, p. e1000289, Feb. 2009.

[87] T. Ursell, K. C. Huang, E. Peterson, and R. Phillips, "Cooperative gating and spatial organization of membrane proteins through elastic interactions.," *PLoS computational biology*, vol. 3, p. e81, May 2007.

[88] O. Yifrach, N. Zandany, and T. Shem-Ad, *Examining cooperative gating phenomena in voltage-dependent potassium channels: taking the energetic approach.*, vol. 466. Elsevier Inc., 1 ed., Jan. 2009.

[89] J. Martens, "Targeting of ion channels to membrane microdomains: localization of KV channels to lipid rafts," *Trends in Pharmacological Sciences*, vol. 25, pp. 16–21, Jan. 2004.

[90] M. N. Rasband, "Clustered K+ channel complexes in axons.," *Neuroscience letters*, vol. 486, pp. 101–6, Dec. 2010.

[91] Z. F. Mainen and T. J. Sejnowski, "Influence of dendritic structure on firing pattern in model neocortical neurons.," *Nature*, vol. 382, pp. 363–6, July 1996.

[92] D. Debanne, "Information processing in the axon.," *Nature Reviews Neuroscience*, vol. 5, no. 4, pp. 304–316, 2004.

[93] P. Nelson, "Biological Physics," *Physics*, vol. 71, no. 2, pp. S419–S430, 2004.

[94] M. Rentschler and P. Fromherz, "Membrane-Transistor Cable," *Langmuir*, vol. 14, no. 2, pp. 547–551, 1998.

[95] F. C. Simmel, "Bioelectronics: Wiring-up ion channels," *Nature Physics*, vol. 5, pp. 783–784, Nov. 2009.

[96] M. Tokarz, B. Hakonen, P. Dommersnes, O. Orwar, and B. Å kerman, "Electrophoretic transport of latex particles in lipid nanotubes," *Langmuir*, vol. 23, no. 14, pp. 7652–7658, 2007.

[97] V. Ruta, Y. Jiang, A. Lee, J. Chen, and R. MacKinnon, "Functional analysis of an archaebacterial voltage-dependent K+ channel," *Nature*, vol. 422, no. 6928, pp. 180–185, 2003.

[98] J. Rigaud and Others, "Reconstitution of membrane proteins into liposomes," *Methods in enzymology*, vol. 372, pp. 65–86, 2003.

[99] S.-Y. Lee, A. Lee, J. Chen, and R. MacKinnon, "Structure of the KvAP voltage-dependent K+ channel and its dependence on the lipid membrane.," *Proceedings of the National Academy of Sciences of the United States of America*, vol. 102, pp. 15441–6, Oct. 2005.

[100] D. Schmidt, S. Cross, and R. MacKinnon, "A gating model for the archeal voltage-dependent K+ channel KvAP in DPhPC and POPE: POPG decane lipid bilayers," *Journal of molecular biology*, vol. 390, no. 5, pp. 902–912, 2009.

[101] F. Cohen, M. Akabas, J. Zimmerberg, and A. Finkelstein, "Parameters affecting the fusion of unilamellar phospholipid vesicles with planar bilayer membranes.," *The Journal of cell biology*, vol. 98, no. 3, p. 1054, 1984.

[102] S. Aimon, J. Manzi, D. Schmidt, J. A. Poveda Larrosa, P. Bassereau, and G. E. S. Toombes, "Functional reconstitution of a voltage-gated potassium channel in giant unilamellar vesicles.," *PloS one*, vol. 6, p. e25529, Jan. 2011.

[103] S. Demarche, K. Sugihara, T. Zambelli, L. Tiefenauer, and J. Vörös, "Techniques for recording reconstituted ion channels.," *The Analyst*, vol. 136, pp. 1077–1089, Jan. 2011.

[104] S. H. White, "The physical nature of planar bilayer membranes. in Ion Channel Reconstitution (ed. Miller, C.)," 1986.

[105] V. a. Frolov, V. a. Lizunov, A. Y. Dunina-Barkovskaya, A. V. Samsonov, and J. Zimmerberg, "Shape bistability of a membrane neck: a toggle switch to control vesicle content release.," *Proceedings of the National Academy of Sciences of the United States of America*, vol. 100, pp. 8698–703, July 2003.

[106] P. V. Bashkirov, "Membrane nanotubes in the electric field as a model for measurement of mechanical parameters of the lipid bilayer," *Biochemistry (Moscow) Supplement Series A: Membrane and Cell Biology*, vol. 1, pp. 176–184, June 2007.

[107] N. Misra, J. a. Martinez, S.-C. J. Huang, Y. Wang, P. Stroeve, C. P. Grigoropoulos, and A. Noy, "Bioelectronic silicon nanowire devices using functional membrane proteins.," *Proceedings of the National Academy of Sciences of the United States of America*, vol. 106, pp. 13780–4, Aug. 2009.

[108] I. Titushkin and M. Cho, "Distinct membrane mechanical properties of human mesenchymal stem cells determined using laser optical tweezers.," *Biophysical journal*, vol. 90, pp. 2582–91, Apr. 2006.

[109] J. Requena, "The lippmann equation and the characterization of black lipid films," *Journal of Colloid and Interface Science*, vol. 51, pp. 315–327, May 1975.

[110] J. Dai, M. P. Sheetz, X. Wan, and C. E. Morris, "Membrane tension in swelling and shrinking molluscan neurons.," *The Journal of neuroscience : the official journal of the Society for Neuroscience*, vol. 18, pp. 6681–92, Sept. 1998.

[111] A. Delcour, B. Martinac, J. Adler, and C. Kung, "Modified reconstitution method used in patch-clamp studies of Escherichia coli ion channels," *Biophysical journal*, vol. 56, no. 3, pp. 631–636, 1989.

[112] F. J. Morera, G. Vargas, C. González, E. Rosenmann, and R. Latorre, "Ion-channel reconstitution.," *Methods In Molecular Biology Clifton Nj*, vol. 400, pp. 571–585, 2007.

[113] A. Battle, E. Petrov, and P. Pal, "Rapid and improved reconstitution of bacterial mechanosensitive ion channel proteins MscS and MscL into liposomes using a modified sucrose method," *FEBS letters*, vol. 583, no. 2, pp. 407–412, 2009.

[114] N. Kahya, "Protein-protein and protein-lipid interactions in domain-assembly: Lessons from giant unilamellar vesicles," *Biochimica et Biophysica Acta (BBA)-Biomembranes*, vol. 1798, no. 7, pp. 1392–1398, 2010.

[115] M. Kreir, C. Farre, M. Beckler, M. George, and N. Fertig, "Rapid screening of membrane protein activity: electrophysiological analysis of OmpF reconstituted in proteoliposomes.," *Lab on a chip*, vol. 8, pp. 587–95, Apr. 2008.

[116] A. Varnier, F. Kermarrec, I. Blesneac, C. Moreau, L. Liguori, J. Lenormand, and N. Picollet-Dhahan, "A simple method for the reconstitution of membrane proteins into giant unilamellar vesicles," *Journal of Membrane Biology*, vol. 233, no. 1, pp. 85–92, 2010.

[117] P. Girard, J. Pécréaux, G. Lenoir, P. Falson, J.-L. Rigaud, and P. Bassereau, "A new method for the reconstitution of membrane proteins into giant unilamellar vesicles.," *Biophysical journal*, vol. 87, pp. 419–29, July 2004.

[118] N. Rodriguez, F. Pincet, and S. Cribier, "Giant vesicles formed by gentle hydration and electroformation: a comparison by fluorescence microscopy," *Colloids and Surfaces B: Biointerfaces*, vol. 42, no. 2, pp. 125–130, 2005.

[119] M. Doeven, J. Folgering, V. Krasnikov, E. Geertsma, G. Van Den Bogaart, and B. Poolman, "Distribution, lateral mobility and function of membrane proteins incorporated into giant unilamellar vesicles," *Biophysical journal*, vol. 88, no. 2, pp. 1134–1142, 2005.

[120] A. Papadopulos, S. Vehring, I. López-Montero, L. Kutschenko, M. Stöckl, P. Devaux, M. Kozlov, T. Pomorski, and A. Herrmann, "Flippase activity detected with unlabeled lipids by shape changes of giant unilamellar vesicles," *Journal of Biological Chemistry*, vol. 282, no. 21, p. 15559, 2007.

[121] P. Streicher, P. Nassoy, M. Bärmann, A. Dif, V. Marchi-Artzner, F. Brochard-Wyart, J. Spatz, and P. Bassereau, "Integrin reconstituted in GUVs: A biomimetic system

to study initial steps of cell spreading," *Biochimica et Biophysica Acta*, vol. 1788, pp. 2291–2300, 2009.

[122] D. L. Richmond, E. M. Schmid, S. Martens, J. C. Stachowiak, N. Liska, and D. a. Fletcher, "Forming giant vesicles with controlled membrane composition, asymmetry, and contents.," *Proceedings of the National Academy of Sciences of the United States of America*, vol. 108, pp. 9431–6, June 2011.

[123] M. Yanagisawa, M. Iwamoto, A. Kato, K. Yoshikawa, and S. Oiki, "Oriented Reconstitution of a Membrane Protein in a Giant Unilamellar Vesicle: Experimental Verification with the Potassium Channel KcsA.," *Journal of the American Chemical Society*, July 2011.

[124] N. Kahya, D. a. Wiersma, B. Poolman, and D. Hoekstra, "Spatial organization of bacteriorhodopsin in model membranes. Light-induced mobility changes.," *The Journal of biological chemistry*, vol. 277, no. 42, pp. 39304–11, 2002.

[125] P. Girard, J. Prost, and P. Bassereau, "Passive or active fluctuations in membranes containing proteins," *Physical review letters*, vol. 94, no. 8, p. 088102, 2005.

[126] S. Ramadurai, R. Duurkens, V. V. Krasnikov, and B. Poolman, "Lateral diffusion of membrane proteins: consequences of hydrophobic mismatch and lipid composition.," *Biophysical journal*, vol. 99, pp. 1482–9, Sept. 2010.

[127] P. Streicher, P. Nassoy, M. Bärmann, A. Dif, V. Marchi-Artzner, F. Brochard-Wyart, J. Spatz, and P. Bassereau, "Integrin reconstituted in GUVs: a biomimetic system to study initial steps of cell spreading.," *Biochimica et biophysica acta*, vol. 1788, pp. 2291–300, Oct. 2009.

[128] K. R. Mahendran, M. Kreir, H. Weingart, N. Fertig, and M. Winterhalter, "Permeation of antibiotics through Escherichia coli OmpF and OmpC porins: screening for influx on a single-molecule level.," *Journal of biomolecular screening the official journal of the Society for Biomolecular Screening*, vol. 15, no. 3, pp. 302–307, 2010.

[129] M. Davidson, M. Karlsson, J. Sinclair, K. Sott, and O. Orwar, "Nanotube- Vesicle Networks with Functionalized Membranes and Interiors," *Journal of the American Chemical Society*, vol. 125, no. 2, pp. 374–378, 2003.

[130] O. Gassmann, M. Kreir, C. Ambrosi, J. Pranskevich, A. Oshima, C. Röling, G. Sosinsky, N. Fertig, and C. Steinem, "The M34A mutant of Connexin26 reveals active conductance states in pore-suspending membranes.," *Journal of Structural Biology*, vol. 168, no. 1, pp. 168–176, 2009.

[131] P. Girard, J. Pécréaux, G. Lenoir, P. Falson, J.-L. Rigaud, and P. Bassereau, "A new method for the reconstitution of membrane proteins into giant unilamellar vesicles.," *Biophysical journal*, vol. 87, pp. 419–29, July 2004.

[132] P. Méléard, L. Bagatolli, and T. Pott, "Giant Unilamellar Vesicle Electroformation:: From Lipid Mixtures to Native Membranes Under Physiological Conditions," *Methods in enzymology*, vol. 465, pp. 161–176, 2009.

[133] K.-i. Akashi, H. Miyata, and H. Itoh, "Preparation of giant liposomes in physiological conditions and their characterization under an optical microscope," *Biophysical journal*, vol. 71, no. December, pp. 3242–3250, 1996.

[134] L. Mathivet, S. Cribier, and P. Devaux, "Shape change and physical properties of giant phospholipid vesicles prepared in the presence of an AC electric field," *Biophysical Journal*, vol. 70, pp. 1112–1121, Mar. 1996.

[135] W. J. Galush, J. A. Nye, and J. T. Groves, "Quantitative fluorescence microscopy using supported lipid bilayer standards.," *Biophysical Journal*, vol. 95, no. 5, pp. 2512–9, 2008.

[136] J. Nagle and S. Tristram-Nagle, "Structure of lipid bilayers," *Biochimica et Biophysica Acta (BBA)-Reviews on Biomembranes*, vol. 1469, no. 3, pp. 159–195, 2000.

[137] S. L. Veatch and S. L. Keller, "Seeing spots: complex phase behavior in simple membranes.," *Biochimica et Biophysica Acta*, vol. 1746, no. 3, pp. 172–185, 2005.

[138] D. Schmidt, S. R. Cross, and R. MacKinnon, "A gating model for the archeal voltage-dependent K(+) channel KvAP in DPhPC and POPE:POPG decane lipid bilayers.," *Journal of molecular biology*, vol. 390, pp. 902–12, July 2009.

[139] A. Wang and G. Zocchi, "Artificial Modulation of the Gating Behavior of a K Channel in a KvAP-DNA Chimera.," *PloS one*, vol. 6, p. e18598, Jan. 2011.

[140] T. M. Suchyna, V. S. Markin, and F. Sachs, "Biophysics and structure of the patch and the gigaseal.," *Biophysical journal*, vol. 97, pp. 738–47, Aug. 2009.

[141] P. Girard, J. Pécréaux, G. Lenoir, P. Falson, J.-L. Rigaud, and P. Bassereau, "A new method for the reconstitution of membrane proteins into giant unilamellar vesicles.," *Biophysical journal*, vol. 87, pp. 419–29, July 2004.

[142] M. L. Molina, F. N. Barrera, A. M. Fernández, J. a. Poveda, M. L. Renart, J. a. Encinar, G. Riquelme, and J. M. González-Ros, "Clustering and coupled gating modulate the activity in KcsA, a potassium channel model.," *The Journal of biological chemistry*, vol. 281, pp. 18837–48, July 2006.

[143] S. Chakrapani, J. F. Cordero-Morales, and E. Perozo, "A Quantitative Description of KcsA Gating I: Macroscopic Currents," *The Journal of general physiology*, vol. 130, no. 5, pp. 465–478, 2007.

[144] W. W. L. Cheng, D. Enkvetchakul, and C. G. Nichols, "KirBac1.1: It's an Inward Rectifying Potassium Channel," *The Journal of general physiology*, vol. 133, no. 3, pp. 295–305, 2009.

[145] S. Uysal, V. Vásquez, V. Tereshko, K. Esaki, F. A. Fellouse, S. S. Sidhu, S. Koide, E. Perozo, and A. Kossiakoff, "Crystal structure of full-length KcsA in its closed conformation," *Proceedings of the National Academy of Sciences of the United States of America*, vol. 106, no. 16, pp. 6644–6649, 2009.

[146] A. Kuo, J. M. Gulbis, J. F. Antcliff, T. Rahman, E. D. Lowe, J. Zimmer, J. Cuthbertson, F. M. Ashcroft, T. Ezaki, and D. A. Doyle, "Crystal structure of the potassium channel KirBac1.1 in the closed state.," *Science*, vol. 300, no. 5627, pp. 1922–1926, 2003.

[147] N. F. Morales-Penningston, J. Wu, E. R. Farkas, S. L. Goh, T. M. Konyakhina, J. Y. Zheng, W. W. Webb, and G. W. Feigenson, "GUV preparation and imaging: Minimizing artifacts.," *Biochimica et biophysica acta*, vol. 1798, pp. 1324–1332, July 2010.

[148] S. L. Veatch, K. Gawrisch, and S. L. Keller, "Closed-loop miscibility gap and quantitative tie-lines in ternary membranes containing diphytanoyl PC.," *Biophysical journal*, vol. 90, pp. 4428–36, June 2006.

[149] T. Baumgart, G. Hunt, E. R. Farkas, W. W. Webb, and G. W. Feigenson, "Fluorescence probe partitioning between Lo/Ld phases in lipid membranes," *Biochimica et Biophysica Acta*, vol. 1768, no. 9, pp. 2182–2194, 2007.

[150] M. Fidorra, a. Garcia, J. H. Ipsen, S. Härtel, and L. a. Bagatolli, "Lipid domains in giant unilamellar vesicles and their correspondence with equilibrium thermodynamic phases: a quantitative fluorescence microscopy imaging approach.," *Biochimica et biophysica acta*, vol. 1788, pp. 2142–9, Oct. 2009.

[151] U. N\\"agerl, K. Willig, B. Hein, S. Hell, and T. Bonhoeffer, "Live-cell imaging of dendritic spines by STED microscopy," *Proceedings of the National Academy of Sciences*, vol. 105, no. 48, p. 18982, 2008.

[152] H. McMahon and J. Gallop, "Membrane curvature and mechanisms of dynamic cell membrane remodelling," *Nature*, vol. 438, no. 7068, pp. 590–596, 2005.

[153] U. V. Nägerl and T. Bonhoeffer, "Imaging living synapses at the nanoscale by STED microscopy.," *Journal of Neuroscience*, vol. 30, no. 28, pp. 9341–9346, 2010.

[154] G. Van Meer, D. R. Voelker, and G. W. Feigenson, "Membrane lipids: where they are and how they behave.," *Nature Reviews Molecular Cell Biology*, vol. 9, no. 2, pp. 112–24, 2008.

[155] K. Simons and G. Vanmeer, "Lipid Sorting in Epithelial-Cells," *Biochemistry*, vol. 27, no. 17, pp. 6197–6202, 1988.

[156] A. Callan-Jones, B. Sorre, and P. Bassereau, "Curvature-driven lipid sorting in biomembranes.," *Cold Spring Harbor perspectives in biology*, vol. 3, Feb. 2011.

[157] M. M. Kamal, D. Mills, M. Grzybek, and J. Howard, "Measurement of the membrane curvature preference of phospholipids reveals only weak coupling between lipid shape and leaflet curvature.," *Proceedings of the National Academy of Sciences of the United States of America*, vol. 106, pp. 22245–50, Dec. 2009.

[158] B. Sorre, A. Callan-Jones, J. Manneville, P. Nassoy, J. Joanny, J. Prost, B. Goud, and P. Bassereau, "Curvature-driven lipid sorting needs proximity to a demixing point and is aided by proteins," *Proceedings of the National Academy of Sciences*, vol. 106, no. 14, p. 5622, 2009.

[159] M. Safouane, L. Berland, A. Callan-Jones, B. Sorre, W. Römer, L. Johannes, G. E. S. Toombes, and P. Bassereau, "Lipid Cosorting Mediated by Shiga Toxin Induced Tubulation.," *Traffic*, pp. 1519–1529, Sept. 2010.

[160] W. Romer, L. Berland, V. Chambon, C. Lamaze, K. Gaus, B. Windschiegl, l. Tenza, M. R. E. Aly, V. Fraisier, J.-C. Florent, D. Perrais, G. Raposo, C. Steinem, PierreSens, P. Bassereau, and L. Johannes, "Shiga toxin induces tubular membrane invaginations for its uptake into cells," *Nature*, vol. 450, pp. 670–675, 2007.

[161] L. Berland, *Étude physique des déformations de membranes induites par la toxine de Shiga*. PhD thesis, 2009.

[162] F. Campelo, G. Fabrikant, H. T. McMahon, and M. M. Kozlov, "Modeling membrane shaping by proteins: focus on EHD2 and N-BAR domains.," *FEBS letters*, vol. 584, pp. 1830–9, May 2010.

[163] B. Antonny, "Mechanisms of Membrane Curvature Sensing.," *Annual review of biochemistry*, June 2010.

[164] D. Danino and J. E. Hinshaw, "Dynamin family of mechanoenzymes.," *Current Opinion in Cell Biology*, vol. 13, no. 4, pp. 454–460, 2001.

[165] J. C. Stachowiak, C. C. Hayden, and D. Y. Sasaki, "Steric confinement of proteins on lipid membranes can drive curvature and tubulation.," *Proceedings of the National Academy of Sciences of the United States of America*, vol. 107, pp. 7781–6, Apr. 2010.

[166] T. Baumgart, B. R. Capraro, C. Zhu, and S. L. Das, "Thermodynamics and mechanics of membrane curvature generation and sensing by proteins and lipids.," *Annual review of physical chemistry*, vol. 62, pp. 483–506, May 2011.

[167] R. Sorre B., Callan-Jones A., Manzi J., Goud B., Prost J., Bassereau P. and A., "Nature of curvature coupling of Amphiphysin 1 interacting with a membrane depends on its bound density," *Proc. Natl. Acad. Sci. U.S.A,*.

[168] Y. Shibata, J. Hu, M. M. Kozlov, and T. a. Rapoport, "Mechanisms shaping the membranes of cellular organelles.," *Annual review of cell and developmental biology*, vol. 25, pp. 329–54, Jan. 2009.

[169] C. M. Waterman-Storer and E. D. Salmon, "Endoplasmic reticulum membrane tubules are distributed by microtubules in living cells using three distinct mechanisms.," *Current biology : CB*, vol. 8, pp. 798–806, July 1998.

[170] G. K. Voeltz and W. a. Prinz, "Sheets, ribbons and tubules - how organelles get their shape.," *Nature reviews. Molecular cell biology*, vol. 8, pp. 258–64, Mar. 2007.

[171] J. Zimmerberg and M. M. Kozlov, "How proteins produce cellular membrane curvature.," *Nature Reviews Molecular Cell Biology*, vol. 7, no. 1, pp. 9–19, 2006.

[172] P. Sens and M. Turner, "Theoretical model for the formation of caveolae and similar membrane invaginations," *Biophysical journal*, vol. 86, no. 4, pp. 2049–2057, 2004.

[173] H. Vacher, D. Mohapatra, and J. Trimmer, "Localization and targeting of voltage-dependent ion channels in mammalian central neurons," *Physiological reviews*, vol. 88, no. 4, p. 1407, 2008.

[174] K. M. S. O'Connell, R. Loftus, and M. M. Tamkun, "Localization-dependent activity of the Kv2.1 delayed-rectifier K+ channel.," *Proceedings of the National Academy of Sciences of the United States of America*, vol. 107, pp. 12351–6, July 2010.

[175] L. Feinshreiber, D. Singer-Lahat, U. Ashery, and I. Lotan, "Voltage-gated potassium channel as a facilitator of exocytosis.," *Annals of the New York Academy of Sciences*, vol. 1152, pp. 87–92, Jan. 2009.

[176] B. Sorre, *Role of Membrane Curvature in Intracellular Trafficking*. PhD thesis, 2010.

[177] W. M. Lee, P. J. Reece, R. F. Marchington, N. K. Metzger, and K. Dholakia, "Construction and calibration of an optical trap on a fluorescence optical microscope.," *Nature protocols*, vol. 2, no. 12, pp. 3226–38, 2007.

[178] D. a. Berk, a. Clark, and R. M. Hochmuth, "Analysis of lateral diffusion from a spherical cell surface to a tubular projection.," *Biophysical journal*, vol. 61, pp. 1–8, Jan. 1992.

[179] A. Roux, D. Cuvelier, P. Nassoy, J. Prost, P. Bassereau, and B. Goud, "Role of curvature and phase transition in lipid sorting and fission of membrane tubules.," *The EMBO journal*, vol. 24, pp. 1537–45, Apr. 2005.

[180] J. Derganc, "Curvature-driven lateral segregation of membrane constituents in Golgi cisternae.," *Physical biology*, vol. 4, pp. 317–24, Dec. 2007.

[181] P.-E. Milhiet, F. Gubellini, A. Berquand, P. Dosset, J.-L. Rigaud, C. Le Grimellec, and D. Lévy, "High-resolution AFM of membrane proteins directly incorporated at high density in planar lipid bilayer.," *Biophysical Journal*, vol. 91, no. 9, pp. 3268–3275, 2006.

[182] V. Ruta, J. Chen, and R. MacKinnon, "Calibrated measurement of gating-charge arginine displacement in the KvAP voltage-dependent K+ channel.," *Cell*, vol. 123, pp. 463–75, Nov. 2005.

[183] Y. Domanov, S. Aimon, G. E. S. Toombes, M. Renner, F. Quemeneur, A. Triller, M. S. Turner, and P. Bassereau, "Mobility in geometrically confined membranes.," *Proceedings of the National Academy of Sciences of the United States of America*, vol. 108, July 2011.

[184] D. Axelrod, "Lateral motion of membrane proteins and biological function.," *The Journal of membrane biology*, vol. 75, pp. 1–10, Jan. 1983.

[185] M. C. Ashby, S. R. Maier, A. Nishimune, and J. M. Henley, "Lateral diffusion drives constitutive exchange of AMPA receptors at dendritic spines and is regulated by spine morphology.," *The Journal of neuroscience : the official journal of the Society for Neuroscience*, vol. 26, pp. 7046–55, June 2006.

[186] G. Saffman and M. Delbruck, "Brownian motion in biological membranes," *PNAS*, vol. 72, no. 8, pp. 3111–3113, 1975.

[187] D. R. Daniels and M. S. Turner, "Diffusion on membrane tubes: a highly discriminatory test of the Saffman-Delbruck theory.," *Langmuir : the ACS journal of surfaces and colloids*, vol. 23, pp. 6667–70, June 2007.

[188] W. Vaz, F. Goodsaidzalduondo, and K. Jacobson, "Lateral diffusion of lipids and proteins in bilayer membranes," *FEBS Letters*, vol. 174, no. 2, pp. 199–207, 1984.

[189] M. Goulian, O. N. Mesquita, D. K. Fygenson, C. Nielsen, O. S. Andersen, and a. Libchaber, "Gramicidin channel kinetics under tension.," *Biophysical journal*, vol. 74, pp. 328–37, Jan. 1998.

[190] D. Cuvelier, I. Derényi, P. Bassereau, and P. Nassoy, "Coalescence of membrane tethers: experiments, theory, and applications.," *Biophysical Journal*, vol. 88, no. 4, pp. 2714–2726, 2005.

[191] S. M. Leitenberger, E. Reister-Gottfried, and U. Seifert, "Curvature coupling dependence of membrane protein diffusion coefficients.," *Langmuir The Acs Journal Of Surfaces And Colloids*, vol. 24, no. 4, pp. 1254–1261, 2008.

[192] E. Reister and U. Seifert, "Lateral diffusion of a protein on a fluctuating membrane," *Europhysics Letters*, vol. 71, no. 5, p. 6, 2005.

[193] E. Evans and A. Yeung, "Hidden dynamics in rapid changes of bilayer shape," *Chemistry and Physics of Lipids*, vol. 73, no. 1-2, pp. 39–56, 1994.

[194] C. Campillo, L. Pontani, P. Bassereau, S. Sykes, P. Sens, and P. Nassoy, "Tether extrusion as a tool to unveil unexpected membrane dynamics,"

[195] T. Heimburg and A. D. Jackson, "On the action potential as a propagating density pulse and the role of anesthetics," *Biophysical Reviews and Letters*, vol. 2, no. 1, p. 13, 2006.

Résumé

Il est difficile d'étudier in vivo le rôle de la membrane dans l'excitabilité des cellules car les paramètres pertinents (composition et état mécanique de la membrane, densité de canaux...) sont activement régulés par la cellule elle-même et donc difficilement ajustables expérimentalement. J'ai donc développé une méthode pour reconstituer un canal voltage-dépendant dans une membrane où ces paramètres peuvent être contrôlés.
Pour cela j'ai exprimé, purifié et marqué KvAP, un canal potassique voltage-dépendant. J'ai ensuite adapté une méthode existante pour le reconstituer dans des Vésicules Unilamellaires Géantes (GUVs). J'ai mesuré la densité des canaux dans les GUVs grâce à la microscopie confocale. Des expériences d'électrophysiologie ont, de plus, montré que le canal reste fonctionnel après reconstitution.
Ce système m'a permis d'étudier tout d'abord l'affinité du canal pour les membranes courbées. Pour cela, j'ai tiré des nanotubes de rayon contrôlé à partir de ces GUVs et j'ai mesuré la distribution du canal entre la vésicule et le tube par microscopie confocale. J'ai montré que le canal est enrichi dans le tube proportionnellement à sa courbure. Ce résultat est en accord avec une théorie basée sur l'élasticité de la membrane. Nous avons également étudié l'effet du confinement de la membrane sur la diffusion de KvAP. Par des expériences de suivi de particule unique, nous avons montré que le coefficient de diffusion le long du tube diminue d'un facteur 3 lorsque le rayon du tube décroît de 250 à 10 nm. Ce résultat est en accord avec le modèle hydrodynamique de Saffman et Delbrück appliqué à la géométrie cylindrique.

Abstract

Studying the role of the membrane in cell excitability is challenging using cells because of the homeostatic feedbacks preventing the external control of the relevant parameters. To circumvent these difficulties, I developed a model system in which a voltage-gated channel was reconstituted in a membrane where the composition, tension and geometry can be controlled.
I thus expressed, purified and fluorescently labeled KvAP, a voltage-gated potassium channel. I then adapted a method to reconstitute the channel in Giant Unilamellar Vesicles, which are liposomes the same size as cells. I used quantitative confocal microscopy to measure the channel density in these GUVs (it can be controlled between few to thousands proteins per square micron). Furthermore, electrophysiology measurements showed that the protein is still functional after reconstitution.
With these GUVs containing reconstituted KvAP, I have studied the affinity of the protein for curved membranes. I have pulled membrane nanotubes of controlled diameter from GUVs and measured the density of the protein in the tube as compared to the vesicle using confocal microscopy. I found that the channel is enriched in the nanotube and that this enrichment increases as a function of curvature, in agreement with an elasticity based theory. The second application was the study of the effect of membrane confinement on KvAP diffusion. Using single particle tracking, we found that the diffusion coefficient decreases by a factor 3 when the tube radius decreases from 250 to 10 nm. This result is in agreement with a hydrodynamic theory that extends the work of Saffman and Delbrück to cylindrical geometries.